

**A Tale of Two Direction Codes in Rat Retrosplenial Cortex:
Uncovering the Neural Basis of Spatial Orientation in
Complex Space**

Ningyu Zhang

Institute of Behavioural Neuroscience, Department of Experimental Psychology, UCL

Supervised by:

Professor Kate Jeffery

Thesis submitted to University College London to fulfil the partial requirements for the
degree of Doctor of Philosophy in Behavioural Neuroscience

May 2021

DECLARATION

I, Ningyu Zhang, confirm that the work presented in this thesis is my own. Where information has been derived from other sources, I confirm that this has been indicated in the thesis.

Signature:

NINGYU ZHANG

Date: May 2021

ABSTRACT

Head direction (HD) cells only become active whenever a rat faces one direction and stay inactive when it faces others, producing a unimodal activity distribution. Working together in a network, HD cells are considered the neural basis supporting a sense of direction. The retrosplenial cortex (RSC) is part of the HD circuit and contains neurons that express multiple spatial signals, including a pattern of bipolar directional tuning – as recently reported in rats exploring a rotationally symmetric two-compartment space. This suggests an unexplored mechanism of the neural compass.

In this thesis, I investigated whether the association between the two-way firing symmetry and twofold environment symmetry reveals a general environment symmetry-encoding property of these RSC neurons. I recorded RSC neurons in environments having onefold, twofold and fourfold symmetry. The current study showed that RSC HD cells maintained a consistent global signal, whereas other RSC directional cells showed multi-fold symmetric firing patterns that reflected environment symmetry, not just globally (across all sub-compartments) but also locally (within each sub-compartment). The analyses also showed that the pattern was independent of egocentric boundary vector coding but represented an allocentric spatial code. It means that these RSC cells use environmental cues to organise multiple singular tuning curves which sometimes are combined to form a multidirectional pattern, likely via an interaction with the global HD signal. Thus, both local and global environment symmetry are encoded by local firing patterns in subspaces. This interestingly suggests cognitive mapping and abstraction of space beyond immediate perceptual bounds in RSC. The data generated from this study provides important insights for modelling of direction computation. Taken together, I discuss how having two types of direction codes in RSC may help us to orient more accurately and flexibly in complex and ambiguous space.

IMPACT STATEMENT

Successful navigation in space is essential for survival, such as for foraging for food and escaping from predators. The research interests and our knowledge of the neural representation of spatial orientation have rapidly grown in the past four decades since James Ranck and Jeffrey Taube discovered direction-sensitive neurons in the rat brain, which they believe function as the brain's compass, signalling 'which direction you are facing'. However, the directional system in the brain seems more heterogeneous and complicated than the canonical view. The study in the thesis aims to tackle an issue of unexplored mechanism of directional encoding, and to provide answers to questions such as: how the brain uses environment features to guide spatial orientation and resolve problems that arise from disorientation. It would foster a more in-depth understanding of spatial cognition.

In addition to the scientific significance of the current study, building up our knowledge by studying the animal navigation and their brain function has promising implications in clinical research, such as investigating disorientation symptoms in Alzheimer's patients. Moreover, spatial navigation is a high-order cognitive function that involves memory processing. The data obtained in my experiments specifically support this view: a multidirectional code in the retrosplenial cortex can represent information of a global environment structure even within a local subspace. This finding would be of particular interests to theoretical neuroscientists for modelling of head direction computation.

Maintaining a sense of direction is not only important for navigation but also provides a sense of "appropriately connecting to the real world". If we don't know where we are in space, we probably will lose a sense of who we are (possibly by a memory loss) eventually. Therefore, advances made in the spatial navigation field may help advance cognitive sciences in general to explore topics on memory and consciousness.

In a broader sense, it is important to understand how environment features and components contribute to one's navigation ability and efficiency. For example, first, understanding how environment symmetry and layout are learned by the brain may provide intuition and guidance for architects, civil engineers, and urban planners to make buildings, streets, large-scale public spaces (especially tube stations and airports) more informative and navigational-friendly. Relatedly, research findings in neuroscience may inspire artificial intelligence to achieve advances in algorithm development and computer sciences, which are useful in analysing complex urban environments for traffic forecasting and intervention. Moreover, understanding of how human beings navigate in complex environments would optimise development of global positioning system (GPS) and boost technological interventions for navigation. Technological development also has profound potential in clinical translations. For example, developing games and wearable devices for people with cognitive deficits (usually include inability in spatial navigation) might be useful for diagnosis, healthcare, and treatments.

CONTENTS

ABSTRACT	3
IMPACT STATEMENT	4
ACKNOWLEDGEMENTS.....	13
PREFACE	16
LIST OF ABBREVIATIONS	18
LIST OF FIGURES.....	20
LIST OF TABLES	23
CHAPTER 1 GENERAL PRINCIPLES OF SPATIAL MAPPING.....	25
 1.1 A tale of directional disorientation in an ambiguous environment.....	25
 1.2 The cognitive map: an internal representation of space	27
1.2.1 Tolman's cognitive map.....	28
1.2.2 A cognitive map in the hippocampus	30
 1.3 Behavioural evidence for spatial mapping: a sense of direction	33
1.3.1 Orientation relative to environment cues	33
1.3.2 Orientation relative to self-movement cues.....	36
1.3.3 Binding internal signals with external references	38
 1.4 Neurophysiological evidence for spatial mapping	39
1.4.1 Place cells.....	40
1.4.1.1 A general phenomenon of location encoding	40
1.4.1.2 Modulation by local sensory cues and a global framework.....	41
1.4.2 Head direction cells.....	44
1.4.2.1 A simplified head direction circuit	44
1.4.2.2 A unitary firing peak	45
1.4.3 Grid cells.....	47

1.4.3.1 An odometry code	47
1.4.3.2 Modulation by internal and external references	48
1.4.4 Boundary-related cells	50
1.4.4.1 Allocentric boundary coding	50
1.4.4.2 Egocentric coding and egocentric boundary vector cells	52
1.5 How does the map system incorporate direction information?.....	54
1.5.1 Integrating environment and self-motion cues	54
1.5.1.1 Cognitive factors in cue control.....	55
1.5.1.2 Local-global reference frames in cue control	56
1.5.2 Deriving direction from the HD system	58
1.5.3 How does the map resolve directional ambiguity?.....	59
1.5.3.1 Spatial field repetition depends on a global direction	60
1.5.4 Local mapping in retrosplenial directional cells	63
1.5.5 Thesis aims in a nutshell	64
CHAPTER 2 THE RETROSPLENIAL CORTEX AND SPECIFIC PRINCIPLES OF HEAD DIRECTION PROCESSING.....	67
2.1 The retrosplenial cortex: converging sensory and cognitive processing.....	68
2.1.1 Neuroanatomy and connectivity.....	69
2.1.1.1 Anatomical sub-regions.....	69
2.1.1.2 RSC-cortical connections	70
2.1.1.3 RSC-(para)hippocampal connectivity	71
2.1.1.4 RSC-thalamic connectivity.....	73
2.1.2 Functional characteristics in spatial navigation.....	74
2.1.2.1 Visual scene and landmark processing	75
2.1.2.2 Reference frame transformation	78
2.1.2.3 Cognitive mapping	81
2.1.3 Summary: towards a capacity for guiding orientation.....	83
2.2 Principles of canonical head direction processing	83
2.2.1 Where is the HD signal?	84

2.2.1.1 Head direction cells in RSC	84
2.2.1.2 A widely distributed direction code.....	85
2.2.2 Where does the HD signal come from?	87
2.2.2.1 Evidence from lesion studies	87
2.2.2.2 Angular head velocity as the HD update signal.....	88
2.2.2.3 Evidence from development studies.....	91
2.2.3 Landmark inputs to HD cells	91
2.3 How does the directional system help maintain a sense of direction?	93
2.3.1 The ring attractor model.....	93
2.3.2 Environmental sensory reset of the HD signal	97
2.3.2.1 Allothetic and idiothetic cue integration.....	97
2.3.2.2 Experience-based cue integration	100
2.3.3 How may the HD system resolve directional ambiguity?	103
2.3.3.1 A global HD signal in multicompartment environments	103
2.3.3.2 Encoding two directions with one cell: an enigma	104
2.4 The current thesis	107
2.4.1 Hypotheses.....	107
Hypothesis 1	107
Hypothesis 2.....	108
Hypothesis 3	109
Hypothesis 4.....	109
Hypothesis 5	109
2.4.2 An overview of experiments	110
CHAPTER 3 METHODS	113
3.1 Animals	113
3.2 Electrophysiology singe-unit recordings.....	113
3.2.1 Workflow	113
3.2.2 Electrodes and microdrives	114

3.2.3 Surgical procedures	115
3.2.4 Electrophysiological recordings	117
3.2.5 General recording procedures	118
3.3 Electrophysiological data analyses.....	120
3.3.1 Single-unit selection.....	120
3.3.2 Cluster quality analyses	121
3.3.3 Head direction tuning analyses	122
3.4 Statistics.....	122
3.5 Histology	123

***CHAPTER 4 ENVIRONMENT SYMMETRY DRIVES A MULTIDIRECTIONAL CODE
IN RETROSPLENIAL CORTEX*** **125**

4.1 Introduction	125
4.2 Methods	128
4.2.1 Animals	128
4.2.2 Experimental apparatus	128
4.2.3 Recording protocols	130
4.2.4 Data analyses.....	134
4.2.4.1 Directional cell analyses.....	134
4.2.4.2 Shuffling.....	138
4.2.4 Statistical analysis	138
4.3 Results.....	139
4.3.1 Does RSC cells' firing symmetry follow the environment symmetry order?	139
4.3.1.1 Bi-directional pattern in the 2-box.....	139
4.3.1.2 Tetra-directional pattern in the 4-box.....	142
4.3.1.3 Unidirectional and non-directional pattern in the 1-boxes	147
4.3.2 Can a multidirectional pattern emerge from Day 1?	151
4.3.3 Does the multidirectional pattern depend on geometry?	152
4.3.4 Do multidirectional cells fire in the dark?.....	153

4.3.5 Do the classic HD cells remain unidirectional?	156
4.4 Discussion	160
4.4.1 The BD-pattern was unlikely to be intrinsic to RSC cells.....	160
4.4.2 The multidirectional firing symmetry followed the environment symmetry order	161
4.4.3 Interim summary	163
CHAPTER 5 RETROSPLENIAL MULTIDIRECTIONAL CELLS ARE NOT EGOCENTRIC.....	165
5.1 Introduction	165
5.2 Methods	168
5.2.1 Animals	168
5.2.2 Experiment design.....	168
5.2.3 Egocentric cell simulation modelling.....	168
5.2.3.1 Position data from random walk.....	170
5.2.3.2 EBC parameters and tuning curves	171
5.2.4 Egocentric spatial tuning analyses	172
5.2.5 Boundary-related firing properties	174
5.2.6 Head direction analyses	174
5.2.7 Statistical analysis	175
5.3 Results.....	175
5.3.1 Are simulated EBCs comparable to real ones?	175
5.3.2 Is head direction tuning of EBCs homogenous?	177
5.3.3 Is there directional symmetry in the simulated EBCs?.....	179
5.3.4 Are the recorded multidirectional cells egocentric?	185
5.3.5 Does the multidirectional cell firing prefer boundaries?	189
5.4 Discussion	191
5.4.1 Summary	191
5.4.2 HD tuning of EBCs as a by-product of egocentric boundary encoding	192
5.4.3 Distinctions between the multidirectional cells and EBCs	195

5.4.4 Limitations and implications	197
CHAPTER 6 MULTIDIRECTIONAL CELLS ARE A SEPARABLE SUBCLASS FROM HEAD DIRECTION CELLS	202
6.1 Introduction	202
6.2 Methods	203
6.2.1 Data analyses.....	203
6.2.2 Histological analysis	204
6.3 Results.....	205
6.3.1 Multidirectional cells were generally confined to dysgranular RSC	205
6.3.2 Is RSC functional dissociation related to the electrophysiological properties?.....	208
6.4 Discussion	212
CHAPTER 7 GENERAL DISCUSSION.....	217
7.1 An overview of results	217
7.2 Review of hypotheses.....	218
7.2.1 Hypothesis 1: the bidirectional pattern is not an intrinsic property of the cells	218
7.2.2 Hypothesis 2: the multidirectional pattern of the cells is driven by environment symmetry	220
7.2.3 Hypothesis 3: egocentric boundary vector cells yield a multidirectional pattern as an artefact	221
7.2.4 Hypothesis 4: the multidirectional cells are not egocentric boundary vector cells.....	222
7.2.5 Hypothesis 5: the multidirectional and HD cells are different subclasses.....	223
7.3 The underlying mechanisms of multidirectional encoding	224
7.3.1 What generates the pattern of multidirectional cells?	224
7.3.2 Is there a theoretical limit on symmetry order?.....	227
7.3.3 Learning multimodal environmental cues	229
7.3.4 Reference frame transformation	230
7.4 Functional significance of two directional systems	232
7.4.1 Assessment of landmark stability.....	232

7.4.2 A working model for the network to resolve spatial ambiguity	233
7.4.3 Future directions	237
7.5 Concluding remarks.....	240
APPENDIX I: Cluster quality	243
APPENDIX II: Multidirectional cells in the multi-fold symmetric environments	245
APPENDIX III: Locomotion and neural encoding in multi-fold symmetric environments..	248
1. Foraging behaviours	248
2. In relationship to neural activity	249
APPENDIX IV: Dwelling time in the multi-fold symmetric environments	253
REFERENCES	256

ACKNOWLEDGEMENTS

My pursuit of a PhD would never have been possible without the support, guidance, help, patience, and love from many who deserve my thanks from deeps of my heart.

First, I must thank my supervisor - Professor Kate Jeffery, an outstanding scientist who always has crystal-clear thinking and leads hypothesis-driven research; a role model who holds big pictures in mind and maintains incredible attention to details at the same time. Kate has enlightened me on research in spatial cognition since 2013. A brief taste in behavioural neuroscience during my undergraduate has made me return to the lab for a PhD later. In the past few years, I have been learning a lot from her. Her recent editing of multiple drafts of our manuscript and this thesis was an invaluable experience to me.

I must also thank members in the Jeffery Lab - especially for a fruitful collaboration with Roddy Grieves and his help in data pre-processing pipeline. Thank Eleonore Duvelle for her patient hands-on trainings, from tetrode-making to implant surgeries. Thank the lab alumnus Jonathan Wilson, a helpful mentor who taught me how to train animals in complex mazes when I was naïve to neuroscience. Thank my ‘lab brothers’ - James Street, Han Yin Cheng, and Merlin Williams for pints of science and non-science chats we had.

To the IBN in general, I should say thank you all for being awesome colleagues. Thank everyone in the Saleem Lab, Solomon Lab, Bendor Lab, Spiers Lab and Joanna Holeniewska for making IBN a great workplace, where I have gained not only knowledge, skills, but also long-lasting friendship.

Thank you, Margot Tirole, Marta Huelin, Zita Patai for being my firm support. Thank Catherine Perrodin, Stefano Zucca (and the coach group), Will de Corthi, and many more. To all the laughter and good times that I have luckily had with you.

The past four and half years have never been easy, especially the year of 2020, filled with rapid changes, bizarreness, and uncertainties. To Min Zhao, my loyal friend who has been standing by me since nonage, thanks for the companionship over the years in London. To Lan Luo, our reunion since 2019 has brought me joy. To all my dear friends who care about me from thousands of miles away: thank Lingxiu Guo and Sheng Wang for being my ‘family’ in Shanghai.

Regarding the financial support, I am indebted to the Chinese Scholarship Council for providing full tuition fees and stipends over the three years of my PhD; I am also indebted to Kate for a generous 12-month fund during my CRS year. While this thesis is being written in Shanghai, I need to thank the Xu Lab at the Institute of Neuroscience, Chinese Academy of Sciences, for hosting and supporting me before I officially embark on a postdoc.

Special thanks go to Zhi Zhou, who humbles me and has been continuously making me become a better self. Our mutual understanding and trusts conquer all.

Finally, I am grateful for my mom and dad being the harbour of love. The constant support (both emotionally and financially) and unconditional love of my family deserve more than my eternal gratitude.

“A journey of thousands of miles must begin with a single step.”

(千里之行，始于足下)

-- *Tao Te Ching*, by Laozi (a 4th-century BC sage in China)

To those who taught me how to walk and navigate in real life

To those who have always been walking with me

To all the little steps that have led me to where I am

To the long journey ahead

PREFACE

We do not live in a vacuum. Rather, we constantly interact with the environment and are intrigued by questions like ‘Where am I? Where is ‘North’? Which way should I go?’.

Acquiring the knowledge of spatial direction information is essential for survival - to return to places that one frequently visits, distinguish one direction from another, and find ways to new places and so on. For human beings, spatial orientation has become less challenging by the help of a magnetic compass and modern GPS on the smart phone – but, what if the phone dies? Without external guidance by technology, how do we get ourselves oriented in a complicated space? Can we rely on a ‘built-in’ compass to know ‘which direction I am facing’, and how might such a compass system work?

This thesis is about the way in which an internal compass (not a magnetic one) within the mammalian central nervous system encodes direction information. Mapping between the brain and behaviours happens at different levels. I would like to describe brain activities at the scale of single units recorded from a specific brain region in the rat brain: the retrosplenial cortex. The neural activity was linked to the animal’s orienting behaviours in different types of environment. The rat brain has highly similar structures with the human brain but is much simpler and accessible. I would also make claims assuming that the single cells endow the animal with some ‘sense of direction’ while it freely forages for food, usually in a given enclosure adorned with different features situated within the laboratory.

In the current thesis, Chapter 1 introduces spatial navigation and general principles of mapping space into the brain. Chapter 2 is dedicated to an overview of mental operations underlying spatial orientation by focusing on their neurobiological foundations and an important region known as retrosplenial cortex (RSC). Part of the RSC function in spatial

cognition has been covered in a collaborative review paper by Mitchell et al. (2018), in which I was one of the authors.

Research questions of my focus are stated at the end of Chapter 1, and the hypotheses are stated at the end of Chapter 2, to which the answers become more evident in the empirical work. Chapter 3 explains the general methodology that I used to conduct experiments in the laboratory. The subsequent chapters are devoted to describing details of each experiment and data that supports the hypotheses. Part of the results in Chapter 4 have been presented in the format of conference abstracts (Zhang and Jeffery, 2019, *SfN*). Chapter 5 is dedicated to a series of data analyses in egocentric coordinates, for which the simulation modelling part was constructed in collaboration with Dr. Roddy Grieves in the Jeffery lab. Chapter 6 includes extended analyses comparing neural properties between cell types in more details. The thesis ends with Chapter 7 with a summary of findings, discussion of results by making connections to theoretical considerations, and implications in a general landscape. It also proposes several future experimental plans. A manuscript based on the thesis work has been prepared and is close to submission (Zhang, Grieves and Jeffery, *in prep*).

A note with regard to style - although I have mostly used 'I' in the thesis, ideas, thoughts and knowledge would not have been collected without meetings, active discussions, reading papers, conferences, comments and feedback from others.

LIST OF ABBREVIATIONS

ADN	Anterodorsal thalamus
AHV	Angular head velocity
AMN	Anteromedial thalamus
AP	Anterior posterior
ATI	Anticipatory time interval
ATN	Anterior thalamic nuclei
AVN	Anteroventral thalamus
BCBD	Between-compartment bidirectional
BCTD	Between-compartment tetradirectional
BD	Bidirectional
BVC	Boundary vector cell
CW	Clockwise
CCW	Counterclockwise
DTN	Dorsal tegmental nucleus
DV	Dorsal ventral
EBC	Egocentric boundary vector cell
HD	Head direction
LEC	Lateral entorhinal cortex
LDN	Lateral dorsal nuclei
LFP	Local field potential
LMN	Lateral mammillary nucleus
MD	Movement direction
MEC	Medial entorhinal cortex
ML	Medial lateral
MRA	Mean resultant angle
MRL	Mean resultant length

MVN	Medial vestibular nucleus
NMDA	N-Methyl-D-aspartate
NPH	Nucleus propositus hypoglossi
NRe	Nucleus reunions
PaS	Parasubiculum
PFD	Preferred firing direction
POR	Postrhinal cortex
PoS	Postsubiculum
PrCM	Medial precentral cortex
PrS	Presubiculum
RSC	Retrosplenial cortex
S1	Somatosensory cortex
SEM	Standard error of mean
SUB	Subiculum
TD	Tetradirectional
TRN	Thalamic reticular nucleus
V1	Primary visual cortex
V2M	Medial secondary visual cortex
VR	Virtual reality
WCBD	Within-compartment bidirectional
WCTD	Within-compartment tetradirectional

LIST OF FIGURES

Figure 1-1. Photo of the Kezar stadium.	25
Figure 1-2. Tolman's L-shape and sunburst maze.	29
Figure 1-3. The hippocampus and single-unit recordings in the rodent hippocampal system.	31
Figure 1-4. Four types of spatially modulated neurons that are building blocks of the map system.	40
Figure 1-5. A simplified diagram of the head direction network.	45
Figure 1-6. An example classic HD cell and cue-rotation.	46
Figure 1-7. The boundary vector cell (BVC) model.	51
Figure 1-8. An example egocentric boundary vector cell.	53
Figure 1-9. Place field repetition depends on direction.	62
Figure 1-10. Schematics of local and global mapping in retrosplenial directional cells.	64
Figure 2-1. Schematics of retrosplenial cortex in the rat brain.	68
Figure 2-2. Schematics of retrosplenial cortex connectivity.	74
Figure 2-3. Detailed schematics of the head direction circuit.	86
Figure 2-4. Schematics of ring attractor dynamics.	94
Figure 2-5. The dual-chamber experiment.	98
Figure 3-1. Workflow of recordings.	114
Figure 3-2. The Axona microdrive.	115
Figure 3-3. Schematics of rat skull and photo of implant surgery.	117
Figure 3-4. Setups of electrophysiological recording in vivo.	118
Figure 3-5. Image of the rotatable holding box.	119
Figure 3-6. Summary of the analysis pipeline.	120
Figure 3-7. Offline analysis of clusters.	121
Figure 4-1. Schematics of the multicompartiment boxes and the cue-controlled recording room.	129
Figure 4-2. Schematic of the 1-boxes.	130
Figure 4-3. Recording protocols for two experiments.	131
Figure 4-4. The 2-box experiment and example BD-pattern cells.	140
Figure 4-5. Multiple directional firing symmetries (BC-BD) in the 2-box.	141
Figure 4-6. Multiple directional firing symmetries (WC-BD) in the 2-box.	142
Figure 4-7. The 4-box experiment and example TD-pattern cells.	144

Figure 4-8. Multiple directional firing symmetries (BC-TD) in the 4-box.	145
Figure 4-9. Multiple directional firing symmetries (WC-TD) in the 4-box	146
Figure 4-10. Directional firing symmetries in the 1-box (arena).	148
Figure 4-11. Directional firing symmetries in the 1-box (cylinder).	149
Figure 4-12. Onefold directional firing symmetry in the 1-box.	150
Figure 4-13. Multidirectional pattern can emerge in Day 1.	152
Figure 4-14. The TD pattern is lost in the square box.	153
Figure 4-15. Example TD-pattern cells in darkness.	154
Figure 4-16. Preserved but reduced TD pattern in darkness.	155
Figure 4-17. Classic HD cells showed a unidirectional firing pattern.	157
Figure 4-18. Co-recorded HD cells and multidirectional cells in the 4-box experiment.	158
Figure 5-1. Schematic flow of egocentric boundary vector cell simulation.	169
Figure 5-2. Example simulated egocentric boundary vector cells in four environments.	176
Figure 5-3. Firing properties of simulated EBC population.	177
Figure 5-4. Head direction tuning of simulated EBCs was not uniformly distributed.	178
Figure 5-5. Homogenous distribution of multidirectional cell HD tuning.	179
Figure 5-6. A fourfold directional pattern of EBCs in the square box but not the circular arena.	180
Figure 5-7. Multiple directional pattern symmetries of simulated EBCs (2-box).	182
Figure 5-8. Multiple directional pattern symmetries of simulated EBCs (4-box).	184
Figure 5-9. Analysing multidirectional cell activity in egocentric coordinates.	186
Figure 5-10. Multidirectional cells did not show significant egocentric boundary representations.	188
Figure 5-11. TD-pattern cells were not EBCs in the square box experiment.	189
Figure 5-12. Distinct spiking preferences of multidirectional cell and simulated EBCs.	190
Figure 5-13. Schematics for EBC bimodal pattern in the square box and the 2-box.	194
Figure 6-1. Histology and locations of tetrode tracks.	205
Figure 6-2. Different distributions of multidirectional and HD cells in RSC sub-regions.	206
Figure 6-3. Distinguishable electrophysiological properties of multidirectional cell from HD cell.	208
Figure 6-4. Multidirectional cells and HD cells are generally not theta-modulated.	210
Figure 7-1. Multidirectional encoding appears from landmark learning and Hebbian plasticity.	225
Figure 7-2. Simulated effects of sub-compartment numbers on HD tuning specificity.	228

Figure 7-3. Model schematics for the network to resolve spatial ambiguity.	235
Appendix Figure 1. BD-pattern in the 2-box experiment.	245
Appendix Figure 2. TD-pattern in the 4-box experiment.	246
Appendix Figure 3. Co-recorded TD-pattern cells in the 4-box experiment.	247
Appendix Figure 4. Locomotion features in multi-fold symmetric boxes.	249
Appendix Figure 5. Speed correlates of multidirectional and HD cells.	251
Appendix Figure 6. Head-motion correlates of multidirectional and HD cells.	252
Appendix Figure 7. Dwelling time in sub-compartment of the multi-fold symmetric boxes.	254

LIST OF TABLES

Table 4-1. Summary of cell types recorded from different environments.....	159
Table 6-1. Summary of cells recorded per animal in the 2-box and the 4-box experiments.....	207
Table 6-2. Summary of cell electrophysiological properties and statistics.....	211
Appendix Table 1. Summary of cluster quality metrics.....	244

CHAPTER 1

CHAPTER 1 GENERAL PRINCIPLES OF SPATIAL MAPPING

1.1 A tale of directional disorientation in an ambiguous environment

Let us start with a true story that happened on October 25th, 1964, at Kezar Stadium (**Figure 1-1**) in San Francisco. Jim Marshall, a former American football player, recovered a fumble, raced for 66 yards in the wrong direction and returned it into his own end zone in the game against the Vikings. This wrong-way-run made it one of the most unforgettable (and embarrassing) moments in the history of the National Football League. During a brief period of running time, this legendary Minnesota player Marshall confused the target position of the rival's goal post with his own goal post, lost track of his own heading and became confused about his 'sense of direction', which is an awareness of knowing which direction one is heading without explicit guidance. As he proceeded in the wrong running direction, his knowledge of rival's goal post position and his whole perception of the orientation of the football field, which he was in, had rotated 180°.



Figure 1-1. Photo of the Kezar stadium. (a) and (b) show two visually identical goal posts on the west and east side of the stadium. c. A bird's eye view of the stadium. Note that the goal posts created an array of two featureally identical points located at two ends of the football field, forming a twofold rotational symmetry. The visual scene of one half of the field looks almost the same as the other half when viewed from opposing directions. Adapted from Google Street View.

The tale of Marshall's directional disorientation reveals that it is not easy to maintain the sense of direction in a visually ambiguous environment such as football field – even professional football players might get lost. It also illustrates some of the basics of spatial navigation: the external references such as positions of the goal posts and one's internal movement information supply direction signals, and the two sources of information may interact. It then opens the research topic of this thesis: how does our sense of direction deal with environmental ambiguity during directional orientation?

In this chapter, I present a selected review of literature on what is currently known of the general principles of spatial navigation, behavioural and neurophysiological. The foundation of the principles was built upon the influential cognitive map theory, which postulates an internal model of the world (e.g., a map of the environment) that captures the relationship between events (Tolman, 1948) and makes predictions of spatial behaviours (O'Keefe and Nadel, 1978). The neural basis of a map-based framework in the mammalian brain is centred on the hippocampus.

In addition to place, representation of direction is another key part of the map framework. The discovery of a directional system (in analogy to a 'compass in the brain' to guide spatial orientation) adds further support to the spatial mapping theory. In this chapter, I first introduce the concept of the cognitive map and how it has been established. Within the map-based framework, I discuss behavioural studies on how a directional sense is supported. Then I review the neurophysiological evidence of how the map system is represented in the mammalian brain, focusing on studies that illustrate why the system needs a directional framework to navigate in ambiguous environments. Specifically, I will ask: how may sensory inputs such as one's local visual panoramas get integrated into the direction system and

become useful for resolving directional ambiguity (or, not useful, as seemed the case in Marshall's disorientation)? Which brain region might handle this operation?

One particular region in the mammalian brain, the retrosplenial cortex (RSC), forms a rather neglected but potentially important component of the direction network. At the end of this chapter, I briefly explain why the RSC is attracting current research interest and is considered a suitable candidate for supporting directional orientation in a flexible manner. A detailed summary of its role in spatial orientation, the origin of the direction signal and how head direction is processed is presented in **Chapter 2**.

1.2 The cognitive map: an internal representation of space

Immanuel Kant (1781) reasoned that we experience the objective external world by constructing an internal perceptual replica of the world within our head: that is, the representing internal world carries corresponding information about the represented external world. To achieve this information mapping, one's perception and knowledge of the surrounding environment is contingent upon sensory systems (Von Helmholtz, 1925).

Early Behaviourists from more than a century ago argued that stimulus-response (S-R) associative learning underpins spatial navigation, and that learning of an environment is sensory or motor sequence based (Honzik, 1936). As inspired by Thorndike's Law of Effect principle (Thorndike, 1898) and Pavlovian classical conditioning (Pavlov, 1927), the S-R school described learning as simple associations to be reinforced by trial-error conditioning associated with utility; a series of actions which lead to reward become more likely to be performed, while actions which lead to undesired experiences become less likely (Mackintosh, 1975). However, rigid action sequences limit flexible navigation, and simple S-R theories were later found unable to explain all types of behaviours such as shortcut taking. For example, rats were able to take shorter of two alternative routes for food,

indicating that the route which requires less effort is preferred (DeCamp, 1921; Sams and Tolman, 1925). As noted by Dashiell (1930), maze learning is not simply a process integrating successive conditioned reflexes but a more cognition-dependent function. As we will see, several studies support the existence of map-based navigation behaviours.

1.2.1 Tolman's cognitive map

In congruence with Kantian intuitions, Tolman (1948) proposed that animals have a 'cognitive map' in which the external space is mirrored internally to set up an internal schema of the environment. The idea arises from Tolman's experimental observation that rats that had learned the route towards a goal location in a pretrained environment (an L-shape maze) were able to take a novel shortcut to the goal direction in the testing choice apparatus (a sunburst maze) when the familiar route was blocked (Tolman et al., 1946; **Figure 1-2**). In short, animals can compute a vector between the starting box and the goal location. This observation implies that the animals must have access to spatial relations between the goal and start box within the familiar L-shape maze, retrieve the direction information of the goal box, and 'infer' the shortcut in the novel choice apparatus. This inferential process requires learning of an overall representation of environment: a cognitive map, an internal representation of an environment based on a cluster of associations between places and responses (Tolman, 1948). The entire process is analogous to retrieving spatial knowledge from a map to guide navigation.

However, it should be noted that several later studies had difficulties replicating the findings in the original study of Tolman et al. (1946). For example, Gentry et al. (1947) argued that Tolman's animals might have referenced a light above the goal box to orient. Instead of the animal using of map, the light functions as a beacon (a single landmark that an animal can just go towards without needing to know its spatial location). However, the

beacon possibility was partially refuted by a repetition of the experiment by Gentry et al. (1948), although in this experiment animals failed to choose novel shortcut more than alternative paths either. More than half of the animals chose pathways immediately adjacent to the blocked one instead of the shortcut path (with light). These studies have casted doubts on the cognitive map hypothesis.

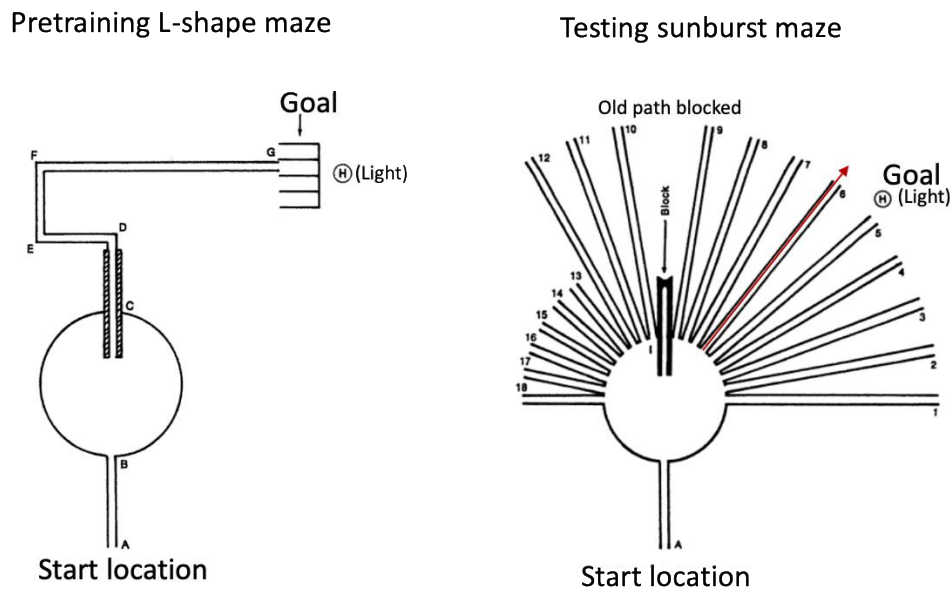


Figure 1-2. Tolman's L-shape and sunburst maze. The pretraining apparatus (left) was used where animals were trained to run from the start to the goal position. In the choice apparatus (right), Tolman et al. (1946) reported that about 36% of the animals chose the novel shortest path (as denoted by the red arrow) to the trained goal when the familiar route was blocked. Adapted from Tolman et al. (1946).

Nevertheless, despite failures of replication, Tolman's proposal of the cognitive map concept has been extremely influential. It has shed light into the long search for a connection between the 'inner perceptual replica' and the external space, and probably a connection to a non-spatial abstract space for making predictions (Stachenfeld et al., 2017) and organising knowledge (Behrens et al., 2018) in contemporary views. The thesis only focuses on its spatial significance. The question arises: where in the brain would this flexible framework be located?

1.2.2 A cognitive map in the hippocampus

The hippocampus (**Figure 1-3a**) became the first candidate for supporting map-based navigation because of its key role in memory and cognition. The hippocampus was originally thought to be important for memory formation, known from the famous patient H.M., who had anterograde amnesia with long-term memory spared but deficits in forming new episodic memories (Scoville and Milner, 1957). Since the early 1970s, the mental map hypothesis has been revitalised and received firm support via neurobiological evidence – this began when John O’Keefe and Jonathan Dostrovsky recorded single units in the hippocampus of rats (**Figure 1-3b**) and discovered that the neurons become active preferentially for specific positions in the environment. This type of hippocampal neuron is termed ‘place cell’ (**Figure 1-3c**) and has been believed to form the neurobiological foundation for a cognitive map of space (O’Keefe and Nadel, 1978).

In further support of the cognitive map theory, the neural signals of ‘where we are going’ as well as ‘which direction we are facing’ have also been found in the brain. James Ranck and Jeffrey Taube reported neurons in parahippocampal region of rats that respond only to an animal’s heading direction (Ranck, 1984; Taube et al., 1990; **Figure 1-3c**). Remarkably, these direction-sensitive neurons share with hippocampal place cells the property of signalling the association between the animal and its surrounding environment. In support of the existence of a neural cognitive map, increasing neurobiological evidence of spatial-selective cells has been reported since then, and I review them in the hippocampus and related structures later in the chapter (section 1.4).

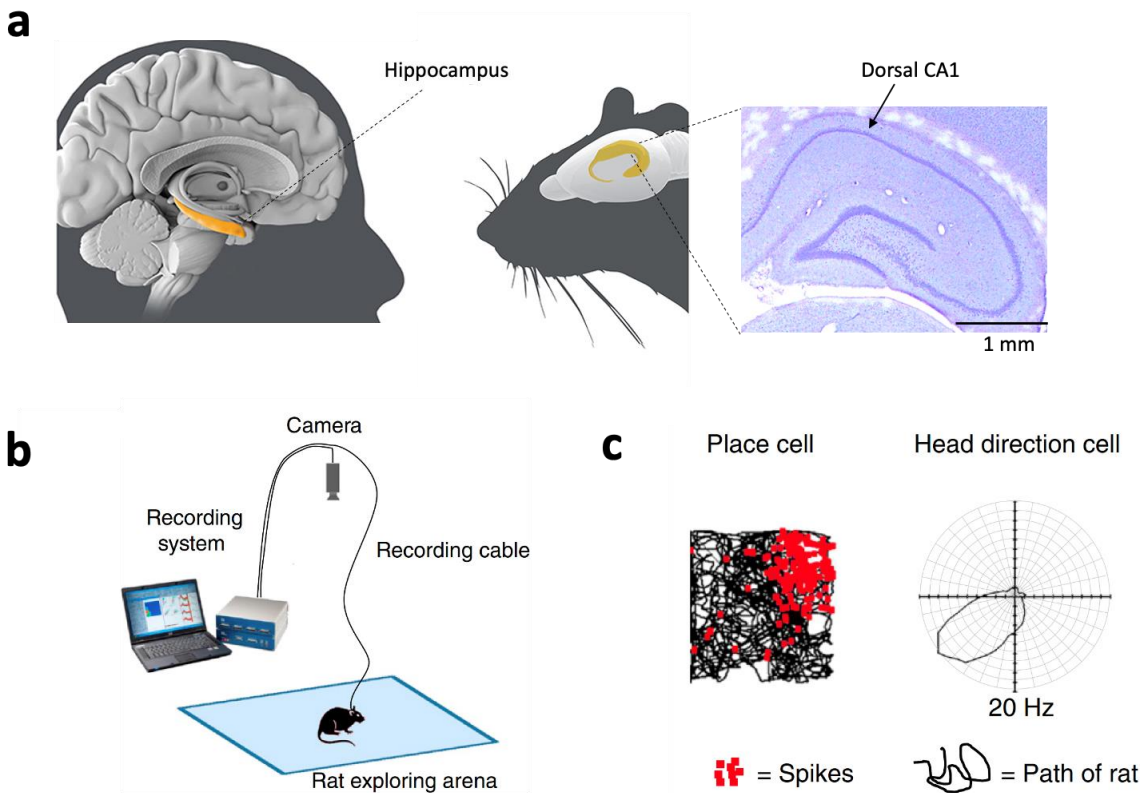


Figure 1-3. The hippocampus and single-unit recordings in the rodent hippocampal system. **a.** Schematics show the hippocampus (yellow) in the human brain (left; a seahorse shape highlighted in yellow) and the rat brain (right); image adapted from www.nobelprize.org. The zoom-out view shows a coronal section of the rat hippocampus taken by the author. Place cells were originally discovered in the dorsal CA1 subregion, denoted by the arrow. **b.** Single-unit recording setup for recording neurons in freely moving animals, with moveable electrodes inside the brain (see **Chapter 3** for details). **c.** Firing patterns of a typical place cell that shows a concentrated pattern of activity in one corner of an arena and a classic head direction cell, which shows a single peak (max firing at 20Hz) pointing the preferred firing direction: south-west direction. (b) & (c) adapted from Marozzi and Jeffery (2012).

Since the discovery of place cells, the hippocampus was proposed to be an important neural substrate of this cognitive map (O’Keefe and Dostrovsky, 1971). Experimental support for the map-based navigation emphasises that animals establish global topographical associations (O’Keefe and Nadel, 1978). For instance, Olton et al. (1978) showed that reference memory of spatial locations on an eight-arm radial maze (in ‘sun-burst’ shape) was hippocampal-dependent, suggesting a vital role of the hippocampus in processing of information about spatial locations and/or general mnemonic processing. In the classic water maze experiment by Morris (1981), rats searched for a hidden platform while swimming in

an opaque water tank filled with water. Through training, animals were able to learn the spatial location of the platform by navigating in the correct direction towards it. The results suggest that rats probably rely on an internal map of the maze layout, having established spatial relationships between distal cues and a known goal location. Further supporting evidence came from a follow-up study by Morris et al. (1982), in which lesions of the hippocampus caused impairments of rats in orienting towards the hidden platform. Similar hippocampal-dependent impairments in place learning were found using a plus maze (Packard and McGaugh, 1996). The results suggest that place learning is hippocampal-dependent. In summary, the cognitive map hypothesis has received extensive support and is widely believed to be the foundation of spatial mapping.

Although a mental map may not be isomorphic to a real geographical map, if the hippocampal system forms a global representation of an environment structure, the spatial relations retrieved from the structure would be sufficient to maintain one's sense of space and sense of direction (O'Keefe and Nadel, 1978). In the experiment of Tolman et al. (1946), the fact that Tolman's animals seem to be able to form a directional measurement (e.g., estimating the goal direction) supports the existence of an internal representation of directional orientation. Similarly, Matthews and Best (1997) showed that rats can travel straight to the platform in the Morris water maze when released from unlearned, novel start locations. Taking direct paths suggests that animals keep a directional sense. Moreover, as we will see later, the hippocampus and its related structures not only support a place system, but also contribute to incorporating direction signals into the map. Next, I review behavioural studies that illustrate the principles underlying directional orientation.

1.3 Behavioural evidence for spatial mapping: a sense of direction

The origin of the hypothesis of having a ‘directional sense’ can be dated back to Darwin’s early proposal that animals acquire a functional architecture which provides information on inertial angular heading and distance travelled for navigation (Darwin, 1873; Barlow, 1964).

The animal’s direction in a given environment is the representation in the system. The system may rely on various sources of inputs, such as allothetic information which informs about the external space and idiothetic information which informs about one’s own movements.

McNaughton et al. (1991) summarised that a compass system in the brain functions by referencing to fixed landmarks and sensory signals generated by self-motion. Supporting behavioural evidence is reviewed below.

1.3.1 Orientation relative to environment cues

In order to register a directional sense, an obvious source of directional information is one or a collection of external cues that have a stable metric relationship in an environment, such as environmental landmarks. Note that they include visual, olfactory, auditory and tactile modalities. Distal visual landmarks are perceived to be more invariant by the animal (Hebb, 1949), hence, they function better in specifying directions (O’Keefe and Nadel, 1978). This is because the further away the landmark is, the less is the parallax error, which is the amount of apparent direction change when one moves orthogonal to the landmark, depending on the distance to the landmarks (Gallistel, 1990).

Celestial landmarks in nature are useful directional referents because they are spatially distant. Insects are impressive navigators despite their relatively simple and small brains compared to mammals; they spatially orient themselves by using landmarks such as contours of mountains, patterns of coastlines and the sun and stars. For example, dung beetles show straight-line orientation during ball-rolling by making use of the celestial cues such as

the sun position and the skylight features (e.g., polarisation pattern and intensity gradient; see Byrne et al., 2003; el Jundi et al., 2014). In order to return to the hive, bees use solar bearing or recognise a configuration of landmark arrays possibly by matching the current view with its remembered view ('snapshots'; Cartwright and Collett, 1983), and so do desert ants (Collett et al., 2013; Freas and Cheng, 2018). The results suggest that distant landmarks can be used by insects to compute compass bearing and the home location via map coordinates to inform spatial orientation.

Mammals also appear to rely heavily on environmental cues and their spatial relations to form an internal representation of orientation. Here, I focus on spatial learning research in rodents in the laboratory context. Animals tend to use configurations of environment cues, rather than just individual features of landmarks for orientation (Benhamou and Poucet, 1998). For example, when rats searched for hidden baited poles in an enclosed circular arena, a fixed relationship between arrays of six intra-maze landmarks with baited poles appeared to be more informative than random pole locations. This indicates that landmark configurations provide compass information in guiding the animal's search behaviour (Greene and Cook, 1997). Moreover, rats used extra-maze cues to facilitate learning of a radial-arm maze task, and the transposition of the cues by altering their configurations (but not cue rotation) disrupted animals' performance (Suzuki et al., 1980). The results show that animals rely on global configurations of cues rather than a single cue for orientation.

Furthermore, many studies have provided us with hints that a directional sense relies on cognitive processing, and that local cues are used together with an established global framework for orientation. In a burrowing task, rats were able to orientate and dig novel tunnels different from the training paths to reach a target box, and visual cues were effective in improving their performances (Zanforlin and Poli, 1970). The results support the mental

map theory and making use of visual cues for orientation. Collett et al. (1986) showed that geometrical relationship between landmarks and goal location can be learned and stored as an internal representation in a form of visuo-spatial memory. In experiments by Collett et al. (1986), gerbils were trained to search for sunflower seeds in a goal location specified by an array of landmarks. Well-trained animals ran straight to the expected goal location when tested by removing or expanding the landmark array transformation, indicating learning of landmarks and their use for route planning. In probe trials, animals were able to reach the seed location defined by a single relevant cue and ignore the unfamiliar and irrelevant landmark, which differed from the familiar cue in features. The result suggests that the animal might match the new landmark with the information held in memory by training. The results suggest that landmark processing is not simply sensory-based but involves transformation of an external reference into an established internal representation.

An early classic place finding task by Ken Cheng (Cheng, 1986) provides strong evidence that animals can rely on a “geometric module” that extracts the geometric properties of an environment, regardless of purely sensory attributes. In Cheng’s task, rats were trained to dig at a target corner location in a rectangular maze with its four corners distinguishable in tactile features and two corners differing in odours. Rats made systematic rotational errors, digging in the location at 180° rotation from the correct goal location, indicating that they probably treated two rotationally symmetrical locations as conceptually the same. The rotational error suggests that animals must have been using the geometric shape of the environment for orientation, rather than the relations to distinguishable sensory features. Using similar paradigms, the findings have been replicated in different species, including human children (Hermer and Spelke, 1994), pigeons (Kelly et al., 1998) and monkeys (Gouteux et al., 2001). These findings show that an overall structure or environment layout is used by animals for spatial orientation.

The findings from previous experiments support that orientation behaviour does not simply rely on sensory processing but probably involves higher-order cognitive processing of the environment layout. Thus, the sense of direction is supported with respect to a global spatial framework. Relatedly, Marshall must have processed identical environment features in the Kezar Stadium (**Figure 1-1**) together with a global geometric shape of the football field. However, he was not correctly keeping track of his own running direction, a process known as path integration, as discussed below.

1.3.2 Orientation relative to self-movement cues

Environment cues might not always be available (e.g., when walking in the dark or a featureless space), so what else can be used for orientation? Path integration (Mittelstaedt and Mittelstaedt, 1980), also known as ‘dead reckoning’ (Gallistel, 1990) allows an animal to return to the start of its journey without explicit guidance from allocentric cues. It is a simple form of spatial learning: animals get knowledge of their current position and direction by integrating with respect to the sum of previous displacements. By keeping track of their own self-movement signals in successive steps, animals can monitor step-by-step changes in direction and distance signals. The self-movement (i.e., idiothetic) cues include vestibular signals, proprioceptive signals (muscle feedback) and kinesthesia, and they can be used to estimate the orientation and distance from previous locations on the trajectory. Therefore, path integration is useful to maintain and update a sustainable sense of direction invariant to changes in allocentric cues (see McNaughton et al., 1991; Etienne et al., 1996; Etienne and Jeffery, 2004 for detailed review).

Several studies on rodents (mice, Alyan and Jander, 1994; gerbils, Mittelstaedt and Mittelstaedt, 1980; hamsters, Etienne et al., 1986) have provided evidence that they use idiothetic directional signals to return home. For example, on a circular platform,

experimenters displaced gerbil pups at random locations from the home base to motivate female gerbils to retrieve the pups. The females were able to carry pups in complete darkness and returned directly back to the home nest via path integration (Mittelstaedt and Mittelstaedt, 1980). Interestingly, when the animal was arbitrarily rotated on the arena before its journey back to the nest, experiencing a conflict in path integration, it compensated for similar amounts of angular displacement by returning to the original location of the nest. However, the animal returned to the new post-rotation location of the nest if the rotation was made below vestibular threshold (Mittelstaedt and Mittelstaedt, 1982), suggesting an involvement of vestibular system in self-motion detection.

Adopting a similar design for food foraging, Etienne et al. (1988) showed that in outgoing trips in the dark, golden hamsters partially compensated the angular shifts of the outward journey for passive angular displacement (i.e., rotation by the experimenter as the animal walked to the arena centre). However, the animals can recalibrate the sense of direction more accurately in an active outgoing journey (i.e., their own exploratory motions around the food source). This suggests that animals rely on self-generated, path-dependent cues during the active outward journey, while the vestibular information dominates during passive outward shift. The authors later suggested that the internal compass system in the brain (Taube et al., 1990) may take over the path integration process to guide behaviours (Etienne et al., 1996). See **Chapter 2** for a detailed discussion on how the vestibular system updates the directional sense in the brain.

In summary, the results show that animals maintain a directional sense through path integration and rely on self-generated inputs especially when external references are limited. However, how may information from different sensory modalities interact to guide spatial orientation?

1.3.3 Binding internal signals with external references

Many studies have shown an interaction between inertial signals and established landmark references, indicating that spatial mapping relies on a combination of idiothetic and allothetic information sources. Etienne et al. (1990) showed that hamsters used either path integration or a salient light in returning to their nest. In their experiment, while the animal was foraging in the dark, if a familiar light spot was made to rotate less than 90°, conflicting with the path-integrated idiothetic signals, hamsters predominantly relied on the light direction in homing, rather than returning back to the departure point using self-motion cues. However, visual cues no longer gained control over path integration as the conflict increased to 180°. The results suggest that familiar external references that are believed to be stable are probably preferred in a cue-conflicting situation, depending on the conflict size (see later sections for further discussion on this point). Alyan and Jander (1994) found similar results in mice in retrieving pups during homing behaviours. However, it was difficult to evaluate the effectiveness of the landmarks in guiding spatial orientation in this experiment, as animals were trained to adopt different orientation strategies at different stages.

In the study by Collett et al. (1986), gerbils successfully reached a goal spot defined by an array of landmarks even if the light was turned off in the middle of their outbound journey. The finding suggests that animals can use previously learned landmark information possibly to plan trajectories, so that a disturbance that happens during execution of the route does not disrupt goal-reaching. These results illustrate an integration of external references and internal signals in guiding spatial orientation behaviours.

In summary, the reviewed results suggest complex aspects of cue integration in spatial mapping for orientation behaviours. Mechanisms of cue integration have been extensively researched in neurophysiological studies and computational models of the hippocampal place

system (to be discussed in the section below) and an internal direction framework (to be discussed in **Chapter 2**). Let us begin by discussing the neural bases that are believed to underlie spatial mapping in the mammalian brain.

1.4 Neurophysiological evidence for spatial mapping

From this section onwards, I focus on the neural representation of space by summarising the literature on neural codes as units of the map system. Here by neural representation, I refer to a connection between experimentally observed activity of single neurons in the brain and the assumed animal's knowledge of allocentric and idiothetic features in navigation. As mentioned earlier, the theoretical notion of the cognitive map has received support from compelling neurobiological findings of spatially modulated single units, first recorded from the hippocampus (O'Keefe and Dostrovsky, 1971) and later from multiple brain regions and neural circuits. The main elements that constitute a map include location, direction, distance, and boundaries (**Figure 1-4**), I briefly introduce cell types that encode these metric features and then focus on their functional aspects. Many more cell types are not covered (e.g., goal, object, conjunctive coding etc; see reviews by Hartley et al., 2014, Grieves and Jeffery, 2017; see anatomical details for spatial neurons in Knierim, 2006).

Akin to the concept of the positional map system in the brain, I briefly introduce the neural compass system and its circuit; note that specific principles on how the direction signal is generated, maintained, and updated within the neural circuit are elaborated in **Chapter 2**.

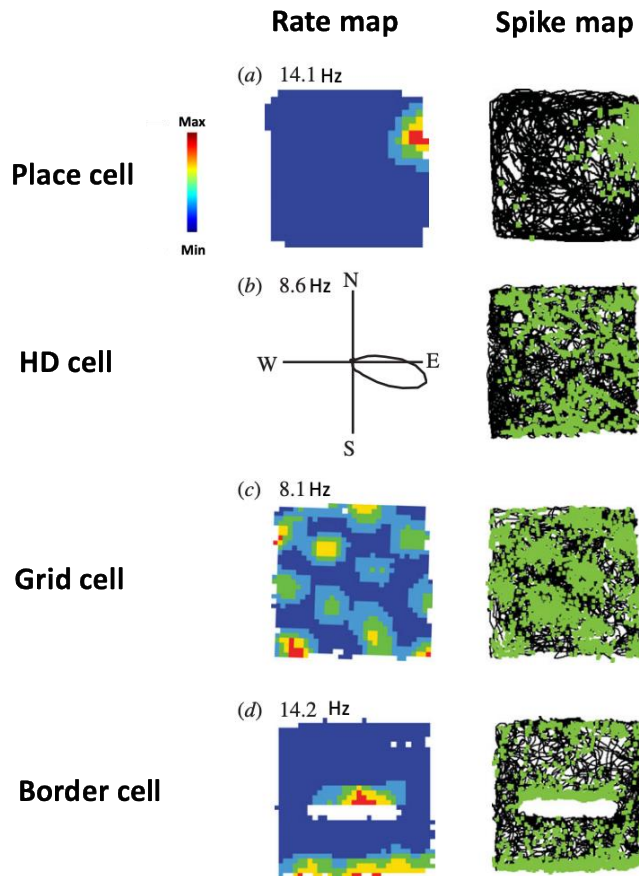


Figure 1-4. Four types of spatially modulated neurons that are building blocks of the map system. Left column: firing rate maps of spatial cells (colour bar denotes activity intensity) and directional tuning polar plot. Right column: spikes (green dots) recorded plotted on the animal's path. The example place cell shows localised firing field on the top-right corner; the head direction (HD) cell shows preferred firing direction towards the East in the polar plot; the grid cell fires in multiple places in a close-packed hexagonal array; the border cell was recorded as a rat explores an arena in which a barrier was inserted; insertion of the barrier led to duplication of firing fields above the lower wall and the barrier. That is, the cell fires regardless of boundary identity. Adapted from Hartley et al. (2014).

1.4.1 Place cells

1.4.1.1 A general phenomenon of location encoding

An internal representation of location is the building block of constructing a cognitive map.

After a technical breakthrough in single unit recording in 1971, John O'Keefe and Jonathan Dostrovsky inserted electrodes in the rat hippocampus and recorded eight putative pyramidal neurons (**Figure 1-4**; also see **Figure 1-3**). These neurons, named place cells, only spike

specifically at particular locations and become nearly silent elsewhere in a testing environment, akin to sending a ‘you are here’ signal (O’Keefe and Dostrovsky, 1971). The region of an environment in which high firing activity occurs is called the place field (O’Keefe, 1979). Different place cells often have different place fields covering the entire surface of the environment, indicating that the whole environment is encoded by place cells as a population.

Originally reported in rats, consistent location-specific single-neuron activity has been reported in other mammals including mice (Rotenberg et al., 1996), gerbils (Mankin et al., 2019), bats (Ulanovsky and Moss, 2007) and directly in the human brain during virtual navigation in epileptic patients (Ekstrom et al., 2003). Similar results (i.e., spatial-viewing) were found in non-human primates when they looked at familiar parts of the environment (Rolls et al., 1998; Rolls, 1999). Ludvig et al. (2004) reported consistent location-specific firing of hippocampal neurons in freely moving squirrel monkeys exploring a three-dimensional space. More recently, a few spatial-location-responsive cells were recorded from the hippocampal formation of freely moving macaques, although many cells showed mixed-selectivity (Mao et al., 2020); and interestingly in non-mammals (titmouse; Payne, Lynch and Aronov, 2020). Together, cross-species place (or place-like) cells suggest that the neural code of location is a substantial and general phenomenon.

1.4.1.2 Modulation by local sensory cues and a global framework

More importantly, place cell activity can drastically change under certain conditions, a phenomenon known as ‘remapping’: the same place cell alters its firing activity when the environment gets changed sufficiently (e.g., cylinder vs. rectangular, Muller and Kubie, 1987; Muller et al., 1987). Remapping of place cells indicates that environmental changes are reflected by changes in the internal representation, supporting the cognitive map theory.

What type of information is fed into the place system which then modulates place cell activity? A short answer comes in two forms: first, local sensory information from different modalities such as visual and self-motion, as well as their interactions; and second, global information about the environment such as layout and structure. As these processes are complicated, the question has received extensive research interests. A more thorough form of the answer is provided later in the chapter (section 1.5), in the context of how the map-based system incorporates direction information.

Briefly, for example, Muller and Kubie (1987) recorded place cells in a cylinder adorned with an on-wall cue card: by rotating the cue card when the rat was removed from the environment, the place fields rotated by a similar amount; by removing the cue card, it was observed that place cells maintained most of their properties but shifted their fields of a random amount. It is important to conduct cue rotation manipulations in a cue-controlled experiment room, so that the animal only registers its sense of direction on selected and controlled cues. In addition to a single cue, place cells are responsive to the configuration of cues. Fenton et al. (2000) observed equal amounts of shifts of 45° in place fields following rotation of a pair of visual cue cards separated by 135°. These results show that place cell activity is modulated by salient visual information in an adaptive, rather than a fixed way.

Moreover, increasing evidence has shown that spatial mapping is more multifaceted than presumed. The hippocampal place cells could respond to more than one category of spatial and sometimes nonspatial elements. For instance, Save et al. (2000) suggested that visual information is crucial for place cell firing, and local olfactory information may be used to compensate visual inputs in the dark. Moreover, a number of studies have reported that place cells show conjunctive responses to multimodal sensory stimuli, including in olfactory-memory (Wood et al., 1999), tactile (Gener et al., 2013), auditory (Aronov et al.,

2017) and taste domains (Herzog et al., 2019). The findings suggest that sensory inputs coming from various sources can be integrated into the map system to modulate place cell activity and thus support cognitive mapping.

Many studies have shown that a global framework, including the structure, geometric layout and general context of the environment, influences place cell activity (Muller and Kubie, 1987). For instance, the scale of place fields changed accordingly to changes in environment geometry: place fields were elongated along the longer wall of a rectangular box compared to a square box (O'Keefe and Burgess, 1996). In addition, global contextual information interacts with local sensory information in influencing place cell firing pattern. Anderson and Jeffery (2003) reported a mix of place cell remapping in response to changes in either wall colour (black/white), odour (lemon/vanilla) of a box, or a combination of both. Nonmetric cues such as the colour and odour supply salient contextual information. A plausible underlying mechanism for observed heterogeneity in the place codes is the contextual gating model proposed by Jeffery et al. (2004), stating that contextual information is incorporated by the map, and may buffer the memorised representations of a familiar environment via synaptic plasticity (also see Hayman and Jeffery, 2008). However, it is still unclear whether hippocampal place cells indeed function as context integrator, or merely a buffer of contextual modulation with the actual integrator being located somewhere else in the brain, for example, possibly the subiculum (Dunn et al., 2018). To summarise, the proposed theory of contextual modulation might be useful to explain nonlinearity in neural activity by considering the heterogeneity of environmental features in spatial mapping.

1.4.2 Head direction cells

1.4.2.1 A simplified head direction circuit

Briefly introduced earlier as a solid support for spatial mapping, the first head direction (HD) cell was recorded from the rat postsubiculum (PoS) by James Ranck in 1984, when he saw a fascinating cell that fired only when the rat's head direction fell within a range of 90 degrees in the horizontal plane, independent of the magnetic field or the animal's location and behaviours (**Figure 1-3; Figure 1-4**). Jeffrey Taube recorded more HD cells from the rat PoS (Taube et al., 1990a; 1990b). Since then, HD cells have been discovered in multiple areas in the mammalian brain, including the subicular cortices (Taube and Burton, 1995; Boccaro et al., 2010; Sharp and Green, 1994), the retrosplenial cortex (RSC; Chen, et al., 1994; Cho and Sharp, 2001; Jacob et al., 2017; Lozano et al., 2017), the medial entorhinal cortex (MEC; Giocomo et al., 2014), the thalamic regions including the anterodorsal thalamic nucleus (ADN; Taube, 1995), the lateral mammillary nucleus (LMN; Stackman and Taube, 1998) and the dorsal tegmental nucleus (DTN; Bassett and Taube, 2001).

In the mammalian brain, HD cells have been reported in multiple interconnected regions, and it is unclear why such a wide distribution exists (**Figure 1-5**). HD cells have been reported in several species (*Drosophila*, Seelig and Jayaraman, 2015; bats, Finkelstein et al., 2014; primates, Robertson et al., 1999; birds, Ben-Yishay et al., 2020). Like the place code, the cross-species finding of HD cells suggests a general phenomenon of direction encoding in the brain.

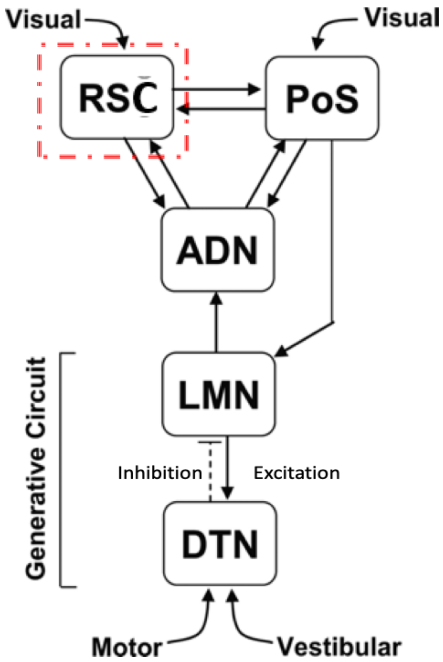


Figure 1-5. A simplified diagram of the head direction network. In the generative circuit, vestibular and self-movement information enters the dorsal tegmental nucleus (DTN) from deeper vestibular system and travels up to the lateral mammillary nucleus (LMN) and anterodorsal thalamic nucleus (ADN) in the thalamus, then to the cortex. Note that the retrosplenial cortex (RSC; highlighted as the focus of the current thesis) and postsubiculum (PoS) receive not only vestibular inputs but also abundant visual inputs from visual areas. Adapted from Clark et al. (2010).

1.4.2.2 A unitary firing peak

Let us take a closer look at the unidirectional HD cell firing pattern as described by Taube et al. (1990). Within a certain range of directions, a typical HD cell fires maximally when the animal faces a specific direction, referred to as its preferred firing direction (PFD). A canonical HD cell firing therefore follows a single Gaussian distribution, with a peak within a narrow range of direction in its activity curve, and near-silent activity (~ 0 Hz) outside of the PFD (Figure 1-6a). The PFDs of the HD cell population are normally homogenously distributed in azimuth around $0\text{--}360^\circ$, supporting its role in representing directions in an allocentric (external environment) space.

In a typical experimental setup searching for HD cells, rats forage in a cylindrical arena adorned with a single cue card on the wall. Crucially, other extra-maze cues such as distal landmarks, room corners are controlled: by placing the cylinder in the centre of the

rooms and inside opaque curtains, to ensure the cue card solely supplies direction information. The cylinder is sometimes rotated to alter the animal's sense of direction as registered with the visual cue. If the animal anchors its directional sense primarily using the intra-maze cue card, rotation of the cue card would consequently shift the PFD of the HD cell (Taube et al., 1990b; **Figure 1-6b**). The single-cued cylinder with cue rotation has become a standard paradigm widely used in HD cell (and place cell) experiments to investigate the effects of visual landmarks in controlling pattern orientation.

Specifically, landmark control observed in place cells has usually been seen in coherence with HD cells by rotating similar amounts (Knierim et al., 1995; Yoganarasimha and Knierim, 2005), supporting that place system and HD system are organised in two different interconnected networks, known as the attractor networks, which may interact with each other (Skaggs et al., 1995; Zhang, 1996; Samsonovich and McNaughton, 1997). The continuous interconnected neural network stores previously computed information, in which neurons behave coherently, see **Chapter 2** (section 2.3.1) for details.

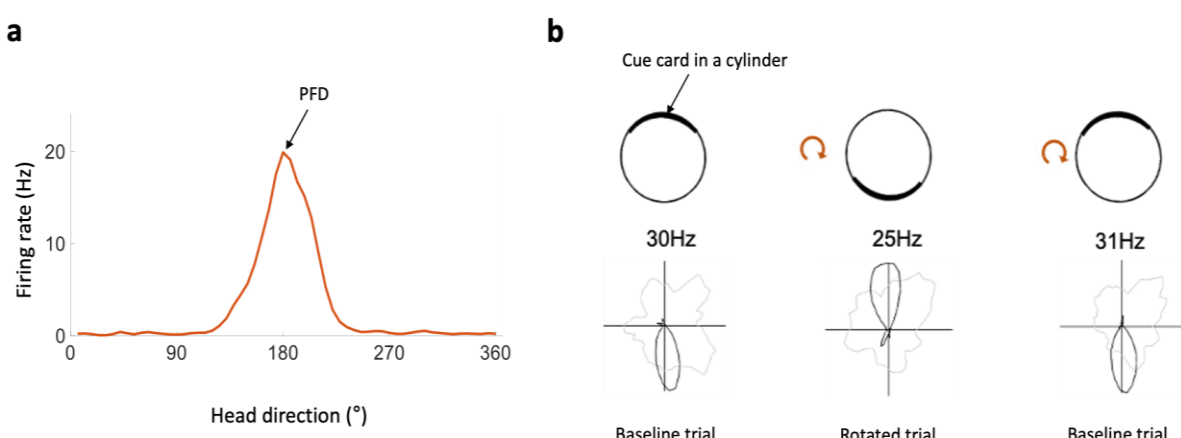


Figure 1-6. An example classic HD cell and cue-rotation. **a.** The tuning curve of an HD cell recorded from the retrosplenial cortex as a rat explored an arena. This cell has its PFD at 180 degrees with max firing rate of 20 Hz and remains silent in directions outside the tuning width. **b.** Polar plots of a different HD cell (cell tuning curve: black; sampling curve: grey). The same cell's PFDs followed correspondingly with the rotations of the cue card in a circular arena. Data obtained by the author.

Across multiple brain regions, this unitary, single-peaked pattern of the classic HD cell has been believed to be consistent (see section 2.2 and section 2.3 for principles of head direction computation). However, a recent finding (Jacob et al., 2017) in the RSC reported populations of noncanonical direction-specific neurons, which intriguingly showed more than one tuning peak in their tuning curves. This type of directional firing pattern is introduced by the end of this chapter (section 1.5.4) and detailed in **Chapter 2** (section 2.3.3). The purpose of mentioning it here is to address that hereafter by HD cell I refer to the classic HD cells with a unidirectional firing pattern as described here.

1.4.3 Grid cells

1.4.3.1 *An odometry code*

Another important component of the map system is odometrical processing by grid cells (see **Figure 1-4**), discovered in the laboratory of Edward Moser and May-Britt Moser (Fyhn et al., 2004; Hafting et al., 2005) in rat entorhinal cortex and adjacent subiculum cortices (Boccara et al., 2010). The grids show highly regular firing patterns in terms of their grid scale (the distance between fields), grid orientation and grid phase (positions of the fields; Hafting et al., 2005). The spacing between firing fields is relatively constant, and this characteristic supports a possible role of grid cells in estimating the travelled distance by the animal.

The regular firing pattern of grid cells is intriguing and suggests that grid cells function as an interconnected network (i.e., attractor network; see Yoon et al., 2013). They may also interact with other spatially modulated cells such as place cells by supplying self-motion related input to the place system (Bush et al., 2014). For example, grid fields rotate coherently with place fields (Fyhn et al., 2007), suggesting interconnected dynamics within the place system (see review by Jeffery, 2011). Moreover, theoretical work proposed that the grid pattern represents movement transition between two locations (Bush et al.,

2015), facilitates position updating and error correction (Fiete, Burak and Brookings, 2008; Sreenivasan and Fiete, 2011), and therefore may support distance coding. However, there is a lack of direct evidence that animals use grid cells to estimate distance.

1.4.3.2 Modulation by internal and external references

Similar to some characteristics of encoding spatial localisation and orientation, grid cells are modulated by internal and external sources of inputs. First, grid cell activity is modulated by environment cues such as geometry. For example, Krupic et al. (2015) showed that when tested in novel environments, the symmetric pattern of grids changed in geometrically different enclosures, and the hexagonal pattern was broken in highly polarized environments such as trapezoids. Although it was unclear whether geometrical shape intrinsically drives the grid pattern, the results support that geometrical cues and global structural information are possibly feeding into the map system via grid cells.

Barry et al. (2007) reported that grid scales varied parametrically with changes in the size and shape of a familiar environment as a function of learning. Changing the global geometric shape from a square to a rectangle induced a conflict between the learned and rescaled environments, thus the grid spacing was enlarged. The finding interestingly suggests that grid cells not only incorporate metric information but are also sensitive to animal's experience. This learning perspective of spatial encoding is revisited later (section 1.5.1.1; section 2.3.2).

Moreover, MEC grid cells showed rate remapping in response to changes made in the local environment cues such as wall features, and the grid pattern drifted in darkness and by removal of visual bars (Pérez-Escobar et al., 2016). The results show that grid cells are sensitive to visual changes, and visual landmarks may be necessary to stabilise the periodic pattern of grid cells, by supplying directional inputs to the grids.

A recent study showed that grid cell spatial firing was preserved when animals ran multiple laps on a 1D ring track (Jacob et al., 2019). Constant spacing between the grid fields across laps indicates that locomotion supports grid cell activity via path integration, complementary to an external reference frame that may be used for correcting accumulated errors in path integration. Furthermore, distance coding is usually associated with linear running speed. In MEC, a group of speed cells were found to code running speed through their firing rates (Kropff et al., 2015), as well as a second type of oscillatory speed coding (Hinman et al., 2016). They may provide speed signals to grid cells for estimating distance during path integration. These results suggest that grid cell activity is influenced by idiothetic and allothetic cues: a general principle of the map system in encoding space.

Furthermore, grid cells are sensitive to nonmetric information change if it is sufficiently salient. Similar to global remapping observed in place cells (Anderson and Jeffery, 2003), by changing different contextual cue combinations (colour, odour), Marozzi et al. (2015) reported repositioning of the grid fields and a shuffling of their firing rate distributions (as analysed in Ismakov et al., 2017). This suggests that contextual cues such as odour and colour are possibly encoded in an upstream interconnected structure before entering the MEC.

Finally, grid cells are not only modulated by sensory cues as discussed in the foregoing experiments; higher cognitive factors such as past experiences and experience with an environment influence grid cell activity. For example, the scale of grid cells is experience-dependent (Barry et al., 2007): if an animal encountered novel environments, grid scales expanded and the grid pattern became less regular but reverted back to the original pattern in the familiar environment (Barry et al., 2012). These results suggest that the grid system is highly plastic. On a related note, the ‘cognitive’ aspects of grid cells recently led

some researchers to relate grid cells to an internal representation at an abstract and conceptual level such as imagination (Bellmund et al., 2016), conceptual knowledge (Constantinescu et al., 2016) and relational knowledge (Garvert et al., 2017). It is possible that potentially, neural codes previously thought to encode specific spatial correlates might be generalised to non-spatial domains.

1.4.4 Boundary-related cells

Boundaries are useful in supplying important geometrical and direction information, because animals can use them as reference points to retrieve angular and linear distance information during path integration. The computational processes to retrieve bearing and distance information can be achieved using two spatial reference frames: allocentric, relative to the boundary or any other external element of the environment and egocentric, relative to the animal. Neurons that encode boundary information in both reference frames have been reported in the rodent brain, as discussed below.

1.4.4.1 Allocentric boundary coding

To explain the observed elongated place fields of place cells in the stretched-environment experiments, O’Keefe and Burgess (1996) proposed an early version of the ‘boundary vector cell model’, in which place cells receives direction and distance information (as referenced to a boundary) from a hypothetical cell type called boundary vector cells (BVCs). Hartley et al. (2000) suggested that the hypothetical inputs to the BVCs come from areas outside the hippocampus, and validated robustness of BVC model in environments with different shapes. Barry et al. (2006) described such hypothetical cells and the boundary vector model in more details: these cells would become active whenever the animal encounters a boundary located within its receptive field at a specific allocentric direction (but irrelevant to the animal’ head direction), and the tuning strength depends on the proximity to the boundary. This type of

neuron has not been reported in empirical experiments at the time the model was proposed.

Where in the brain would it exist?

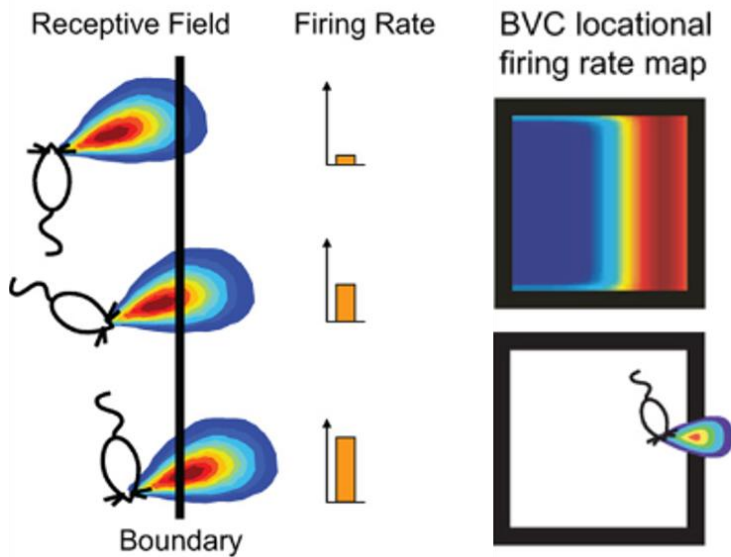


Figure 1-7. The boundary vector cell (BVC) model. In presence of a boundary at a preferred allocentric direction and distance, a BVC increases its rate (bar chart) and fires maximally if the boundary gets closer to the centroid of the receptive field (red colours). For an example BVC recorded in the square arena, its East boundary fell within the firing receptive field (Gaussian sum of preferred distance and direction with thresholds), as shown in the firing rate map. Adapted from Lever et al. (2009).

An earlier work by Sharp (1999) noted the importance of environmental boundaries for firing of subiculum place cells, implying that the subiculum complex may be a potential site for the BVCs. The first empirical border-related cells were reported in the MEC and adjacent parasubiculum; PaS (Solstad, Boccara, et al., 2008). When rats approached the walls of an enclosure in allocentric space, the cells fired maximally and showed edge-proximal activity along the wall, as well as when the square was stretched to a rectangle. Similar boundary cells were found in response to local borders within a larger environment, treating them as ‘landmarks’ (Savelli et al., 2008). These cells were different from the BVCs because the responses depend on geometric border, rather than vector-based computation.

Lever et al. (2009) argued that these cells might be a subtype of the BVC category with short distance tuning and reported more prominent BVC cells in the subiculum. In the experiment by Lever et al. (2009), by inserting a wall into a square box to split the box into two rectangular boxes, the subicular BVCs developed new firing fields along the new boundary (**Figure 1-4**, row4). This indicates that these cells are able to incorporate environmental changes into the system, possibly sending inputs to hippocampal place cells (Barry et al., 2006; Bush et al., 2014; Grieves et al., 2018).

1.4.4.2 Egocentric coding and egocentric boundary vector cells

To some extent similar to the journey of BVC discovery, experimental confirmation of egocentric coding comes after theoretical proposals. The idea of egocentric coding of environment features can be traced back to the consideration that whether self-localisation is based purely on associating multiple egocentric sensory snapshots (e.g., visual panorama, landmarks) with a given location (Leonard and McNaughton 1990; McNaughton et al., 1991). Later theoretical models proposed that the brain should contain a sensory origin of egocentric local views, such as visual-scene information and mental imagery processes, and that egocentric information could be supplied or translated to the map system for comparison with the encoded environments features (Burgess et al., 2001; Byrne et al., 2007; Bicanski and Burgess, 2018). It has been suggested the parietal cortex (Pouget and Sejnowski, 1997) and RSC (Byrne et al., 2007) in particular, may be important brain regions where the egocentric-allocentric reference frame transformation takes place. I discuss the specific role of RSC in **Chapter 2**.

More specific to egocentric boundary coding, Derdikman (2009) proposed a preliminary idea that to some extent, the boundary encoding observed in the subiculum by Lever et al. (2009) may actually be explained if analysing the cell firing from an egocentric

perspective. After a decade, recent advances have been made in the empirical discovery of egocentric cells that encode spatial information from the animal's perspective. For example, egocentric boundary vector cells (EBC) have been reported in the rat striatum (Hinman et al., 2019) and the RSC (Alexander et al., 2020). As shown in **Figure 1-8**, an egocentric boundary vector cell fires maximally when the distance and bearing of the boundary falls within its egocentric preferred firing field (e.g., presumably sending a message of 'a boundary is 10 cm in front of me', or 'the wall is 20 cm on the right' etc). This type of egocentric tuning is invariant to the shape or size of the environments, suggesting that they encode local boundary information. Further EBC tuning characteristics were introduced and examined in **Chapter 5**.

Other types of egocentric coding such as egocentric landmark coding was found in the lateral entorhinal cortex (LEC; Wang et al., 2018), and egocentric coding of the centre of space was found in the postrhinal cortex (POR; LaChance et al., 2019). Together, the egocentric neural codes reflect an interplay of environmental feature representation (through bottom-up processes) and visuospatial memory (via top-down processes). This characteristic supports cognitive mapping (see a detailed review by Bicanski and Burgess, 2020).

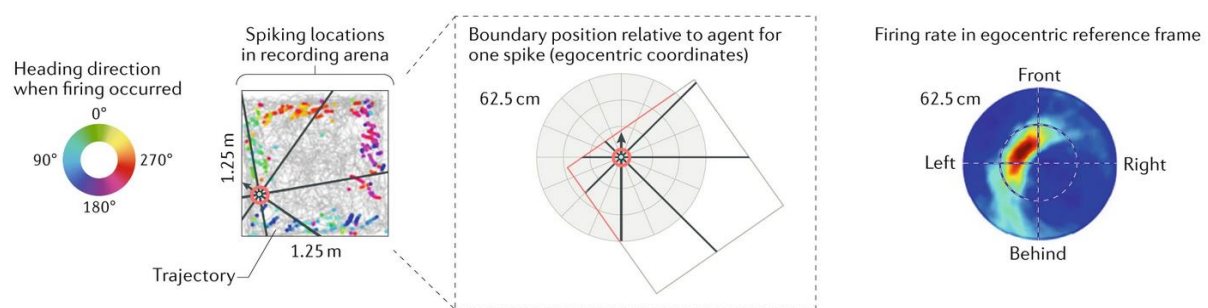


Figure 1-8. An example egocentric boundary vector cell. When an animal explores a square arena (grey lines denote trajectory) and at a specific location (red circle) an egocentric boundary cell fires (dots denote spikes, colour-coded according to the animal's movement direction). The middle panel shows egocentric reference frame, in which the boundary positions (red lines) were plotted relative to the animal when one spike was emitted. The firing rate map is shown on the right: this EBC fires whenever the egocentric coordinates of a boundary fall within its firing field (showing the maximal firing). Adapted from Bicanski and Burgess (2020); also see Chapter 5 for how this method was used to analyse data obtained in the current thesis.

In summary, a map-like system in the brain is supported by neurons like the place cells, grid cells, HD cells, as well as many other cell types reported in the neocortex, hippocampal formation, parahippocampal structures and the thalamus. The selected review above only covered a part of the large pool of neural encoding of spatial information. Although the types of spatial representation vary in the brain, as we have seen, the map-based system follows some general principles to encode space: a sense of place and direction relies on both internal signals and external references; and both local, sensory cues and a global, cognitive framework modulate the firing pattern of spatial neurons. To elaborate, next, I discuss how these rules are implemented by the map system when it needs the sense of direction.

1.5 How does the map system incorporate direction information?

In this section, first, I emphasise the neurophysiological evidence of how allothetic and idiothetic cues supply directional information to the hippocampal place system. Second, I discuss how a local-global reference frame translation influences spatial mapping and the sense of direction in ambiguous environments, as well as how such influences are reflected in place cell activity. This discussion aims to highlight why the map needs a direction system.

1.5.1 Integrating environment and self-motion cues

As supported by behavioural evidence (section 1.3), two major sources of directional information are idiothetic cues via locomotion and a constellation of allothetic cues as external references. How does the place system use them for direction processing?

It has been proposed that the inertially-based signals primarily drive the place cells (McNaughton et al., 1991; Knierim, 1996), and place cell activity relies on the vestibular system during spatial orientation (Best and Thompson, 1989; Jeffery et al., 1997; Stackman et al., 2002). However, since errors are easily accumulated during the path integration

process, external cues such as visual landmarks specifying directions reset the direction signal in the system when it drifts. It was found that self-motion signals interact with local visual cues to control the orientation of place fields (Knierim, 2002; Yoganarasimha and Knierim, 2005) and HD cell activity (Taube and Burton, 1995).

Extensive research studies have shown that the recalibration is subject to at least these two factors: first, cognitive factors such as the animal's past experiences or perceived cue (Knierim et al., 1995; Jeffery, 1998; Jeffery and O'Keefe, 1999; and second, arrangement of cues from which animals compute spatial relationship between different reference frames (Shapiro et al., 1997; Tanila et al., 1997; Knierim, 2002; Yoganarasimha and Knierim, 2005). Details are discussed below.

1.5.1.1 Cognitive factors in cue control

Early studies demonstrated that place fields follow the rotation of salient distal cues when running a plus-shaped maze (O'Keefe and Speakman, 1987) and intra-maze cue in circular arenas (Muller and Kubie, 1987). Importantly, the effectiveness of external visual landmarks in influencing place cell activity is subject to landmark stability as perceived by the animal. In the study by Knierim et al. (1995), better cue-control in place fields has been reported in non-disorientated animals than disorientated ones, as landmarks might not be perceived as stable enough for the latter group. Thus, they used idiothetic cues 'by default' for orientation. Jeffery (1998) showed that a landmark gained better control of place fields if it was perceived as stable from the beginning, but once the animal learned that the visual cue was mobile and unstable, it no longer served as a reliable directional reference, and the animal would rely more on idiothetic cues. Thus, the animal's experience modulates cue efficacy in orientation.

This interpretation is supported by a follow-up study by Jeffery and O'Keefe (1999). When rats were slowly rotated on a rotating platter below the vestibular threshold, they

experienced continuous conflicts in visual (e.g., a salient cue card) and idiothetic directional inputs by rotations in different amounts. If the cue card rotation was out of the animal's sight and knowledge, visual landmarks predominated over idiothetic cues in controlling place cell activity. For instance, place fields rotated 90° following the 90°-rotation of cue card while the rat was rotated by 180°. However, the place fields followed rat rotation more if the cue card rotation was visible to the animal. Furthermore, visual cues showed more dominance over idiothetic cues if a small conflict (e.g., 45°) was experienced (Knierim et al., 1998).

These results support that animals maintain a sense of direction by referencing to one or a set of distributed cues (such as a visual panorama) interacting with idiothetic inputs. This process is not purely sensory but is modulated by cognitive aspects such as prior experiences and learning. This point is revisited again in the context of HD cell findings in the next chapter.

1.5.1.2 Local-global reference frames in cue control

Cue effectiveness in controlling cell activity may also depend on its reference frame: being local or global, and the relative relationship between the cues as perceived by the animal. Place fields followed rotation of a group of objects if they were at the periphery of the enclosure but not when they were in central places (Cressant et al., 1997). Several studies have shown that place cells exhibited mixed responses when proximal (local to the animal) cues and distal (global to the animal) cues were placed in conflicts. When salient distal cues were rotated in the opposite direction to local cues, producing a cue conflict or mismatch with each other, noncoherent responses (split cue control) were observed in place cells. In a mismatch scenario, Shapiro et al. (1997; also see Renaudineau et al., 2007) showed split cue control in place fields: cells that followed the distal cue were simultaneously recorded with cells that followed the local cues, suggesting that place cells respond to distinct subsets of the cues in a complex environment.

Knierim (2002) delineated this issue further and found similar nonlinear responses of place cells that were not simply related to the size of mismatch (i.e., whether local and global cues were in 45° or 180° mismatch). In that study, it was proposed that the heterogeneity in place cell firing in response to local-global cue hierarchy was probably because the cells received different input strengths from local cues versus distal cues. An interconnected network structure (i.e., an attractor model; Skaggs et al., 1995) is important for the system to ‘initialise’ its representation, then through learning and experiences (as discussed earlier), the strengths of inputs (i.e., in a form of synaptic weights) onto the cells get modulated and then further mediate cell activity. This reflects a plastic characteristic of the map system.

The flexibility of the map-based system has been supported by several recent studies that suggest an interaction of local sensory cues and global, distal external references. Using cutting-edge technology with virtual reality and augmented-reality setups, experimenters tried to decouple vestibular and proprioceptive signals and visual information by manipulating the gain between the animal’s locomotion and the visual scene, therefore creating continuous conflicts between self-motion and landmark anchoring. Grid cells showed remapping during gain changes (Campbell et al., 2018). Additionally, grid firing may rely on self-motion more than vision in a 2D virtual reality environment where the animal is able to move its head and body (Chen, Lu, et al., 2019).

Furthermore, visual landmarks can recalibrate path integration to update the place system. In a dome apparatus, by moving projected visual landmarks proportionally to animal’s movements on a circular track, rats experienced sustained exposure to cue conflict between idiothetic signals and feedback from external references (Jayakumar et al., 2019). The place fields shifted dynamically based on the conflict: they shifted towards the landmark reference frame if the animal ran less than the amount of landmark rotation (e.g., rat: 90°

rotation; landmark: 180° rotation); and shifted backwards towards the landmark if the animal overran the landmark (e.g., rat: 90° rotation; landmark: 45° rotation). Prolonged and predictable changes in place cell activity could be estimated in absence of landmarks after training, suggesting high flexibility and plasticity of the system. Overall, these findings indicate that the map system relies on a combined signal (locomotion and environmental landmarks) to register and recalibrate the sense of direction in a rapid and flexible manner.

In summary, the map-based system incorporates direction signals from salient environment cues, ongoing self-motion cues and integration of both sources. The processes are not purely sensory based, but also depend on cognitive factors such as learning and prior experiences.

1.5.2 Deriving direction from the HD system

During path integration, from where might the map system receive the idiothetic inputs and world-centred direction signal? The place system in the hippocampus predominantly processes positional information and may receive direction inputs from elsewhere (O'Keefe and Nadel, 1978; also see evidence in Alyan and McNaughton, 1999). Therefore, the HD circuit, as mentioned earlier, might be a more plausible candidate to supply directional information to the hippocampal map.

Many studies have shown that the map can be direction-modulated and incorporates direction directly from the HD system. Early work showed that hippocampal place cells have directional specificity while rats move outward or inward from the end of arms on a radial maze (McNaughton et al., 1983), and place fields also show directional selectivity in the cylinder (Muller et al., 1994; Markus et al., 1995). Care should be taken to consider potential influence of task correlates and environment geometry, which might lead to stereotyped behaviours and sampling bias. More direct evidence comes from findings of conjunctive

place-by-HD cells in the pre- and parasubiculum, of which the direction modulation seemed to be more stable and stronger than location modulation, as examined in different environments (Cacucci et al., 2004). Likewise, conjunctive grid-by-HD cells have been reported in the deep layers of MEC (Sargolini et al., 2006).

Lesion studies also support the idea that the hippocampal-entorhinal map system derives directional inputs directly from HD cells in their circuit (**Figure 1-5**). This is partly supported by the finding that inactivation of the ADN impaired HD signals in MEC, albeit some neurons remained weakly direction-specific (Winter et al., 2015). In contrast, place fields from PoS-lesioned animals were not controlled by rotation of landmarks and shifted randomly, whereas the effect was mild for place fields in ADN-lesioned animals (Calton et al., 2003). This suggests that landmark information directly from PoS, rather than ADN, may supply finer directional precision for the spatial map.

More direct evidence comes from sophisticated juxtacellular recording studies finding that presubiculum (PrS) layer III HD cells appeared to project directly and prominently to MEC layer III, which contains grid cells (Preston-Ferrer et al., 2016). However, currently there is a lack of direct anatomical evidence for cell-specific mapping from HD cells to place cells or grid cells, although place cells and a small number of HD cells, as well as conjunctive coding have been reported in the hippocampus (Leutgeb et al., 2000). To summarise, the orientation of the map-based system may be supplied by path integration and direct signal inputs from the HD system.

1.5.3 How does the map resolve directional ambiguity?

When navigating in an ambiguous environment, such as the one with visually similar features and multi-folded symmetry like the football field, the map system would need to properly

connect local visual information with a global sense of direction. Otherwise, think about Marshall's disorientation scenario. Can the system achieve this? If so, how?

1.5.3.1 Spatial field repetition depends on a global direction

The findings reviewed so far suggest that place cells and grid cells encode global spatial features, but they also encode local spaces in specific conditions, by showing repeating firing fields when the animal moves between multiple visually similar sub-compartments or segments (Skaggs and McNaughton, 1998; Fuhs et al., 2005; Derdikman, 2009; Spiers et al., 2015). To disambiguate visually similar environments, direction information specified by the orientation of the local subspaces is important in order for the map to connect them to a global structure (Grieves et al., 2016; see review by Grieves et al., 2017).

In multi-compartmented mazes with a parallel design (i.e., multiple sub-compartments aligned in the same direction), Skaggs and McNaughton (1998) found that many place cells showed firing fields in a similar position in each of the two connected compartments, rather than a unitary representation of the whole apparatus. With the same design, Tanila (1999) found comparable results, but the remapping and repetition of place fields depend on the animal's recent experience. Grid cells also showed repeating firing between the two sub-compartments, although would become less repeating when animal gained more experience (Carpenter et al., 2015).

In an extended version of the two-parallel-box, place field repetition was found in a four-connected box: four parallel sub-compartments connected with a common corridor (Spiers et al., 2015; Grieves et al., 2016), suggesting that the animal seemed to treat the four visually identical compartments as the same. However, when one of the boxes could be distinguished by colour or odour, place cells remapped in the changed sub-compartment but

maintained repeated fields in the other three, suggesting that local contextual cues are sufficient in inducing remapping (Spiers et al., 2015).

Interestingly, a number of studies have shown that place field repetition depends on the environment structure and the relative orientation between the connected boxes, possibly because different arrangements provide different directional references for the spatial map. Fuhs et al. (2005) replicated the repeating place field in the design of Skaggs and McNaughton (1998) and additionally recorded cells from the same animals in a two-box-apparatus, where the compartments were rotated 180° (**Figure 1-9a**). However, in the latter experiment, place cells showed unique representations across the two sub-boxes and repetition of place fields was rarely seen, suggesting that their place cells encode the global apparatus information.

Moreover, place field repetition depends on a global directional reference. Grieves et al. (2016) conducted experiments in a rectangular box with four connected sub-compartments arranged either in radial (60° to each other) or in parallel (0° separation; the same configuration as in Spiers et al., 2005). The two types of configurations were shown in **Figure 1-9b**. Importantly, they observed that place field duplication occurred only in the parallel maze, indicating that the animal might treat four sub-boxes similarly in that case, which was supported by a set of behavioural experiments in a different group of rats. Taken together, the results suggest that directional information supplied by the environment structure, even small, enables the animal to distinguish otherwise visually identical subspaces.

Where might a global direction information come from? As discussed earlier, the map system incorporates directional information from the HD system (section 1.5.2). Properly functioning vestibular nuclei in the HD circuit (section 1.4.2) are essential for the place

system to disambiguate visually similar environments (Harland et al., 2017). Adopting the same design used by Grieves et al. (2016), Harland et al. (2017) replicated the findings only in control animals that had an intact HD system but not in LMN-lesioned animal that were supposed to have disrupted HD generational signals (**Figure 1-9b**). Place field repetition was also present in the radial maze for the LMN-lesioned group, suggesting that without a properly functioning HD system, the place system failed in angular disambiguation.

However, to what extent does global mapping interact with local mapping?

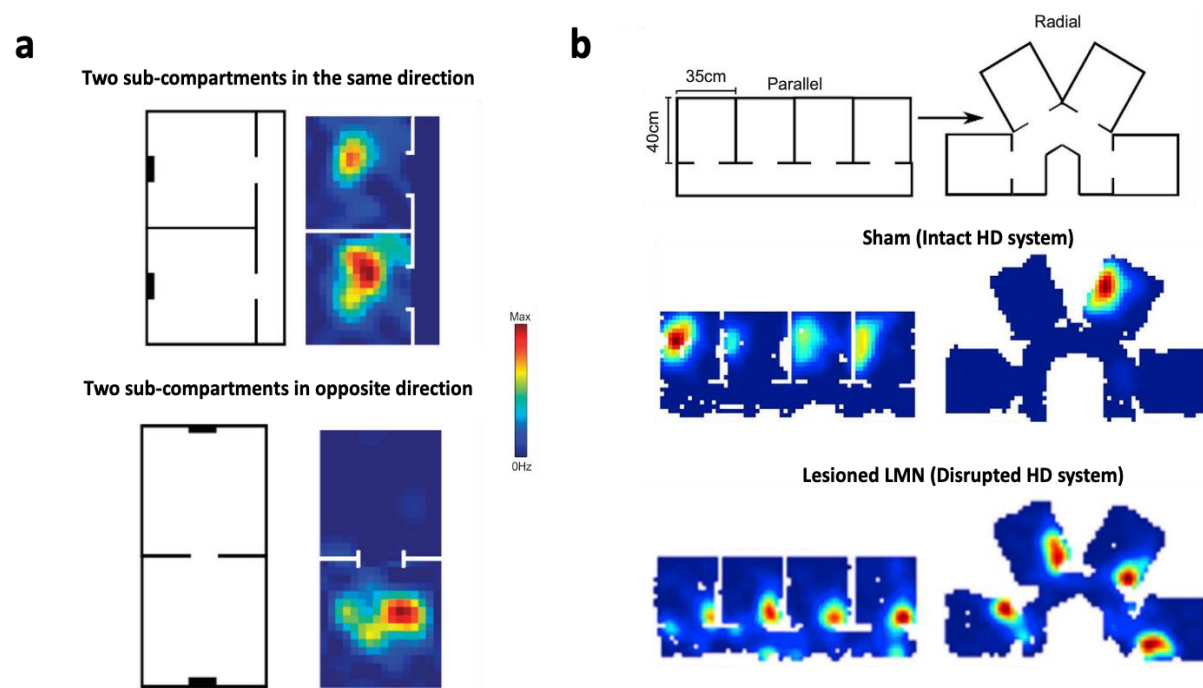


Figure 1-9. Place field repetition depends on direction. **a.** Maze schematics by Fuhs et al. (2005) and the place cell firing maps. Place field repetition was observed when the sub-compartments were in parallel (top), and rarely when they are in opposite directions (bottom). Adapted from Grieves et al., 2017; **b.** Maze schematics by Harland et al. (2017) and the place cell firing maps. Place fields repetition disappeared in the radial formation in the control animal (middle) but persisted in the LMN-lesioned animal (bottom). Adapted from Harland et al. (2017).

Derdikman et al. (2009) found that on a hairpin maze with multiple zigzag pathway segmentations, grid cells and place cells displayed repeated, fragmented fields when the animal was running in the same direction between pathways. In the same setup, while grid cell activity was fragmented, MEC HD cells showed unidirectional firing and the PFDs were

constant between different alleyways (Whitlock and Derdikman, 2012). These results suggest that global direction information is coded upstream of the place and grid cells and then gets integrated into the map system (also see Taube and Burton, 1995; section 2.3.2.1). Where about in the brain might global and local mapping happen simultaneously?

1.5.4 Local mapping in retrosplenial directional cells

Importantly, a recent discovery in rat RSC (part of the HD system as mentioned) provides us some hints. Jacob et al. (2017) reported a subpopulation of rat RSC neurons that, surprisingly, fired in two opposite directions in a visually ambiguous box that consisted of two connected sub-compartments. The two sub-compartments were in a 180° rotational symmetry (i.e., a twofold rotational symmetry), creating a conflict between local directions as specified by visual cue cards and global direction as specified by the whole structure (**Figure 1-10**). Jacob et al. (2017) found that the dysgranular RSC cells displayed bidirectional (BD) tunings in which one PFD flipped to the opposite direction when animal crossed the central doorway between the two sub-compartments. These neurons were believed to encode two opposite local directions by showing reversing tuning curves, as specified by two landmarks (i.e., cue cards) in the apparatus. In contrast, simultaneously recorded HD cells from the RSC and ADN displayed coherent tuning between the two sub-compartments, signalling a global direction in the apparatus.

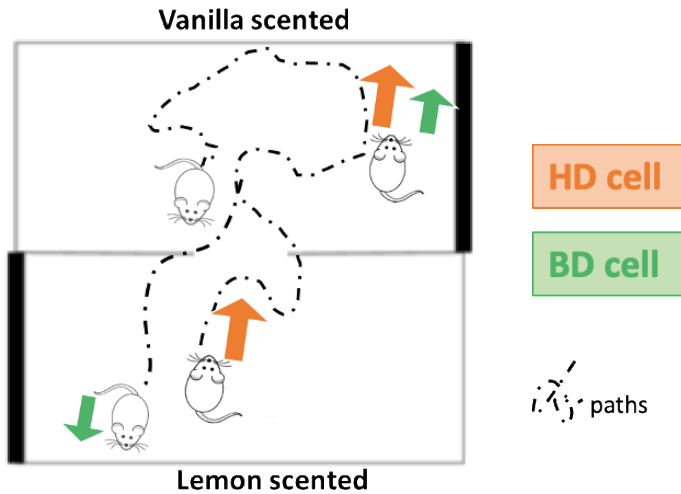


Figure 1-10. Schematics of local and global mapping in retrosplenial directional cells.

In the experiment by Jacob et al. (2017), rats foraged between the two connected rectangular boxes, adorned with an on-wall cue card (denoted by the black bar). The two sub-compartments were scented differently to help compartment disambiguation. The unidirectional HD cells (orange) and bidirectional cells (green) were simultaneously recorded, displaying decoupled directional tuning. Arrows denote the preferred firing directions of the cells: as the animal crossed the central doorway, a BD cell flipped its PFD by 180° , while the HD cell maintained its unidirectional firing pattern.

Intriguingly, such split or decoupled tuning of direction in a multicompartment environment had never been reported in the HD system. The discovery of these RSC bidirectional neurons indicates that local mapping of direction information coexists with global mapping of direction in the same brain region, the RSC. The underlying mechanism of such dissociated RSC neuron populations in local and global mapping requires further investigation and has motivated the current work.

1.5.5 Thesis aims in a nutshell

The main aim of the thesis was to explore the formation of the intriguing bidirectional pattern in RSC. Whether the twofold symmetry of firing derives from the twofold symmetric environment or is a built-in property of the bidirectional cells? It is possible that the brain may be specifically interested in reversing the traveling paths and directions in wayfinding. While Jim Marshall was running in the twofold symmetric football field (section 1.1), his brain might either be constantly encoding two opposite directions, or his sense of direction

was mainly triggered by the goalposts that were 180° apart, relying on the environment symmetry. These possibilities were tested in the current thesis, in the context of investigating retrosplenial directional firing in environments with different symmetry orders.

Furthermore, the current thesis also aimed to address these questions: how do egocentric-referenced sensory cues (e.g., local visual views) interact with allocentric-referenced cues to form a coherent directional sense in RSC? How do local sensory cues get mapped onto a global directional framework? Might the pattern arise from egocentric encoding of local boundary relationships? These questions were unfolded in specific forms in **Chapter 2**.

In the next chapter, let us go one or several synapses backward from the hippocampal formation, and focus on the RSC function as well as the origin of its directional encoding. After reviewing an extensive number of studies on the role of RSC in spatial cognition, discussing specific principles of direction processing in the HD circuit, and a discussion on the noncanonical direction encoding (e.g., Jacob et al., 2017), we will converge to the proposed experiments to test several hypotheses regarding the BD pattern formation. This is a critical issue, because the mechanisms of firing symmetry point to a postulation that RSC direction code serves as credible representation of local-global spatial mapping and may be important to resolve directional ambiguity.

CHAPTER 2

CHAPTER 2 THE RETROSPLENIAL CORTEX AND SPECIFIC PRINCIPLES OF HEAD DIRECTION PROCESSING

In **Chapter 1**, behavioural and neurophysiological studies revealed the general principles underlying spatial mapping. Neural encoding of space depends on processing of allothetic and idiothetic cues and their integration to maintain a directional sense. However, when navigating in an ambiguous environment such as Marshall's football field, how does the HD system coordinate with different sources of information to maintain a coherent directional sense? As reviewed in the previous chapter, clearly, there is a faculty in the brain (upstream of the hippocampal-entorhinal system) that is part of the HD system and may be specifically involved in spatial disambiguation. A potential candidate has drawn our attention: the retrosplenial cortex (RSC). The current research interest in RSC arises mainly from the discovery of the intriguing local directional tuning, which co-exists with but dissociates from the global HD cells in an ambiguous twofold symmetrical environment (Jacob et al., 2017).

In this chapter, I first review an extensive body of research on the anatomical connectivity of RSC with multiple brain regions and its function in spatial cognition: especially in landmark processing, reference frame switching, cognitive mapping, and direction encoding. Then, starting from direction encoding in RSC, we travel down the hierarchy of canonical HD circuit to discuss how HD signals originate from and are updated in the vestibular system and thalamic regions. This is then followed by an introduction to theoretical modelling of HD processing and a discussion of the noncanonical directional signals, including the RSC bidirectional pattern as described in Jacob et al. (2017), as well as a few other types reported recently. The discussion points towards an enigma of noncanonical pattern formation, and the current thesis aims to address the issue. By the end of the chapter,

it is hoped that it will become clear that RSC may be the faculty to convert local sensory inputs onto a global directional framework, so that it may contribute to resolving spatial ambiguity.

2.1 The retrosplenial cortex: converging sensory and cognitive processing

The RSC (**Figure 2-1**) is a multi-layered cortical region that forms the posterior part of the cingulate cortex. It derives its name from the position in relationship to the splenium of the corpus callosum (Hopkins, 2005). Research interest in RSC has been initiated by the discovery of abundant reciprocal connectivity to multiple brain regions (Van Groen and Wyss, 1990; 1992; 2003). The connectivity allows RSC to process information from multiple sources.

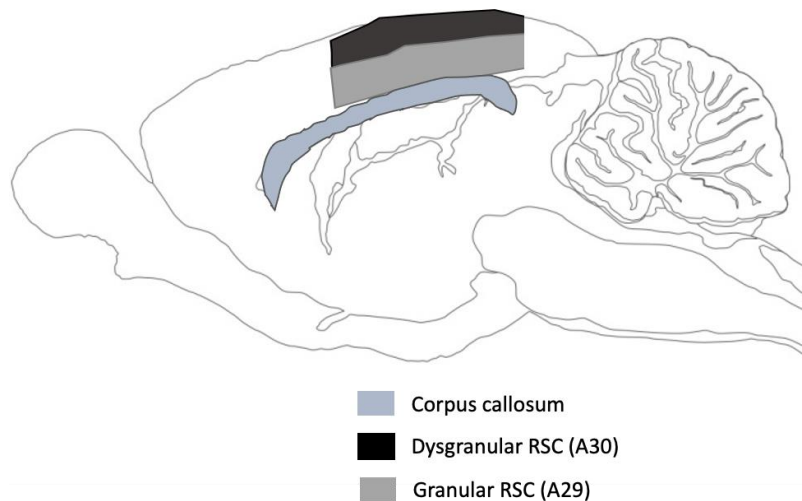


Figure 2-1. Schematics of retrosplenial cortex in the rat brain. The dorsal-medial part of the rat brain (shaded areas) denotes the retrosplenial cortex, located above the corpus callosum (blue). The two sub-regions, dysgranular RSC (referenced as Brodmann area 30 in literature; dark) and granular RSC (referenced as Brodmann area 29; light) are denoted in different shades. Drawn by the author by adapting the rat brain schematics from <https://scidraw.io/>.

More importantly, accumulating evidence has suggested an ‘incontrovertible’ role of RSC in spatial navigation (see detailed reviews by Epstein, 2008; Vann et al., 2009; Mitchell et al., 2018; Alexander et al., 2020). It has been shown that RSC is important for a general

cue-associative learning beyond the spatial domain (see review by Todd et al., 2019), mnemonic processing (Wagner et al., 2005), and even conscious states (Fox et al., 2017; Vesuna et al., 2020), reflecting the capacity of RSC in cognitive processing. In this section, I review the neuroanatomical evidence on how different sources of inputs (e.g., allothetic and idiothetic) converge in RSC.

2.1.1 Neuroanatomy and connectivity

2.1.1.1 *Anatomical sub-regions*

RSC is one of the largest neocortical areas in the rodent brain, taking up half of the anterior-posterior axis on the brain surface (Vogt and Peters, 1981). The rodent RSC consists of dysgranular (Brodmann area 30; dorsal) and granular (Brodmann area 29; ventral) subregions (Wyss and Sripanidkulchai, 1984; Van Groen and Wyss, 1992). In some early studies, the dysgranular subregion of RSC was referred to as 29d, and the granular RSC was divided in to two subregions (gRSCa and b; Van Groen and Wyss, 2003) or three subdivisions: Rga (29a), Rgb (29b), Rgc (29c) (see review by Sugar et al., 2011). For simplicity, this thesis only considers RSC anatomical segregation as dysgranular and granular in general.

The two sub-regions can be distinguished by their laminar characteristics. For example, packing and density of neurons are different in laminar layers of two sub-regions: neurons in the dysgranular part are loosely distributed, making layer II/III and layer V (big pyramidal neurons) wider than granular RSC; whereas in the granular part, layer I and layer II neurons are more densely packed than that in the dysgranular RSC (Vogt and Peters, 1981; Van Groen and Wyss, 1992). Would the two sub-regions contain neurophysiologically distinct sub-populations? The current thesis explored this issue in **Chapter 6**.

Importantly, anatomical segregation might be related to functional differences. Pothuizen et al. (2009) found that there is a difference in granular and dysgranular contribution when animals navigated in the dark versus the light conditions, in which granular RSC was heavily involved in processing memory components, whereas the dysgranular RSC was more responsible for visual-spatial cue information (also see Vann and Aggleton, 2005). As a further support, in Jacob et al., (2017), landmark-dominated directional cells were reported exclusively in the dysgranular RSC. These findings suggest potential differences between the two sub-regions in processing visual information.

2.1.1.2 RSC-cortical connections

The RSC sits within an interconnected cortical-hippocampal-thalamic network. First, a number of studies have shown that it has dense connections with the visual cortex (Van Groen and Wyss, 1992), Brodmann areas 17 and 18a/b (Vogt and Miller, 1983; Van Groen and Wyss, 2003; Makino and Komiyama, 2015), prefrontal cortices (Shibata et al., 2004), auditory cortex (Vogt and Miller, 1983; Todd et al., 2016), posterior parietal cortex (Olsen et al., 2017) and secondary motor cortex (Yamawaki et al., 2016). The connection with multiple sensory areas suggests that RSC is involved in multimodal sensory processing.

The visual system has been shown to have close anatomical interconnection with RSC. The primary visual cortex (V1) forms a cortico-cortical feedback loop with RSC in mice, in which RSC receives strong inputs from V1 (Oh et al., 2014) and projects processed inputs back to the visual cortex (Makino and Komiyama, 2015; Vélez-Fort et al., 2018). These results provide a neurobiological basis for visual information to arrive in RSC, in which Murakami et al. (2015) found strong neural responses to visual gratings presented with low speed, indicating a preference for stable visual features in the visual scene.

RSC is not simply a visual-responsive area but is involved in processing of visual landmark information for navigation in humans (Auger et al., 2012; Epstein and Vass, 2014) and rodents (Fischer et al., 2020; Powell et al., 2020; Mao et al., 2020b), especially in respect of direction encoding (Knight et al., 2014; Jacob et al., 2017). Human patients with a lesioned RSC fail to remember directional information as specified by familiar landmarks, although their ability to identify visual landmarks is spared (Takahashi et al., 1997). Therefore, RSC is involved in processing visual landmark information for maintaining a sense of direction. I return to this point in more details later (section 2.1.2.1).

2.1.1.3 RSC-(para)hippocampal connectivity

RSC receives substantial inputs via projections from the hippocampus (see review by Cenquizca and Swanson, 2007; Miyashita and Rockland, 2007) and the subiculum complex (Van Groen and Wyss, 1992; 2003; Honda and Ishizuka, 2015), including the presubiculum (PrS), postsubiculum (PoS) and parasubiculum (PaS) (Kononenko and Witter, 2012) and the MEC (Van Groen and Wyss, 1992; Burwell and Amaral, 1998). As discussed in **Chapter 1**, the hippocampal-entorhinal network is demonstrably involved in spatial navigation. Anatomical connection to this network ensures an interaction between RSC and the hippocampal system for information exchange.

A recent developmental study reported that in rat pups the projections from the hippocampal-parahippocampal region to the RSC show low density around birth, but they develop rapidly and reach adult-like level around the time of eye-opening (Haugland et al., 2019). Postnatal development in anatomical connectivity implies that neuronal wiring and synaptic plasticity develop through learning and experiences. This is in agreement with a recent finding suggesting RSC-hippocampal connectivity is important for memory formation during sleep (Opalka et al., 2020).

Specifically, Yamawaki et al. (2019) elegantly delineated the connectivity within the RSC-subiculum hippocampal circuit. They found that layer V pyramidal neurons in granular RSC receive excitatory inputs from the subiculum pyramidal neurons. The excitatory inputs converge in layer 1 of granular RSC with long-range inhibitory inputs from the hippocampal CA1 as well as excitatory axons from the anterior thalamic nuclei (ATN) of the thalamus, a part of the HD circuit (Taube, 1995). Although the function of this circuit requires investigation, one may infer that HD information could be supplied by ATN to RSC.

The parahippocampal regions, including the postrhinal cortex (POR), PrS, PaS, and MEC, where spatially modulated cells are clustered, receive dense inputs originated from RSC (Jones and Witter, 2007; Sugar et al., 2011; Kononenko and Witter, 2012; Czajkowski et al., 2013). It has been found that from the first postnatal day (P1), afferents originating in rat dysgranular RSC layer V arrive all layers of PrS and deeper layers of MEC and mature at around P12, before the spatial cell activity patterns appear (Sugar and Witter, 2016). Although the function of the afferents is unknown, this rapidly developed connectivity may facilitate development of other spatial cells in the parahippocampal regions by receiving upstream sensory inputs from RSC.

Interestingly, Sugar and Witter (2016) reported differentiations in dysgranular and granular RSC projections to the PaS/MEC. They found that dysgranular RSC is connected preferentially to medial MEC, distal subiculum and distal PrS. In contrast, granular RSC is densely connected to lateral MEC, proximal subiculum, and proximal PrS. A route of axonal origination from dysgranular RSC to medial MEC is very interesting, suggesting potential inter-region information flow. It may be tentatively related to a recent finding of visually driven directional cells in the PaS and MEC (Kornienko et al., 2018) that share some properties with cells in the dysgranular RSC (Jacob et al., 2017).

2.1.1.4 RSC-thalamic connectivity

RSC is reciprocally connected with subcortical regions (see detailed connections in Mathiasen et al., 2017), especially the limbic thalamus in rats (Van Groen and Wyss, 1990; 1992) and primates (Baleydier and Mauguiere, 1985). Many of these thalamic nuclei are part of the HD circuit. Specifically, the lateral dorsal nucleus (LDN) and the ATN of the thalamus provide major inputs to the RSC, and layer VI neurons in dysgranular and granular RSC project back to the ATN and LDN (Aggleton, 2014). Moreover, it has been reported that RSC sends excitatory synaptic inputs to the thalamic reticular nucleus (TRN), which may control the gain of sensory inputs and mediate ATN HD cell tuning (Vantomme et al., 2020). These findings provide a biological basis for directional information processing between RSC and the thalamus within the HD circuit.

The thalamic inputs into the RSC have some segregation. ADN of the thalamus, one of the subdivisions of ATN, is also a key component of the HD circuit, and seems to only project to the granular RSC (Van Groen and Wyss, 1990b; Shibata, 1993; Lomi et al., 2021), or very sparsely to dysgranular RSC. Lomi et al. (2021) also reported that the afferents from ventral-lateral part of the anterior thalamus target both dysgranular and granular RSC, suggesting distinct thalamocortical pathways in RSC.

Furthermore, an interesting columnar structure has been found in granular RSC and may be important in regulating thalamic inputs. The module consists of a combination of prominent apical dendritic bundles from layer II pyramidal neurons and thalamo-cortical patchy inputs, which are spatially matched with the dendritic bundles (Wyss et al., 1990). The columnar dendritic bundles were visible early from development in rat pups at P10 (Ichinohe, 2012), prior to HD signal maturation at P12 (Bassett et al., 2017). Modular

computation within granular RSC may help process thalamic inputs (i.e., HD signal) more efficiently.

In summary, the anatomical findings reviewed above show that RSC is connected reciprocally to and interacts with many cortical and subcortical regions (as summarised in **Figure 2-2**). The connectivity of RSC with many brain regions provides the neurobiological basis for its function, such as sensory landmark information processing (possibly via the cortical-RSC connection), spatial and cognitive function (via the RSC-para-hippocampal circuit) and HD computation (via the RSC-thalamic connectivity), as discussed in the next section.

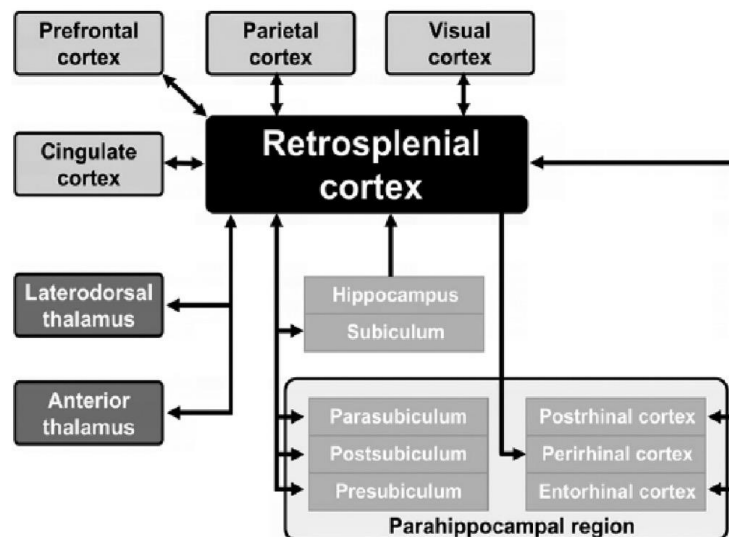


Figure 2-2. Schematics of retrosplenial cortex connectivity. RSC is interconnected with multiple brain regions in the cortex, the hippocampal formation, parahippocampal areas and the thalamus. See the texts for detailed description of the connectivity. Different shadings are for only illustration purpose. Arrows denote connections. Adapted from Mitchell et al., (2018). Also see Figure 7-3 in Chapter 7 for a proposed network that incorporates the current experimental data.

2.1.2 Functional characteristics in spatial navigation

In this section, I review the neuropsychological and neurophysiological evidence that supports a crucial role of RSC in spatial navigation from the following aspects: landmark

processing, reference frame transformation and cognitive mapping. These functional characteristics are the foundation in service of its capacity in maintaining a sense of direction to support a map-based framework.

2.1.2.1 Visual scene and landmark processing

RSC plays a particular role in landmark processing during spatial orientation and navigation. Evidence appears from clinical human studies in which RSC amnesic cases (with compromised Brodmann's area 30 on the right) showed severe orientation deficits: the patients were able to recognise landmarks but unable to locate landmark positions on a map (Takahashi et al., 1997; Suzuki et al., 1998; note extended lesion to the medial parietal lobe). The patients were unable to make use of landmarks to learn new routes and find ways in a familiar environment (see review by Maguire, 2001), suggesting that RSC is critical in helping to retrieve spatial relations from familiar landmarks.

In rats, lesions in the dysgranular RSC impair landmark-based navigation and animals use motor-based strategy instead (Vann and Aggleton, 2005). Similarly, rats with bilateral lesions in RSC fail to use directional cues for directional alternation whereas sequential alternation behaviours are spared (Pothuizen et al., 2008). Interestingly, Hindley et al. (2014) showed that rats with extensive RSC lesions are unable to use distal landmarks to discriminate between two target places for digging. Elduayen and Save (2014) showed that lesioned animals were impaired in path integration in the dark but not in light, suggesting a role of RSC in incorporating visual-dominant information. These results support the contribution of RSC to using environmental landmarks for direction orientation.

Moreover, it is particularly interesting that RSC is active while human subjects perceive landmarks as 'permanent' when they are in view and used for navigation (Auger et al., 2012; Auger and Maguire, 2013). Furthermore, a follow-up study by Auger et al. (2015)

showed that RSC also supports learning of featureless, abstract landmarks. This suggests that RSC also represents cognitive factors in landmark processing rather than the local features: for example, the perceived stability of landmarks. As discussed in **Chapter 1**, this modulates the effectiveness of landmarks in supplying direction information to the spatial localisation system. This point is revisited in HD system later in the chapter.

RSC is part of the broader network involved in visual scene processing: for example, the parahippocampal-RSC-occipital place area, known from research in human brain imaging (Park and Chun, 2009; Epstein and Vass, 2014) and macaque monkeys (Kornblith et al., 2013). Studies have revealed that RSC and parahippocampal place area compute different properties of the visual scene: RSC is involved in integrating similar panoramic scenes whereas the other areas selectively discriminate them (Park and Chun, 2009). The result supports the role of RSC in viewpoint integration, which is related to transforming local view information from an egocentric perspective to an allocentric map framework (Byrne et al., 2007; see **Chapter 1** and below). This point may account for the clinical findings that RSC deficits usually cause impairments in associating visual panoramas with estimated heading (Maguire, 2001).

Of note, landmark processing for orientation has been found in the parietal cortex (Brodmann A31, sometimes not differentiated from RSC in human imaging studies). Baumann and Mattingley (2010) presented human subjects with salient visual landmarks at the end of a corridor in a familiar virtual-reality environment. The parietal cortex was more engaged when subjects associated viewpoint-independent landmarks with different heading directions and suppressed when the facing direction remained the same. The results suggest that recalling landmarks and their associative allocentric directional information recruits the medial parietal cortex, which may be a supplement to RSC functions.

More specifically, neurophysiological studies in rodents demonstrated encoding of landmark information in RSC at the neuronal level. First, RSC is involved in beaconing for orientation in a goal-directed task. In a light-cued T-maze task, RSC neurons increased responsiveness to the light cue signalling the reward location (Vedder et al., 2017). Second, RSC cell activity usually couples with visual landmarks while the animal is actively performing navigational tasks. Fischer et al. (2020) imaged mouse RSC and the afferent axons from V1. They found supralinear responses in RSC neurons when head-fixed mice were actively engaged in a landmark-cued task searching for reward in virtual reality corridors. The responses were greater than the sum of activity when animals were just running or passively viewing the landmarks. The result reveals an integration of visual landmark signals and task information (e.g., whether animal was in an engaged state) in the RSC. Powell et al. (2020) similarly reported that excitatory RSC neuron responses show supralinear integration of visual and locomotion signals, whereas inhibitory RSC neurons are more locomotion-modulated. The visually evoked activity in excitatory neurons is limited to the posterior part of dysgranular RSC, which is anatomically closer to the visual area, suggesting comparable functions of dysgranular RSC and the visual cortex.

The RSC characteristics reported by Powell et al. (2020; also see multimodal responses by RSC neurons to optic flow and head motion signals in Keshavarzi et al., 2021) are in accordance with a multimodal property found in mouse V1: integrating visual information from optic flow and locomotion during spatial navigation (Saleem et al., 2013). Moreover, Mao et al. (2020) recently showed that a subpopulation of RSC cells (12%) displayed landmark-position-locking activity during locomotion in a virtual reality environment, and many cells (35%) selectively represented three vertex locations that were distinguishable in their local visual scene features on a triangular tunnel. The results suggest

that encoding of visual landmarks in RSC is modulated by spatial locations in virtual reality reference frames, comparable to V1 neurons reported by Saleem et al. (2018).

Furthermore, Mao et al. (2020) found that landmark representations were disrupted if only optic flow information was presented to the animal dissociated from its own locomotion, suggesting that RSC landmark encoding depends on an integration of coherent internal idiothetic and external allocentric inputs. Clancy et al. (2019) also suggested that an animal's behavioural state modulates the coupling activity between RSC and the sensory cortices: linear running induced dramatic shifts in RSC neurons, from being locally suppressed to diffused coupling with other sensory areas; whereas V1 neurons became more locally correlated. Therefore, locomotion is important in modulating, or even gating information flow between RSC and other sensory regions (see the current experiment data in **Appendix III**).

These results are in agreement with recent imaging findings that while an animal is running on a ball in virtual reality environments, RSC and associated posterior parietal cortex integrate multimodal sensory information (Minderer et al., 2019) and accumulate visual information (Koay et al., 2019) to facilitate navigation. These results together indicate that sensory responses in the posterior retrosplenial-parietal-visual network are also modulated by primary visual information and self-motion signals during locomotion.

2.1.2.2 Reference frame transformation

As mentioned earlier in **Chapter 1**, integration of inputs from internal-external and local-global coordinates is essential for spatial mapping and orientation. RSC has been believed to be particularly important in transforming egocentric-referenced information (e.g., visual scene, imagery) to the allocentric worlds (e.g., structure, map; see Burgess, 2002; Byrne et al., 2007). A rich body of human imaging studies reported that the most active

responses in RSC are observed when human subjects attempt to orient relative to different viewpoints, and/or changes in their perceived heading relative to a global or local space (see detailed review by Epstein et al., 2017).

Importantly, in a study by Marchette et al. (2014), human subjects learned landmark locations inside two different museum environments in virtual reality and were asked to imagine the viewing direction towards the landmarks. RSC activity showed similar patterns when subjects faced in similar directions or at the similar local places in different contexts of two museums. The result suggests that RSC primarily encodes local directions and environment features. This observation of local mapping may be reminiscent of the flipping BD cells found by Jacob et al., (2017), as described earlier (section 1.5.4; also see section 2.3.3.2). However, care needs to be taken because it was unclear whether the human subjects actually acquired knowledge of the global environment layout and if local information was mapped onto a global reference frame. Moreover, in a different study, when human subjects were making direction judgements by viewing a familiar environment learned through walking, responses relating to global orientation signals were seen in both RSC and thalamic regions (Shine et al., 2016), suggesting a recruitment of the HD system in retrieving familiar directional relations.

Data from single unit recordings also support a role of RSC in switching spatial reference frames for navigation. When animals ran on two identical ‘W’-shaped tracks located at different places in a room, Alexander and Nitz (2015) found that RSC neurons encoded conjunctions of local positions, turning sequences, maze locations within the experiment room and the animal’s head directions. It reflects mapping of egocentric, local cues to allocentric, global spatial representation in RSC. Interestingly, Alexander and Nitz (2017) showed that after extensive training, some RSC neurons showed substantial firing

peaks in their activity, that were periodically corresponding to the animal's trajectories around the edge and corners of a plus maze. The periodic activation at multiple scales (quarter, half, and full route) across sessions suggests that RSC simultaneously encodes local fragmented subspace such as routes and a global structure of the maze.

However, Alexander and Nitz (2017) also reported periodical activity in a ring track placed in the same location as the plus maze. The intriguing pattern casts some doubts on whether the periodic patterns truly emerged from the maze structure, or rather from distal cues around the maze. One interpretation is that 70% of ring track trials were run after the plus maze, leading to a possibility that ring track patterns might be a carry-on effect from the plus maze; and in the rest of the trials, the pattern might have emerged from the non-controlled, familiar cues in the experiment room.

As mentioned in egocentric coding in **Chapter 1**, direct evidence in support of allocentric-egocentric transformation comes from a particular kind of border representation found in RSC, known as the egocentric boundary vector cells (EBCs; see section 1.4.4.2). When environmental boundaries are at a certain bearing and distance relative to the animal itself, a subpopulation of RSC neurons, named egocentric boundary vector cells, become active and encode a vector-based signal (Alexander et al., 2020). Moreover, egocentric border cells were found in RSC that increase firing only when the animal gets near to environmental boundaries, with the boundary-related inputs likely being supplied by MEC (van Wijngaarden et al., 2020). Recently, Vale et al. (2020) showed RSC tuning reminiscent of egocentric goal vector cells when freely moving mice escape to their shelters. The results of egocentric coding in RSC reveal the existence of a transformation between egocentric and allocentric coordinate systems to guide spatial navigation (also see **Chapter 5** for further discussion and how egocentric coding was examined in the current thesis).

The findings reviewed so far suggest that RSC converts the perceived (egocentric) visual scene and landmark information to an allocentric reference frame during navigation. Next, I review studies demonstrating how RSC is involved in cognitive mapping of spatial information.

2.1.2.3 Cognitive mapping

Multiple studies have shown that RSC is importantly involved in mnemonic processing, including accessing information from an established environment schema or a map. When human subjects navigated in a familiar, versus recently learnt campus, the RSC was only engaged in tracking distance in the familiar environment, suggesting a role in retrieving remote spatial knowledge and established spatial relations (Patai et al., 2019). In further support of its role in higher cognitive functions, RSC has been proposed to contribute to multiple forms of spatial learning. Lesion studies in rodents (Aggleton, 2010) highlighted a role of RSC in memory retention and cognitive control (Hindley et al., 2014; Nelson et al., 2014). Likewise, in primates, impaired memory retrieval of positional information of objects was observed following RSC removal, but anterograde memory was unimpaired (Buckley and Mitchell, 2016).

Moreover, as discussed earlier, cognitive factors in landmark processing are encoded by RSC, and effective use of landmarks interacts with mnemonic processes in RSC. Lesion studies showed that rats with RSC lesions failed in making use of distal cues to navigate in Morris water maze (Sutherland et al., 1988; Harker and Whishaw, 2002; Vann and Aggleton, 2004) and showed deficits in a radial arm maze reference memory task (Vann and Aggleton, 2005; Pothuizen et al., 2008; also see an involvement of RSC in spatial memory in Milczarek et al., 2018). Therefore, RSC is required to retrieve a map-like structure for spatial navigation. These findings together support a role of RSC in integrating external landmark information and possibly forming internal knowledge through learning.

The notion that RSC may comprise a map-like structure received support from neurophysiological evidence of a place code in RSC. Mao et al. (2017) imaged RSC when mice locomoted on a treadmill adorned with tactile cues and found encoding of position information. However, it is unclear if these responses are specific to the motor sequences or sensory cue representations associated with running on a treadmill. In addition, Cooper and Mizumori (2001) observed hippocampal place cell remapping following temporally inactivation of RSC, suggesting that mnemonic spatial information is processed by RSC which probably can update the map system.

Smith et al. (2012) similarly reported that RSC neurons develop large, sparse ‘place fields’ around reward-associated locations on a plus maze. The number of place fields substantially increased with the animal’s experience, and unlike focal hippocampal place fields, some RSC fields could cover the whole trajectory on an arm. This leads to the possibility that RSC encodes distinguishable contexts (e.g., rewarded east arm vs. non-rewarded west arm) by reward outcome, rather than precise locations on the maze. Therefore, it remains to be explored whether RSC encodes spatial location specifically in the same way as the hippocampal place cells.

Nevertheless, Mao et al. (2018) showed that the place-like code in RSC was disrupted by bilateral lesions in the hippocampus, providing strong support for a functional link between RSC and the neural basis of the map system (see anatomical link discussed earlier). Similar to the method (i.e., lesioning) of ‘shutting down’ the hippocampus, optogenetic inactivation of hippocampal-RSC efferents led to impairment in contextual memory acquisition (Opalka and Wang, 2020). Furthermore, Opalka et al. (2020) showed that hippocampal ripples activated RSC interneurons during slow-wave sleep and caused a temporary inhibition of RSC. This provides direct evidence for signal mediation from the hippocampal system to RSC, possibly for the purpose of refining the integrated cue

information in RSC by specific entities formed in the hippocampal system (Ranganath and Ritchey, 2012).

2.1.3 Summary: towards a capacity for guiding orientation

To summarise, the reviewed neuroanatomical studies show abundant cortical and subcortical connections of RSC in the rodent brain. The connectivity makes it well-situated as an integrative hub to process internal and external information from different modalities. The connections with many sensory cortical areas may help visual landmark processing; the hippocampal-parahippocampal circuitry would ensure information exchange with the place system; and multiple thalamic nuclei in the thalamus provide a solid biological basis for direction inputs to the RSC (also see section 7.4.2 for a proposed working model).

Visual, self-motion and cognitive inputs all converge to RSC, a multimodal region that also forms part of the HD network. Then the question arises as to how exactly does RSC recruit these faculties to guide spatial orientation? What role the RSC might play during spatial disambiguation, such as in the Jim Marshal incident? How may RSC contribute to supply HD signals to the system for a coherent directional sense? Before we discuss how the current thesis plans to tackle this issue in more specific terms, we need to know fundamentally where the RSC direction signal comes from and how it is generated. Next, let us dive into the head direction system, starting from directional representations found in RSC, then discuss specific principles underlying head direction computation, which are also implemented by RSC neurons.

2.2 Principles of canonical head direction processing

The map system needs a directional framework to function properly (section 1.5). In the preceding section, several lines of evidence support a prominent role of RSC in processing internal and external sources of information for navigation. More importantly, RSC is

specifically involved in head direction processing and forms part of the HD system. How is the head direction processed within the HD system before being incorporated into the map? In this section and the next one, let us consider what is known about head direction processing.

2.2.1 Where is the HD signal?

The basic firing properties of HD cells and a simplified HD circuit have been introduced briefly in **Chapter 1** (section 1.4.2). Here, we zoom into the hierarchy and its components in more details, starting from the top of the circuit: the RSC.

2.2.1.1 Head direction cells in RSC

HD cells in rat RSC were first reported by Chen et al. (1994), displaying unimodal tuning curves and comparable firing properties similar to the HD cells originally discovered in PoS (Taube et al., 1990; **Chapter 1**). Likewise, Cho and Sharp (2001) characterised HD cells in RSC and found that they fire slightly in advance of the actual head direction as an effect of angular head velocity (AHV). For example, if an HD cell anticipates arrival at a northward heading, then the cell is more likely to fire when the head direction is about to reach the exact north. Similar anticipatory properties have been reported by Lozano et al. (2017) in RSC and PoS; and RSC HD signals were found to come ahead of the PoS ones, supporting a hierarchy of signalling in the HD circuit.

Interestingly, neurons that specifically encode AHV were recently found in mouse RSC. This AHV coding was dependent on vestibular systems processed by semi-circular canals (e.g., such as during passive rotations), and the gain of AHV coding increased when optic flow signals were available (Keshavarzi et al., 2021). A significantly higher amount of AHV cells were reported in active exploratory animals provided with visual information, suggesting that AHV neurons may incorporate visual optic flow to improve navigation

accuracy. The authors also reported conjunctive AHV-HD cells in RSC. AHV signals, as we will see later, are important for HD signal generation and updating during locomotion. The results may suggest that HD signal in RSC could also be generated locally, rather than being purely inherited from thalamus.

Apart from a small population of HD cells, a majority of RSC neurons show complex firing profiles (Chen et al., 1994; Alexander and Nitz, 2015; Jacob et al., 2017). Cho and Sharp (2001) also described that RSC neurons are not only modulated by direction but also conjunctively by turning direction, locomotion speed and location. This is consistent with evidence in the preceding section that RSC integrates multiple spatial correlates, and it is possible that cue integration is essential for directional encoding in RSC. The recent discovery of noncanonical RSC directional cells that encode two opposite directions provide evidence in support of this claim (Jacob et al., 2017), as to be revisited later in this chapter.

2.2.1.2 A widely distributed direction code

The unidirectional HD cells have been reported in many areas throughout the rodent limbic system (also known as the Papez' circuit; Papez, 1937), and different regions have different proportions of HD cells (see a detailed review by Taube, 2007). In the main HD circuit, it has been found that 25% of the recorded cells are HD cells in PoS (Taube et al. 1990), with roughly 10% in RSC (Chen et al., 1994; 9% in Jacob et al., 2017; Lozano et al., 2017), 60% in ADN (Taube, 1995; Yoganarasimha et al., 2006); 25% in lateral mammillary nucleus (LMN) (Stackman and Taube, 1998) and 11% in dorsal tegmental nucleus (DTN) in the brain stem (Bassett and Taube, 2001; 14% in Sharp et al., 2001).

Other thalamic nuclei that contain HD cells are, anteroventral thalamus (AVN; 69% in Tsanov et al., 2011; Yoganarasimha et al., 2006), anteromedial thalamus (AMN; 10%, Jankowski et al., 2015), lateral dorsal nuclei (LDN; Mizumori and Williams, 1993), and

nucleus reunions (NRe; 11%, in Jankowski et al., 2014). Additionally, a small population of HD cells have also been reported in other structures involved in spatial cognition, including the medial secondary visual cortex (V2M; Chen et al., 1994), the striatum (Wiener, 1993; Mizumori et al., 2000; Mehlman et al., 2019), medial precentral cortex (PrCM; Mehlman et al., 2019), posterior parietal cortex (Wilber et al., 2014), and a few in the hippocampus (Leutgeb et al., 2000). Recently, HD cells (4%) have also been reported in rat somatosensory cortex (S1; Long and Zhang, 2021). HD cells across regions share highly similar characteristics of tuning curves, albeit some minor differences from one region to another.

It is believed that the cells work together in an interconnected network (the attractor network; Zhang, 1996; see section 2.3.1) within the hierarchical HD circuit. Next, I discuss how HD signals are generated and updated within this hierarchy (**Figure 2-3**; also see **Figure 1-5**).

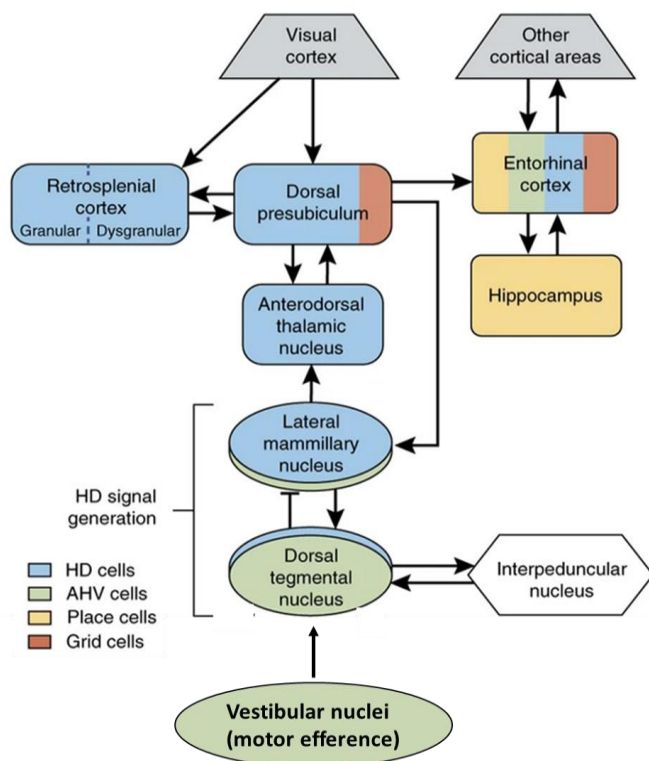


Figure 2-3. Detailed schematics of the head direction circuit. The diagram shows multiple regions that hold HD cells (blue), AHV cells (green), place cells (yellow) and grid cells (orange), as indicated by different colours. The arrows denote anatomical connectivity between these regions. The

canonical HD circuit includes RSC, PoS (dorsal presubiculum), ADN/ATN, LMN, DTN; in which the LMN and DTN form the signal generation circuit, receiving vestibular signals from deeper nuclei; also see description in Chapter 1. The AHV cells are introduced in detail in the section below. Adapted from Cullen and Taube (2017).

2.2.2 Where does the HD signal come from?

Vestibular inputs are vital for HD signal generation (see review by Clark and Taube, 2012), as evident in a large number of lesion studies in the HD circuit. Relevant evidence is visited in this section.

2.2.2.1 Evidence from lesion studies

An extensive body of lesion studies has illustrated the hierarchy of HD signalling, in which the inputs were propagated from the deep thalamic nucleic and travelled upward to cortical regions such as PoS and RSC (Cullen and Taube, 2017; Taube, 2007). For example, blocking components of the vestibular system such as the semicircular canals disrupts HD firing in the ADN (Muir et al., 2009). Valerio and Taube (2016) specifically showed that the horizontal canals, which are sensitive to angular head movements in the horizontal plane, are critical for HD signal formation. Likewise, ADN HD cells lost their direction-specific firing pattern following either permanent or temporary inactivation of vestibular hair cells (Stackman and Taube, 1997; Stackman et al., 2002). These results suggest vestibular signals, carrying head-motion information, are conveyed to HD cells via an ascending stream in the HD circuit.

Specifically, the pathway is delineated in this way: head movement signals in the yaw plane originate from the semicircular canals and the medial vestibular nucleus (MVN), then travel from MVN to the nucleus propositus hypoglossi (NPH). The NPH projects to and receives inputs from the DTN in the midbrain and forms a reciprocal loop with the LMN. The LMN then projects rostrally to the ADN and then PoS and RSC (Winter and Taube, 2014).

Critically, the HD signal is thought to be generated subcortically via the reciprocal connections between the DTN and LMN (Taube et al., 1996). Supportive evidence for this claim comes in three forms. First, retrograde tracing studies showed connectivity within the LMN-DTN circuit (Graf et al., 2002). Second, combined lesion and electrophysiological studies showed that lesions to the DTN-LMN complex tend to eliminate the HD signal in downstream areas. For example, HD cell activity in the ADN was shown to depend on an intact LMN (Blair et al., 1999; Bassett et al., 2007) and largely on DTN (Bassett and Taube, 2001; Bassett et al., 2007). This was further verified by an observation of ADN HD cell drifts, following optogenetic inactivation of DTN-projecting cells in the NPH (Butler et al., 2017).

In contrast, a complementary study showed that PoS HD cells depend on an intact ADN (Goodridge and Taube, 1997), but lesioned PoS or RSC did not disrupt subcortical HD signals in the LMN (Yoder et al., 2015). Lesions in RSC did not abolish the HD signals in the ADN, but the ADN HD cells become less stable even in presence of visual landmarks (Clark et al., 2010). The results further support the hierarchical circuit in which HD signal is propagated into the ADN from the LMN, then further transferred from the ADN to cortical areas including RSC.

2.2.2.2 Angular head velocity as the HD update signal

The AHV signal serves as a major source of vestibular information during head movements. In the rat brain, a high concentration of neurons tuned to AHV has been reported in the deeper vestibular nuclei down the LMN-DTN circuit (see **Figure 2-3**). AHV cells exhibit either positive or negative correlations between the firing rates and angular speed of head movements. In DTN, around 75% of the recorded neurons are AHV-modulated (Bassett and Taube, 2001; 83%, Sharp et al., 2001) and nearly half of neurons in LMN are AHV cells

(44%, Stackman and Taube, 1998). In addition to structures in the vestibular system, AHV encoding has recently been reported in the RSC (Keshavarzi et al., 2021) and the parahippocampal regions (rat MEC, PaS, PrS in Spalla et al., 2021; and mouse MEC in Mallory et al., 2021), further supporting idiothetic cue processing in the HD circuit.

The HD signal is thought to be the computational outcome through path integration, by transforming incremental angular head displacement to head direction during head turning and locomotion (McNaughton et al., 1991; Redish et al., 1996). AHV-modulated HD cells provide direct evidence for AHV inputs into the HD system. A small but significant group of HD cells in the ADN of the thalamus are modulated by an animal's angular head velocity (Taube, 1995). In addition, AHV information in the ADN is propagated downstream from the LMN-DTN circuit. HD cells in the ADN are abolished by bilateral lesions of LMN but not unilateral lesions in LMN (Blair et al., 1999). In contrast, in animals with unilateral lesions in LMN, HD cells in ADN develop AHV-modulated activity similarly to the HD cells in the intact LMN (Blair et al., 1999). This suggests a key role of LMN in maintaining angular head rotational signals and but an indirect role in HD signal generation. Furthermore, Butler et al. (2017) disrupted AHV signals by optogenetically inactivating DTN-projecting cells in the NPH. They consequently saw drifts of ADN HD cells in the dark, as well as some degraded performance in homing behaviours. This result strongly supports a role of AHV signal from deeper vestibular nuclei in driving the thalamic HD signal in the HD circuit.

Computational work points to AHV as an important input for driving the HD signal and updating heading information during path integration (McNaughton et al., 1991). Experimentally, HD cells in some brain regions within the HD circuit show anticipatory firing properties (Blair and Sharp, 1995; Taube and Muller, 1998; Stackman and Taube, 1998). To be more precise, an HD cell anticipates the animal's future head direction and fires

optimally a few tens of milliseconds before animal's head points at the cell's PFD. This period is known as anticipatory time interval (ATI).

Temporal analyses showed that the ATIs for HD cells in each region within the HD circuit vary. It has been found that the HD cells in LMN have a large interval of approximately 70 ms, and they lead that in ATN by about 15-20ms (Blair et al., 1998). The interval was about 49 ms in the ADN (Stackman et al., 2003), 48 ms in RSC, but not evident in PoS (~14ms, not significantly different from 0; Lozano et al., 2017). This stepwise decrease in ATIs observed in the ascending stream of the HD circuit implies that HD cells in the subcortical region may drive the cell firing in cortical regions through AHV inputs (although note that ADN and RSC have similar ATI). This generally supports the HD hierarchy.

Pure head movement signals are not the only source to account for anticipatory firing of thalamic HD cells. It has been shown that passive movements do not abolish, but instead increase ATIs in HD cells in the ADN (Bassett et al., 2005). The result could potentially be explained by modelling work on the network dynamics of HD anticipation. Modelling work by van der Meer et al. (2007) proposed that rather than pure head movement velocity, the HD network can be updated by a high-pass filtered vestibular AHV signal (i.e., ATI) through the medial vestibular nucleus (MVN). Passive and active movements may produce variations in this vestibular adaptation. Moreover, Redish et al. (1996) proposed that following head rotations, ATN leads HD cell activity in the PoS by changing the strength of their interconnections in the network, revealing dynamic characteristics of the system.

Taken together, vestibular signals from the tegmento-mammillary ascending pathway are clearly critical for HD signal generation and for AHV signals to update the system during head movements and locomotion.

2.2.2.3 Evidence from development studies

Development studies reported that the internally generated signals develop from early on, even before eye-opening in rat pups (Bjerknes et al., 2014), suggesting the HD system develops early and rapidly in the rodent brain. HD cells emerge at P12, the earliest among the other types of spatially modulated neurons (place cells, P16; grid cells, P20; see Wills et al., 2010; Langston et al., 2010; see review by Tan et al., 2017).

It was interesting that HD cells appear even before the eye opening of rat pups at around P12, suggesting that at least part of the HD network exists before visual information processing begins. HD cell responses in the ADN of rat pups showed low directional information and were directionally unstable at P13 when the pups were crawling in a large box before eye-opening. However, refined tuning of HD cells appeared in a small box, suggesting that environmental geometric features like corners and boundaries supplied direction information, possibly through internal vestibular system during self-motion (Bassett et al., 2018). The developmental evidence suggests that the directional system develops early and depends on the integration of vestibular signals and other sensory inputs.

In sum, HD cells found in multiple brain regions in the circuit encode accurate directional information. The vestibular system plays a significant role in generating and updating the HD signal during head movements. Next, I discuss another important source of information feeding into the HD system: the visual landmark inputs.

2.2.3 Landmark inputs to HD cells

Although idiothetic motion signals are the major inputs to generate and update HD signal during locomotion, errors can accumulate over a long period of navigation, especially when visual information is inadequate or unstable. For instance, HD cells in the ADN and PoS shifted their PFDs by at least 30° in the dark (Goodridge et al., 1998). Visual inputs have

been believed to recalibrate the HD attractor in order for the system to maintain an accurate orientation bearing (Skaggs et al., 1995). Clearly, landmarks dominate HD cell activity in many cases, as evident in several recording experiments in which established HD cells follow salient cue rotation in the environment and shift their preferred firing direction by an equal amount (Taube et al., 1990; Taube, 1995; Goodridge et al., 1998). For instance, Goodridge and Taube (1995) recorded HD cells in the classic cylinder paradigm in three conditions: first with a single cue card, then cue-removal, and finally 90° rotation. ADN and PoS HD cells first shifted their tuning drastically when the cue was removed, but remarkably, shifted their PFDs to realign with the rotated cue card. Thus, it appears that allothetic inputs from familiar landmarks are capable of overriding the HD signal developed by idiothetic inputs.

Where does the visual landmark information come from? As discussed in section 2.1, RSC is heavily involved in landmark processing and forms part of the HD circuit. Following RSC lesions, ADN HD cells have increased tuning widths, exhibiting more intra-trial drifts and reduced stability following visual landmark cue control (Clark et al., 2010). Furthermore, PoS is another important source of landmark information, and PoS projects directly to the ADN (Van Groen and Wyss, 1990). Although HD cells in the ADN of the thalamus still show directional specificity after bilateral lesions of PoS, the HD cells fail to follow a prominent visual cue during rotation trials (Goodridge and Taube, 1997). This effect suggests that landmark information from PoS provides finer spatial resolution to thalamic HD cells. In addition, Yoder et al. (2015) reported that PoS lesions impair LMN HD cell activity in darkness and disrupted landmark control.

Therefore, visual landmark information is highly likely to travel from PoS/RSC to ADN and LMN (see review by Yoder et al., 2011), and recalibration of HD cells by visual inputs depends on at least an intact and functional cortical-thalamic descending pathway. As

landmark information gets processed in parallel with vestibular inputs in the HD circuit to maintain the HD signal, how do these two sources of information converge in the system for HD signal processing, then maintain a sense of direction?

2.3 How does the directional system help maintain a sense of direction?

The behavioural evidence for spatial orientation (see section 1.3) and the neurophysiological findings (see section 1.5) point out that the system needs direction information for spatial disambiguation. One might wonder - what would HD cells do in ambiguous environments? In this section, I continue discussing the principles implemented by the HD system with a focus on RSC neurons. This then leads to my research topic on whether and how HD signalling in RSC may help resolve directional ambiguity.

As briefly mentioned earlier, the theoretical ring attractor network serves as a powerful model accounting for head direction processing. First, I review the theoretical considerations and then relevant findings in empirical HD cell activity.

2.3.1 The ring attractor model

In the past three decades, the research into the underlying mechanisms of HD cells has taken large strides. A single HD cell, exhibiting a unitary firing peak (i.e., persistent firing that forms a single Gaussian peak), only signifies directional signal within a narrow range of directions of 90° (Taube, 1995; Blair and Sharp, 1995). To encode the whole 360 degrees on the azimuth plane, in an abstract space, the HD cell population has been conceptualised to be arranged in a ring structure: thus all PFDs are homogeneously distributed, by analogy with a compass system (Skaggs et al., 1995; Redish et al., 1996; Zhang, 1996).

On a hypothetical one-dimensional ring structure (**Figure 2-4a**), HD cells are considered to form recurrent connections with their nearby cells so that the dynamics follow

a rule of ‘winner-takes-all’: neighbouring cells with similar PFDs excite each other but inhibit other distant cells with different PFDs. Zhang (1996) provided the first mathematical formulation of the HD model as an attractor network, which maintains a stable activity packet (the ‘bump’; **Figure 2-4b**) that can be shifted without deformation.

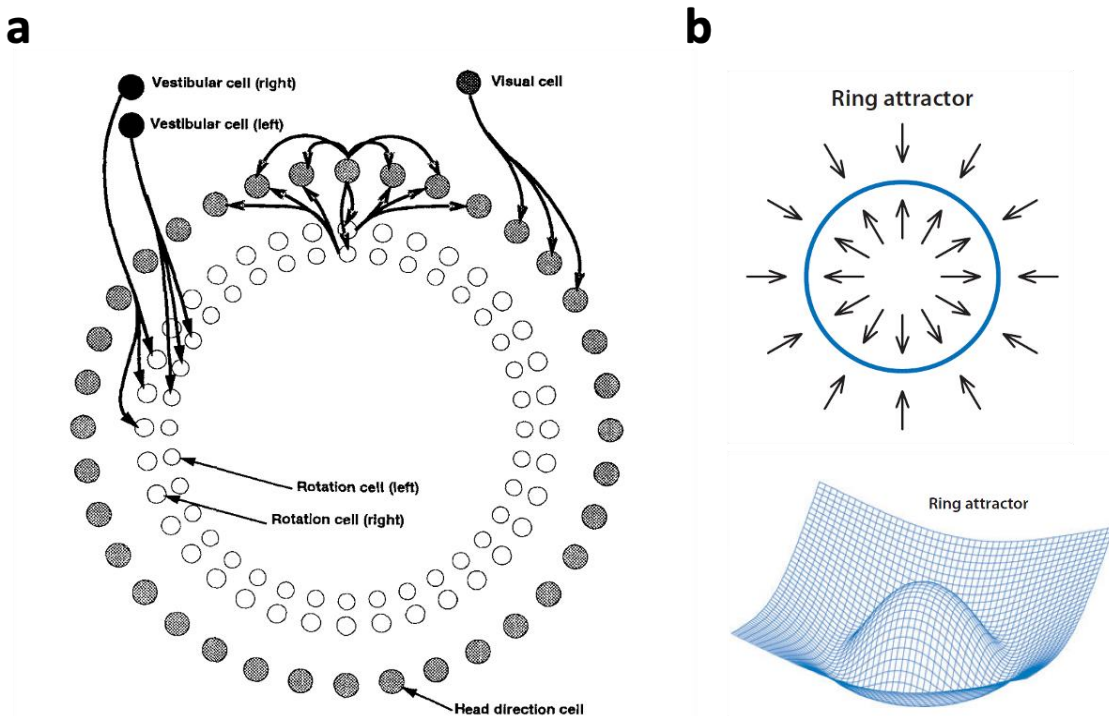


Figure 2-4. Schematics of ring attractor dynamics. **a.** HD cells are arranged in a ring structure by connecting probability to its neighbours. Rotation of the activity packet in the clockwise and counterclockwise directions is controlled by HD cells (the most outer ring layer) and vestibular cells (i.e., angular head velocity cells; inner ring layers with empty dots). As the animal turns its head, vestibular cells receiving clockwise motion signals project to the right of the HD cells; those receiving counterclockwise motion signals project to the left. The ring structure stabilises when there is no motion. The visual cell (possibly in visual areas) helps to correct the accumulated error via landmark inputs. Note that the structure does not reflect the biological organisation in the rat brain. Adapted from Skaggs et al. (1995). **b.** Function of the ring attractor and its schematics. Arrows show how the state of the network changes, and symmetry (arrows equal in opposite directions) indicates a state of no head movements. To be able to move the ‘bump’ on a ring attractor, the connectivity state needs to be changed to asymmetric. Adapted from Knierim and Zhang (2012).

It was believed that the strength of excitation and inhibition is appropriately tuned possibly via AHV signals from head movements (McNaughton et al., 1991) as well as visual inputs (Skaggs et al., 1995), such that the ring exhibits attractor dynamics (see review by McNaughton et al., 2006; Knierim and Zhang, 2012). In this way, the architecture is self-

stabilised when the animal's head is still, and the angular separation in PFDs of different HD cells stays consistent in different environments. When the head moves, both visual inputs and idiothetic inputs decide how the activity bump is shifted, and the strongest input takes control. The animal is thus believed to acquire a coherent directional sense free of dissonance.

The ring attractor network captures several key features of the canonical HD cell population: first, the population of HD cells in the network shows a coherent shift of the activity bump; second, HD cells can update the activity bump position by self-motion cues; and third, HD cells anchor to landmarks, and the activity bump can be controlled by sudden shifts of salient visual cues (Taube et al., 1990; Taube and Burton, 1995; Knierim, 1995). Briefly, the 'bump shift' has been reported in a large number of studies showing that HD cell population behaves cohesively by shifting their PFDs by similar amounts as an ensemble in response to cue rotation (Knierim et al., 1995; Goodridge et al., 1998; Yoganarasimha et al., 2006). As mentioned in **Chapter 1**, a similar cue-control effect on place field orientation has been reported in place cells (Knierim et al., 1995; Knierim et al., 1998; Jeffery, 1998). The finding of coupled activity of place cell and HD cells further supported interconnected structures of the network (Yoganarasimha and Knierim, 2005).

Several models have been proposed to capture the characteristics of the attractor dynamics of the HD cell population. For example, the recurrent network dynamics are believed to be updated by self-motion (i.e., idiothetic) inputs (McNaughton et al., 1991), angular head velocity and head turning (Sharp et al., 2001), interaction between idiothetic inputs and the learned input from external landmarks (Knierim et al., 1995), and connections with landmark information via an experience-dependent plasticity change (Jeffery et al.,

2016; Page and Jeffery, 2018). The latter two theoretical constructs were elaborated in the next section.

The conceptualised ring attractor network has been the most plausible and prominent theory underling HD signal processing (Skaggs et al., 1995; Zhang, 1996). Although still a hypothetical theory in the mammalian brain with no biological evidence supporting a ring topographical organisation, the model has received strong support by empirical findings, as we have seen in the AHV section, and more to be discussed in the next section. Interestingly, the circular anatomical arrangements have been found in *Drosophila*, its ellipsoid body encodes the heading of flies, matching strikingly with the hypothesised ring attractors (Seelig and Jayaraman, 2015; see Hulse and Jayaraman, 2020 for a thorough review of a directional system in the fly).

Furthermore, experimental recordings of offline HD cells in mice provide evidence in support of an intrinsic attractor dynamic. Peyrache et al. (2015) co-recorded HD cell ensembles from mouse ADN and PoS during sleep. The temporal correlation structure of HD cell populations in both regions is preserved during sleep and waking: that is, HD cells with similar PFDs tend to fire at a similar time, whereas the pairs with more separate PFDs are less correlated (Peyrache et al., 2015). This finding strongly suggests that the HD signal is internally generated and persists during the immobile period. Furthermore, adopting an unsupervised learning algorithm, a recent model showed that responses of these HD cells tend to cluster on a one-dimensional ring attractor manifold (Chaudhuri et al., 2019).

To summarise, the attractor network theory has been a powerful theoretical conceptualisation of the HD network structure. It has provided useful predictions about the mechanisms underlying HD signal processing.

2.3.2 Environmental sensory reset of the HD signal

As illustrated in the attractor model, the strongest inputs into the network exert control over the cells' encoding of direction. Surrounding environments are usually complex and comprise multiple cues. Then, will environment landmarks always take over HD cell activity (see section 2.2.3)? What would happen if allothetic cues conflict with idiothetic cues?

2.3.2.1 *Allothetic and idiothetic cue integration*

McNaughton et al., (1991) pointed out that landmarks may only develop saliency if they have been experienced as useful in specifying directions and mapped with the inertial signals through path integration. This hypothesis has received support from several studies, as partially shown in findings in place cell activity (see section 1.5.1; Jeffery, 1998). HD cells similarly prioritise using idiothetic inputs when landmarks are perceived as 'nonstable' (Knierim et al., 1995) and in novel environments (Taube and Burton, 1995). This reveals that environment cue control depends primarily on the animal's experience.

To be more precise, the effectiveness of landmark control over HD cell activity largely depends on an animal's experience in two ways: first, the extent to which the animal perceives an incoherence or conflict between the visual and vestibular inputs; and second, its mnemonic or learning experiences, suggesting involvement of learning related dynamics. The latter point is elaborated in the next subsection (2.3.2.2). For example, to create a conflict between an experienced directional sense and a pre-registered (learned) directional sense, Taube and Burton (1995) adopted a dual-chamber experiment. In their experiment (**Figure 2-5**), HD cells were first recorded when the rat was in a 'familiar' cylinder and then get connected to a 'novel' rectangular chamber via a passageway. The animal freely walked through the alleyway when the door was open and could maintain a consistent directional bearing via path integration. As the doorway was closed, the animal had no knowledge of the

fact that the cue card in the cylinder was rotated 90°. The HD cells subsequently shifted the PFDs to similar amounts of rotation when it returned to cylinder after rotation. Then, as the rat walked back to the ‘now-familiar’ rectangular box, HD cells returned to their original registered PFDs. The cells showed mixed responses when the rat returned to the cylinder: this was probably because the cylinder visual cue was now less ‘trustworthy’ to the animal. The results suggest that when an animal encounters inconsistency or errors in perceived heading direction in a familiar environment, more reliable familiar landmarks take over the cell’s activity and reset the HD attractor. The findings also supported that local landmarks are learned and associated to the global HD signal.

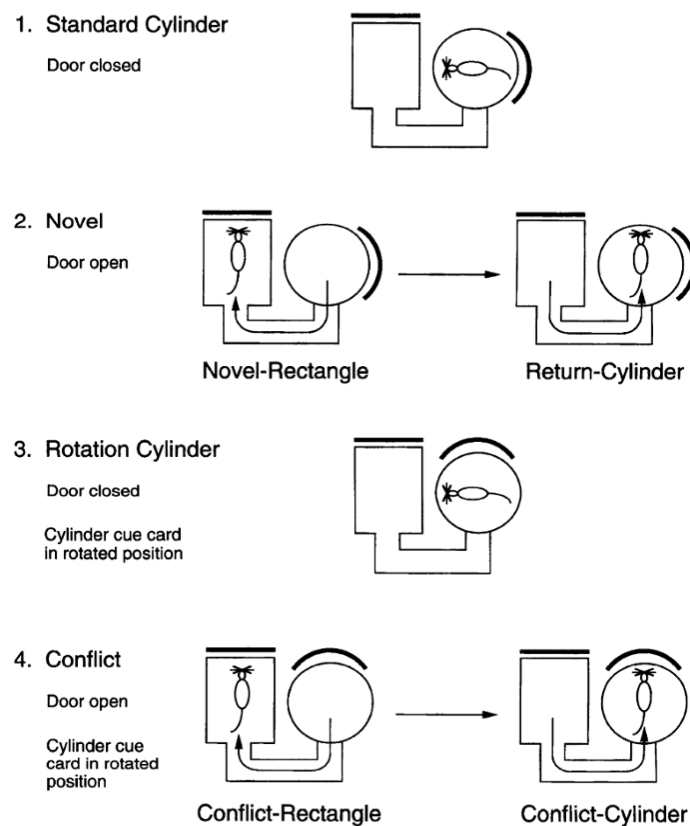


Figure 2-5. The dual-chamber experiment. The dual-chamber apparatus consists of a cylinder and a rectangle chamber, connected with an alleyway through doors. Thick bold lines indicate the cue card in the apparatus. Repositioning of the cue card indicates cue rotation. The four recording sessions are shown sequentially. The orientation of the rat denotes example HD cell activity, as it changes in different experimental sessions. See the text for details of the experiment. Adapted from Taube and Burton (1995).

As mentioned in **Chapter 1** (section 1.5.1.2), local-global reference frames of landmarks also coordinate the effect of cue control. Zugaro et al. (2000) adopted double-cue rotation paradigm by rotating local proximal cues (cue card within the cylinder) and global cues (distal ones: floor plus the cue card on the wall of a cylinder), either together, or separately in various combinations (45° , 90° , or 180°) in the presence of the animal. Regardless of the condition, ATN and PoS HD cells followed the rotation of global cues for 90% of the time with 10% incomplete control. This indicates that distal visual cue control dominates over proximal cues, and an under-rotation by HD cells may be due to an influence of conflicting idiothetic cues and visual cues.

In addition, Zugaro et al. (2001) also showed that ADN HD cells only followed rotation of a group of objects if they served as background cues inside a cylinder enclosure, but not when the enclosure was removed (thus the objects become proximal local cues). Similar preference of distal landmark over proximal cues by HD cells has been reported by Yoganarasimha et al. (2006), in which all HD cells coherently shifted the firing direction by similar amount equal to the distal cue rotations. As mentioned earlier, distant landmarks serve as more stable directional reference because they can be dissociated from animal's positions and viewing perspectives, producing less parallax error (Gallistel, 1990). Thus, animals might prefer to rely on distal landmarks for orientation.

Other factors such as conflict size should also be taken into account. Knierim et al. (1998) described an interesting phenomenon of HD activity drift, which could be reset accurately by landmarks within a specific 45° -window. If the apparatus was quickly rotated 45° , the tuning curves of HD cells and place cells reliably followed the rotation for 45° . In contrast, in only half of the experiment sessions, the cells followed when the apparatus was rotated 180° . The result suggests the capacity of landmark control is mediated by the effect of conflict size. In addition, in successive light-dark-light sessions, HD cell showed drifts during

the middle darkness trial, but the subsequent light trial could normally correctly reset the cell's PFD to original only the drift was small. This suggests a dominant effect by visual inputs to overcome a slow drift in the system.

Comparable findings regarding the conflict size were reported in RSC HD cells. Knight et al. (2014) created a cue-conflict scenario for rats: following an initial environmental cue, animals were presented with a second light cue at a different position on the wall of a large arena. The cue positions varied with different angles, to deliver a conflict between an established sense of direction registered with the initial cue and the shifted light. They observed that RSC HD cells reliably followed the light cue as the inter-cue angle increased, reaching a peak at 120°, then under-rotation occurred beyond 120°. This may suggest an effect of conflict size in landmark control over HD cells, however, experience was a confounding factor because the conflicts increased over days. Moreover, it should be noted that undershoot of HD cell activity occurred following cue rotation intermediate with animal's exposure experiences, and HD cells recorded from naïve animals tended to follow the cue more accurately. This leads to my second point: efficacy of landmark control appears to depend on learning experience and cognitive factors, as discussed below.

2.3.2.2 Experience-based cue integration

As reviewed earlier, landmarks appear to exert control over HD cell if a stable mapping between the external landmark and internal directional references has been established (Knierim et al., 1995). Goodridge et al. (1998) demonstrated prominent cue control within eight minutes when the animal is exposed to a novel environment adorned with a single cue card, whereas degraded cue control is observed if the exposure is too short such as less than three minutes. The result suggests a cue learning process in HD cells.

Interestingly, Dudchenko and Zinyuk (2005) recorded HD cells in a four-room apparatus where the landmarks within each room were distinguishable. In the familiarisation phase, HD cells developed association with landmarks in two of the diagonal rooms separately. Then in the test phase, as the animal walked freely between the four rooms, in less experienced animals, the pre-registered PFDs were maintained from the 1st familiar to a novel room and shifted back to the 2nd familiar room, indicating cue learning and interaction with path integration. However, as the animal become more familiar with the connected four-room apparatus, HD cells displayed homogeneous PFDs in all four rooms. The findings suggest learning of the environment layout and cue weighting processes occurred in experienced animals, and they might have treated the apparatus as a global space after learning.

This interpretation to some extent is supported by a recent finding that place cells display a unique place code as animal learn the connectivity between four visually-identical rooms. Instead of showing place field repetition in each sub-compartment, hippocampal place cells showed a global firing pattern in the connected four-room maze, indicating disambiguation between subspaces, possibly by a global directional signal as supplied by distal room cues (Duvelle, Grieves, et al., 2021).

Importantly, acquiring the knowledge about visual landmarks reflects potential cognitive processes, which probably involve learning and mnemonic processing (Knierim et al., 1995; Samsonovich and McNaughton, 1997; Jeffery and O’Keefe, 1999; Knierim, 2002; Jeffery et al., 2016; Page and Jeffery, 2018). That is to say, the HD system may learn or ‘memorise’ how environment cues specify direction information and consequently tune the synaptic connection between HD cells and the inputs through long term potentiation, forming prolonging changes in the synapse conductance (i.e., level of change in the postsynaptic

membrane potential), as the result of association between pre- and postsynaptic activity (Hebb, 1949; also see Jeffery, 1997).

This cognitive aspect of learning landmark inputs by the HD system has been delineated in recent modelling work. Specifically, it has been proposed that the connectivity weights between the feedforward connections from the visual inputs to the HD attractor are modulated by learned salient environmental cues on a basis of experience (Jeffery et al., 2016; Page and Jeffery, 2018). Thus, the HD network achieves an ‘optimal’ choice by combining self-motion, visual landmark inputs and knowledge of the landmark stability, such as seen in the finding of Knight et al. (2014). This point is particularly relevant to the current experiments and revisited in **Chapter 7**.

Interestingly, recent findings from the *Drosophila* HD system provide strong support for weighted cue integration in the HD system. Ring neurons (i.e., the tangential neurons) in the fly ellipsoid body were found to convey visual landmark information to the HD system in the central complex. More remarkably, the connectivity between the mapping of landmark and cell packet could be altered through physical experiences, in which a visual cue was rotated 180°. The experiences of visual landmark shift not only led to remapping of the activity packet but also changed the synaptic weights (Fisher et al., 2019).

Likewise, Kim et al. (2019) elegantly induced a similar effect of shifting the cell packet using optogenetics, mimicking an effect of visual landmark shift, and observed a global remapping of the compass due to Hebbian plasticity change between the co-active ring-compass neurons. The experiments of cue control and integration of HD cells in flies provide solid evidence that mapping of landmark information onto the HD network involves changes in plasticity in sensory processing. Such change can be combined with established

attractor dynamics to reconcile flexibly to achieve a coherent sense of direction. The findings are in concordance with the findings in rodents and theoretical predictions.

In summary, environmental cues are useful in the sense that they probably prevent cumulative errors and drifts in representing orientation. Learned landmarks can recalibrate the HD system to a previous registration or re-anchoring in a familiar environment. However, the effectiveness of the cue largely depends on the animal's prior experience and how the external cues interact with internal self-motion inputs when the animal experiences a conflict. The conflict size and knowledge of landmarks also influences the pre-registered sense of direction in a flexible manner.

2.3.3 How may the HD system resolve directional ambiguity?

Given that the HD system may incorporate environment cues in a dynamic way, how do HD cells respond to directional ambiguity? Turning back to the Jim Marshall's wrong-way-wrong incident (section 1.1), how does the HD system function in visually ambiguous environments?

2.3.3.1 A global HD signal in multicompartiment environments

As shown earlier, Dudchenko and Zinyuk (2005) reported that when several subspaces are experienced more as connected (i.e., a whole global space), HD cells exhibited consistent firing across subspaces, indicating encoding of a global directional reference, rather than the following of local distinguishable landmarks in each compartment. Similarly, repetition of place field depends on directional orientation (section 1.5.3; Grieves et al., 2016; Harland et al., 2017). The HD signal in LMN forms a coherent global signal in the radial four-room apparatus that is passed on to the hippocampal place cells. Recently, using the same parallel-radial apparatus, the global HD signal has been confirmed in MEC and subiculum HD cells: regardless of the parallel or radial version of the maze, unidirectional HD cells showed

homogeneous PFDs in all four rooms without prominent shifts between subspaces (Smith et al., 2021).

More relevant to the current experiments, in the two-compartmented environment in the study by Jacob et al. (2017), when the animal walked between the two connected, odour-distinguishable but visually similar sub-compartments (**Figure 1-10**), the canonical HD cells recorded from the ADN, PoS and RSC displayed a coherent unitary firing peak between the two sub-compartments without any shift in their PFDs. This indicates that the canonical HD cells in the HD circuit encode a global directional signal by displaying a unidirectional, single peak in the tuning curve.

However, as mentioned earlier (section 1.5.4), what is intriguing is that a subset of simultaneously recorded neurons in RSC displayed local mapping of opposite directions (Jacob et al., 2017). Let us take a closer look at this issue below.

2.3.3.2 Encoding two directions with one cell: an enigma

To reiterate, in the experiment of Jacob et al., (2017), rats freely foraged in a visually ambiguous environment: a square box that consists of two visually identical rectangular sub-compartments connected with a central doorway (referred to as the 2-box thereafter; **Figure 1-10**; also see **Chapter 4**). Each sub-compartment is adorned with one cue card and has onefold symmetry. Each sub-compartment is arranged in 180° rotation to the other: thus, together they have a twofold symmetry. In addition, the two sub-compartments are scented with discriminable odour cues to help the animal distinguish one box from another.

Specifically, Jacob et al. (2017) found that some cells in the dysgranular RSC encode two opposite directions while the animal travelled in the 2-box. The cells showed bimodal tuning activity, with their PFDs of 180° apart and thus were named bidirectional (BD) cells. 11% of cells recorded in the RSC were classified as BD cells, and these were recorded almost

exclusively from dysgranular RSC. The BD cell population was subdivided into subgroups based on the firing pattern within each single sub-compartment of the 2-box. Between-compartment BD cells (40%) exhibited unimodal tuning curves in single boxes, and remarkably flipped the PFDs as the animal stepped from one box to another through the central doorway. In contrast, the second group, within-compartment BD cells (60%) maintained bimodal tuning activity even inside the single boxes, with a slightly asymmetrical shape of the tuning curves between boxes, but with 180° offset in the bearing between two peaks.

However, the underlying mechanism of bidirectionality is extremely intriguing. This type of neurons has only been reported in RSC but not the co-recorded ADN and PoS in Jacob et al. (2017). Considering a special role that RSC plays in landmark processing (section 2.1.2.1), Page and Jeffery (2018) hypothesised that these two groups of BD-pattern cells reflect an interaction of local direction as specified by landmarks and a global direction as signalled by the canonical HD network. It was hypothesised that the noncanonical cells may function to gate and map the landmark information onto the HD system by linking the perceptual views to an established global directional reference. This theoretical mechanism needs experimental validation, and is one of the motivations for the current study.

Moreover, in addition to the RSC BD pattern, a subgroup of neurons in the subiculum and MEC have also been found by others that displayed bi-directional tuning in certain environment conditions. In a study by Olson et al. (2017), rats foraged on a complex maze (a triple-T shape) with multiple sub-routes. The whole apparatus has a mirror symmetry design. A group of subicular neurons encoded two opposite directional headings along any path segments on the maze. However, it is unclear whether movement signals or running speed may drive the pattern (i.e., more egocentric like) and if the cell would continue firing in

motionless state, like HD cells (allocentric). Nevertheless, both cell types share some intriguing similarities: the BD pattern persisted in the dark and was lost in an open arena, although this is based on preliminary results from Jacob et al., (2017). This leads to the question of whether a 180° bidirectional coding is a built-in characteristic of the brain, possibly to allow for reversing routes? Alternatively, both cell types might emerge from the twofold symmetric environment structure.

Additionally, in mouse PaS/MEC, Kornienko et al. (2018) reported a small number of visually driven directional cells with bidirectional tuning curves in a square box adorned with one stable landmark and an orienting cue alternating in two positions (one occupies the full-length of the ‘North’ wall; and the other one occupying half of the ‘West’ wall). Some cells showed two peaks in their tuning curves and some had a 90° between-peak offset and some showed 180° offset, possibly due to the arrangement of visual cues. Notably, these visually driven directional cells do not behave coherently, and only a few were theta-modulated, whereas all canonical HD cells were theta-modulated. It is believed that these new types of cells are outside the HD attractor and controlled mainly by visual landmarks.

Would these visually driven cells relate to RSC BD cells? One possibility is that, these cells are the downstream of RSC BD cells, because PaS/MEC receives direct input from the RSC (Czajkowski et al., 2013; Koganezawa et al., 2015; van Wijngaarden et al., 2020). This interpretation assumes that visual landmark inputs might be processed in the RSC as the upstream site (also see discussion in section 7.4.2), echoing with the hypothesis that landmark information is gated via RSC BD cells into the HD system in an integrative manner (Page and Jeffery, 2018; section 7.3.1), as to be examined further in the current thesis.

2.4 The current thesis

So far, the directional system in the brain is considered as a nexus between sensory and cognitive representations, involving both low-level, bottom-up, and high-order, top-down mental operations. Hence it can be used as a proxy to investigate how different sources of cues are integrated into the system to establish a coherent directional sense.

Following this logic, RSC is of research interests because it sits in an anatomical and functional position for both bottom-up and top-down information processing, as well as for egocentric-allocentric transformation. More importantly, RSC forms part of the canonical HD circuit for encoding a global direction signal. Recent findings of local direction mapping are intriguing, pointing towards a missing link in direction processing: how does the local, perceptual, and egocentric information get translated into a directional signal and linked to the global, cognitive, allocentric spatial framework? The formation of the noncanonical firing pattern requires further experimental investigation in the current study.

2.4.1 Hypotheses

To perform a detailed investigation into the properties of RSC neurons, and to figure out what drives the symmetric firing pattern, the current study examined five hypotheses, as listed below. The subpopulation of neurons showing a BD firing pattern as reported by Jacob et al. (2017) is referred to as ‘the RSC BD cells’ below.

Hypothesis 1

There is an intrinsic propensity for the RSC BD cells to express directional tuning curves that are 180° apart.

This hypothesis was mainly derived from the observation by Jacob et al. (2017).

Additionally, the subiculum (Olson et al., 2017) and MEC (Kornienko et al., 2018) neurons

also showed a twofold symmetry in the cell's directional tuning. Since these areas all form part of the HD circuit, then the question arises as to whether a twofold pattern is a built-in characteristic of the system? If intrinsic, the bi-directional pattern should persist in a simple open field (i.e., onefold symmetry). If not, then, what aspect of the environment could produce the atypical directional firing pattern?

Hypothesis 2

There is a fundamental relationship between environment symmetry order and the tuning curve pattern of the RSC BD cells.

Based on the preliminary result reported by Jacob et al. (2017) that the BD pattern was absent in a square box, as well as the fact that the retrosplenial BD pattern has not been reported in other types of environment, the BD pattern is unlikely to be intrinsic but arises from the environment. The 2-box has a twofold-symmetrical design and comprises polarising landmark arrays that are 180° apart. The landmark inputs are hypothesised to be transformed into the canonical HD system by the RSC cells (Jacob et al., 2017; Page and Jeffery, 2018). If the twofold symmetric environment drives firing symmetry in these cells, as the symmetry order changes (i.e., landmark arrays are in different angular offsets), the firing pattern of the cells may change accordingly.

Moreover, this hypothesis has also been inspired by the modelling work, which predicted that the RSC cell activity can form a trifold firing pattern with peaks that are 120° apart in a three-compartment environment (Page and Jeffery, 2018). However, the model also suggested that the firing symmetry would deform if the order exceeds a threshold, because of wide tuning widths of multiple peaks (see section 7.3.2). Thus, the current experiments aimed to test whether the symmetry is present in a fourfold symmetric environment.

Hypothesis 3

The egocentric boundary vector cells show multidirectional HD tuning due to egocentric sampling.

Briefly, as mentioned earlier (section 1.4.4.2), vectorial encoding of egocentric boundaries has been reported in RSC (Alexander et al., 2020). These cells (EBCs) respond to boundaries located at a given distance and direction from the animal's direction of travel in an egocentric reference frame. The authors observed that the HD tuning of some retrosplenial EBCs exhibited a fourfold pattern in a square box, showing four peaks aligning with the boundary directions of the box (Alexander et al., 2020). Accordingly, it is important to test whether the EBCs display a bidirectional firing pattern in the 2-box due to their egocentric coding of boundaries. This hypothesis was tested with a simulated EBC dataset in **Chapter 5**.

Hypothesis 4

The RSC BD cells are intrinsically egocentric, encoding egocentric boundary relationships.

A follow-up hypothesis appeared from speculations by Alexander et al. (2020), the authors suggested that egocentric coding in RSC might account for the bidirectional firing pattern through encoding of the environment boundaries. Therefore, it is important to investigate whether the recorded RSC BD cells show any egocentric boundary vector tuning, hence Hypothesis 4. Note that Hypothesis 3 focused on the EBC property *per se*, while Hypothesis 4 focused on properties of RSC BD cells. A detailed introduction of Hypothesis 3 and 4 can be found in **Chapter 5**.

Hypothesis 5

The RSC BD cells are a distinct subclass of neurons from HD cells.

An interesting finding in Jacob et al. (2017) was that local directional tuning was found exclusively in the dysgranular sub-region of RSC, whereas the classic HD cells were found in both dysgranular and granular RSC. This was also examined in the current dataset. To investigate whether the RSC cells and the canonical HD cells belong to the same or different neuronal subclasses. A comparison of their electrophysiological characteristics has been performed.

2.4.2 An overview of experiments

In the final section, the flow of the experiment design is summarised briefly. To test the proposed Hypotheses 1 and 2, I explored the cell's activity in environments having different levels of symmetry. For instance, a circular arena adorned with a single cue card or surrounded by multiple distal cues was considered as having onefold symmetry. The 2-box with 180° rotational symmetry and two opposite visual cue cards, was considered as having twofold symmetry. A novel 4-box was a four-connected-box with 90° rotational symmetry a central doorway and four visually identical boxes, and it was considered as having fourfold symmetry. Directional encoding of the RSC cells recorded in these environments was presented in **Chapter 4**.

Hypothesis 3 and Hypothesis 4 were tested by a series of extended analyses in **Chapter 5**, in which I attempt to examine two different but related questions: whether (simulated) EBCs display symmetric HD tuning in the current experimental setups, and whether the recorded RSC cells are EBCs and encode egocentric boundary vectors.

Hypothesis 5 was examined in **Chapter 6**, in which I compared the anatomical and electrophysiological characteristics of the directional cells in RSC.

It is hoped that, by conducting a series of experiments and several in-depth analyses, the current thesis uncovers the formation of the atypical directional pattern of RSC neurons, enumerates the underlying mechanisms of direction signal processing within RSC. Thus, the overall findings may provide insights into the role of RSC in HD computation, landmark learning and cognitive mapping in service of resolving spatial ambiguity in complex environments.

CHAPTER 3

CHAPTER 3 METHODS

To study the neural representation of head direction at a single-neuron level in the rat brain, a chronic electrophysiological method was adopted to extracellularly record single-units in awake and freely moving rats foraging in different types of apparatus. In this chapter, I introduce the general recording procedures, surgical procedures for implants, experimental setups, and the basics of neural activity analyses. Detailed descriptions of the experiments and analyses can be found in the results chapters.

3.1 Animals

All animals were adult male Lister Hooded rats (Charles River UK, Margate). They were individually housed in a temperature ($22\pm2^{\circ}\text{C}$) and humidity-controlled ($55\pm10\%$) holding room with a 12-hour light-dark cycle, with 1h of simulated dusk/dawn. A hanging hammock or nesting box was provided as enrichment. Animals received an implant surgery at a weight range between 350g-550g. Animals had free access to food and water during a seven-day recovery period after the surgery, then they were put on a mild food restriction diet (to 90% of free-feeding weight) throughout the experiment period. All procedures were carried out in compliance with the Animals (Scientific Procedures) Act, 1986, United Kingdom and the European Communities Council Directive of 24 November 1986 (86/609/EEC) legislation for use and maintenance of laboratory animals.

3.2 Electrophysiology single-unit recordings

3.2.1 Workflow

As shown in **Figure 3-1**, before the implant surgery, animals were handled by the experimenter on the daily basis for at least a week and habituated to single housing for at least one day. Then, after a full recovery from the surgery, daily screening sessions

(sometimes twice/day) were carried out, and the experiments started if single units were detected. It was planned to sample new cells for every recording session on different days; therefore, the tetrodes were lowered after every complete recording session or if no cell activity was detected.

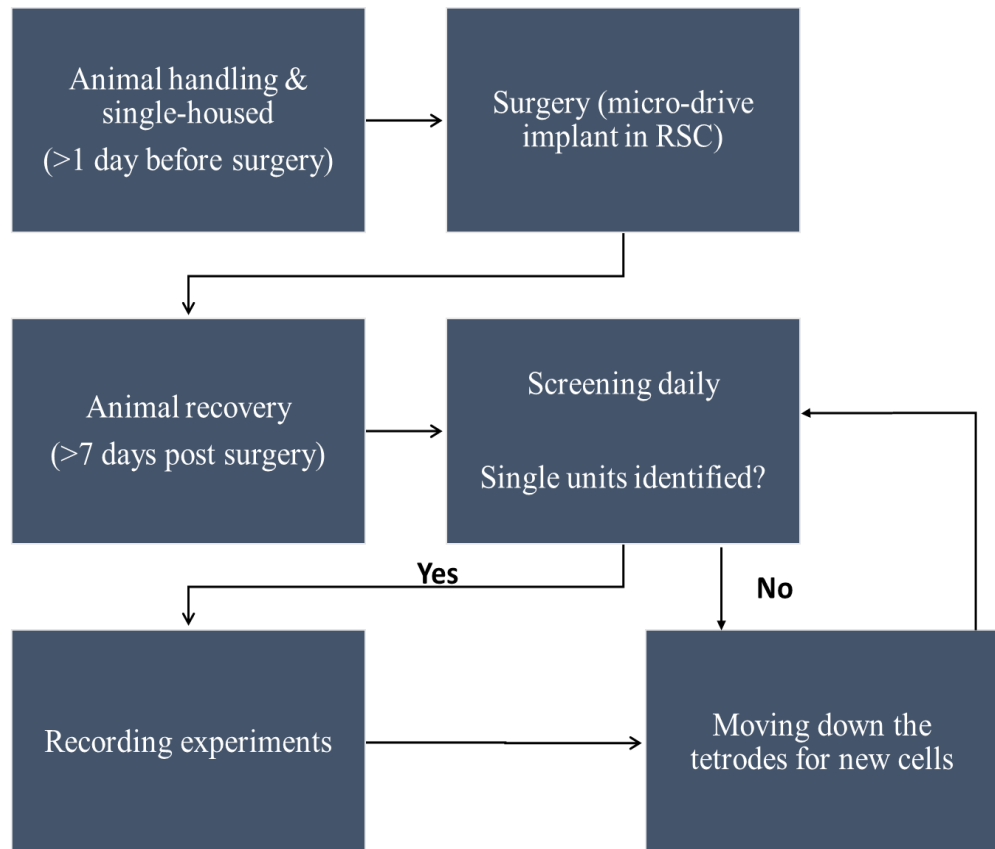


Figure 3-1. Workflow of recordings. The flow chart shows the general workflow of recording procedures and the timeline, from the surgery preparation to the experiments. Normally, it took at least 3-4 days of screening before the experiments.

3.2.2 Electrodes and microdrives

Movable microwires were inserted into the brain to direct electrical voltage changes induced by action potentials of cells. Recordings were made via a microdrive (Axona Ltd, St Albans, UK) attached with four tetrodes (16-channels) or 8 tetrodes (32-channels) loaded in a microdrive cannula connected to a moveable screw allowing tetrode advancements. Each tetrode consists of four twisted 25- μm polyimide-coated platinum-iridium (90%:10%) wires

(California Fine Wire, CA, USA). All tetrodes were cut to proper length (~5 mm) using fine scissors to obtain shining tips at the end the tetrodes (**Figure 3-2**). To optimise signal detection to prevent mechanical noise (e.g., eating or grooming), the electrode tips were gold plated (NanoZ, Neuralinx, USA) on the same day of the surgery to lower the wire impedance at around 200-220 kΩ.

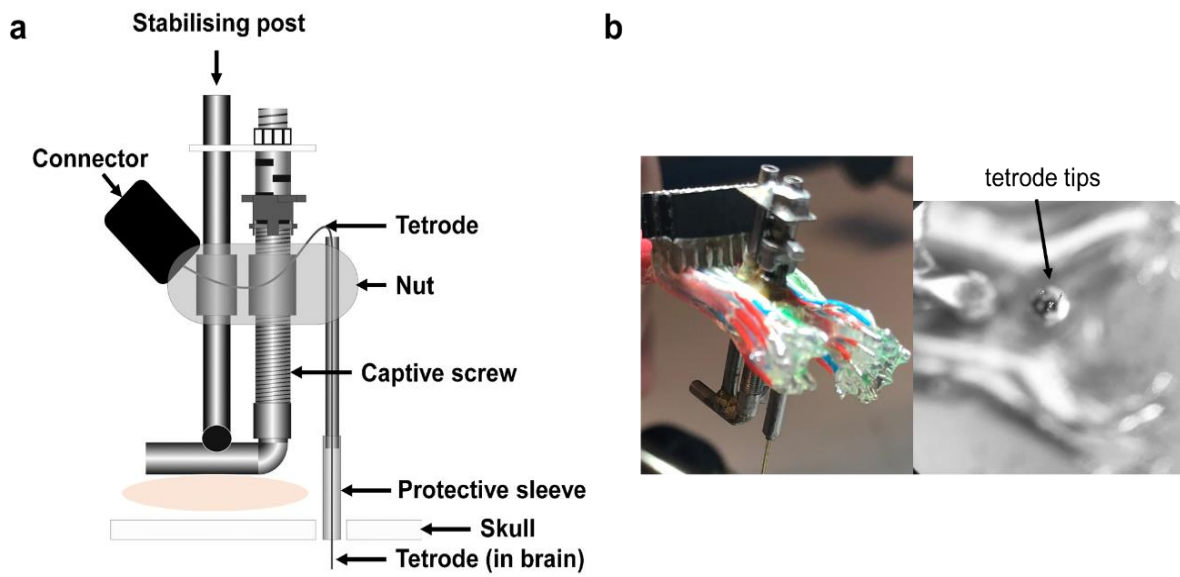


Figure 3-2. The Axona microdrive. a. Schematic of the construction of an Axona microdrive; Adapted from Jeffery et al. (2018). b. Images of a wired micro-drive (32 channels) and the shining tips of tetrodes are shown under the microscopy. Photo taken by the author.

3.2.3 Surgical procedures

Animals were handled by the experimenter daily and transferred to a larger transparent cage for single-housing at least 24 hours before surgeries. Enrichment items (e.g., nesting box, toys, wooden biting bars or balls) were provided. Each rat received chronic implantation surgery of one microdrive to either left or right hemisphere.

In preparation for surgery, all required surgical material and tools were autoclaved and the theatre surfaces were wiped with ethanol to create highly sterile conditions. The head fur of the animal was shaved, and iodine applied on the top surface of the head. The animal

was subcutaneously injected with an analgesic solution (0.2ml of Carprofen, 0.1ml/100g, Norbrook Laboratories, UK) mixed in a sterile saline solution (2ml, 0.9%). Under a delivery of isoflurane (3% in 2L/min oxygen) through the anaesthetic mask, the animal's head was fixed on the stereotaxic frame (Kopf David Kopf Instruments, CA) by two ear bars and a bite bar. The animal's body temperature was kept stable at 37°C by a heating pad throughout the surgery. The eyes were kept moisturised with carbomer (Viscotears, Novartis Pharmaceuticals Ltd.). After an incision was created in the midline through the skin covering the skull, 4-6 curved haemostatic forceps, covered with sterilised Vaseline at the tips, were used to grip the inner skin layer to expose the Bregma and Lambda sites on the skull (**Figure 3-3**, left). The height of two sites were checked to be equal before taking the implant coordinates (the median of all animals: AP: -5.5; ML: ±0.83; DV: 0.5).

Next, at least six holes were created using a small drill bit, and jeweller's screws were inserted into each of the holes (**Figure 3-3**, right). One of the screws contacted the dura was soldered with a wire that served as the ground wire, and the others were for the purpose of anchoring the dental cement. After applying the first layer of cement (Super-bond, C&B, Japan), an entry craniotomy at the marked implantation coordinates was created using drill bits and trephine to expose the dura. The dura was removed carefully using a fine needle (30 gauge), and caution was taken to avoid bleeding from the central sinus. With a clear view of the craniotomy, the electrodes were lowered into the brain to a depth of 0.5 mm. The guiding (outer) cannula was pulled down to cover the remaining electrodes and sit on the skull surface, covered with Vaseline. Final layers of dental cement were applied to fix the microdrive to the skull. At least 24 hours after the surgery, the meloxicam (15mg/ml, 0.15ml for a 500g-rat) mixed in some condensed milk was given to the animal for three consecutive days. All animals were given at least one week of recovery under ad libitum feed before any experiment.

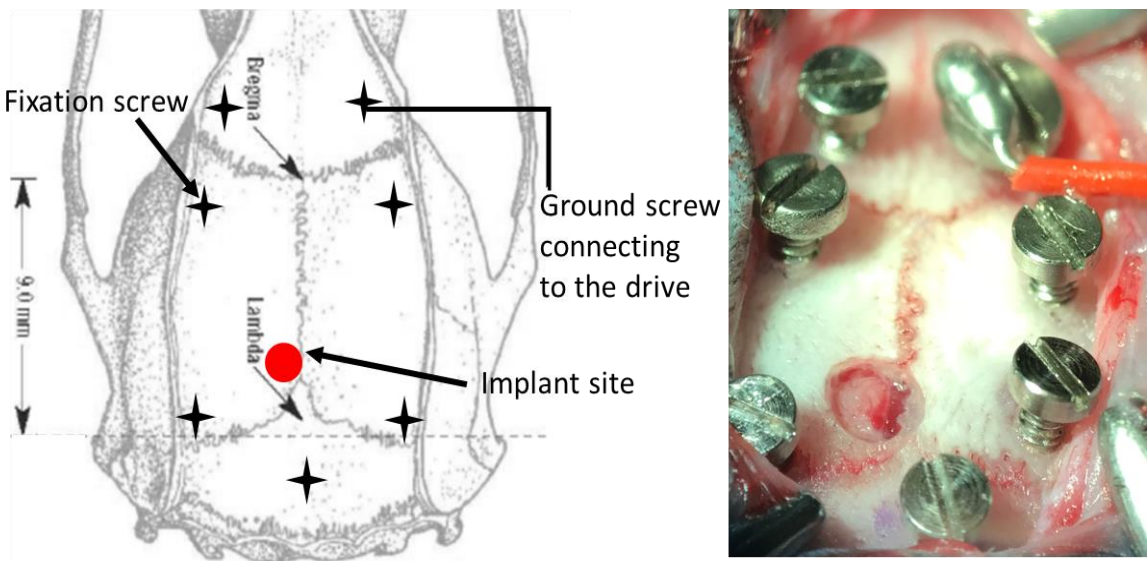


Figure 3-3. Schematics of rat skull and photo of implant surgery. Left: on the schematic of the rat skull, the star denotes the positions of fixation screws, and one of which (top-right) was a ground screw connecting to the microdrive by ground wires. Red circle denotes the implant site (either on the left or right hemisphere). Adapted from Paxinos and Watson (2006). Right: the photo shows an implant craniotomy window on the left RSC during surgery performed by the author. Note that extra caution needs to be taken when making an RSC craniotomy near the central sinus.

3.2.4 Electrophysiological recordings

The electrophysiological recording setup is illustrated in **Figure 3-4**. Single-unit activity was recorded using an acquisition system (Axona Ltd, St Albans, UK), monitored online with thresholds set by the experimenter. The microdrive was attached to a head-stage, connected to a pre-amplifier and a digitizer (at 48 kHz). Single-unit signals were amplified 5,000-8,000 times and band-pass filtered between 300 and 7,000 Hz; local field potential (LFP) signals were amplified 1,000-2,000 times and lowpass filtered at 500 Hz. The heading and position information of the animal's travelling in space was determined by tracking the positions of two LEDs based on differential brightness at each site of the head-stage assembly. The LEDs were separated by 5 cm. The spatial information was monitored by a camera mounted in a central position on the ceiling relative to the apparatus, at a sampling rate of 50Hz. Right next to the camera, a radio was constantly playing white noise. During recordings, the

environmental sound level was maintained over 70 dB to minimise any extra-maze auditory influence.

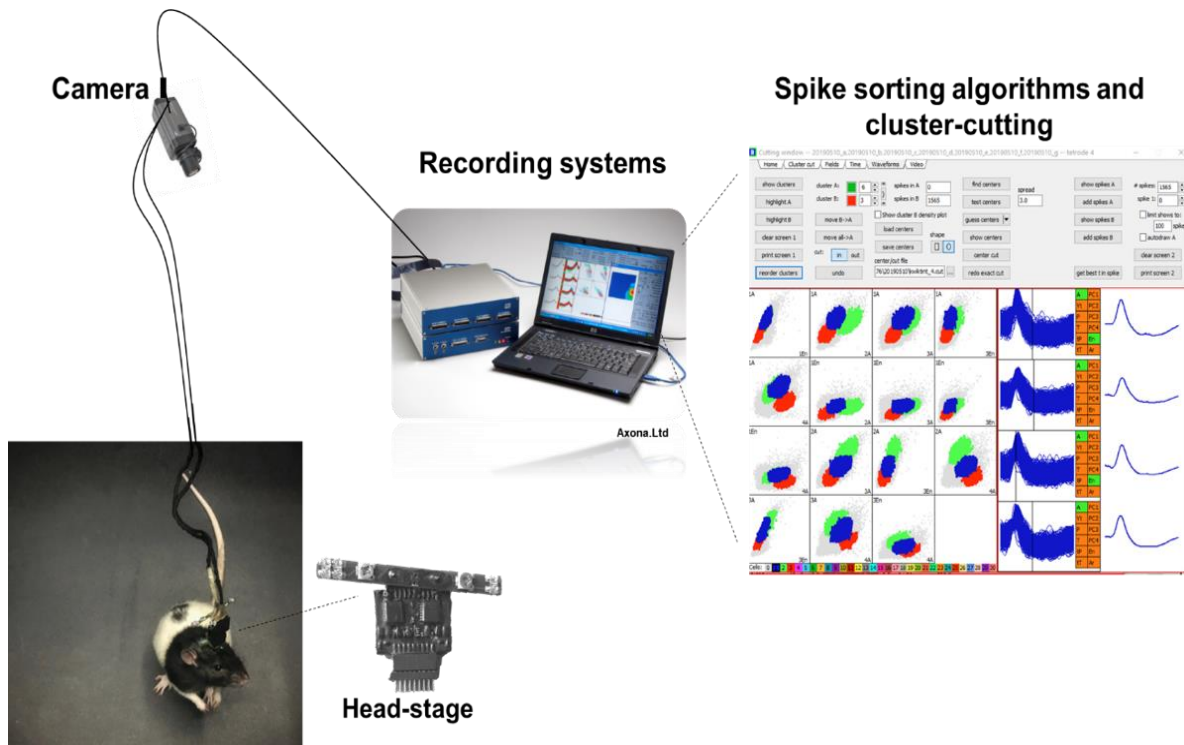


Figure 3-4. Setups of electrophysiological recording in vivo. The head-stage connects the microdrive implanted inside the brain and the recording systems, to which the camera is connected to capture animal's spatial positions and directions. Signals are then processed by the spike sorting algorithms for cluster-cutting, implemented in the TINT software (Axona Ltd., St Albans, UK).

3.2.5 General recording procedures

As shown in the flowchart in **Figure 3-1**, before the experiment started, animals were acclimated to the screening room only and screened daily for single-unit activity. To identify single unit activity, screening sessions were carried out daily in a circular arena (the screening environment). Tetrodes were lowered at multiples of 50 μm (50-150 μm ; occasionally 25 μm if no cell activity was detected) after every successful experiment session. In the cue-controlled condition, to minimise any effect of extra-maze cues, experimental apparatus were placed in the middle of the experiment room surrounded by black

curtains, a central radio was playing white noise constantly during recordings to minimise potential extra-maze influence or effect of uncontrolled directional auditory cues.

In between each trial during a session, the animal rested inside a holding box attached to a rotating plate (**Figure 3-5**), inside the curtain to prevent its knowledge of any room cues or experimenter's manipulation of the apparatus. Before the next trial, the holding box was quickly rotated by the experimenter for a few seconds, at a speed (roughly around 60-120 rpm) above the animal's vestibular threshold, so that the animal was mildly disoriented. During screening and recording sessions, the animal was motivated to explore and sample all directions in each apparatus as much as possible while foraging randomly for scattered rice or coco-pops. At the end of the recording session, the animal was taken out of the apparatus, carried in an opaque box to prevent its knowledge of any distal cues, and sent back to the home cage.

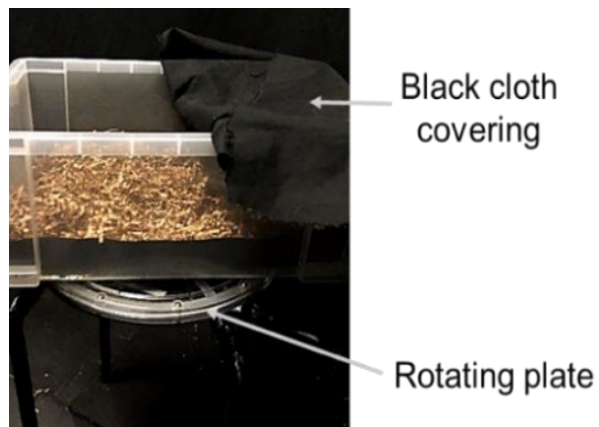


Figure 3-5. Image of the rotatable holding box. This box was used for disorientation and resting in between trials. The black cloth covering was to prevent animal's knowledge of any room cues. Bedding and water were provided to the animal inside the holding box.

3.3 Electrophysiological data analyses

A general analysis pipeline is shown in **Figure 3-6**. In this chapter, I describe how raw signals were processed and the standard analysis procedures for unidirectional head direction cells. Detailed description of specific analyses could be found in later chapters.

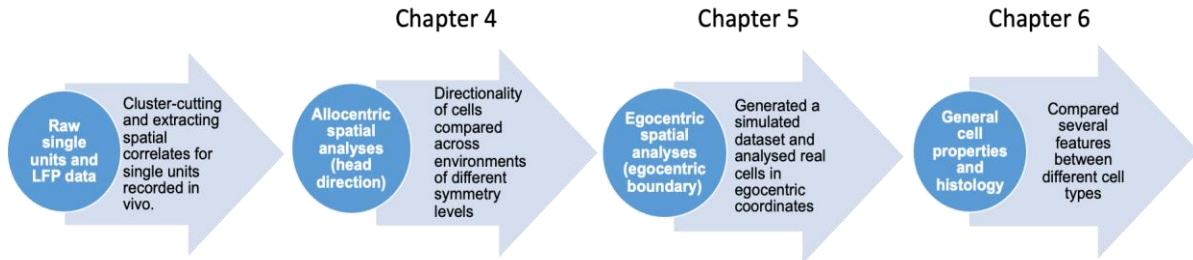
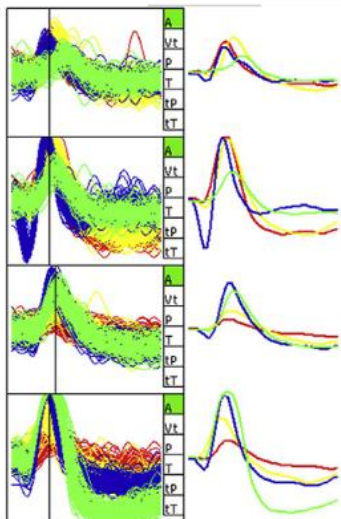


Figure 3-6. Summary of the analysis pipeline. Each part briefly summarises the analyses in each chapter. Here I introduce the processing of raw unit signals. Chapter 4 focuses on head direction analyses in an allocentric reference frame. Chapter 5 focuses on analyses of the cell activity in an egocentric reference frame as well as a simulation model. Chapter 6 focuses on analysis of histological and electrophysiological characteristics.

3.3.1 Single-unit selection

The raw electrophysiological signals were pre-processed by the recording system. Single unit activity was analysed offline using an automated spike sorting algorithm (Klustakwik v3.0; Harris et al., 2000), packaged in a cluster-cutting software with a graphical user interface (TINT, Axona, St Albans, UK). The waveform characteristics were extracted and reduced to the first three principal components and sometimes a fourth (e.g., amplitude) for each electrode. The expectation maximisation algorithm runs over this feature space. The outcome was further refined by the experimenter with reference to the spike auto-correlograms and cluster feature space.

Waveform features



Example cluster space

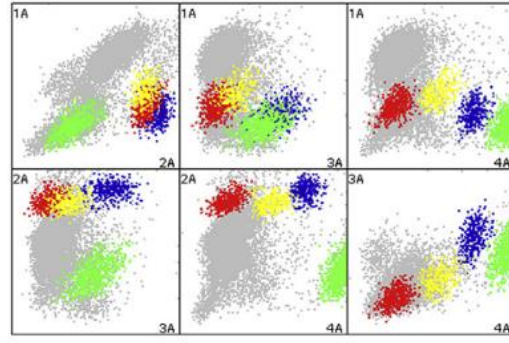


Figure 3-7. Offline analysis of clusters. Left: spikes collected from the same tetrode were analysed based on their waveform features on the four different electrodes (channels). Therefore, the waveforms can be well separated. Right: using an automated clustering algorithm implemented in TINT, the four clusters were isolated (as denoted by four different colours; light grey points are unassigned ‘noise’ spikes). Different metrics are calculated to measure the cluster quality for each tetrode (see below). Adapted from Jeffery et al. (2018).

3.3.2 Cluster quality analyses

Cell cluster quality was assessed over a recording session that consists of multiple trials recorded from different environments. Before cluster-cutting, spike data collected from all trials within a session were compiled to one overall cluster space, so that cluster centre of mass remained constant across trials. Cluster quality was monitored by calculating three metrics: the isolation distance, L-ratio (both measures make use of the Mahalanobis Distance; Schmitzer-Torbert et al., 2005), and refractory period contamination rate (Fee et al., 1996). The larger the isolation distance and the smaller the L-ratio, the better isolation of cluster is. The refractory period contamination rate was calculated as the number of spikes in the refractory period (2 ms duration) in proportion to the total number of spikes within a trial. The results of cluster quality analyses were summarised in **Appendix I**.

3.3.3 Head direction tuning analyses

The animal's head direction information was obtained by tracking the relative position of two LEDs as the animal moved on the horizontal plane. To assess whether a cell is directionally tuned, the activity is usually visualised in polar plots, by plotting the cell's firing activity as a function of animal's heading in polar coordinates. A single cell's firing rate refers to the spike count occurred in an interval of duration, divided by the measurement time. A directional tuning curve is a circular distribution of the firing rate over the range of 0-360°, the scale in which the head direction was measured. The samples were binned into 60 bins.

For each cell, the mean firing rate (no. spikes/sec) was computed by dividing the number of spikes of a cell firing in each angular bin (i.e., 6°) by the time spent facing a direction in the angular bin (sampling). The resulting circular histogram was smoothed by a boxcar kernel (MATLAB function *imfilter*; width = 5 bins). The peak firing rate indicates that the cell has the most spikes during the time facing towards the angular bin. The preferred firing direction was determined by the bin of maximal firing. See **Chapter 4** for detailed metrics used to assess the head direction tuning characteristics.

3.4 Statistics

The circular statistic toolbox (Berens, 2009) was used, and parametric tests and post hoc nonparametric tests were applied to compare population means and medians. In one-way ANOVA, Games-Howell post hoc procedure was used if the data violated the homogeneity of variance assumption. The statistical tests were performed in MATLAB (MathWorks, R2018) and SPSS packages (IBM, SPSS 25). Where appropriate the effect sizes for each test were stated clearly. All statistical tests are two-tailed (p value threshold at 0.05) unless stated otherwise. In all figures * = significant at the 0.05 level, ** = significant at the 0.01 level,

*** = significant at the 0.001 level. For all box plots, red lines denote the sample mean, dotted lines denote the sample median, and boxes denote interquartile range.

3.5 Histology

At the end of the experiment - normally after the electrodes passed through the relevant structures in the brain, or occasionally after loss of the implanted microdrive - animals were anaesthetised with isoflurane and injected with an overdose of sodium pentobarbital for euthanasia. Half of the animals underwent an electrolytic lesion by passing a small 15~20 µA current through one to two electrical channels for 6~12 seconds prior to perfusion. After the animal's breathing ceased, trans-cardiac perfusion was performed using saline (0.9%) and then paraformaldehyde (4%). Then, the brain was extracted from the skull, fixed in cold paraformaldehyde (4%) for at least two weeks, and then transferred to sucrose solution (30%) for cryoprotection. The brains were sliced using a freezing cryostat (Leica Biosystems, UK) under -21°C, and 35-40 µm coronal sections through caudal extent of the RSC were taken. The sections were stored in wells containing PBS and wet-mounted on the slides. After they were dried for at least a week, the sections were stained with a 0.1% cresyl violet solution for imaging preparation.

The slices best representing the electrode tracks were then imaged using an Olympus microscope (Olympus Keymed, UK). The deepest point of the electrode track was identified by referencing to the Paxinos and Watson rat brain atlas (Paxinos and Watson, 2006). The history of tetrode movements was used together with these points to calculate the tetrode depth for each recording session, so that each single unit had its depth recorded. The records were used to compare the localisation of the recorded cells in dysgranular versus granular sub-regions in RSC (see histology data presented in **Chapter 6**).

CHAPTER 4

CHAPTER 4 ENVIRONMENT SYMMETRY DRIVES A MULTIDIRECTIONAL CODE IN RETROSPLENIAL CORTEX

4.1 Introduction

A complex environment with a symmetrical design (e.g., a football field) is usually visually ambiguous, therefore being challenging for accurate spatial orientation. Maintaining a stable sense of direction requires integrating information from the perceived environment together with information from ongoing movements. As reviewed in previous chapters, in sensory-conflict conditions in which visual inputs are mismatched with self-motion inputs, an interplay of local, sensory information and a global direction signal is involved in landmark learning. The system needs to decide which source of information is more informative or reliable for spatial orientation (Knight et al., 2014; Jeffery et al., 2016). Investigating how this process is represented in the brain is important to understand direction signal computation and how to resolve spatial ambiguity.

As introduced in **Chapter 2**, retrosplenial cortex (RSC) is thought to be a candidate for this integrative process. Anatomical and functional evidence suggests its close interactions with sensory cortices such as visual cortex, the hippocampal place system, and the thalamic vestibular system. Therefore, RSC is considered as an interface for the sensory and cognitive components to converge, and to facilitate spatial orientation (Vann et al., 2009; Mitchell et al., 2018). Among different heterogeneous spatial tuning characteristics of RSC neurons, it is particularly intriguing that RSC seems to comprise two types of directional cells: first, the consensus HD cells sensitive to heading in a global reference frame, displaying a unitary tuning peak (Chen et al., 1994); and second, the landmark-sensitive

bidirectional cells that express a two-way firing pattern in a two-compartment space having twofold rotational symmetry (Jacob et al., 2017).

The twofold-symmetric environment (termed ‘the 2-box’; also see **Figure 4-1a**) comprised two rectangular sub-compartments connected by a central doorway, each was adorned with a single cue card at one end and being a 180° rotated copy of the other. It was found that as the animal stepped from one box to another through the central doorway, HD cells maintained their preferred firing whereas the bidirectional cells switched preferred firing directions by a 180° between sub-compartments, exhibiting a *globally* bimodal pattern (with two tuning curves when the 2-box was considered as a whole). Their firing pattern was locally unidirectional – a single tuning curve in each sub-compartment. Interestingly, a further subset of cells was *locally* bidirectional, expressing a two-way arrangement of tuning curves within each sub-compartment. These neurons were unexpected and raised questions as to how their firing patterns arise and what they might be for. This forms the first hypothesis of the study: that the atypical encoding of two opposite directions is an intrinsic neural property of these RSC neurons.

Since the bidirectional pattern has not been reported in other environments, it suggests that the pattern could instead derive from the twofold symmetry of the 2-box. Page and Jeffery (2018) devised a computational model to account for the BD pattern and suggested that the landmark inputs that are 180° apart may be mapped onto the HD network through Hebbian learning. The model predicted that the BD pattern would become tri-directional in a trifold-symmetric environment, but that the directional specificity may break down in higher symmetries (Page and Jeffery, 2018; see detailed discussion in **Chapter 7**). As inspired by the modelling results, this forms the second hypothesis of the study: experimentally, that the

firing symmetry of cells follows the order of environment symmetry but may be degraded by a level as high as fourfold.

Moreover, Jacob et al., (2017) reported that the BD-pattern cells were located exclusively in the dysgranular RSC, suggesting that these cells may be anatomically segregated from the HD cells. The hypothesis thus concerns whether the noncanonical cells were a distinct cell type from the HD cells by showing different electrophysiological features. This was examined in **Chapter 6**.

In the current thesis, I tested these hypotheses by recording RSC neurons in single- or multi-compartment environments with different symmetry orders. If the symmetry of cell's tuning curve changes accordingly with the environment symmetry order, this would favour the environment account and refute the 1st hypothesis. Specifically, I conducted two sets of experiments by systematically changing the order of environment symmetry to investigate whether the noncanonical directional cells are driven by environment symmetry. Adopting a similar design as with the 2-box, a fourfold symmetric environment was designed – a ‘4-box’ with four visually identical compartments, in 90° rotation symmetry to each other. I thus set out to explore whether the cells would express a fourfold symmetric pattern in a 4-box and compared this with a 2-box and with onefold environments. The latter term, the 1-boxes, refers to two circular environments (one with low and one with high walls) and one square box. In this chapter, I present the 2-box data first (the 2-box Experiment), then the 4-box data (the 4-box Experiment). The associated 1-box trials which flanked the box trials are presented after the multicompartment box data.

4.2 Methods

4.2.1 Animals

A total number of 18 adult male Lister Hooded rats (Charles River UK, Margate) were used in the study (10 animals only in the 2-box experiment; 4 animals only in the 4-box experiment; and 4 animals had experiences in both experiments). All animals received an implant-surgery with one 16-channel ($n = 14$) or 32-channel microdrive ($n = 4$) in either right or left RSC, initially targeting the dysgranular sub-region. All procedures were carried out in compliance with the Animals (Scientific Procedures) Act, 1986, United Kingdom and the European Communities Council Directive of 24 November 1986 (86/609/EEC) legislation for use and maintenance of laboratory animals.

4.2.2 Experimental apparatus

A total number of five recording apparatus were used in two experiments (multicompartment environments, **Figure 4-1**; 1-boxes, **Figure 4-2**). For the 2-box (120 x 120 x 60 cm), here I used the same apparatus as in the previous study (Jacob et al., 2017) – two connected equal-sized rectangular boxes with 180° rotational symmetry, each adorned with a white on-wall cue card and scented with lemon or vanilla odour. The 4-box (120 x 120 x 60 cm) contained four equal-sized square sub-compartments interconnected with a central doorway (width = 10 cm). Each sub-compartment was polarised by two environmental features: the doorway in the innermost corner, and a white cue card (20 x 40 cm) mounted on the wall. The spatial relationship between the cue card positions relative to the doorway remained the same for all four sub-compartments, forming a 90° rotational symmetry overall. At the start of each recording session, two adjoining sub-compartments were scented with lemon odour and the other two with vanilla odour made from bakery concentrates (Dr. Oetker, Bielefeld, Germany). The scents were to help the animal differentiate the visually identical

environments, and to help set in global reference frames. The floor and walls of the apparatus were covered with black vinyl sheets and cleaned after each session. The multicompartiment boxes were placed in the same experimental room (**Figure 4-1c**), with floor-to-ceiling black curtains surrounding the apparatus to minimise distal cue influence (i.e., cue-controlled).

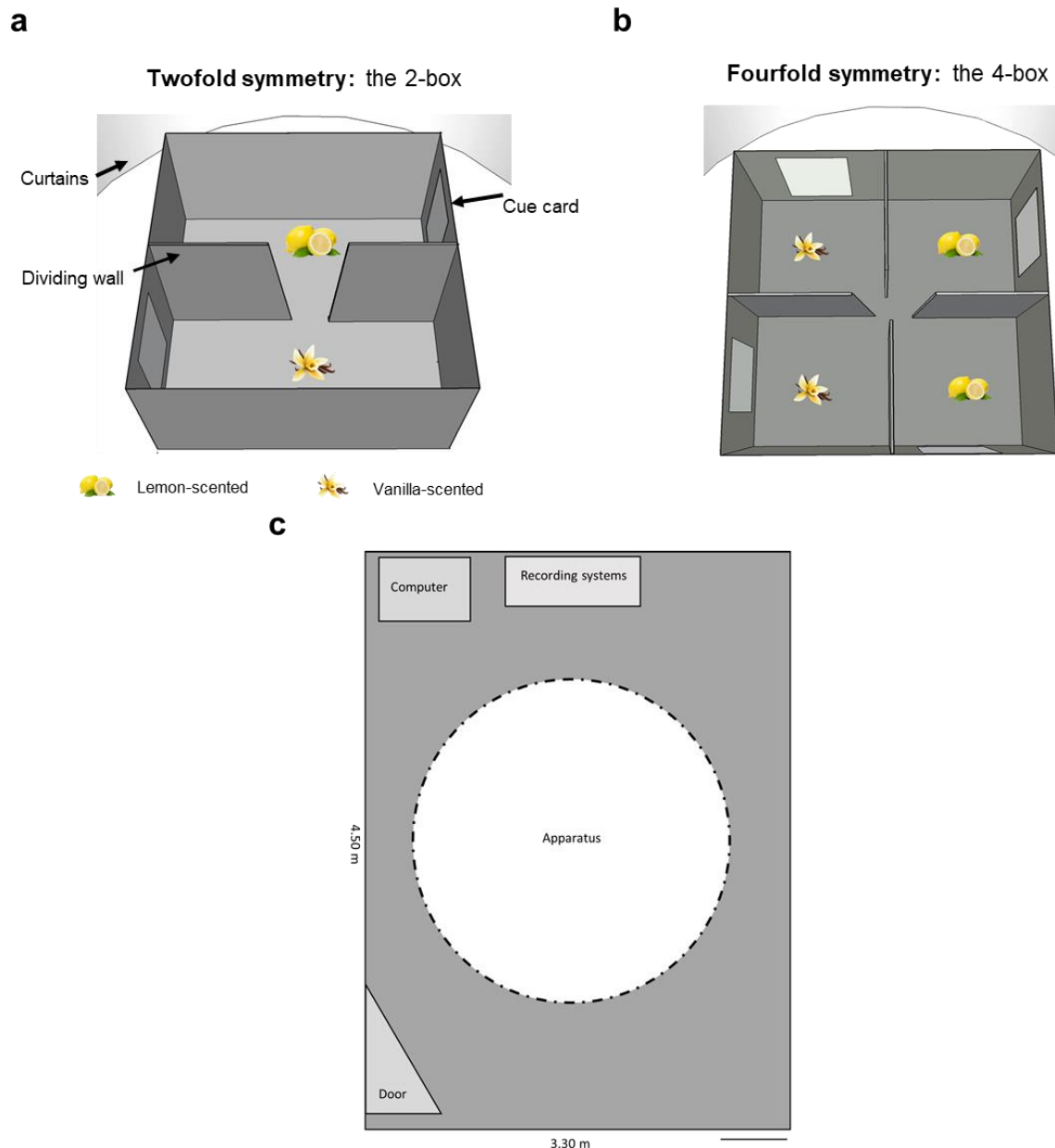


Figure 4-1. Schematics of the multicompartiment boxes and the cue-controlled recording room. **a.** Schematic of the 2-box, with a 180° rotational symmetry. Two compartments were scented differently to make them contextually distinguishable. **b.** Schematic of the 4-box: four equal-sized square boxes connected by a central doorway, forming a four-way 90° rotational symmetry. Two adjacent sub-compartments were scented with lemon odour and the other two with vanilla odour **c.** Top-down schematics of the cue-controlled experimental room, where the 4-box and 2-box recordings were carried out. Dashed line denotes the curtain area where the apparatus is placed. Scale bar denotes 0.5 metres.

Regarding simpler onefold environments, two circular arenas (1-boxes) were used, located in two different experiment rooms. A bigger and low-walled circular arena (**Figure 4-2a**, diameter = 100 cm, height = 10 cm) was used with the 2-box only, lifted (50cm) from the floor, surrounded by distal room cues. Intra-maze cues were limited. The high-walled cylindrical arena (**Figure 4-2b**, diameter = 80 cm, height = 72 cm) was in a cue-controlled room (different from the multicompartiment box shown above) and used with all 4-box experiments and for a few sessions in the 2-box experiment. Finally, a few sessions ($n = 6$) were recorded in a novel square box (**Figure 4-2c**, 100 x 100 x 60 cm), which was adorned with a single white cue card (20 x 60 cm) in the middle of one side of the wall in a cue-controlled room.

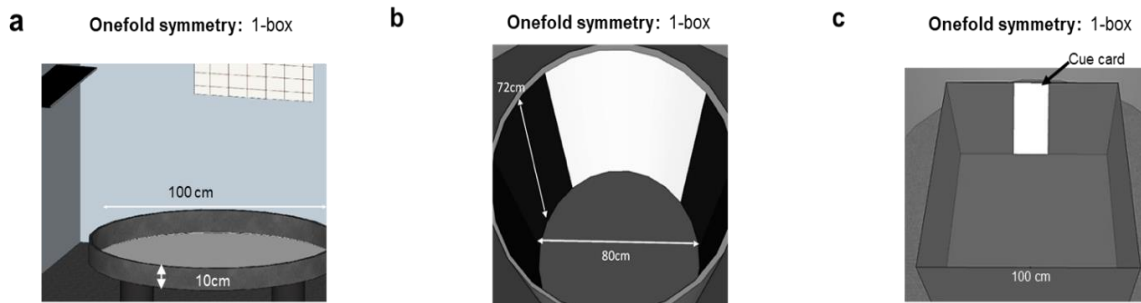


Figure 4-2. Schematic of the 1-boxes. **a.** Schematic of a low-walled circular platform: the only apparatus that did not have a cue-controlled condition. **b.** Schematic of the high-walled circular arena with a single cue card inside (forming a 90° arc). **c.** Schematic of a novel square box polarised with a single white cue card on one side of the wall. Note that only a few sessions have been performed in this environment. These environments were not compartmentalised, thus were considered as onefold symmetric environments.

4.2.3 Recording protocols

Recordings started once single units were identified from screenings (screening procedure described in **Chapter 3**). One standard recording session consisted of seven trials (**Figure 4-3**), with the first and last trial in the 1-box and five multicompartiment box trials in between. In all trials, animals were motivated to explore and sample all heading directions in the apparatus as much as possible while foraging for randomly scattered rice or coco-pops.

Between trials, the animal was carried out gently from the apparatus, placed in a holding box inside the curtain to prevent its knowledge of any room cues or experimenter's manipulation of the apparatus, and then mildly disoriented by rotating the holding box before the next trial. See **Chapter 3** for details of the holding box. Experiment room change happened between the trials in the 2-box/4-box from and to the 1-boxes, and the animal was carried in an opaque box and disorientated to prevent knowledge of any distal cues.

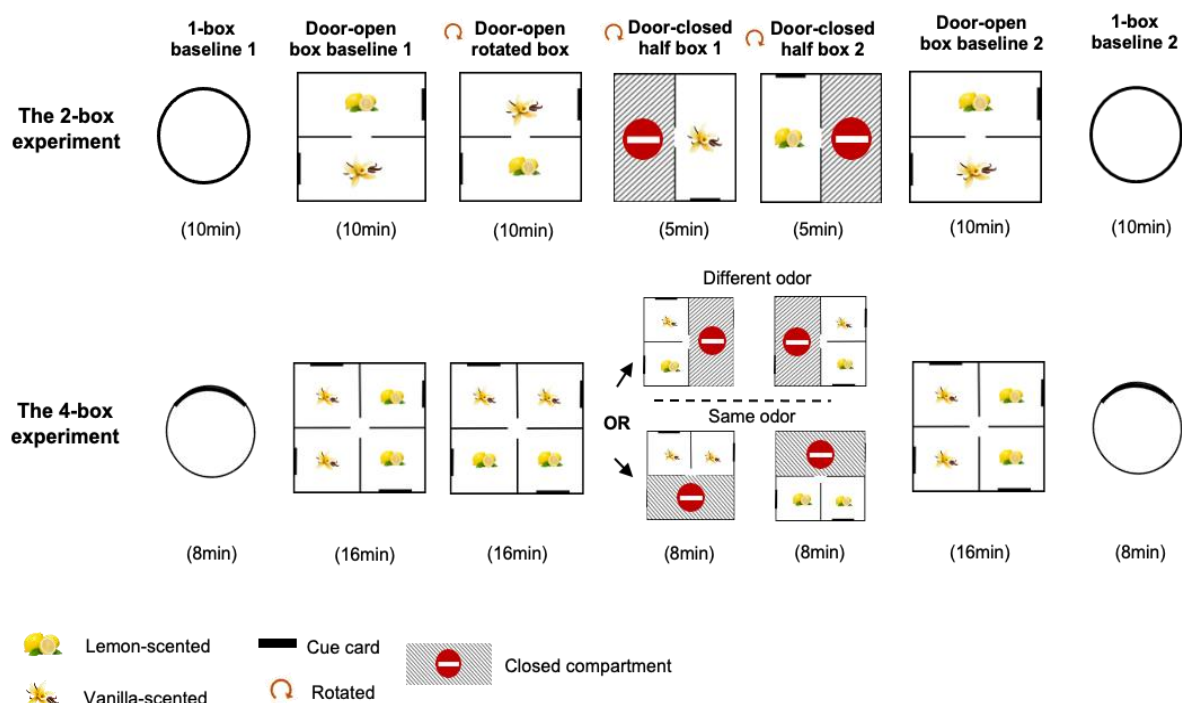


Figure 4-3. Recording protocols for two experiments. Top: seven-trial recording procedure of the 2-box experiment. In all trials, the animal freely and randomly moves in each apparatus. The trial duration is shown in brackets. Bottom: seven-trial procedure for the 4-box experiment. Note that the 1-boxes were different in two experiments. The 2-box experiment: a low-walled circular platform in an open room. The 4-box experiment: a high-walled circular arena with a single cue card forming a 90° arc around the inside wall. Switching to the cylindrical environment was to test if the cells form onefold pattern in a cue-controlled condition, and the pattern was compared with unidirectional cells (see Figure 4-12).

Details of experimental trials are described as follows:

- Trial 1 (1-box baseline): For high-walled cylinder trials, the cylinder was randomly placed in the centre of the room and oriented in multiples of 90° in camera-defined coordinates at the beginning of the trial. The aim of pseudo-random rotation in a

cue-controlled room was to check whether the cell tuning follows the local cue rotation with the apparatus. Note that for low-walled circular arena trials, the arena was lifted 50cm from the floor, and rotated randomly to a new orientation to avoid any intra-maze olfactory bias.

- Trial 2 (door-open box baseline): The apparatus was randomly placed in the centre of the room and oriented in multiples of 90° in camera-defined coordinates at the beginning of the trial. Animals were placed in a randomly chosen sub-compartment at the beginning of the trial.
- Trial 3 (door-open rotated box): As in trial 2 except that the apparatus was pseudo-randomly rotated by multiples of 90°.
- Trial 4 (door-closed half box1): The central doorway was closed so that the animal was restricted to only half of the apparatus. Note that, to test whether visual symmetry (formed by landmarks in 90°-offset) within the same context was sufficient to influence the cell's firing pattern, two protocols were used in the 4-box (**Figure 4-3**): the halves of the apparatus (two sub-compartments) were either scented the same or different. If two peaks that are 90° apart could be observed in the two sub-compartments scented the same, this would support that the contextual odours are not necessary for the peaks to emerge (which was the case, see **Figure 4-7**).
- Trial 5 (door-closed half box 2): As in trial 4, the animal was recorded in the other half of the apparatus.
- Trial 6 (door-open box baseline): As in trial 2, the door was open, and the apparatus was rotated back to its starting orientation.
- Trial 7 (1-box baseline): As in trial 1, the animal returned to the circular environment.

All recording sessions included in the study consisted of at least these seven trials as described above. In addition to the seven standard trials, the following procedures were performed:

- Darkness trials: To test whether the firing pattern was primarily dependent on vision, in some 4-box recording sessions ($n = 28$), two darkness trials were added after the last door-open box baseline trial. The cue cards were removed from the apparatus and the lighting sources in the room were switched off, then the animal was disorientated and reintroduced into the apparatus. The 4-box was again randomly rotated in the last darkness trial.
- Rotated cylinder trials: To investigate if the onefold firing pattern of the cells is similar to unidirectional HD cells, in some recording sessions of the 2-box ($n = 8$) and 4-box experiments ($n = 43$), at least two extra cylinder trials were added following the last cylinder baseline trial. The cylinder was randomly rotated from the baseline orientation, the animal was disorientated and reintroduced into the apparatus. Note that the rotated cylinder trials were also performed on the first day of two naïve animals before recording in the multicompartment box trials. This was to examine whether any potential intrinsic directional tuning exists before the first multicompartmented box exposure.
- Square box trials: in a few recording sessions of the 4-box experiment ($n = 5$). After the last circular baseline trial, two extra 10-min trials were carried out in a novel square box in the same cue-controlled room. This was to test the influence of simple geometry and to investigate any possible relationship to egocentric boundary coding (see the latter part in **Chapter 5**).

4.2.4 Data analyses

The basic procedures of electrophysiological signal processing were described in **Chapter 3**.

4.2.4.1 Directional cell analyses

- *HD polar plot:* For each trial, all direction samples were binned into 60 bins of 6° width, the number of spikes emitted in each bin divided by the total dwell time for that direction. The directional tuning curve was the cell's firing rate over 360° . A boxcar kernel (width = 5) was applied to smooth the raw tuning curve. The peak firing rate was defined as the maximal firing rate of bin of the smoothed tuning curve, and this angular bin was defined as the cell's preferred firing direction.
- *BD/TD score:* The scores reflected the level of spatial periodicity in the tuning curves and were calculated using a similar circular autocorrelation procedure as described previously (Jacob et al., 2017). Each cell's tuning curve was rotated in steps of 6° . The Pearson's correlation coefficient between the rotated and non-rotated tuning curves at each step was calculated. Periodicity appears as a sinusoidal modulation of the circular auto-correlogram, with the number of peaks reflecting the order of symmetry. The BD score was defined as the difference between the mean correlation coefficient at the expected peak ($\pm 180^\circ$) and the expected troughs ($\pm 90^\circ$). The TD score was calculated in the same way, but the expected peaks were at $\pm 90^\circ$ and $\pm 180^\circ$ and the expected troughs at $\pm 45^\circ$ and $\pm 135^\circ$. Computation of the scores for the shuffle control (see Shuffling section below) was performed in the same manner.
- *Directional specificity:* Normally, directional specificity would be assessed using mean resultant vector length – the Rayleigh vector length (Giocomo et al., 2014). However, multi-fold directionality violates the assumption of the Rayleigh

distribution: I thus performed the directionality analysis by angle-doubling (as used before in Jacob et al., 2017) and angle-quadrupling procedures in which the heading direction of each spike (in radians) was doubled or quadrupled and wrapped to 2π . In this way, multi-fold symmetric data is converted into a unimodal distribution (Landler et al., 2018). Then Rayleigh vector length was computed from the converted data.

The Rayleigh vector length was not sufficiently sensitive to characterise the broad unidirectional tuning pattern in the 1-box. Instead, an area under the correlation curves between 1-box baselines was computed using the trapezoidal method approach (MATLAB function *trapz*). The trapezoidal numerical integration method computes an approximation of the integral of the cross-correlogram, and a stable unidirectional pattern would yield a high, positive value while non-selective cells had low, negative values. Therefore, this value could be used to represent the cell's directional selectivity. Computation for the shuffle control was performed in the same way. Then the cell's value was compared with the 95th shuffle threshold.

- *Selection criteria:* A classic head direction cell was defined as meeting the following criteria: peak firing rate at least 1Hz and Rayleigh vector length greater than 0.26 – the same threshold as used in Jacob et al. (2017). A BD-pattern cell was defined as meeting the following criteria: the cell's peak firing rate should be no less than 1 Hz; the 95th percentile criterion of shuffle was applied to the cell's BD score; and the cell's Rayleigh vector length (angle-doubled) exceed either 95th percentile criterion of shuffle or a population threshold at 0.18. The population threshold was applied when a cell passed the first two criteria but not its own Rayleigh vector length threshold.

Similarly, a TD-pattern cell was defined as meeting the following criteria: the cell's peak firing rate should be no less than 1 Hz; its TD score should be greater than

the 95th percentile criterion of shuffle control; and the cell's Rayleigh vector length (angle-quadrupled) greater than either 95th percentile criterion of shuffle or a population threshold at 0.15. The population thresholds of Rayleigh vector length were obtained in this way: the 95th percentile threshold computed in three door-open box trials of all cells recorded in that experiment were collated (i.e., the shuffle procedures were done for 478×100×3 times in the 2-box experiment and 660×100×3 times in the 4-box experiment), and the population mean was calculated. Note that the mean was higher than the median, so more stringent thresholds were taken. All criteria above were applied to both baseline trials in the 2-box and 4-box. The same criteria were also used in analyses of cell activity in 4-box darkness trials.

For the within-compartment activity, we further analysed the cell's firing in single sub-compartments in the 1st baseline trial separately. A between-compartment BD cell was defined as meeting these additional criteria: the Rayleigh vector length (without angle-doubling) of single-compartment activity greater than the shuffle or mean Rayleigh vector length of two single sub-compartments greater than 0.18; and the BD score of single compartments did not exceed the shuffle control. A within-compartment BD cell was defined as meeting the following criteria: the BD score greater than 0.26 (the shuffle population median) in both single sub-compartments; and mean Rayleigh vector length (angle-doubled) of two single sub-compartments greater than 0.18. Similarly, for between-compartment TD cells: the Rayleigh vector length (without angle-quadrupling) of single compartments greater than 0.15 (the shuffle population median) in at least three sub-compartments; and the TD score of single compartments did not exceed the shuffle control. For within-compartment TD cell: the TD score and Rayleigh vector length (angle-quadrupled) of single sub-compartments greater than 0.15 in at least three sub-compartments.

As discussed earlier, in the 1-boxes (circular baselines), cells that were considered broad-unidirectional had their area under the correlation curve higher than its 95th percentile criterion of shuffle. In rotated cylinder trials, cells that were considered unidirectional had their Rayleigh vector lengths higher than the 95th percentile criterion of shuffle in all three successive cylinder trials. In the novel square box, to check for any potential TD pattern, the 95th percentile criterion of shuffle was applied to a cell's TD score and angle-quadrupled Rayleigh vector length.

- *Symmetry analyses:* To examine the directional pattern (onefold, twofold and fourfold) across environments and their sub-compartments, I calculated the cross-correlation (Pearson's correlation coefficient) between two tuning curves in each angular bin in steps of 6°. For the 2-box, the tuning curve pairs were from lemon and vanilla sub-compartments of the baseline trials. For the 4-box, the tuning curve pairs were from any adjacent two sub-compartments (i.e., four pairs: vanilla 1 vs. lemon 1; lemon 1 vs. lemon 2; lemon 2 vs. vanilla 2; and vanilla 2 vs. vanilla 1) were pooled together, and the final cross-correlation was averaged over these four comparisons. For 1-boxes, the tuning curve pairs were from two baseline trials. Periodicity would appear as a sinusoidal modulation of the circular cross-correlogram in a range from -180° to 180°, with the number of peaks reflecting the order of symmetry. Computation for the shuffle control was performed in the same manner. Statistical tests were performed to compare the data and the shuffle.
- *Pattern similarity:* In the dark trial analysis, the criteria for TD pattern were applied first. Cross-correlation of a cell's tuning curve pairs in the light (4-box baseline 1) and dark was computed, as well as for two dark trials. Although the cells have passed the criteria, to examine if there is a drift of pattern periodicity from light to dark, the cross-correlations between light vs. dark 1 and with dark 1 vs. dark 2 were computed

respectively. To measure the strength of sinusoidal modulation (i.e., periodicity), a sine wave (two terms, MATLAB functions *sin2*, curve fitting toolbox) was fitted to the circular cross-correlogram, and the goodness of fit (*r-squared*) was calculated using a non-linear least-squares approach. The higher the goodness of fit, the stronger the sinusoidal modulation, thence more similar the pattern between different conditions (i.e., light vs. dark; dark 1 vs. dark 2).

4.2.4.2 Shuffling

A shuffling procedure was used to obtain control distributions and chance-level estimation in directionality and egocentric tuning analyses. In the HD analyses, for each permutation trial, the entire spike train of each cell was time-shifted by random intervals ranging from 20s to the trial duration (usually 600s for 2-box and 960s for 4-box baseline trials) minus 20s relative to the positional/directional data. Spike times shifted past the end of the trial were wrapped around to the beginning. One hundred permutations were performed for each trial of a given cell in the shuffling procedure. For each permutation, an HD tuning curve was constructed, and the associated Rayleigh vector length and TD/BD scores were determined. Thresholds were identified from the overall distribution of the measurements of the shuffled data (e.g., 95th percentile).

4.2.4 Statistical analysis

See description in **Chapter 3**.

4.3 Results

4.3.1 Does RSC cells' firing symmetry follow the environment symmetry order?

4.3.1.1 Bi-directional pattern in the 2-box

Let us begin with the twofold environment symmetry, where I first replicated the previous findings (Jacob et al., 2017). In the 2-box experiment (**Figure 4-3**), RSC cells were recorded for five trials in the 2-box, flanked by two trials in the 1-box (rats, $n = 14$; cells, $n = 478$). Consistent with the previous work (Jacob et al., 2017), the directionally tuned cells with bidirectional tuning curves were found in the current study: a twofold-symmetric firing pattern with a 180° offset between two tuning curves (**Figure 4-4**). This was quantified with a bidirectionality score and angle-doubled Rayleigh vector length (see **Methods**); 48/478 cells passed the criteria for bidirectionality, with a median BD score of 0.85 and median angle-doubled Rayleigh vector length of 0.23. A total of 48 cells (10%) showed such firing pattern in the 2-box when the doorway was open. More example BD-pattern cells were shown in **Appendix II**.

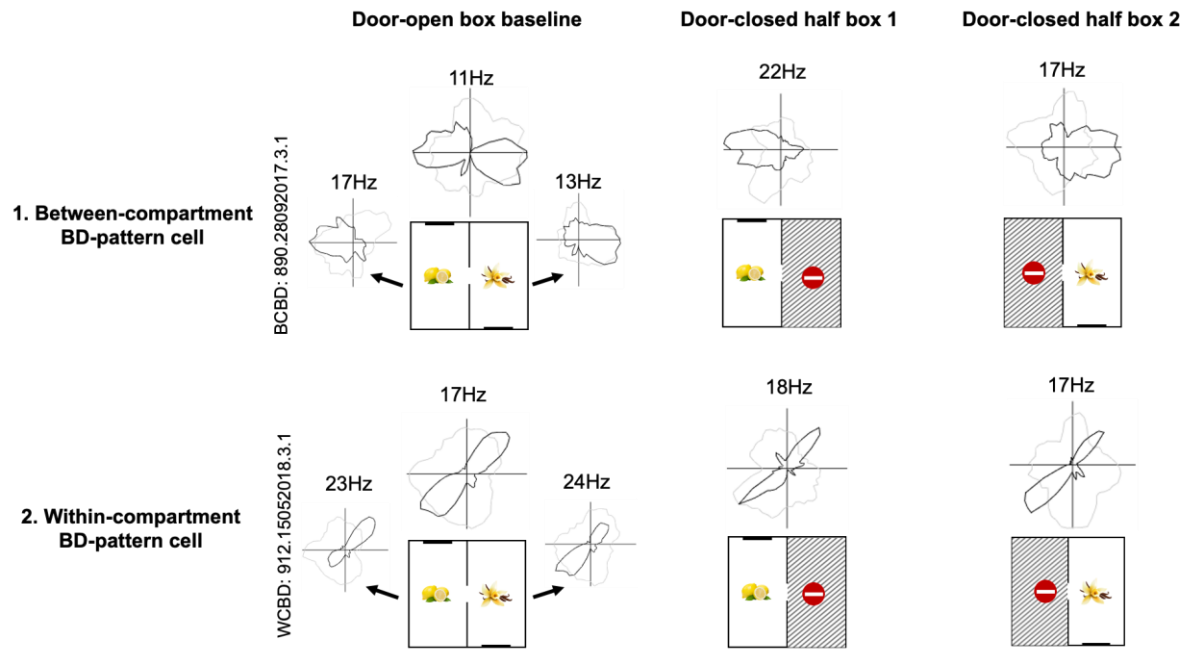


Figure 4-4. The 2-box experiment and example BD-pattern cells. Here, the figure only shows three trials. An example between-compartment BD-pattern cell (top) and within-compartment BD-pattern cell (bottom) recorded from the 2-box. Polar plot depicts cell's tuning curve (black) normalised to animal's head direction sampling (light grey) inside the whole apparatus (on top of the schematic) as well as its firing within each sub-compartment (as indicated by the black arrow next to the affiliated single sub-compartments). Number denotes peak firing rate in Hz (the largest peak for within-compartment cells). Note that the between-compartment single peak and the within-compartment two peaks persist in door-closed trials.

Consistent with the previous findings (Jacob et al., 2017), these BD-pattern cells displayed three main types of bidirectional pattern within single sub-compartments. The so-called between-compartment bidirectional cells (BC-BD, $n = 9/48$, 19%, **Figure 4-5**) lost their bidirectionality in the local sub-compartments, as shown by the fact that BD scores were not significantly different from 0 (median lemon = 0.11, $t(8) = 0.94$, $p = 0.37$; vanilla = -0.13, $t(8) = 1.07$, $p = 0.32$). However, they maintained unidirectional firing (median Rayleigh vector length: lemon = 0.22; vanilla = 0.23), as the within-compartment autocorrelations were significantly different from a shuffle control (**Figure 4-5b**, KStest, lemon, $D = 0.65$, $p < .001$; vanilla, $D = 0.59$, $p < .001$), revealing persistence of local correlation structure. Thus, only the global pattern was bidirectional (**Figure 4-5c-d**,

cross-correlations significantly different from shuffle, KStest, $D = 0.58$, $p < .001$; peaked at 174° , circular v-test against 180° , $V = 4.76$, $p = 0.012$.

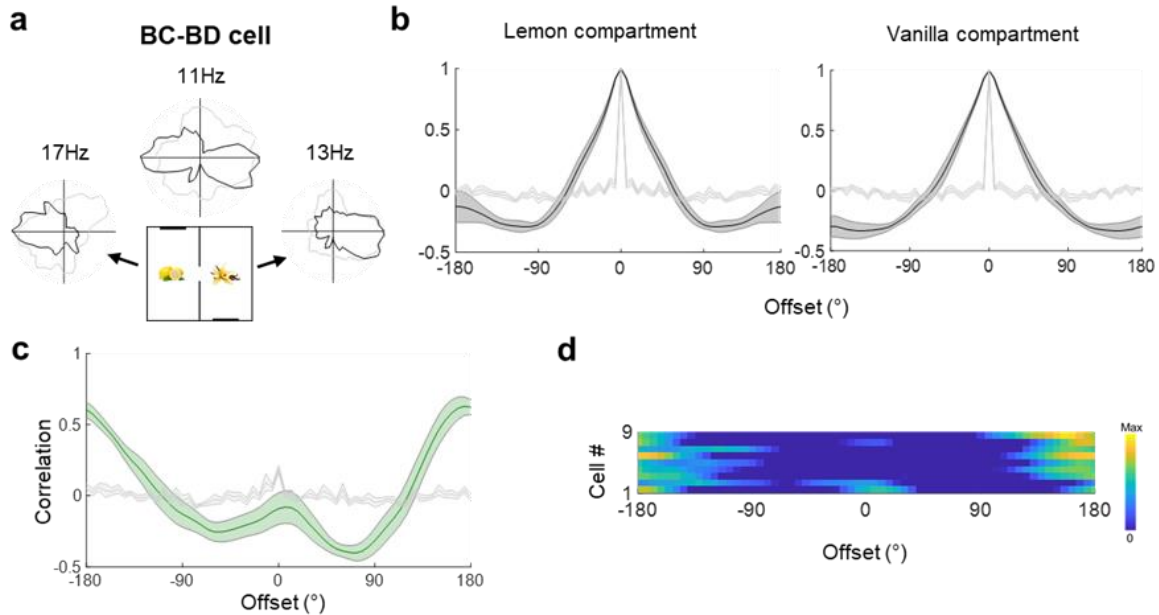


Figure 4-5. Multiple directional firing symmetries (BC-BD) in the 2-box. **a.** Global and compartment-specific polar plots of a between-compartment bidirectional cell (BC-BD). Top polar plot: bipolar directional tuning curve for the whole apparatus (dark line) and directional behavioural sampling (pale line). Numbers show peak firing rates. Side plots: Tuning for each sub-compartment showing locally opposite direction. **b.** Auto-correlograms of the within-compartment firing showing single peak for the BC-BD cell. Pale line shows the shuffle control. **c.** Population tuning curve cross-correlation between sub-compartments shown as a line (green), population mean (solid line) and SEM (shaded) of the correlation coefficients. Pale line shows the shuffle control. **d.** Heatplots of the cross-correlograms for individual cells, sorted by Rayleigh vector lengths, maximum at the top.

Second, the within-compartment bidirectional cells (WC-BD; $n = 22/48$, 46%, **Figure 4-6b**), expressed a bidirectional pattern even within single sub-compartments (**Figure 4-6b**, BD scores above shuffle control, median lemon = 0.90; vanilla = 0.61; within-compartment autocorrelations significantly differed from a shuffle: KStest, lemon, $D = 0.52$, $p < .001$; vanilla, $D = 0.52$, $p < .001$). Angle-doubled Rayleigh vector lengths within sub-compartments were high: median lemon = 0.27; vanilla = 0.31. Where the two within-compartment tuning curves were asymmetric, their largest peaks were shifted by around 180° between two sub-compartments (**Figure 4-6c-d**, between-compartment correlations significantly different from shuffle: KStest, $D = 0.51$, $p < .001$;

mean $\Delta\text{PFD} = 188^\circ$, circular v-test against 180° : $V = 6.54, p = 0.024$). A third category of BD-pattern cells (17/48, 35%) fell below the statistical threshold (shuffle criterion) for directionality in the sub-compartment analysis and remained unclassified.

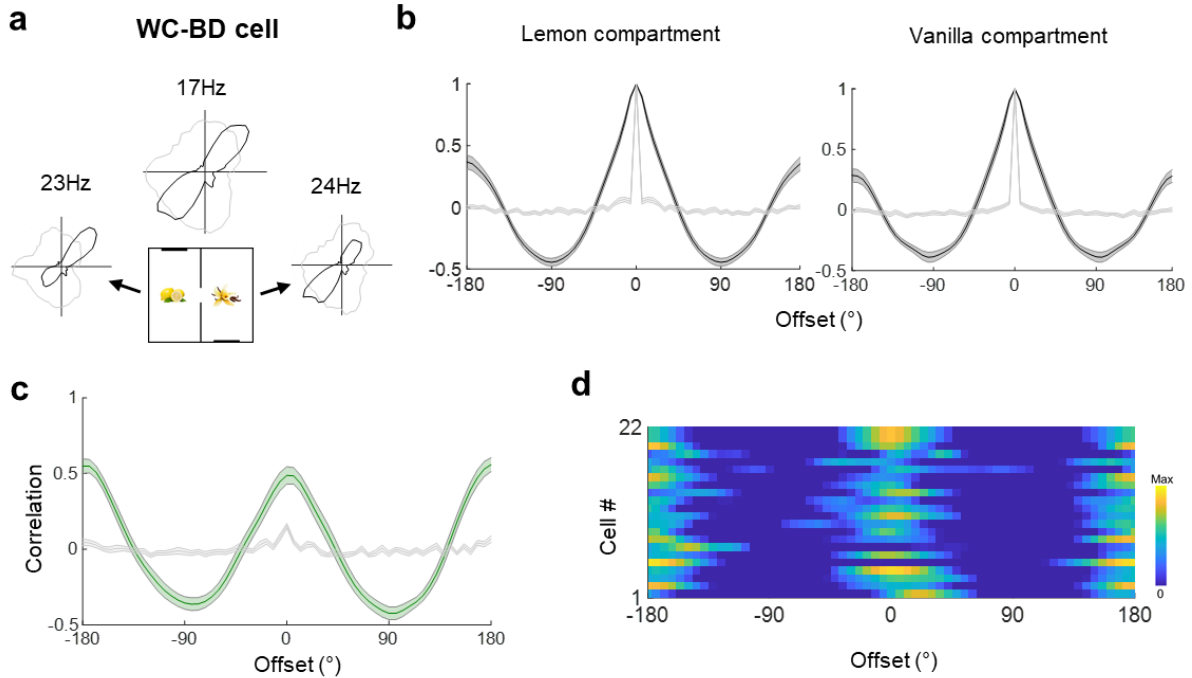


Figure 4-6. Multiple directional firing symmetries (WC-BD) in the 2-box. **a.** Polar plot depicts the tuning curve of a within-compartment BD cell inside the whole apparatus (top) and cell's firing within each sub-compartment (as shown by the black arrow next to the affiliated single sub-compartment). Number denotes the largest firing peak. Bidirectional tunings for each sub-compartment are shown in the side plots, showing PDFs at opposite directions. **b-d.** Analyses as in Figure 4-5; b: Auto-correlograms of the within-compartment firing; c: cross-correlation between sub-compartments shown as a line (green). Pale lines show the shuffle control. Note that in contrast to single-peaks around 0° for BC-BD cells, the auto-correlograms of the within-compartment firing and the cross-correlation between compartments show double peaks at $\pm 180^\circ$ for the WC-BD cell. In (d), the heatmap of the cross-correlograms is shown, sorted by angle-doubled Rayleigh vector lengths, maximum at the top.

4.3.1.2 Tetra-directional pattern in the 4-box

Having replicated the basic observation, I next increased the level of environment symmetry from twofold to fourfold, to test our prediction that the symmetry of firing would follow that of the environment. In the 4-box Experiment (Figure 4-3), I designed a fourfold symmetric environment – the 4-box, as described earlier (Figure 4-1b). In the door-open baselines,

animals freely and randomly moved through four sub-compartments. Adjacent pairs of sub-compartments were scented the same, with lemon or vanilla, to break the symmetry and allow the head direction signal to stabilise. This also created a chunking of the subspaces that might reveal a hierarchical organisation of directionality, for instance, whether a cell is directionally consistent across both lemon sub-compartments but rotates in vanilla.

In the 4-box experiment, RSC cells were recorded for five trials in the 4-box and at least two trials in the 1-box (rats, $n = 8$; cells, $n = 660$). I saw no bidirectional cells in the 4-box, but many cells showed a fourfold-symmetric ‘four-leaved clover’ firing pattern, with a 90° offset between four directional tuning peaks (**Figure 4-7**). This fourfold directionality was quantified as a tetradirectional (TD) score (see Methods): 67/660 (10.2%) of the cells met the criteria for tetradirectionality, yielding a median TD score of 0.90 and angle-quadrupled median Rayleigh vector length of 0.20. As with the BD cells, three subgroups of TD-pattern cells were identified – that were unidirectional, multidirectional, and non-directional in single sub-compartments.

To prevent carry-over effects from experience of previous environment symmetries, I mostly used naïve rats except for four rats that had little experiences (9 sessions in total) in the 2-box experiment. Of note, three rats that showed BD pattern in the 2-box also yielded 15 TD cells when tested in the 4-box – this strongly refuted Hypothesis 1 that the multidirectional pattern is intrinsic, rather, it is driven by the environment.

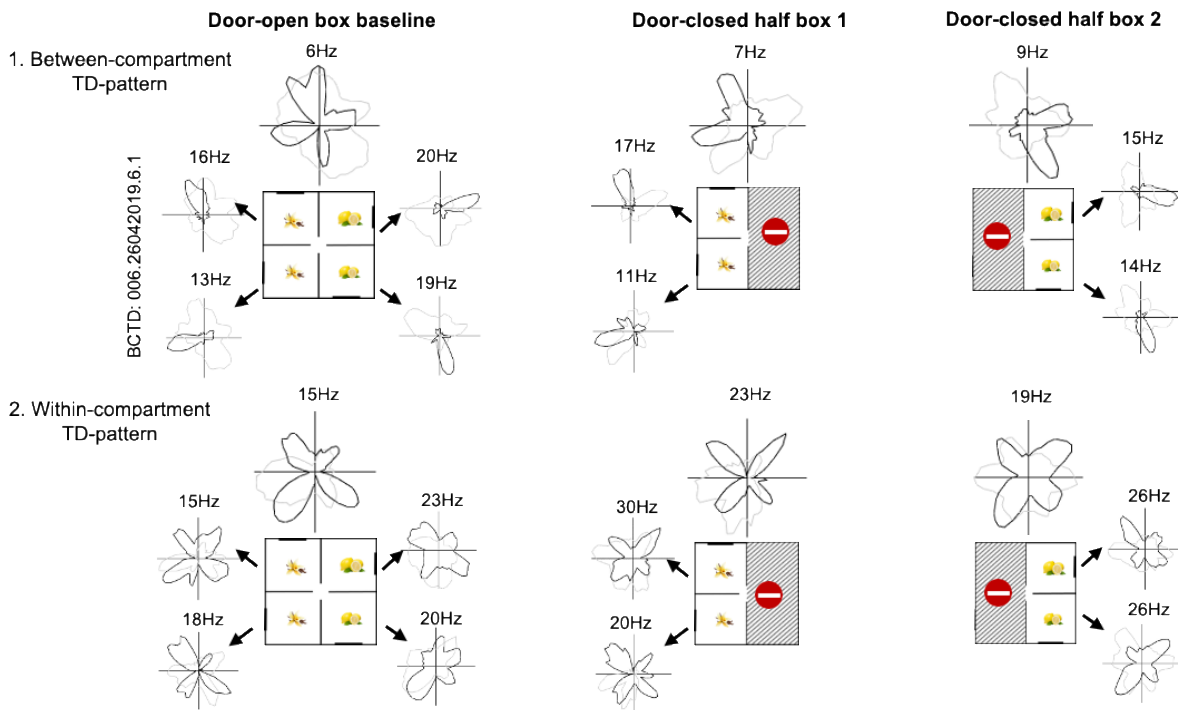


Figure 4-7. The 4-box experiment and example TD-pattern cells. Schematics of the 4-box (three trials) and example of two TD-pattern cells (top: BC-TD cell; bottom: WC-TD cell). Polar plot depicts cell's tuning curve inside the whole apparatus (top) and its firing within each sub-compartment (as indicated by the black arrow next to the affiliated single sub-compartments). Number denotes the largest firing peak. The BC-TD cell shows tetradirectionality of the overall tuning but unidirectionality within each sub-compartment. The WC-TD cell shows overall and local tetradirectionality in the 4-box.

Similar to the two subgroups observed in the 2-box experiment, two sub-populations of TD-pattern cells were separated in 4-box experiment. The between-compartment tetra-directional cells (BC-TD; $n = 9/67$, 13%, **Figure 4-8**) expressed unidirectional but not tetradirectional tuning curves in individual sub-compartments. Unidirectionality was shown by a high Rayleigh vector length (median vanilla1 = 0.27, vanilla2 = 0.22, lemon1 = 0.25, lemon2 = 0.32) and by the fact that the within-compartment correlations significantly differed from a shuffle in every sub-compartment (**Figure 4-8b**, KStest, vanilla1, D = 0.67, $p < .001$; vanilla2, D = 0.66, $p < .001$; lemon1, D = 0.72, $p < .001$; lemon2, D = 0.52, $p < .001$). Loss of tetradirectionality was shown by the fact that within-compartment TD scores were not significantly different from 0 (median vanilla1 = -0.06, $t(8) = 0.03$, $p = 0.98$; vanilla2 = 0.03,

$t(8) = 0.35, p = 0.74$; lemon1 = -0.10, $t(8) = 0.46, p = 0.66$; lemon2 = 0.01, $t(8) = 0.44, p = 0.67$). The preferred direction in each sub-compartment rotated for 90° in successive sub-compartments relative to the global direction: cross-correlations of tuning curves from adjacent sub-compartment pairs differed from a shuffle (**Figure 4-8c-d**, Ktest, $D = 0.68, p < .001$) and peaked at ~90° (circular v-test against 90°: $V = 7.98, p < .001$).

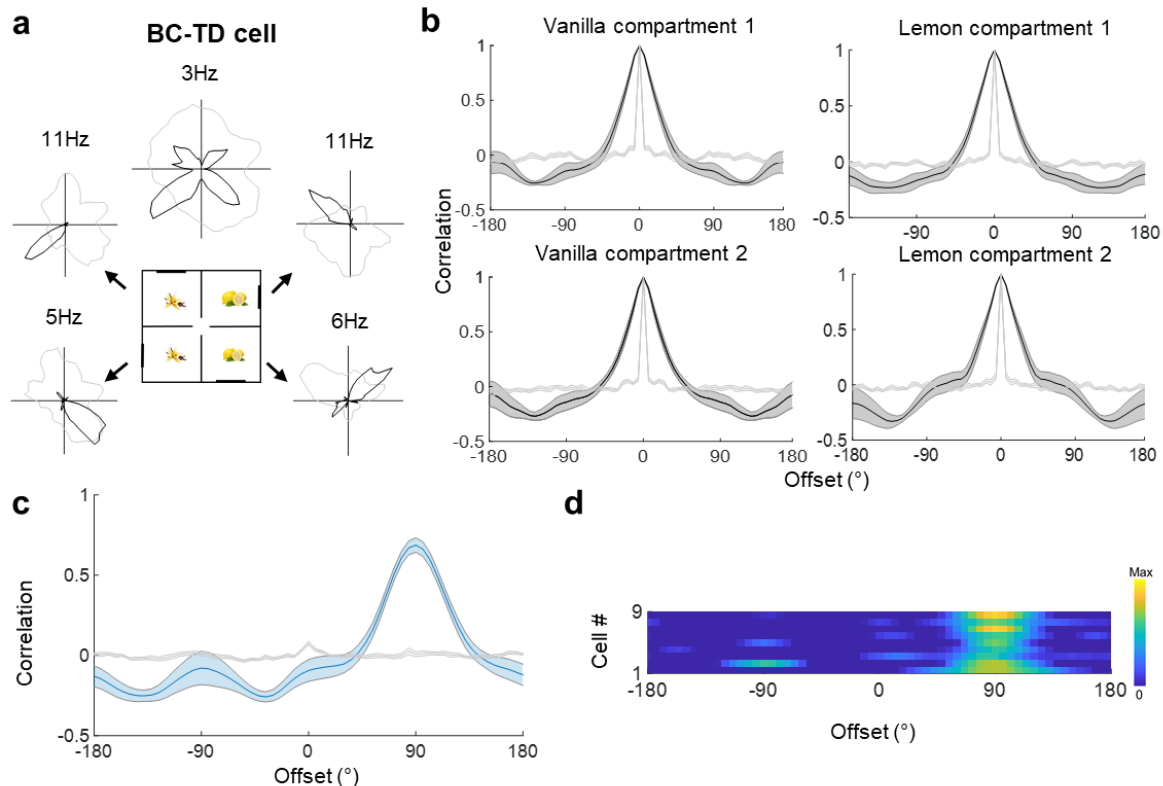


Figure 4-8. Multiple directional firing symmetries (BC-TD) in the 4-box. **a.** Schematic of the 4-box baseline and an example BC-TD cell (top). Polar plot depicts the tuning curve inside the whole apparatus (top) and cell's firing within each sub-compartment, as indicated by the black arrow. **b-d.** analyses as in Figure 4-5. Note that the cross-correlograms were obtained by averaging four cross-correlograms of tuning curve pairs from any two adjacent sub-compartments. A single peak was found at 90° angular offset in auto-correlograms of the within-compartment firing and the cross-correlation between compartments. In (d), the heatmap of cross-correlograms was sorted by Rayleigh vector lengths, maximum at the top.

A second subgroup of TD-pattern cells, the within-compartment cells (WC-TD; $n = 29/67, 43\%$, **Figure 4-9**) exhibited a multidirectional pattern (usually fourfold, but occasionally a fourth peak was smaller) even in single sub-compartments (**Figure 4-9b**;

within-compartment TD scores significantly greater than shuffle control, 0.15: median vanilla1 = 0.43, $t(28)= 6.03$, $p <.001$; vanilla2 = 0.35, $t(28)= 4.04$, $p <.001$; lemon1 = 0.32, $t(28)= 5.31$, $p <.001$; lemon2 = 0.21, $t(28)= 1.70$, $p = 0.05$; high quadruple-angled Rayleigh vector length: median vanilla1 = 0.32, vanilla2 = 0.28, lemon 1 = 0.30, lemon 2 = 0.27); coefficient of within-compartment correlations significantly different from shuffle, Kstest, vanilla1, $D = 0.49$, $p <.001$; vanilla2, $D = 0.47$, $p <.001$; lemon1, $D = 0.52$, $p <.001$; lemon2, $D = 0.50$, $p <.001$). The tuning curve peaks varied in size and the direction of the largest peak usually rotated 90° between the sub-compartments.

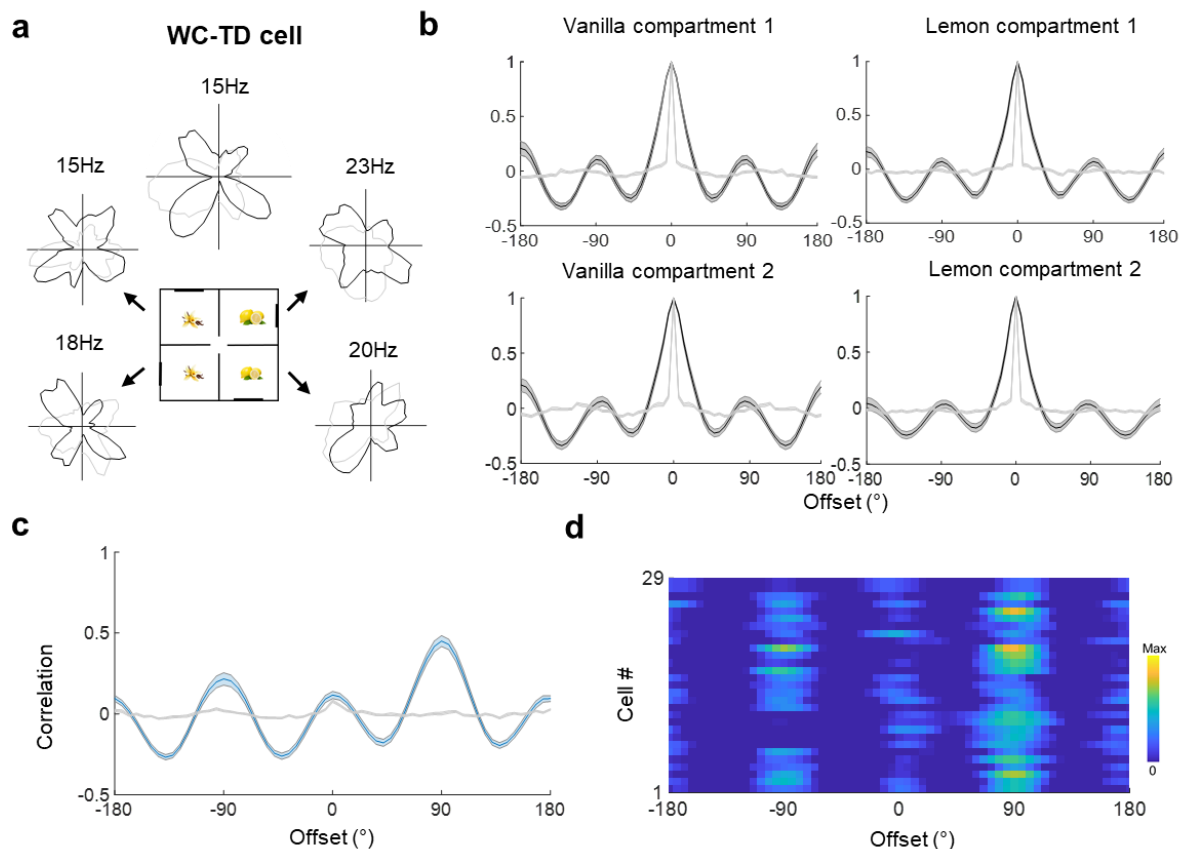


Figure 4-9. Multiple directional firing symmetries (WC-TD) in the 4-box. a. Schematic of the 4-box baseline and an example WC-TD cell (top). **b-d.** analyses as in Figure 4-8. Note that auto-correlograms (b; grey) of the within-compartment firing and the cross-correlations (c; blue) between compartments show four peaks in 90° offset for the WC-TD cells. The correlations were significantly different from the shuffle control. The heatmap (d) was sorted by angle-quadrupled Rayleigh vector lengths, with maximum at the top.

Cross-correlograms of tuning curves from adjacent sub-compartment pairs significantly differed from a shuffle (**Figure 4-9c-d**; KStest, $D = 0.47, p <.001$) and peaked at $\sim 90^\circ$, circular v-test against 90° : $V = 13.69, p < .001$). The third group (29/67, 43%) lost directionality and remained unclassified in the sub-compartments. In all findings, cells with only two or three peaks were rarely seen in the whole 4-box. Moreover, in all results I did not see any cells that were directionally stable across similarly-scented sub-compartments but that rotated between lemon and vanilla. This indicates that there was no hierarchy of sub-compartment encoding.

4.3.1.3 Unidirectional and non-directional pattern in the 1-boxes

Having established that cells could express twofold and fourfold symmetric patterns, I then looked at the two onefold conditions (1-boxes), which were run before and after the multicompartment trials, to see whether there would be either singlefold tuning or no directional tuning at all. For cells that were BD in the 2-box, in the open arena (**Figure 4-10**), the correlation between the two baselines significantly differed from the shuffle (KStest, $D = 0.63, p <.001$), showing above-chance directionality preserved in the 1-box (median Rayleigh vector length = 0.11). To quantify this preserved directionality, the area under the correlation curves between 1-box baselines was computed, representing the cell's directional selectivity, and compared with its shuffle control (the 95th percentile of the area computed from the shuffle). A KStest showed significant difference between the cell population ($n = 32$) and shuffle ($D = 0.44, p = 0.0028$). In the big arena, it was found that 15/32 cells passed this selectivity criterion (exceeded 95th percentile of shuffle control), showing a broad unidirectional pattern (area median = 1.07), and 17/32 lost directional specificity (**Figure 4-10d**).

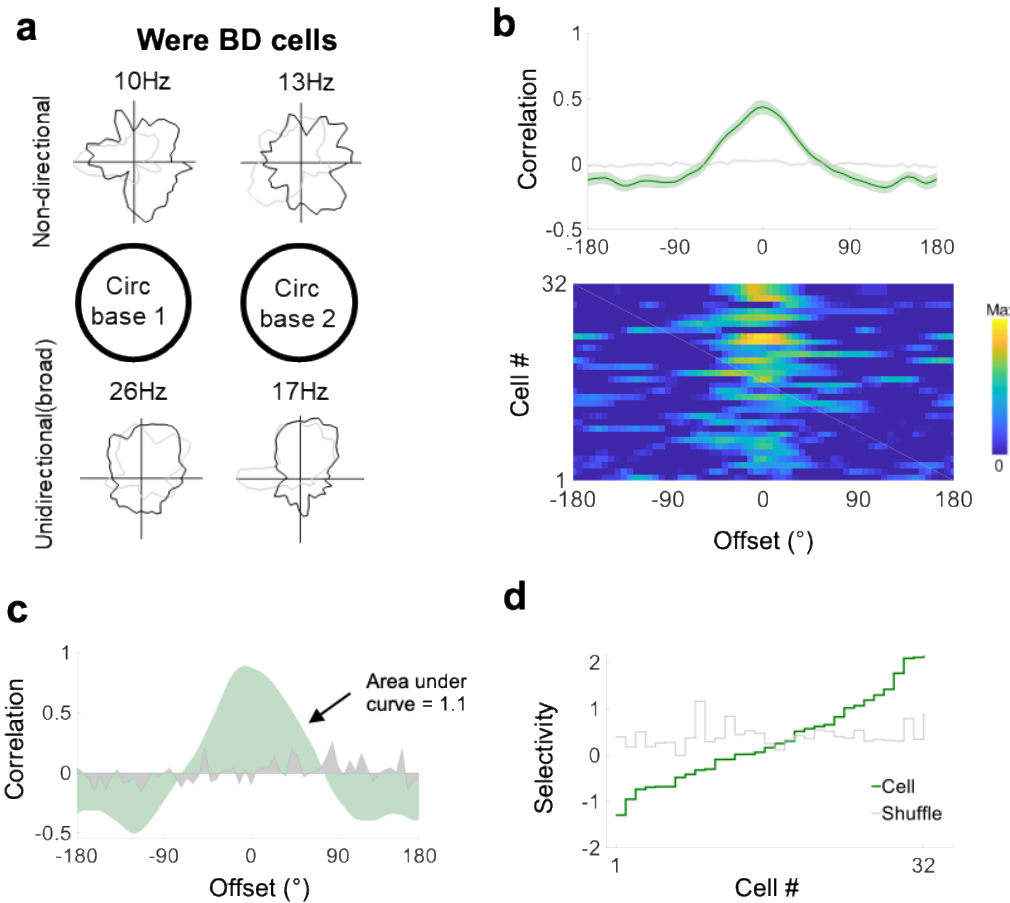


Figure 4-10. Directional firing symmetries in the 1-box (arena). Two BD cells **a-b**, in the 1-boxes; analyses as in Figure 4-5. Note the occurrence of onefold (0°) symmetries for the global pattern in both 1-box environments even if many cells lost directionality. The heatmap (from top to bottom) was sorted according to the cell's Rayleigh vector length (descending). Note the occurrence of onefold (0°) symmetries for the global pattern in both 1-box environments even if more than half of cells lost directionality. **c.** Area under correlation curve (green) of an example BD cell (the bottom in a) that showed broad unidirectional pattern in two trials and its shuffle (grey). **d.** Stair plot shows BD cell's area under curve (sorted by the value, green) and corresponding shuffle value (95th, grey). 15 cells had a value above the shuffle threshold: the green line is above the grey line.

Similarly, in the cylinder (**Figure 4-11**), as a population ($n=73$), the multidirectional cells' correlations between the two baselines was significantly different from shuffle (KStest, $D=0.67, p<.001$), indicating above-chance directionality preserved in the 1-box (median Rayleigh vector length = 0.12). As before, I compared the arena under curve of the cell to its shuffle control, and the KStest showed significant difference for the cell and shuffle (KStest, $D=0.62, p<.001$). I then looked at cells on cases-by-case basis: the majority of

multidirectional cells (49/73) became nondirectional but 24/73 (4 were BD; 20 were TD)

became unidirectional in the 1-box (area median = 0.96; **Figure 4-11d**).

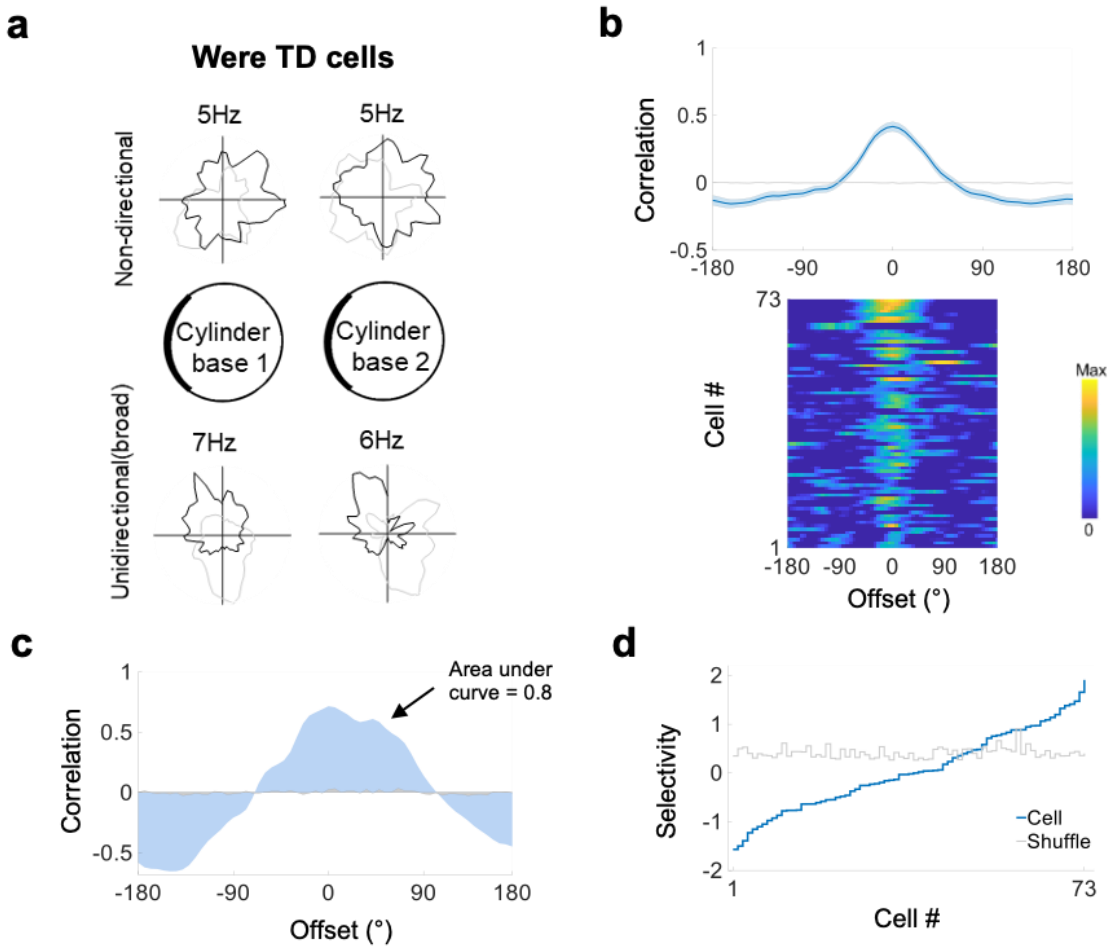


Figure 4-11. Directional firing symmetries in the 1-box (cylinder). a. two TD-pattern cells in 1-boxes; b-d. analyses as in Figure 4-10. In b, the heatmap (from top to bottom) was sorted according to the cell's Rayleigh vector length (descending). Note some occurrence of onefold (0°) symmetries for the global pattern in both 1-box environments at the top. An example broad singlefold tuning is shown in c. In d, most multidirectional cells lost directionality ($n = 49$), as evidenced in their values (blue line) being below their shuffled threshold (grey line).

Even if some multidirectional cells showed singlefold firing pattern in the 1-box, the next question is – is the onefold pattern comparable with the unidirectional pattern of classic HD cell, in terms of their peak firing rate, tuning width, and Rayleigh vector length? To answer this question, during some recording sessions, two extra cylinder trials were added following the cylinder baseline to collect more data stable across trials. In total, it was found that 19 multidirectional cells (TD, $n = 15/43$; BD, $n = 4/9$) maintained a consistent

unidirectional pattern in all three successive 1-box trials (had Rayleigh vector length above shuffle control in all three cylinder-trials, indicating highly stable onefold pattern; **Figure 4-12a**). Although unidirectional, the tuning curve characteristics of the multidirectional cells were significantly different from that of HD cells ($n = 19$): their Rayleigh vector lengths, although higher than their shuffle control, were significantly lower than the HD cells (**Figure 4-12b**; Multidirectional: median = 0.21; HD: median = 0.59; Wilcoxon rank-sum $Z = -4.34$, $p < .001$). This was also the case for peak firing rate (Multidirectional: median = 8.91Hz; HD: median = 21.35Hz; $Z = -2.95$, $p = 0.003$), and tuning width (Multidirectional: median = 143.99°; HD: median = 102.98°; $Z = 4.38$, $p < .001$).

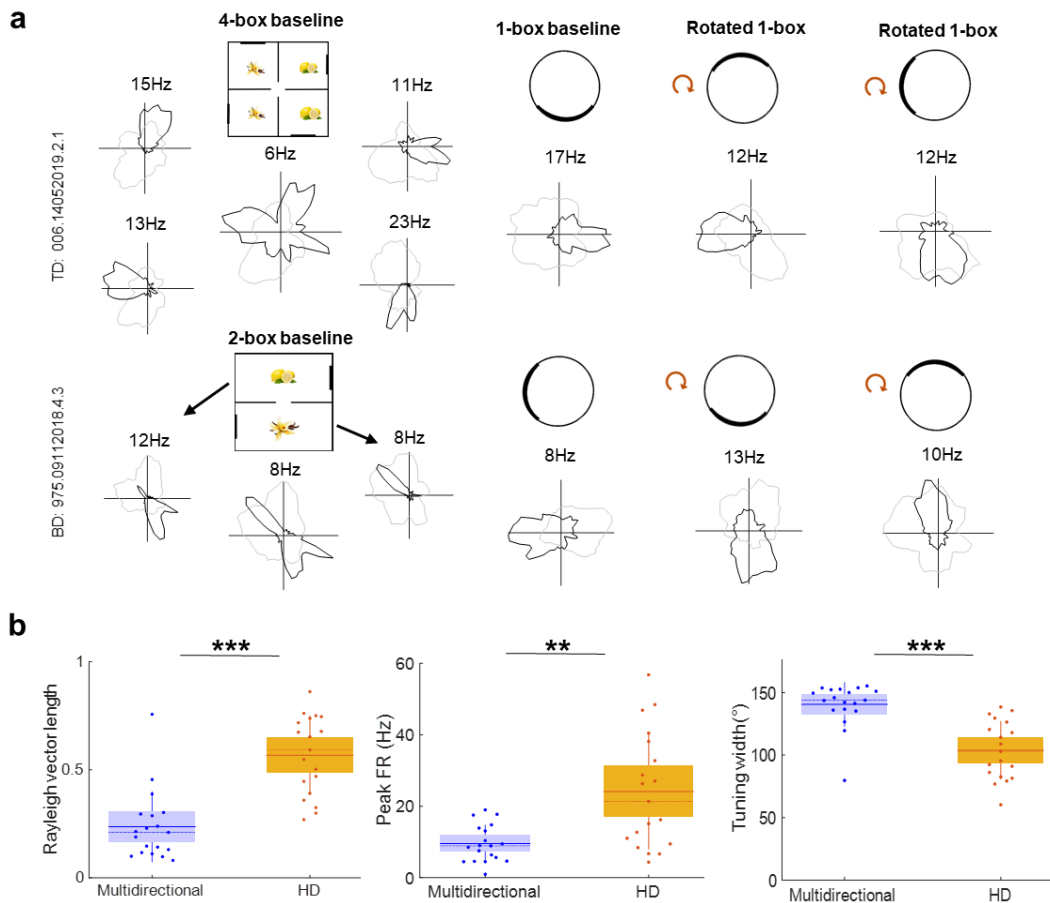


Figure 4-12. Onefold directional firing symmetry in the 1-box. **a.** Examples of one TD-pattern (top) cell and a BD-pattern cell (bottom) in the multicompartmented box baseline (sub-compartment tuning curves were also shown), 1-box baseline and two extra trials, the rotation mark denotes that the 1-box orientation was different from the baseline. Note that these multidirectional cells showed unidirectional pattern in the 1-box and the preferred firing directions followed the cue rotation. **b.** Box plots show directional tuning characteristics of 19 multidirectional cells (15 TD-pattern and 4 BD pattern, violet) compared with 19 HD cells (orange).

In summary, the results here show that the symmetry of multidirectional cell firing pattern follows the order of environment symmetry such as onefold (although some cells become zero-fold, i.e., nondirectional), twofold and fourfold. See **Appendix II** for more example cells from all seven trials in the two experiments.

4.3.2 Can a multidirectional pattern emerge from Day 1?

To further investigate whether the BD-pattern is an intrinsic firing pattern, I looked at whether the cells would show any hint of twofold symmetry in their pre-exposure trials in the 1 box. The activity of one TD-pattern cell and one BD-pattern cell was examined in the 1-boxes when the animal was naïve to the multicompartment environments. Although preliminary, the data showed that the multidirectional pattern was clearly absent in naïve animals in cylinder trials before exposure to the 2-box and the 4-box (**Figure 4-13**). In both cases, the multidirectional pattern emerged after a few minutes when the animals explored the whole environment. For the BD-pattern cell of a naive animal, although was not unidirectional in the 1-box, the inter-peak offset got stretched from 120° to 160° in the 2-box baselines. The offset was decreased again in the last cylinder baseline trial. This result strongly suggests a cue learning process in the multidirectional cells; that is to say, the cell could either develop other peaks or gain stronger response to the other peak by the influence of the landmarks. The Day 1 data also suggested that the pattern can be formed in the multicompartment boxes rapidly, further supporting that the multidirectional pattern was specific to environments with multi-fold symmetry.

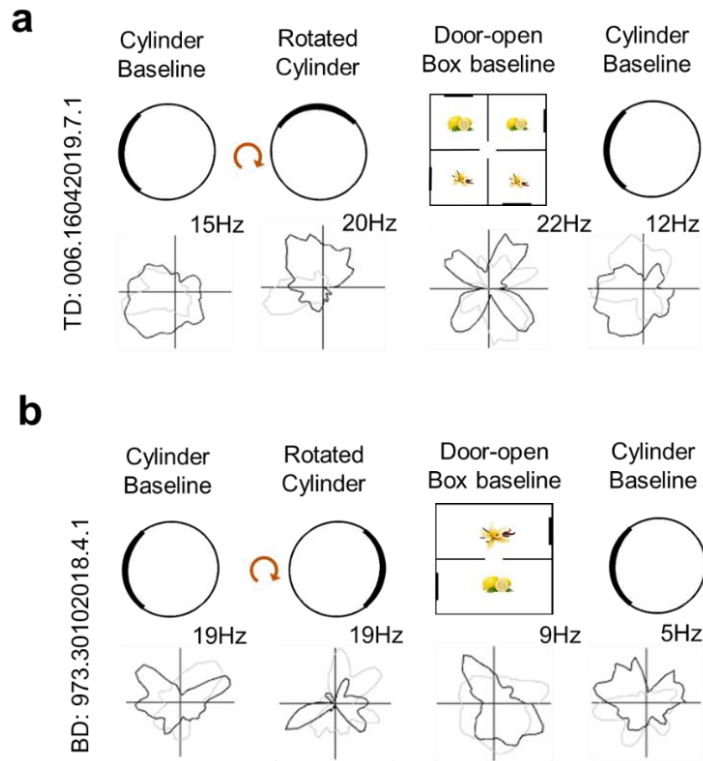


Figure 4-13. Multidirectional pattern can emerge in Day 1. **a.** The TD pattern was absent but broad unidirectional in the cylinder before and after the 4-box exposure. **b.** The BD-pattern cell showed the inter-peak offset decreasing to less than 120° in the cylinder trials, whereas the BD pattern was prominent in the 1st 2-box baseline trial.

4.3.3 Does the multidirectional pattern depend on geometry?

In order to examine whether geometric features such as corners contribute to the fourfold pattern formation, the activity of TD-pattern cells was further examined in a novel square box (**Figure 4-14**). Although the square box was polarised with a single cue card, the four corners that could also supply some directional references. However, the TD-pattern cells failed the criteria for TD cells (median TD score: -0.01; $t(5) = 0.06, p = 0.952$). It was found that the multidirectional cells lost the fourfold HD tuning pattern but reinstated it on return to the 4-box (**Figure 4-14a**). The results suggest that the fourfold firing pattern did not rely solely on geometric features such as corners. This also supports that the multidirectional pattern is unlikely intrinsic.

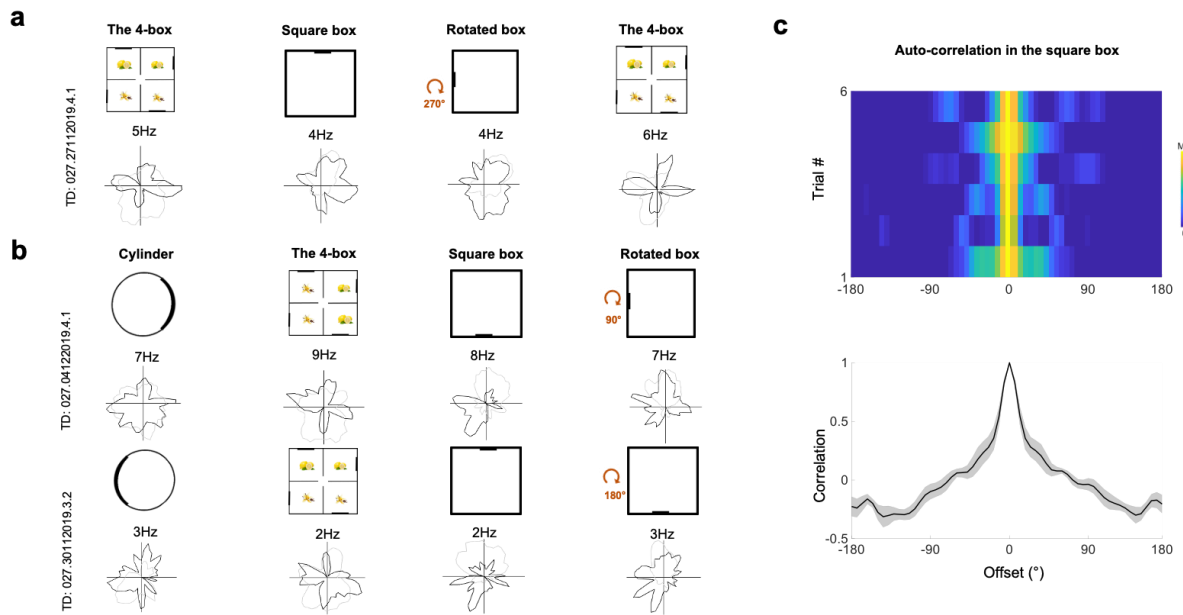


Figure 4-14. The TD pattern is lost in the square box. **a.** One TD-pattern cell was additionally tested and lost the pattern in two trials in the square box, then the TD pattern reappeared when the animal subsequently returned to the 4-box. **b.** Note that the TD specificity was disrupted in other environments except in the 4-box. **c.** The heatmap of the auto-correlograms of tuning curves in the square box trials, sorted by TD score, maximum at the top. The mean (grey) and SEM (shaded) are shown as a line below.

4.3.4 Do multidirectional cells fire in the dark?

Is the multidirectional pattern primarily dependent on vision? I also recorded the firing activity of 28 TD-pattern cells in the dark after the last 4-box baseline trial (**Figure 4-15**), finding that most TD-pattern cells ($n = 25$, 85.7%) maintained the four-way firing activity in the first dark trial, although only 64% of cells ($n = 16$) passed the threshold criteria in both dark trials.

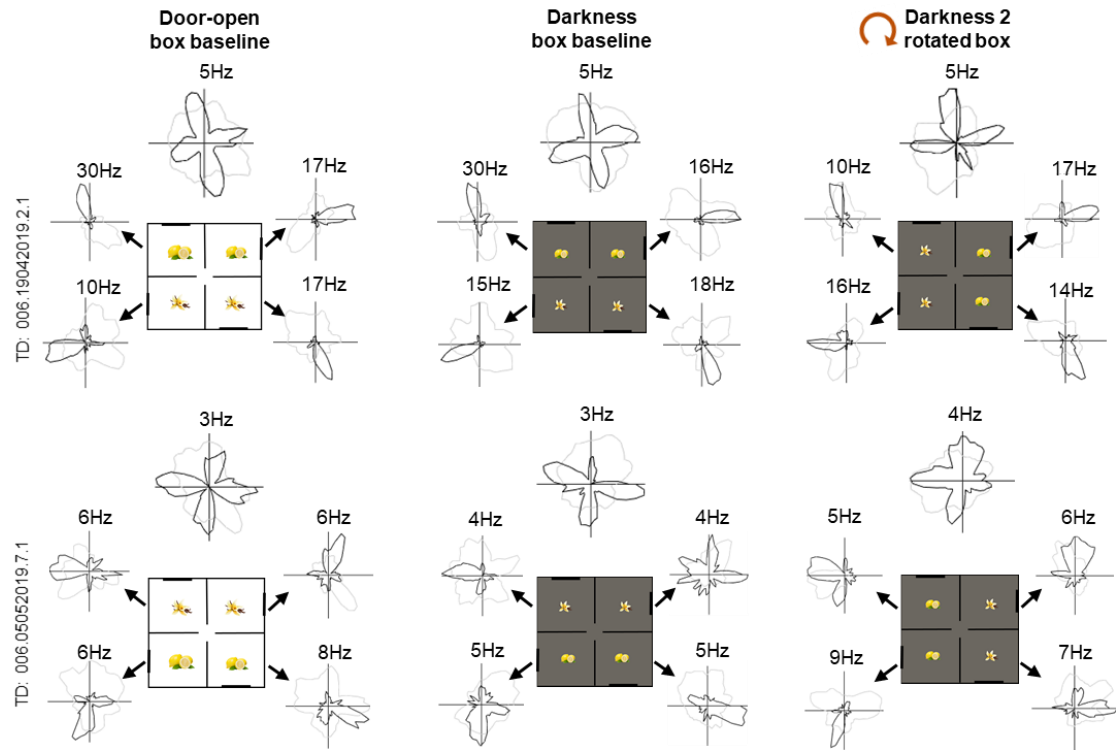


Figure 4-15. Example TD-pattern cells in darkness. Schematics of the 4-box trials and example of two TD-pattern cells that kept the four-way firing pattern in two darkness trials following the box baseline. Note that the animal was removed, mildly disorientated, and reintroduced to the apparatus before the dark trials started.

As shown in **Figure 4-16**, the TD score of the cells was reduced in darkness, compared to those in light condition (significant difference between light vs. dark1: t-test, $t(27) = 2.51, p = 0.018$). The TD score was decreased further in the second dark trials (significant difference between dark1 vs. dark2: $t(24) = 2.54, p = 0.018$). The directional specificity (Rayleigh vector lengths) was decreased from the light to dark condition but not between two darkness trials (repeated-measures ANOVA: $F(2,78) = 3.36, p = 0.04$; t-tests: significant difference between light vs. dark 1, $t(27) = 4.35, p < .001$; non-significant between two dark trials, $t(24) = -0.52, p = 0.61$). The findings suggest that reduced visual information of darkness might affect the reliability of direction encoding to some extent but not drastically.

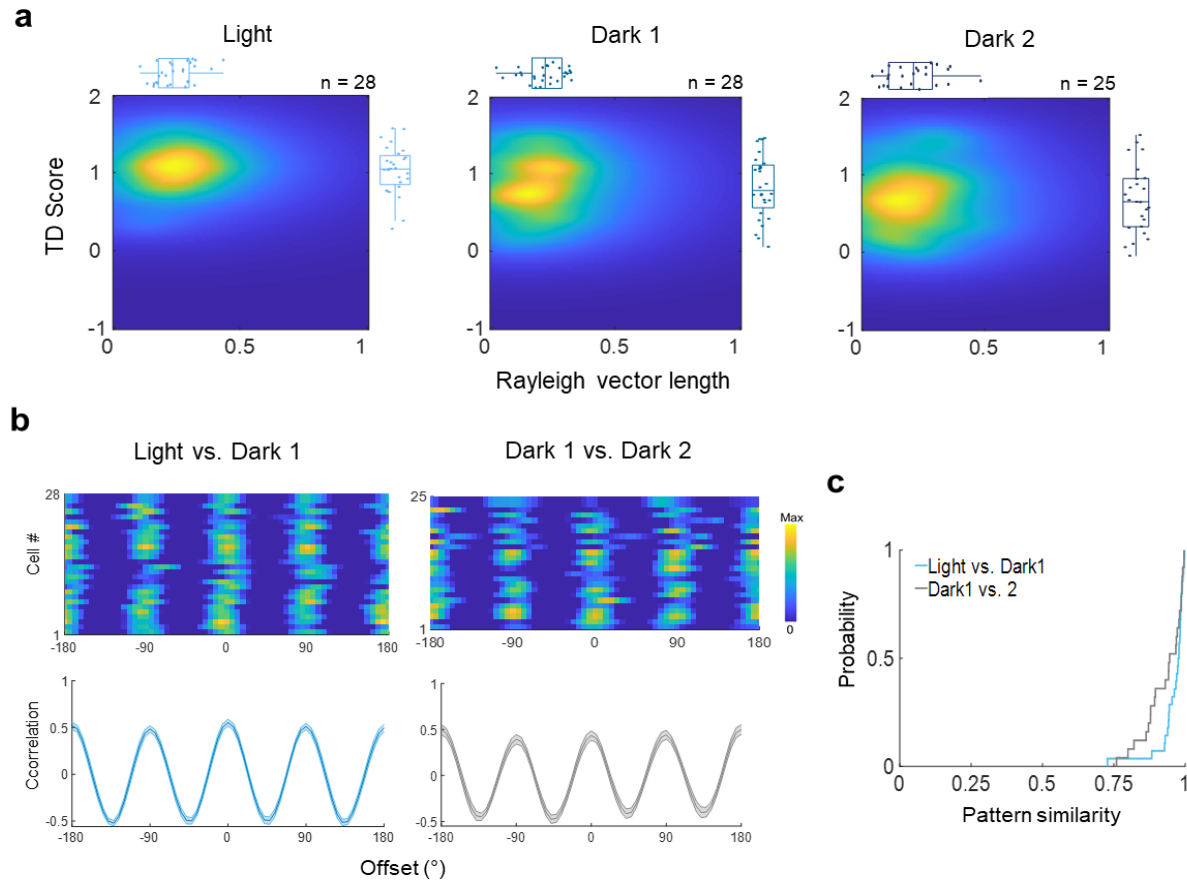


Figure 4-16. Preserved but reduced TD pattern in darkness. **a.** Density and box plots showing distribution of TD scores as a function of Rayleigh vector length in light (1st box baseline) and two dark trials. **b.** Cross-correlograms of tuning curves in light vs. dark 1 (left) and two dark trials (right). The population mean was plotted as the solid line, with shaded area denoting the SEM. **c.** Related to b, the level of (periodic) pattern similarity in light vs. dark 1 comparison (blue) and in two dark trial comparison (grey) respectively.

Nonetheless, the fourfold pattern, although decreased from the light condition, was generally preserved in the dark. The population means computed from the two cross-correlograms (light vs. dark1; dark1 vs. dark2) were not significantly different (**Figure 4-16b**; KStest, D = 0.165, $p = 0.142$). Furthermore, the fourfold pattern similarity between light-dark trials was not significantly higher than dark-dark trials (see **Methods**; **Figure 4-16c**; Wilcoxon rank-sum, Z = 1.49, $p = 0.137$). Persistent firing of the BD-pattern in darkness was reported in the 2-box (Jacob et al., 2017). Due to the technical difficulties in obtaining these types of cells in the first exposure, it was not practical to start recording the cells from complete darkness at the start. Together with the findings from that study, the

present results suggest that the multidirectional cells were not solely dependent on vision, and multimodal information could maintain HD tuning of these cells, possibly through path integration.

4.3.5 Do the classic HD cells remain unidirectional?

In addition to the bi-and tetra-directional pattern firing patterns, it was found that the canonical directional cells expressed the classic HD cell pattern of globally stable unidirectional tuning in both experiments (rats, $n = 6$; cells, $n = 27$; 5.6% in the 2-box experiment; rats, $n = 8$; cells, $n = 75$, 11.4% in the 4-box experiment). To be more precise, if they are classic HD cells, they should show a consistent unidirectional firing pattern across sub-compartments. As expected, the preferred firing directions did not shift between single sub-compartments and remained the same relative to the global layout (**Figure 4-17**; correlation coefficients peaked only at 0° offset, circular v-test: $V = 100.69, p < .001$). The results were consistent with previous findings of the canonical HD cell activity in RSC, ADN and PoS in the 2-box (Jacob et al., 2017).

Furthermore, in the 4-box experiment, unidirectional HD cells and TD-pattern cells were simultaneously recorded (**Figure 4-18**). The result clearly showed decoupled directional firing patterns of the two direction codes in the fourfold symmetric environment, as in the 2-box (Jacob et al., 2017). Thus, the finding also supported that the multidirectional pattern was not simply due to any non-controlled movement correlates (i.e., stereotyped sampling) in the complex environments.

Together, the TD-pattern and BD-pattern cells are henceforth collectively referred to as multidirectional cells. I compared the electrophysiological properties between the two types of directional codes in **Chapter 6**, where a table containing details of contribution by

individual animals is available. A summary of number of cells of each cell type recorded from two experiments, including different environment type and conditions can be found in **Table 4-1** below.

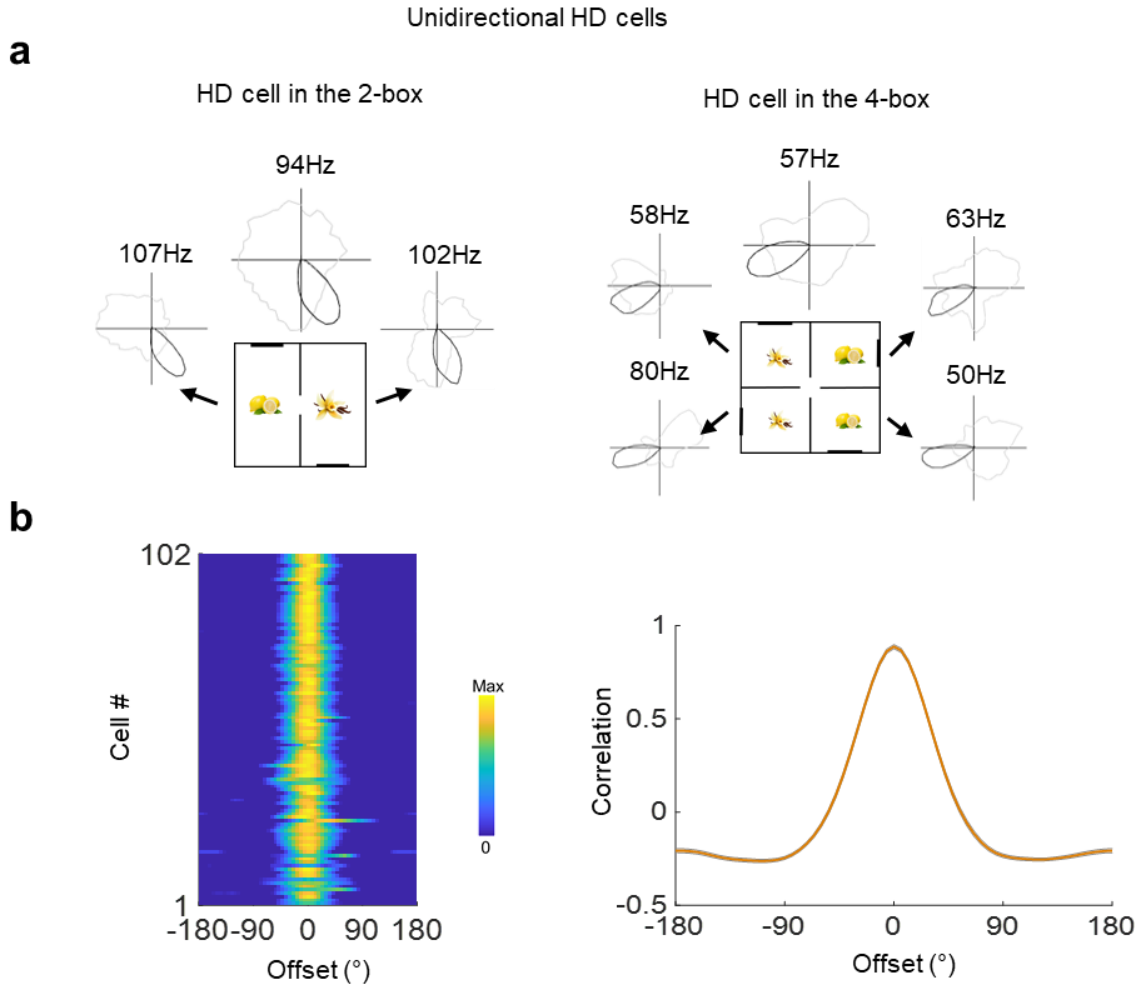


Figure 4-17. Classic HD cells showed a unidirectional firing pattern. a. Unipolar directional tuning curve of an example HD cell in the 2-box (left) and another HD cell in the 4-box (right). **b.** Analysis as in Figure 4-5, population ($n = 102$) tuning curve cross-correlation between different sub-compartments, as shown as a heatmap (sorted by the Rayleigh vector lengths, max at the top) and a line (mean and SEM).

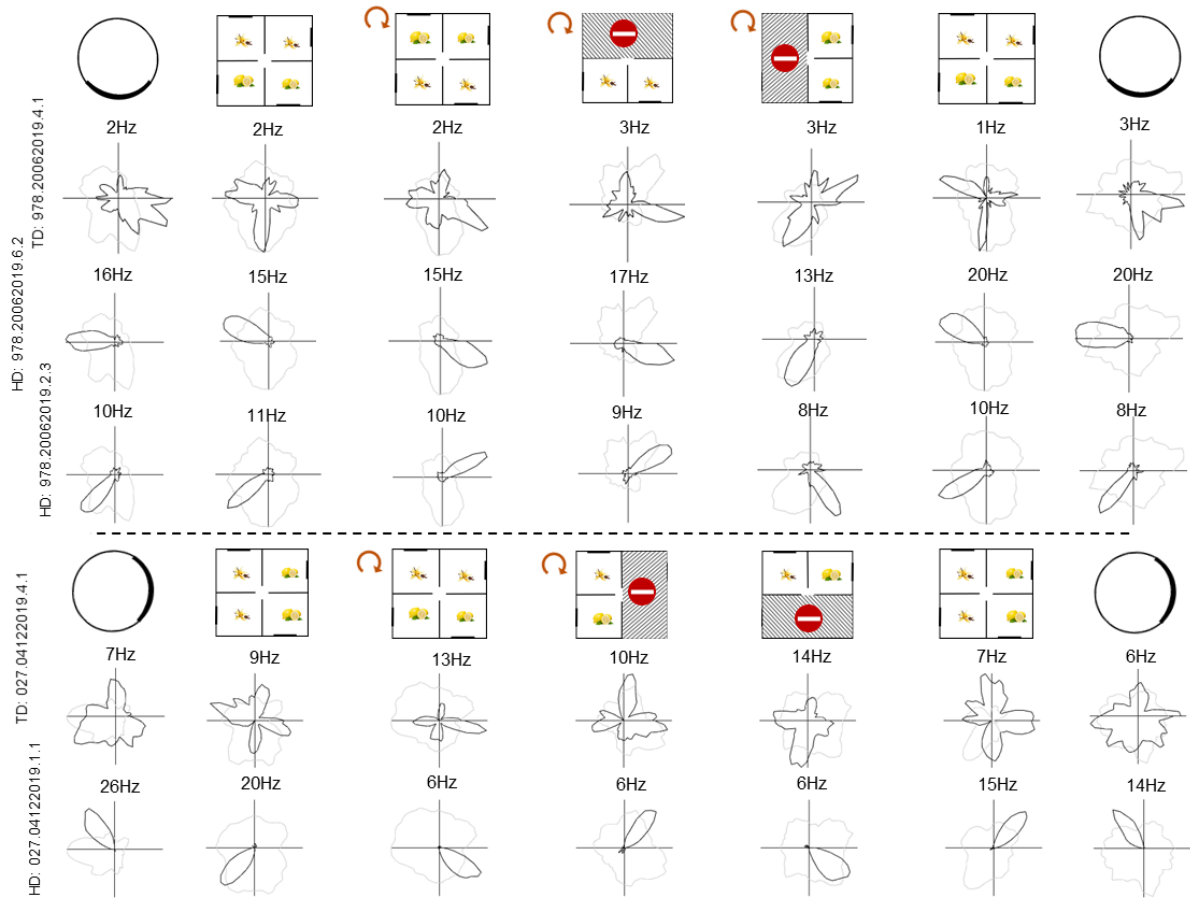


Figure 4-18. Co-recorded HD cells and multidirectional cells in the 4-box experiment.
Examples of one TD-pattern co-recorded with two HD cells in one session (upper), and another TD-pattern cell co-recorded with an HD cell in a different recording session (bottom). Simultaneous recordings of the HD cell and the TD-pattern cell reveal dissociation in direction encoding of the two groups. This strongly supports that directional encoding of the cells is unlikely due to simply movement-related factors of the animal during recordings.

Table 4-1. Summary of cell types recorded from different environments.

Apparatus	Trial type	Trial duration	Total n cells	Cell type			
				Multi-directional	Uni-directional broad	Uni-directional narrow	Non-directional
				(HD cells)			
4-box	Door-open	16 min	660	TD: 67	-	75	518
	Darkness*	16 min	28	TD: 28	-	-	9
2-box	Door-open	10 min	478	BD: 48	-	27	403
1-box (cylinder)	Baseline	8 min	148	Were** TD: 65	20	75	45
				Were BD: 8	4		4
	Rotated	8 min	70	Were TD: 43	15	19	28
				Were BD: 8	4		4
1-box (arena)	Baseline	10 min	59	Were BD: 32	12	27	20
1-box (square)	Baseline	10 min	5	Were TD: 3	2	2	1
	Rotated	10 min	5	Were TD: 3	2	2	1

*28 TD-pattern cells had at least one darkness 4-box trial, and 25/28 had a second rotated box darkness trial.

** “Were” refers to the firing pattern in the preceding 4-box or 2-box.

4.4 Discussion

The main findings of the two experiments showed that RSC neurons express a multi-directional code that reflects the rotational symmetries of the environment. The firing pattern of the cells follows concordantly with symmetry order: a pronounced TD pattern (four peaks in a 90° offset) in the fourfold symmetric 4-box and a BD pattern (two peaks in a 180° offset) in the 2-box, and the number of tuning peaks and inter-peak angular offsets changed accordingly in door-closed box conditions. In addition to classic HD cells that have a unitary global directional tuning, the reported noncanonical “multidirectional” cells had onefold-symmetric tuning in a single sub-compartment of the multicompartiment box but multi-fold tuning globally, while others also expressed multi-fold symmetry locally, providing an instantaneous readout of the global symmetry from within each of the sub-compartments. The results are interpreted briefly in the result sections and discussed below by relating to the first two hypotheses. A more in-depth discussion is presented in **Chapter 7.**

4.4.1 The BD-pattern was unlikely to be intrinsic to RSC cells

First, the main findings refuted the first hypothesis that the BD-pattern is intrinsic to the cells. This was evident in the following: a) the BD pattern established in the 2-box did not persist outside the twofold-symmetric environment, such as in onefold and fourfold environments; b) four animals that had experiences in both experiments, of which three not only showed a BD-pattern while tested in the 2-box, but also yielded 15 TD cells in the 4-box. Moreover, it has been found that in Day 1, the multidirectional pattern was absent in naïve animals before exposure to the multicompartiment environments – suggesting that learning happens rapidly. These findings strongly supported our view that the multidirectional pattern is driven by the environment, rather than being a built-in feature of the cells. Otherwise, one would expect to

see the twofold symmetric firing pattern across environments regardless of the symmetry order.

However, it should be noted that data from naive animals are still preliminary (section 4.3.2). Due to the low proportion of the multidirectional cell distributed in RSC (10%) and their environment-dependent firing, it is particularly challenging to successfully track the ‘multidirectional’ cell activity from the 1-boxes to the multicompartment environments from the first recording day. During screening in the 1-box, without knowing whether a cell would become multidirectional in the 2-box or 4-box, the experimenter had to ‘guess’ the outcome, and then decide whether to record in the multicompartment environment at a cost of animal’s exposure; and if the cell did not pass the criteria in the multicompartment box (which was usually the case), the one-shot chance was lost. Thus, only two of the multidirectional cells passed the criteria in Day 1. Although they are unlikely to be intrinsically multidirectional in the 1-boxes, it is inconclusive whether the cells have any form of intrinsic pattern, such as the broad onefold pattern observed in the 1-boxes.

4.4.2 The multidirectional firing symmetry followed the environment symmetry order

Having replicated previous findings in the 2-box (Jacob et al., 2017), the present results reported the between-compartment BD pattern (i.e., globally BD) and within-compartment BD pattern (i.e., locally BD) in the 2-box. Similarly, in the 4-box experiment, both global and local tuning curve symmetries of the same order (fourfold) were found. Furthermore, the multidirectional cells become either singlefold (unidirectional) or zero-fold (nondirectional) in 1-boxes. The results clearly illustrate a dominant effect of the environment symmetry in driving the firing symmetry, supporting the second hypothesis.

Importantly, the carryover of the global symmetry into a single sub-compartment reflected some kind of plasticity process, in which the local directional information specified

by visual landmarks possibly is hypothesised to be mapped onto the global HD network (Page and Jeffery, 2018). That model predicted that the BD pattern would become tri-directional in a trifold-symmetric environment but that the directional specificity would break down with higher symmetries. Thus, it was slightly surprising that the empirical cells indeed expressed a fourfold-symmetric tuning and exceeded a proposed theoretical threshold (Page and Jeffery, 2018). This point is further discussed in **Chapter 7**.

Rather than a simple sensory-based encoding, the present findings support a learning perspective of the RSC cells in encoding multisensory environmental cues; that is, the multidirectional pattern is acquired through experience in multi-fold environments that comprise multiple landmarks and symmetric structures. This is particularly evident in the observation of retention of the multidirectional pattern in the single sub-compartments in the 2-box and 4-box after experience. This point is further supported by the finding that a loss of the fourfold pattern in a simple square box (onefold), but the pattern was recapitulated when the animal returned to the 4-box (section 4.3.3). The latter result supports the notion that the fourfold pattern cannot be formed simply due to low-level geometric features of the box.

Furthermore, the multidirectional code was not purely sensory-dependent. It was evident that the firing pattern did not depend entirely on visual inputs, as TD-pattern cells generally maintained the pattern in darkness, as did the BD-pattern cells of Jacob et al. (2017). Although it should be noted that it was unclear whether the cells would emerge in darkness. The results supported the notion that multimodal information helps maintain directionality. Additionally, decoupled HD tuning in simultaneously recorded multidirectional and HD cells suggests that the direction encoding was independent of merely locomotion correlates. Otherwise, the same behavioural sampling would have produced the same HD tuning of cells. Nevertheless, the reduced directional specificity observed in dark

trials suggests that vision, although not necessary, may be crucial in registering the initial sense of direction, as directional information is most appropriately conveyed through stable and salient cues (Knierim et al., 1995), and visual landmarks could recalibrate errors accumulated through path integration (see previous chapters).

4.4.3 Interim summary

In summary, in addition to the BD pattern observed in the 2-box, the study found a novel directional firing pattern – a fourfold firing pattern of RSC cells recorded when animals freely foraged in a fourfold symmetric environment. The BD-pattern and TD-pattern cells share a high degree of similarity in terms of their function and properties and are thus considered as multidirectional cells. Further support of this point is presented in **Chapter 6**. Thus, the findings strongly supported that the multi-directionality is a product of the environment symmetry, rather than intrinsic properties of the cell. This means that one may be able to decode the environment symmetry from the cell activity, even from subspaces of the whole environment. It reflects high flexibility of the system.

What contributes to the pattern formation? Briefly (see detailed discussion and proposed model in **Chapter 7**), it is believed that it arises from the environment layout, from which the multidirectional cells learn to encode environment symmetry. Therefore, these cells have the capacity to report on the symmetry and orientation of both the current compartment (via the unidirectional tuning curves) and the global space. Possibly via interacting with the classic HD cells, these cells provide environment-driven directional signals to the network (Page and Jeffery, 2018). This nested symmetry-encoding may play a key role in cognitive mapping of complex spaces in RSC. The data presented in this chapter have supported this hypothesis, although another possibility such as egocentric coding needs to be excluded to reach a full conclusion; see the extended analyses in the next chapter.

CHAPTER 5

CHAPTER 5 RETROSPLENIAL MULTIDIRECTIONAL CELLS ARE NOT EGOCENTRIC

5.1 Introduction

In **Chapter 4**, recordings from rat RSC in two experiments showed that the multidirectional cells encode multiple head orientations in different symmetric environments: two opposite directions in the 2-box and four directions in the 4-box. The data were analysed in allocentric reference frames by considering each animal's navigational information (path and heading) relative to a static spatial environment. The findings suggest that the multidirectional pattern was unlikely to be an intrinsic property of the retrosplenial cells but is driven by environment symmetries.

Multiple environmental components such as visual landmarks, boundaries and other geometric features define environment symmetry. For example, in addition to four visual landmarks, the 4-box also contains multiple corners and four inner walls. Borders were shown to modulate post-subiculum HD cell activity relative to an animal's egocentric positions in a square box (Peyrache et al., 2017). How might the HD pattern look in its neural representation of border-related features? Do multidirectional cells encode any of these features egocentrically (i.e., referenced to the animal)? To be able to fully support the previous hypothesis (Hypothesis 2 of the thesis) that the cell's multidirectional pattern is primarily driven by head direction encoding in symmetric environments, other possibilities need to be considered, such as whether the cells encode any egocentric boundary relationships.

The egocentric boundary coding property has been reported in a number of brain regions (see section 1.4.4 in **Chapter 1**; see detailed review by Wang et al., 2020; Bicanski

and Burgess, 2020), including the RSC (Alexander et al., 2020). This type of cell, known as an egocentric boundary vector cell (EBC), has been shown to respond specifically to physical boundaries found at a given distance and angle from the animal's travelling direction (or head direction) in an egocentric reference frame: for instance, a boundary to the animal's left or right. Moreover, also in RSC, another study (van Wijngaarden et al., 2020) recently reported egocentric border cells that increase firing near boundaries proximal to the animal. These studies revealed that RSC is part of the border-encoding neural circuit.

In particular, Alexander et al. (2020) reported that the structure of head direction tuning in RSC EBCs differs in the square box and circular arena: the alignments of HD tuning to the box walls were absent in the circular arena. The authors suspected that such a difference in HD tuning arises because the firing of EBCs in nature would be restrained by any two walls that are orientated in 90°-rotation along the allocentric axes. They thus proposed a tentative interpretation of the BD-pattern data of Jacob et al. (2017), specifically suggesting that “The bimodal directional tuning … may arise from constrained egocentric sampling along two axes as a consequence of the multicompartment environment segmenting two opposing walls.” This speculation implies first that there might be a substantial but unexplored relationship between the twofold allocentric directional pattern and egocentric boundary encoding; and second, that the cells reported by Jacob et al. (2017; and relatedly, multidirectional cells in this thesis) might be EBCs.

Thus, these speculations form two hypotheses that concern a). the relationship between the geometric features such as boundary arrangement or inner segmentation and HD tuning of EBCs; and b). the relationship between the RSC multidirectional cells and EBCs. The first hypothesis to be examined here is: the allocentric HD tuning pattern of EBCs could in principle arise from environmental boundary and geometric constraints on the cell's

encoding of egocentric boundary relationships; and the second hypothesis is: are multidirectional cells EBCs?

Specifically, regarding the first hypothesis, what pattern of HD tuning would the EBCs yield in the current environmental set-ups? According to Alexander et al. (2020), first, the EBC population is expected to yield four peaks along the walls in the square box, although the authors commented that it was not always the case (see their Figure 5A), and the proportion was not reported; multiple peaks should vanish in the circular arena. Second, the EBC population is expected to show a bimodal pattern in the 2-box, possibly because of the two opposing inner walls. Third, as with a square box, an EBC is thus predicted to show a tetradirectional tuning pattern in the 4-box that consists of four inner walls. These predictions were tested in this chapter.

It is clear that the predictions listed above would imply firing patterns that resemble the HD pattern reported in the RSC multidirectional cells (**Chapter 4**). Accordingly, the second hypothesis importantly concerns whether the recorded RSC multidirectional cells are EBCs and show boundary related tuning characteristics? If the cells are indeed an independent population from the EBCs and primarily encode truly allocentric head direction orientations, they should not pass the criteria for EBCs and should show characteristics distinct from the EBCs.

Three approaches were taken to test these two hypotheses. To examine the first hypothesis: a population of simulated EBCs that shared similar features with the biological RSC EBCs (Alexander et al., 2020) were generated from a computational model. The simulation not only validated the EBC detection methods reported previously (Hinman et al., 2019; Alexander et al., 2020) in the current environmental set-ups, but also produced datasets

for analyses to be applied such as the directional symmetry analyses used in Chapter 4. This validation is critical to confirm the robustness of the analysis methods.

To test the second hypothesis, I examined the recorded directional cells' firing properties in egocentric reference frames using the validated methods. Other spatial features including the spiking preference to boundaries of the cells were compared with the simulated EBCs.

5.2 Methods

5.2.1 Animals

The recorded data presented here are from 18 rats, the same sets as described in the previous chapter.

5.2.2 Experiment design

In order to test whether the methods that others used (Hinman et al., 2019; Alexander et al., 2020) are robust in detecting potential EBCs in the current experimental set-up, especially the 2-box and 4-box that comprises complex boundary arrangements, I (in collaboration with Roddy Grieves) first conceived a simulation computational model to produce a dataset of simulated units that encode EB relationships. Then, after the units were generated from the simulation, I applied the same analysis methods and criteria (as described in section 5.2.3 below) first on the simulated data to select significant EBCs, and then to the recorded cells. The egocentric analyses were applied to cell activity in the 1st baseline trials while the animal was freely foraging in the 1-boxes, 2-box and 4-box.

5.2.3 Egocentric cell simulation modelling

To obtain a large EBC dataset, a simulation model was designed to produce EBCs that acquire similar egocentric boundary encoding characteristics with the real cells in RSC (Alexander et al., 2020). A schematic of the simulation is shown in **Figure 5-1**. Intuitively, the activity of an EBC at a specific time point was calculated as the product of two weighting functions: the first is a Gaussian that weights walls at the cell's preferred distance highly and other walls low, and the second is a von-Mises function that weights angles around the cell's preferred angle highly and other angles low. The product of these two is high only when an intersection is at both the preferred egocentric distance and angle to the agent. Lastly, spike times were simulated for each cell by normalising and rounding the results of $f(t)$ and assigning that many spikes to the corresponding position time point t .

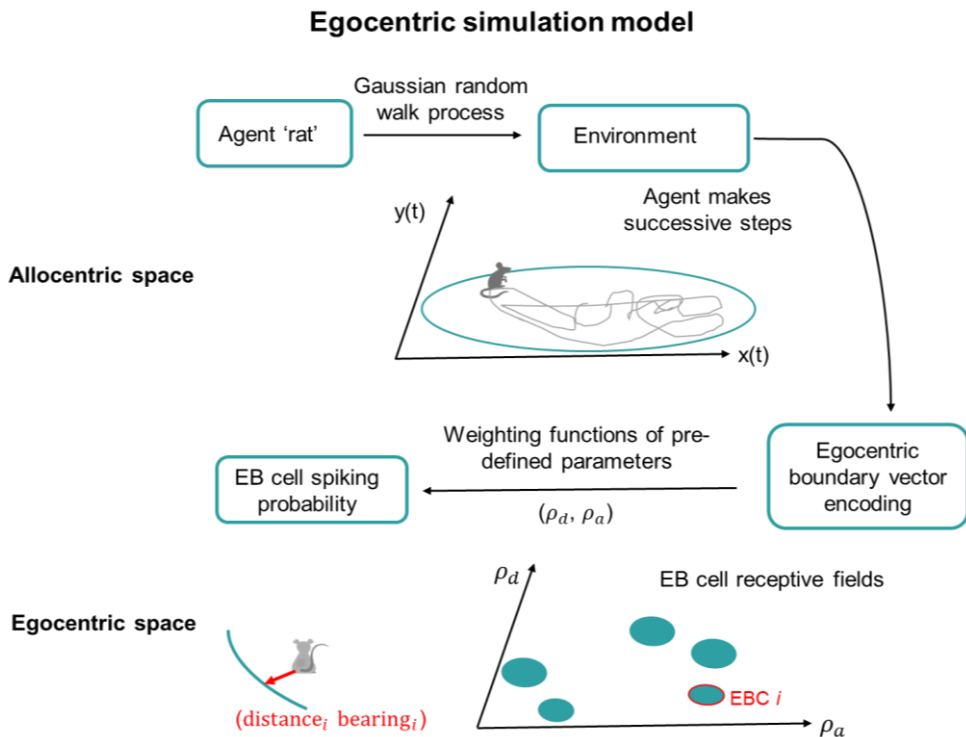


Figure 5-1. Schematic flow of egocentric boundary vector cell simulation.

In the allocentric space, the model simulated an agent's random walk paths (grey line) in different environments. The agent explored each type of environment (i.e., the circular arena, square box, 2-box and 4-box) for 10 minutes, position and head direction data in each environment were obtained. The behavioural sampling for different EB cells remained the same, ensuring that the cell's firing as well as its allocentric spatial correlates were only determined by egocentric parameters, rather than any non-controlled factors. In the egocentric space, the agent weighted its nearest physical boundaries differently according to pre-defined EB vectors (ρ_d, ρ_a), which decide cell's firing probability. The EB relationships varied between different cells.

After generating a pool of simulated cells ($n=1,000$) using the simulation methods described below, the same set of EBC selection criteria was applied to the simulated pool to check the model performance and then to the real cells.

5.2.3.1 Position data from random walk

To simulate rat exploratory and foraging behaviour in four environments (namely, the cylinder, 2-box, 4-box and the square box), a Gaussian random walk process was employed. The trajectories were different for each environment but remained the same for all cells generated from that environment. Each environment was recreated as a binary grid map, with a resolution of 0.5 cm, where 1's represented viable positions an animal could occupy and 0's represented walls, regions within 50 mm of the walls or other inaccessible areas. The agent started in the geometric centre of the environment with a random starting heading between $-\pi$ and π in radians. The agent then made successive steps through the environment, with each step representing one second of walk time. At each time point the agent's next position was calculated as:

$$g(x) = \operatorname{argmax} \left(\frac{1}{\sigma\sqrt{2\pi}} e^{\frac{-(D-\mu)^2}{2\sigma^2}} \times \frac{1}{2\pi I_0(\kappa)} e^{\kappa \cos(A - \alpha_{t-1})} \times occ \times d_w \times d_c \times m \right)$$

where D is the distance to every pixel in the grid map, $\mu = 48 + (-8, 8)$ cm (controlling the shape of the distance distribution). The distance sigma $\sigma = 48$ cm (the width of tuning relative to wall) is controlled by an exponential curve. The first σ controls the initial height of the curve (i.e., the smallest possible sigma) and the second controls the rate of slope (i.e., how quickly does tuning width expand with distance). I_0 is the modified Bessel function of order zero, A is the angle to every pixel in the grid map, α_t was the angular heading of the animal at time step t , κ is the concentration of the von-Mises distribution which was set to 1, occ is the total occupancy in each grid map pixel divided by the maximum value and subtracted from 1, m was the binary grid map, d_w and d_c are the distance to every pixel from

the nearest wall in the environment and the distance to every pixel from the centre of the environment respectively, Gaussian weighted according to:

$$f(x|\mu, \sigma) = \frac{1}{\sigma\sqrt{2\pi}} e^{\frac{-(x-\mu)^2}{2\sigma^2}}$$

For d_c , $\mu = 0$ cm and $\sigma = 150$ cm and the resulting values were rescaled by dividing by the maximum value. For d_w , $\mu = 0$ cm and $\sigma = 50$ cm and the resulting values were rescaled by dividing by the maximum value and subtracting from 1. Once $g(x)$ was found the Euclidean optimal route between the current and next point, avoiding obstacles (finding the best path between the current point the next point), was taken as the agent's path which was then up-sampled by a factor of 50. This was to match the 50 Hz positional sampling rate of our recording systems. Lastly, 50 mm random jitter was added to the raw position data to make the trajectories more realistic. Then the path was smoothed using an unsupervised, robust, discretized, n-dimensional spline smoothing algorithm (MATLAB function *smoothn*) (Garcia, 2011; Le Tarnec and Garcia, 2012).

5.2.3.2 EBC parameters and tuning curves

To simulate the firing characteristics of EBCs, each simulated cell was assigned with a preferred distance (ρ_d) which was drawn from a beta distribution with parameters $\alpha = 1$ and $\beta = 3$, truncated between 5 and 60 cm. This distribution was designed to match as closely as possible the one reported by Alexander et al. (Alexander et al., 2020; see their figure 1) for biological EBCs. We also assigned preferred angles (ρ_a) which were drawn from two von-Mises distributions with parameters $\mu = \pm 1.9199$ rads ($\pm 110^\circ$) and $\kappa = 10$. Again, these were designed to match as closely as possible the left and right-side bias reported by Alexander et al. (2020). Next, for each position sample t we calculated the activity of EBCs as:

$$f(t) = \sum \left(\frac{1}{\sigma\sqrt{2\pi}} e^{\frac{-(\beta_t - \rho_d)^2}{2\sigma^2}} \times \frac{1}{2\pi I_0(\kappa)} e^{\kappa \cos(\alpha - \rho_a)} \right)$$

where β is the distance to the nearest boundary at every egocentric angle, α are the egocentric angles at which β was measured, κ is the concentration of the von-Mises weighting function, which was set to 20, I_0 is the modified Bessel function of order zero and σ is the standard deviation of the Gaussian weighting function which was set to:

$$\sigma = 5e^{0.02\rho_d}$$

the exponent here was intended to reflect distance estimation inaccuracies as rats move away from the walls (Barry et al., 2006; Grieves et al., 2018). For α , every egocentric angle between 1.5° and 360° in 3° increments was used.

5.2.4 Egocentric spatial tuning analyses

The same set of analyses as described previously (Hinman et al., 2019; Alexander et al., 2020) was adopted. For each cell recorded in an environment, the animal's allocentric position data points were used to get the following: movement direction (current moving directions of travel, calculated by taking instantaneous derivative of successive position samples in the travelling path), the distance from a point to all environment boundaries by finding all possible surrounding boundaries in every time frame (20 ms), and the angle from a point to all boundaries (in 3° increments). The spiking activity over the animal's trajectories was colour-coded by the animal's movement directions.

- *Egocentric rate map:* To construct the two-dimensional egocentric boundary rate maps, angular bins were referenced to the current movement direction so that 0° was to the animal's front, 90° to its right, 180° to its back and -90° to its left. For every spike, its distance to the walls was computed within a range from zero to half of the length of the most distant possible boundary. The number of distance bins was 20,

and the distance bin size and the maximum possible distance varied adaptively for each type of environments due to different environment dimensions (e.g., 40 cm for the circular arena, 50 cm for the square box, 60 cm for the 2-box and 30 cm for the 4-box). For a given 2D bin, the number of spikes within that spatial bin was divided by the dwell time. Rate maps were smoothed using a 2D Gaussian kernel (width = 5).

- *Egocentric boundary tuning criteria:* The same methods and criteria used previously (Alexander et al., 2020) were applied. The mean resultant length (MRL) was computed as the measure of egocentric boundary directionality. The mean resultant was calculated as:

$$MR = \frac{(\sum_{\theta=1}^n \sum_{D=1}^m F_{\theta,D} \cdot e^{i*\theta})}{n \cdot m}$$

in which θ is the egocentric bearing to boundaries, D is the distance, $F_{\theta,D}$ is the firing rate in a given egocentric spatial bin, n is the number of orientation bins, m is the number of distance bins. Then MRL is calculated as the absolute value of MR. The mean resultant angle (MRA) is the preferred egocentric boundary orientation of a cell, which was calculated as:

$$MR \text{ angle} = \arctan2\left(\frac{\text{imag}(MR)}{\text{real}(MR)}\right)$$

The preferred egocentric boundary distance was calculated based on MR angle by fitting a Weibull distribution to the firing rate along the MRA. The distance bin with the maximal firing rate was taken as the preferred boundary distance. For a cell to be a significant EBC: the MRL would exceed 99th percentile of the shuffle, preferred distance would shift less than 50% in the 1st half vs. 2nd half of a trial and the MRA would shift less than 45° in the 1st and 2nd half of a trial. The above criteria

were applied to examine recorded directional cells and simulated cells (see section 5.3.2. for EBC simulation modelling) and calculated the proportion that passed all three criteria in different environments.

5.2.5 Boundary-related firing properties

To examine whether the cells show any preference of spiking in proximity to the wall or the centre of arena, boundary-related firing properties were characterised. The spiking preference index was calculated as:

$$\text{Preference index} = \frac{\text{Outer firing rate} - \text{Inner firing rate}}{\text{Outer firing rate} + \text{Inner firing rate}}$$

Specifically, the number of spikes emitted in the inner 50% area of an apparatus and the 50% area near the outer walls were computed. To normalise for the dwell time, the preference index was computed as the ratio of the difference in firing rates of a cell in vs. out of the 50% over the sum.

Notably, in real experimental recordings, the LED tracking of the animal was not available at the very edge of boundaries due to its snout. To minimise any potential confounds of boundary sampling in real data versus the simulation, the region 3 cm from the boundary was excluded when calculating the inner and outer firing rate for the real cell data. Nevertheless, a preliminary analysis without this exclusion did not show any difference in the results.

5.2.6 Head direction analyses

The same set of analyses on head direction tuning and directional firing symmetry were used as described in **Chapter 4**.

5.2.7 Statistical analysis

The same set of statistical analyses was used as described in the previous chapter.

5.3 Results

Multiple analyses were performed on two datasets. First, the EBC simulation results are presented, followed by HD tuning of the simulated EBCs in comparison with the recorded multidirectional cells. The results are presented in a similar way as in **Chapter 4**. Then, the multidirectional data analysed in egocentric coordinates are presented, and finally the results of spiking preference to boundaries.

5.3.1 Are simulated EBCs comparable to real ones?

The egocentric analyses used by others (Hinman et al., 2019; Alexander et al., 2020) were applied to the pool of simulated EBCs in four different environments to confirm the EBC detection methods (section 5.2.4).

First, the simulation model (**Methods**; **Figure 5-1**) produced a surrogate dataset containing 1,000 units with egocentric boundary vector tuning in environments of different levels of symmetry. When analysed using the established methods, significant simulated EBCs showed prominent egocentric boundary vector representations when a simulated rat randomly walked through the environment (example EBCs shown in **Figure 5-2**), and the EB tuning was stable in all four environments.

In total, 94% ($n = 940$) of the simulated cells were identified as significant EBCs, passing the criteria in all four environments (**Figure 5-3a**). Some cells that failed the criteria had their EB tuning fields close to the centre of arenas. A high proportion of significant simulated EBCs support the robustness of the analysis methods in detecting EBCs in symmetric environments. The simulated EBCs shared comparable tuning characteristics with

the RSC EBC firing properties (Alexander et al., 2020; as adapted in **Figure 5-3d**): the preferred distances were distributed close to the boundaries and the preferred bearings were concentrated on the left or right to the animal (**Figure 5-3b**, **Figure 5-3c**). The results of the simulated data confirmed the performance of the simulation model in generating EBCs and the robustness of the egocentric analyses. This means that if any occult EBCs exist in the recorded dataset, they should be detected and show similar EB tuning relationships consistently in different environments, as seen in the simulation data.

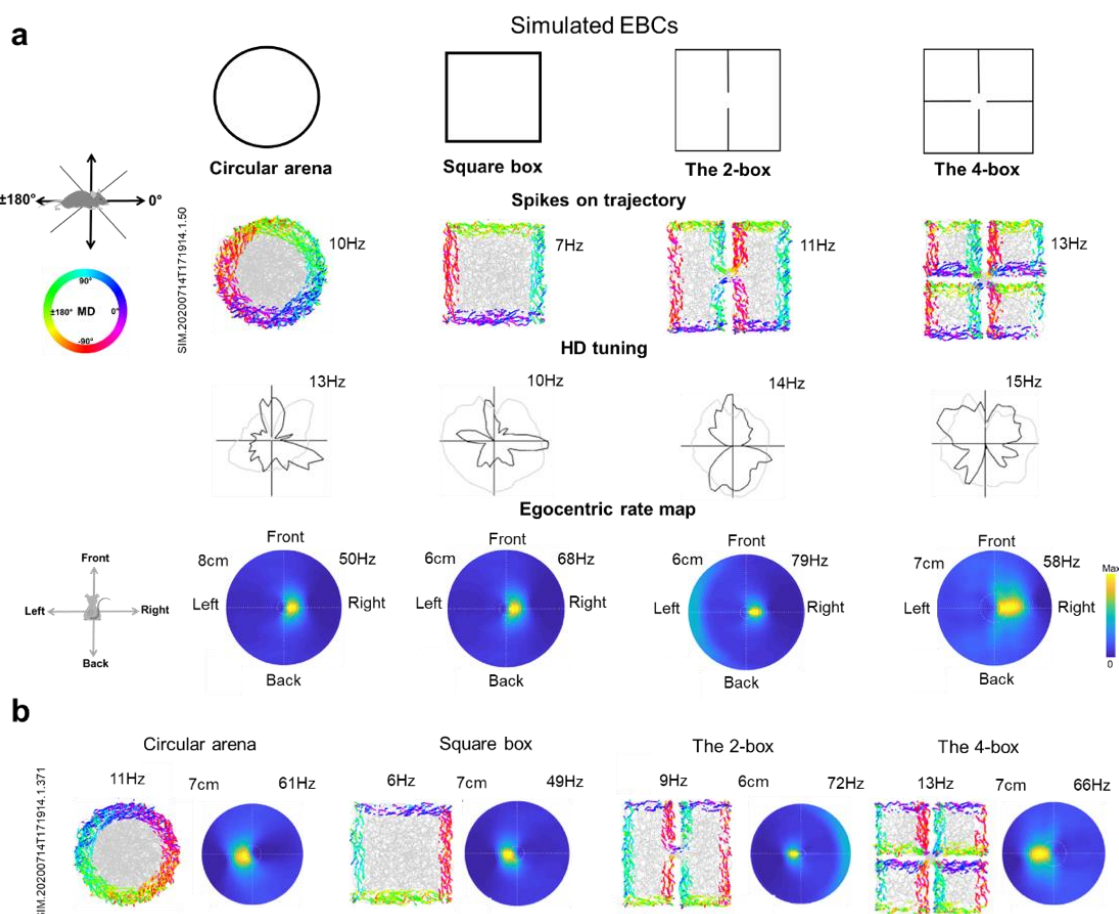


Figure 5-2. Example simulated egocentric boundary vector cells in four environments. Example of two simulated EBC in the 1-boxes and multicompartiment boxes, showing spiking preference towards environmental boundary (colour-coded by an agent rat's travelling direction as depicted in the schematics; number denotes the mean firing rate). The schematics show the movement direction reference. In the row below, the HD polar plots show HD tuning of the EBC, analysed in the same way as the recorded multidirectional cells in Chapter 4. See section 5.3.2 for more detailed analysis on EBC HD tuning. The schematics in the third row shows the egocentric reference frame, and the egocentric firing rate maps show consistent EB firing fields across four environments (heatmap, numbers denote the preferred distance and peak firing rate). A different EBC is shown in b. The cell in (a) has preferred EB tuning when the boundary is within 6~7cm to the agent's right, while the cell in (b) has preferred EB tuning to boundaries within 6~7cm to its left.

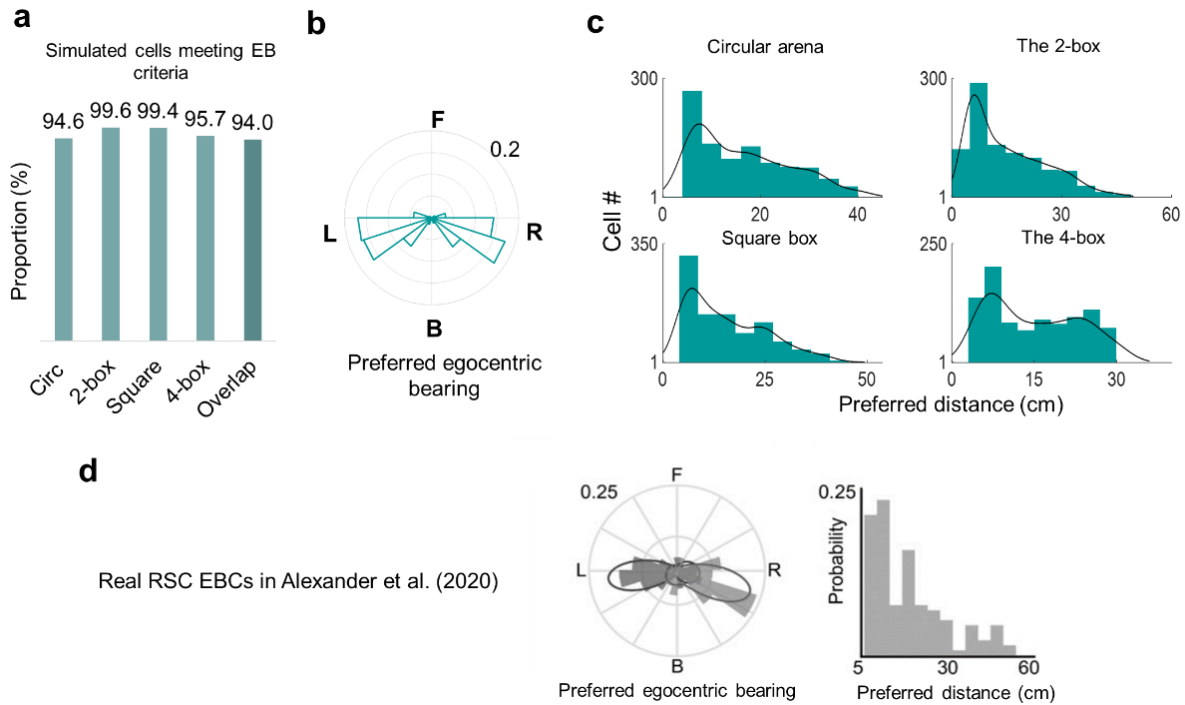


Figure 5-3. Firing properties of simulated EBC population. **a.** Proportions of simulated EBCs that passed criteria in different environments - an overall of 940 simulated EBCs (overlapping ones in all four environments) were included for analyses. **b.** Polar histogram of the preferred orientation of egocentric receptive field across the significant simulated EBCs ($n = 940$, four environments collated). Number denotes probability. **c.** Histograms show that distribution of preferred distance of simulated EBCs in four environments, the fitted line denotes kernel density. **d.** Distribution of preferred orientation of EB fields and distance of real RSC EBCs reported by Alexander et al. (2020). Adapted from the Fig 1J-K in Alexander et al. (2020). Note that the current results shown in (b) and (c) were comparable to (d), confirming satisfactory performance of the simulation model.

5.3.2 Is head direction tuning of EBCs homogenous?

One important feature of the RSC EBCs as reported by Alexander et al. (2020) was that many cells showed allocentric directional peaks aligned with the walls in the square box but not in circular arena. What about in the 2-box and 4-box that possess more complex arrangements of boundaries? I first examined how allocentric directional peaks are distributed, then analysed the simulated EBC HD tuning in environments with different arrangements of boundaries, namely, the circular arena, the square box, the 2-box and the 4-box.

As predicted by the first hypothesis, the preferred directions of the simulated cell's HD tuning were distributed non-uniformly in different environments (**Figure 5-4**, Rayleigh

test, circular arena: $z = 61.46, p < .001$; square box: $z = 61.82, p < .001$; 2-box: $z = 71.05, p < .001$; 4-box: $z = 48.03, p < .001$). Moreover, to confirm the robustness of the non-uniformity, the analysis was repeated in a subset of the simulated EBCs ($n = 100$) randomly drawn from the entire population ($n = 940$). The down-sampled size matched with the multidirectional cells ($n = 115$) and HD cells ($n = 102$). Again, the preferred directions of the cell subsets were distributed non-uniformly in all four environments (Rayleigh test, circular arena: $z = 9.0, p = 0.001$; square box: $z = 11.70, p < .001$; 2-box: $z = 5.57, p = 0.004$; 4-box: $z = 5.57, p = 0.001$). Note that the actual PFD distributions of empirical EBCs have not been reported in Alexander et al. (2020), so it was not possible to make direct comparisons with their data. It remains unclear why a bimodal distribution occurs in the circular arena. One possibility would be that the HD tuning of EBCs was sensitive to any occult bias in the random walk produced by the simulation. Nevertheless, the PFDs in the square box shown in **Figure 5-4** showed clustering of HD tuning parallel to walls, consistent with previous recorded results (Alexander et al., 2020) and the current intuition.

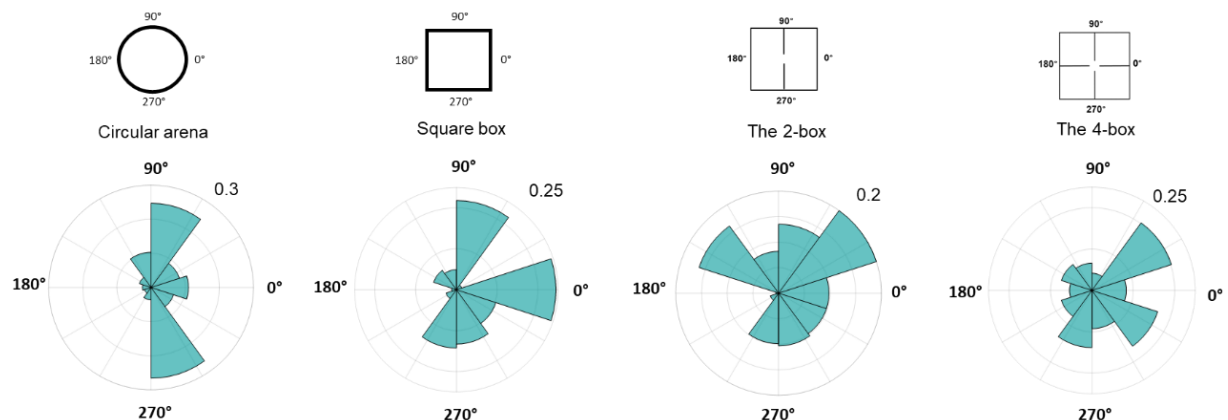


Figure 5-4. Head direction tuning of simulated EBCs was not uniformly distributed.
Polar histograms of the preferred firing directions of the simulated EBCs in the circular arena, square box, 2-box and 4-box. Note that the HD tuning was not homogeneously distributed, showing biases in all environments by influences of EB tuning relationships.

Next, the same analysis was applied to the real directional cells recorded in RSC from the two experiments. In contrast to the simulation data, the preferred directions of the

recorded directional cells including the unidirectional HD cells and multidirectional cells were distributed uniformly in the 2-box and 4-box. Like the RSC HD cells reported previously (Jacob et al., 2017), in the current two experiments, the preferred directions of the RSC directional cells were distributed homogeneously around the whole environment (**Figure 5-5**, Rayleigh test: TD: $z = 0.76, p = 0.47$; BD: $z = 0.63, p = 0.53$; HD: $z = 0.04, p = 0.96$). The findings suggest that the HD tuning of the multidirectional cells was not anchored to environment boundary directions. Thus, the multidirectional pattern seen in the current two experiments (see **Chapter 4**) was unlikely due to inhomogeneous sampling or ambulatory constraints by boundaries.

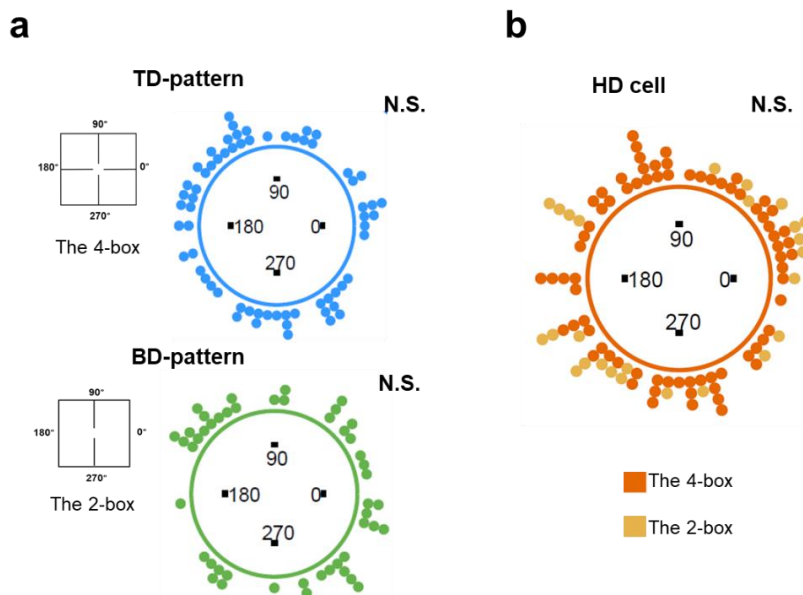


Figure 5-5. Homogenous distribution of multidirectional cell HD tuning. **a.** Circular distribution of preferred directions (the biggest peak) of TD-pattern (blue) and BD-pattern (green) cells. Each dot stands for one cell in the 1st baseline trial. **b.** Circular distribution of HD tuning of the canonical HD cells (orange: the 4-box; yellow: the 2-box) pooled from the two experiments.

5.3.3 Is there directional symmetry in the simulated EBCs?

To examine whether EBCs exhibit symmetric HD tuning patterns in the square box, 2-box and the 4-box, the same symmetry analyses (see **Chapter 4**) used for multidirectional cells were applied to the simulated EBCs. (**Figure 5-6**). Consistent with the observation by

Alexander et al. (2020), the simulated EBCs showed four peaks in their HD tuning patterns, separated by a 90° angular offset (mean TD score was significantly higher than 0.15, the population threshold of the recorded cells: $t(939) = 18.93, p < .0001$). However, the fourfold pattern was absent in the circular arena compared to the square box (median TD score, circular: -0.14; square box: 0.46; $t(1878) = 36.59, p < .0001$). The results also confirmed the robustness of the simulation model in producing EBCs comparable to the biological RSC EBCs.

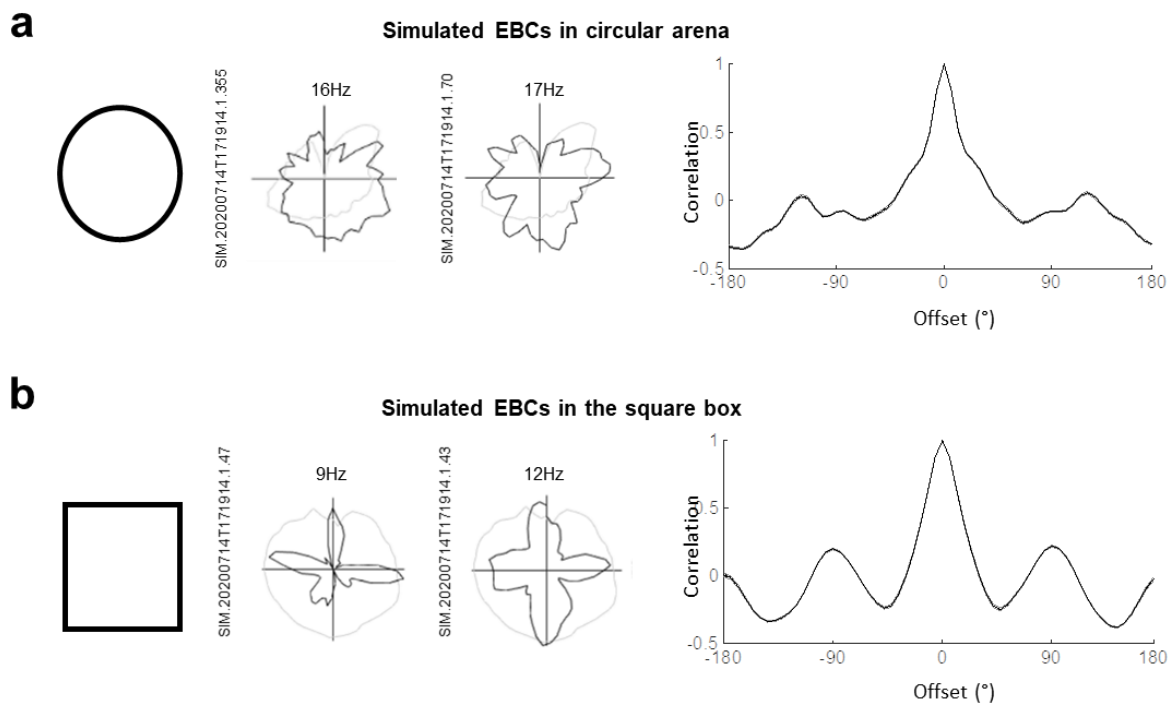


Figure 5-6. A fourfold directional pattern of EBCs in the square box but not the circular arena. HD polar plots of two example simulated EBCs in the circular arena (a) and another two cells in the square box (b) that show four-way pattern in HD tuning. Note that their peaks are in alignment with the box boundaries. The mean and SEM of the auto-correlograms of tuning curves are shown as lines.

Next, the symmetries of HD tuning curves were examined in the multicompartment boxes. First, the Rayleigh vector lengths (i.e., measurements for directional specificity) of the EBCs and multidirectional cells were compared. The simulated EBCs showed low Rayleigh vector values (angle-doubled in the 2-box: median = 0.15; angle-quadrupled in the 4-box:

median = 0.07). They were significantly lower than the real multidirectional cells (vs. all BD-pattern cells: $D = 0.55, p < .001$; vs. all TD-pattern cells: $D = 0.91, p < .001$). This suggests that the HD tuning curves of EBCs were not as sharply tuned as real multidirectional cells.

Interestingly, as predicted by the first hypothesis, many of the simulated EBCs showed symmetric patterns: a prominent twofold pattern in the 2-box (median BD score = 1.2, significantly higher than the recorded BD-pattern cells, KStest, $D = 0.39, p < .001$; **Figure 5-7a**). It should be noted that, although the overall pattern showed a two-way symmetry in the 2-box, some simulated EBCs showed a four-way pattern (example cell 2 in **Figure 5-7a**), and the population mean TD score in the whole 2-box was significantly higher than zero (t-test: $t(939) = 5.68, p < .001$) but lower than 0.15 ($t(939) = -11.87, p < .001$). The HD tuning widths of the simulated EBCs were significantly higher than the BD-pattern cells in the 2-box (width median, EBC: 159.4° ; BD: 156.7° ; KStest, $D = 0.52, p < .001$). It was possible that the tuning widths of two 90° -neighbouring peaks were too wide (as evident in low Rayleigh vector lengths) to be distinguishable: thus the pattern was probably deformed to twofold overall in EBCs (see below).

A high level of bimodal pattern was seen in the two rectangular sub-boxes in the 2-box. The twofold symmetric pattern shown in the sub-boxes (median BD score = 1.02 in sub-box 1; 0.93 in sub-box 2) was not significantly different from the within-compartment BD cells recorded in the 2-box (sub-box 1: $D = 0.1, p = 0.911$; sub-box 2: $D = 0.2, p = 0.16$). The cross-correlation between the tuning curves of the two sub-compartments was shown in **Figure 5-7b**. All individual cells were shown in the heatmap (sorted by the BD score values), indicating no evidence of between-compartment bimodality (i.e., correlation peak only at $\pm 180^\circ$ but decreased in other bins, as illustrated in Figure 4-5). Critically, none of the cell's Rayleigh vector lengths (without angle-doubling) exceed 0.23 (the median of the recorded

between-compartment BD cells), suggesting absence of unidirectional peaks within single sub-boxes. This was different from the recorded multidirectional cells.

The cross-correlation showed that the maximal angular bins were bimodally distributed around 0° (37% of the cells) and 180° (63% fell within a range of $150-210^\circ$; circular V-test against 180° , $V = 197.34, p < .001$), suggesting that around 2/3 of the EBC population showed a 180° -rotation of the HD tuning between the sub-boxes while 1/3 did not ‘flip’ the preferred firing directions. Moreover, unlike the recorded within-compartment BD cells, the trough angular bin positions were found at $\pm 72^\circ$, slightly off from $\pm 90^\circ$, indicating some correlations at $\pm 90^\circ$.

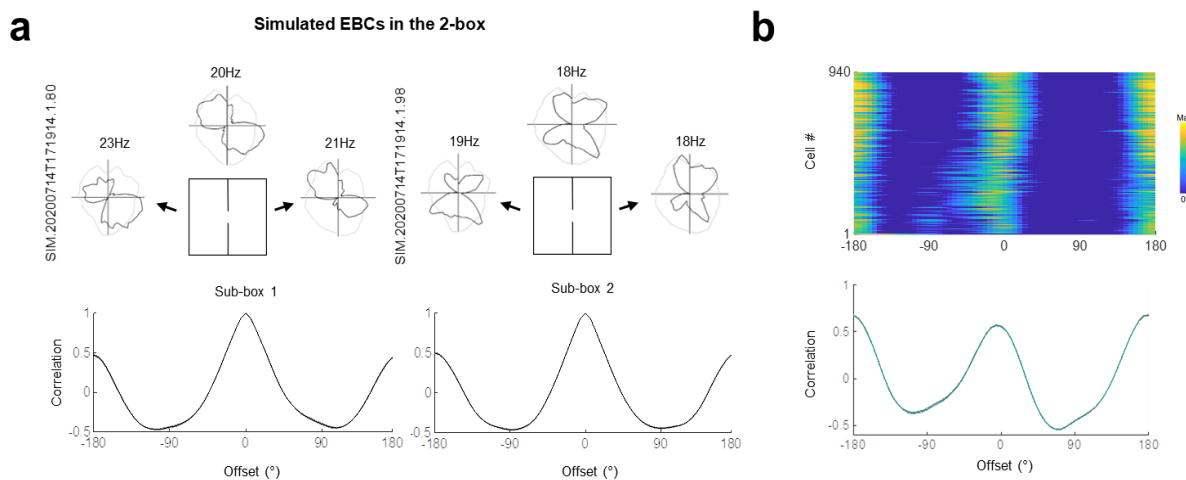


Figure 5-7. Multiple directional pattern symmetries of simulated EBCs (2-box). **a.** HD polar plots of two example simulated EBCs. Top plots show directional tuning curve for the whole apparatus (dark line) and directional behavioural sampling (pale line). Numbers show peak firing rate. Side plots show tuning for each sub-compartment. The twofold pattern was shown in the auto-correlograms (mean and SEM, shown in black line). **b.** Heatplot of the cross-correlations by taking the mean between sub-compartments for individual cells, the population mean, and SEM are shown in the cyan line below. The heatmap is sorted by angle-doubled Rayleigh vector lengths, maximal at the top. (a)-(b) analysed as in Figure 4-6.

Similar to the results in the single square box, a fourfold symmetric pattern was observed in the 4-box (median TD score = 1.2; significantly higher than the recorded TD-pattern cells, KStest, $D = 0.63, p = 0.009$; **Figure 5-8a**). The four-way pattern was the generally preserved in four square sub-boxes with some disruptions (median TD score:

sub-box 1: 0.01; sub-box 2: 0.30; sub-box 3: 0.04; sub-box4: 0.11), possibly due to the missing corner in the central doorway. The EBC autocorrelation was compared with the within-compartment TD cells recorded in the 4-box, and they were significantly different in two sub-boxes (sub-box 1: $D = 0.23, p = 0.06$; sub-box 2: $D = 0.17, p = 0.34$; sub-box 3: $D = 0.35, p < .001$; sub-box 4: $D = 0.13, p = 0.63$), indicating that the four-way periodic patterns of EBCs were not entirely preserved in single sub-compartments.

As before, the cross-correlation of the tuning curve pairs in the sub-compartments (i.e., by taking the mean of four) was computed. Overall, the population cross-correlation showed that the median maximal offset was found at -90° (60% showed peak angular bins within a range of $240\text{-}300^\circ$; circular V-test against 270° , $V = 82.56, p <.001$), 37% of the peaks were within a range of $60\text{-}90^\circ$ and 3% were around zero. The results suggest that the majority of EBCs showed a 270° -rotation of the HD tuning between the sub-boxes. This asymmetry should not be present in theory and is discussed later. Nevertheless, the result was in contrast with the multidirectional cell data that the peak was found at 90° , following rotational symmetry by visual landmarks.

All individual EBCs are shown in the TD-score-sorted heatmap (**Figure 5-8b**). Notably, those with low TD scores (the bottom part) showed singular correlation peaks at an angular bin around -90° , suggesting a potential wide onefold pattern in some sub-boxes (such as the example cell 2 in **Figure 5-8a**). This was further quantified by considering the single Rayleigh vector lengths in individual sub-boxes: by taking the average in four sub-boxes: 9.8% ($n = 93$) cells had mean TD scores below zero and mean Rayleigh vector lengths above 0.15 (the threshold for real cells; median in sub-box 1 = 0.16; sub-box 2 = 0.13; sub-box 3 = 0.21; sub-box 4 = 0.17; **Figure 5-8c**). However, the cross-correlation peaks of

simulated EBCs were located at 270° , in contrast to 90° for the between-compartment TD-pattern cells.

In short, the results in this section supported that the HD tuning by EBCs do reflect the geometric features of simple environments (circular and square box) with peripheral boundaries and complex environments (the 2-box and 4-box) with both outer and inner boundaries. Therefore, the speculation proposed by Alexander et al. (2020) that the BD pattern could be formed by egocentric boundary vector encoding was valid and needs to be assessed with the real data (see below).

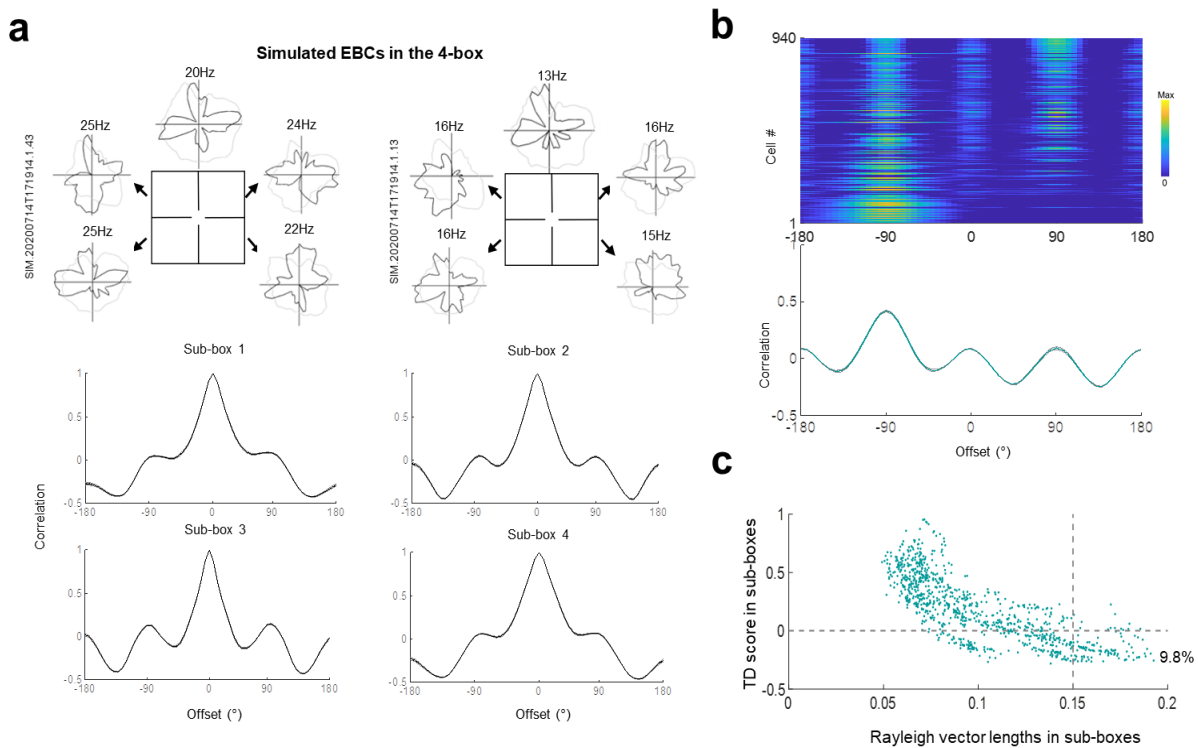


Figure 5-8. Multiple directional pattern symmetries of simulated EBCs (4-box). **a.** HD polar plots for two example simulated EBCs in the 4-box, showing fourfold symmetry. The auto-correlograms for four sub-boxes of the 4-box are shown below. **b.** Heatplot shows the cross-correlations (by taking the mean of four tuning curve pairs) between sub-compartments for individual cells, the population mean, and SEM are shown in the cyan line below. The heatmap is sorted by angle-quadrupled Rayleigh vector lengths, maximal at the top. (a)-(b) are analysed as in Figure 4-9. **c.** Scatter plot shows the mean TD scores and the mean (single) Rayleigh vector lengths of all simulated EBCs in four sub-boxes. In the bottom-right part, a few cells (9.8%) had their TD scores below zero (denoted by the line) and intermediate level of Rayleigh vector lengths (above 0.15, denoted by the line).

5.3.4 Are the recorded multidirectional cells egocentric?

The results presented in this section were to test the hypothesis that multidirectional cell are EBCs. Following the method validation in simulated data, I applied the established egocentric analyses (Hinman et al., 2019; Alexander et al., 2020; see **Methods**) to the recorded multidirectional cells to examine potential EB tuning. Briefly, for every spike emitted by cells, the distance and angle of the surrounding walls relative to the animal's movement direction were computed (schematics shown in **Figure 5-9a**) and from these data I constructed the egocentric firing rate map and calculated the egocentric tuning strength in the 1-boxes, 2-box and 4-box.

The egocentric boundary firing fields of an example multidirectional cell in the 1-box and another example in the 4-box were shown in **Figure 5-9**. Note that the cell in the 1-box was non-representative and for illustration purpose. It was found that rather than showing selective EB tuning, multidirectional cells generally showed multiple and uniform egocentric firing fields in their rate maps (**Figure 5-9b**). This homogeneous EB tuning was consistently seen in the 1-box, 2-box and 4-box (**Figure 5-10a**; also see more square box data in **Figure 5-11**), suggesting no tuning selectivity to egocentric spatial features by the recorded cells.

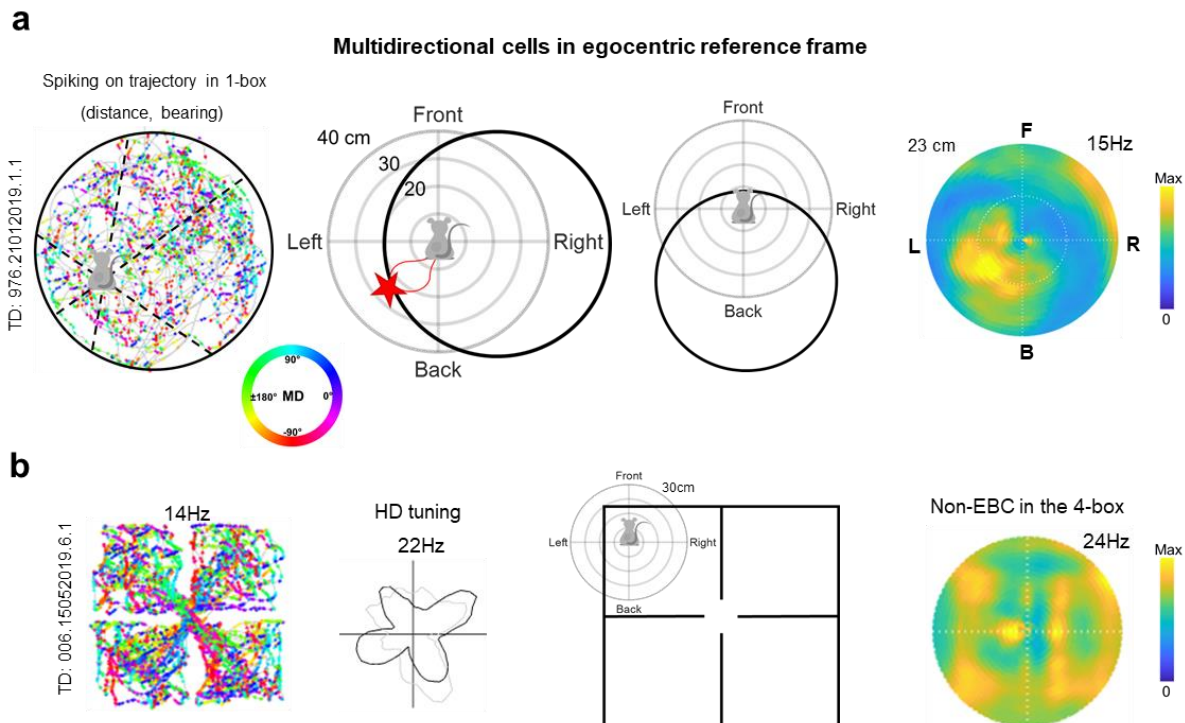


Figure 5-9. Analysing multidirectional cell activity in egocentric coordinates.

a. Schematic illustrates egocentric firing map construction for multidirectional cells, as same as for simulated EBCs. Column1: individual spikes are colour-coded by the movement direction of the animal in the circular arena. Angular bearing and distance to all intersections for 360° (in 3° bin) was determined for each frame (simplified as dashed lines) in egocentric coordinates. Column2: red star denotes an example emitted spike when a cell responds to the egocentric boundary (falling within the firing field, denoted by red line). Column3: no spike was emitted if the boundary fell outside the preferred distance and angle. Column4: an example cell's egocentric firing field, number denotes the max firing rate. Note that this example cell was one of only four that showed an intermediate level of EB tuning in the cylinder, but the EB field is not as focal as the simulated EBCs. **b.** An example TD-pattern cell (the polar plot shows its fourfold HD tuning curve) that did not show significant egocentric tuning in the 4-box. Numbers above the spike map on trajectories denote mean firing rates.

Critically, as shown in **Figure 5-10b**, most multidirectional cells (BD, 70.8%; TD, 74.6%) fell below the EBC detection threshold in any baseline trials of all environments (see assessment criteria in **Methods**). Slightly more (BD = 7; TD = 9) cells passed the EB criteria in one multicompartment box single trial than in the circular arenas (BD = 3; TD = 4). This was probably because the former held a higher number of boundaries in the environment and thus an increased chance of yielding false positives of EBC classification. Nevertheless, very few multidirectional cells (the overlapping proportion was no more than 3% as shown in

Figure 5-10b) showed significant, stable, or reproducible egocentric tuning across two trials or environment types.

The proportion of multidirectional cells that passed EB criteria was significantly higher than HD cells (Chi-squared test: group: χ^2 (8, N = 217) = 22.45, p = 0.004; TD vs BD: χ^2 (4, N = 115) = 0.22, p = 0.994; TD vs HD: χ^2 (4, N = 169) = 18.47, p <.001; BD vs HD: χ^2 (4, N = 150) = 20.05, p <.001). This was probably because HD cells only encode a single head orientation and thus less likely to coincide with cell activity along the walls. This probability, however, was doubled for within-compartment BD-pattern cells encoding two opposite directions and quadrupled for within-compartment TD-pattern cells encoding four directions in subspaces.

Moreover, the activity of a few TD-pattern cells was examined in a square box in experiments (**Figure 5-11**; also see 1-box results in the previous chapter), which was the main geometrical shape used in the original RSC EBC experiment (Alexander et al., 2020) and the striatal EBC experiment (Hinman et al., 2019). The results showed that the multidirectional cells exhibited homogeneous egocentric firing fields, and none of the trials (n = 6) passed the statistical thresholds for EBCs. The multidirectional cells also lost the fourfold HD tuning pattern, in contrast to the directional pattern of RSC EBCs in the experiment by Alexander et al. (2020) and current simulated EBCs.

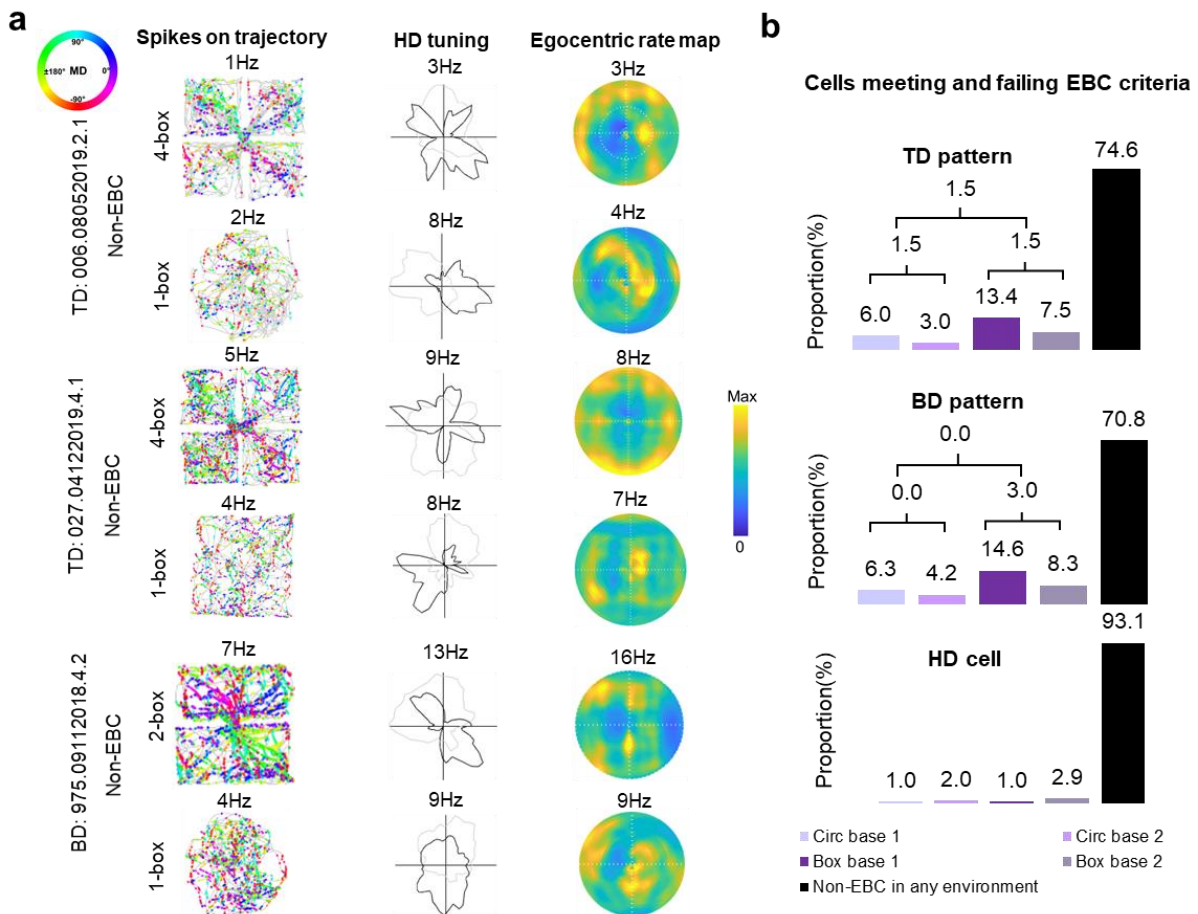


Figure 5-10. Multidirectional cells did not show significant egocentric boundary representations. **a.** Example of two TD-pattern (top and middle) and one BD-pattern cells in environments with different symmetry orders. Note that the EB firing fields were usually homogeneous with multiple ‘hot spots’, suggesting non-selective activity. **b.** Proportion of directional cells assessed with EB criteria: colour: cells that passed in at least one trial. The branch denotes overlaps between trials. Different shades of violet denote different trials. The black bar denotes the cells that did not pass the criteria in any single trial.

In short, the results of multidirectional cell analysed in egocentric coordinates contrasted with real EBCs that showed stable EB tuning regardless of the environmental geometry (Alexander et al., 2020), suggesting that egocentric boundary vector coding was not a robust feature of the recorded directional cells.

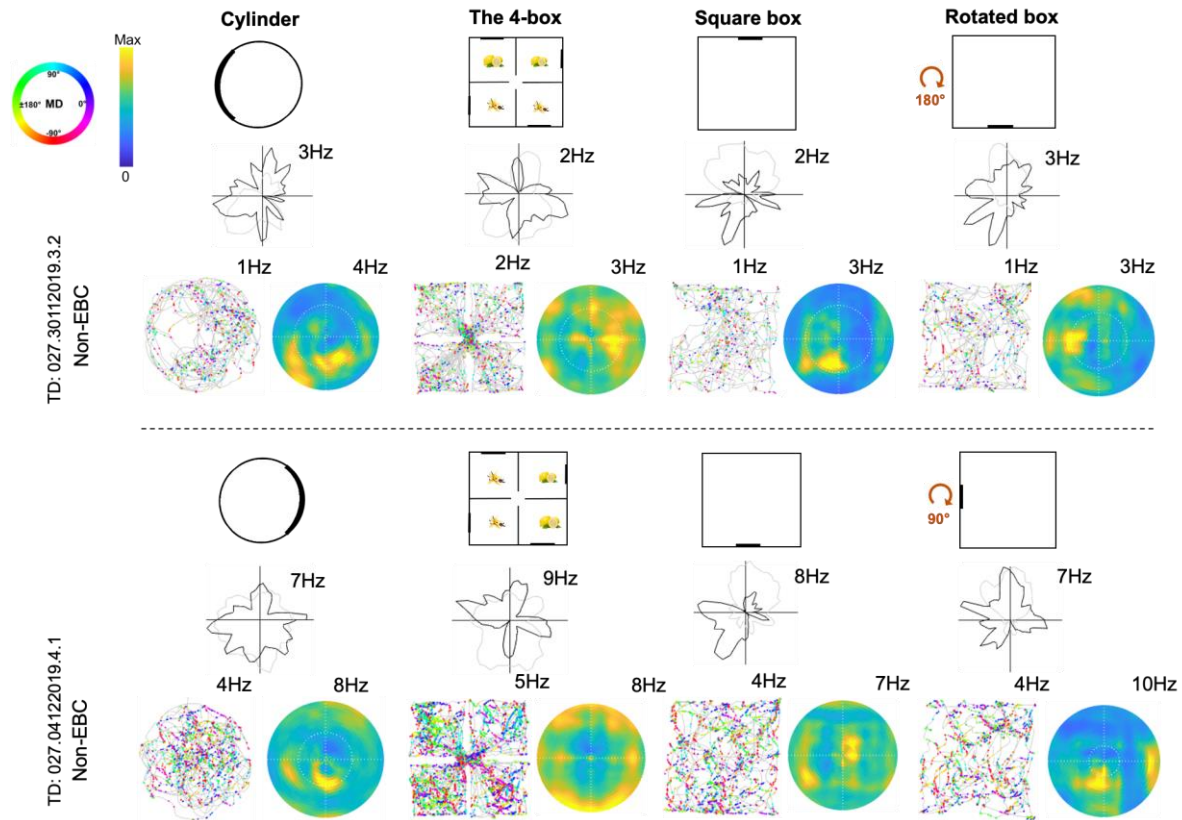


Figure 5-11. TD-pattern cells were not EBCs in the square box experiment. Examples of two TD cell HD tuning, spiking activities and egocentric tuning in the cylinder, 4-box baseline and two extra trials in the square box. Note that the TD specificity was disrupted in other environments except in the 4-box, and egocentric rate maps show unstable and homogeneous patterns across different trials.

5.3.5 Does the multidirectional cell firing prefer boundaries?

Finally, the spiking preference index was computed to examine if the multidirectional cells show any boundary-related firing activity, such as firing in proximity to boundaries. It is one of characteristics of the RSC EBCs (note that a minority showed centre-preferred firing; Alexander et al., 2020) and egocentric boundary cells (van Wijngaarden et al., 2020). The recorded multidirectional cells did not show any firing preference in proximity to the boundaries or the centres in the 1-boxes, 2-box and 4-box and their subspaces (circular arena: median = -0.01, KStest for a normal distribution centred at zero, $D = 0.38$, $p < .001$; square box: note a very small sample size, median = 0.11, $D = 0.49$, $p = 0.077$; the whole 2-box: median = -0.07, $D = 0.40$, $p < .001$; rectangular sub-boxes of the 2-box: median = -0.06,

$D = 0.41, p < .001$; the whole 4-box: median = -0.02, $D = 0.37, p < .001$; square sub-boxes of the 4-box: median = -0.04, $D = 0.39, p < .001$). Although the index values in the onefold square box were marginally significantly higher than zero (due to only six data points), they were significantly different from the spiking preference index in the simulated EBCs, as shown in **Figure 5-12**.

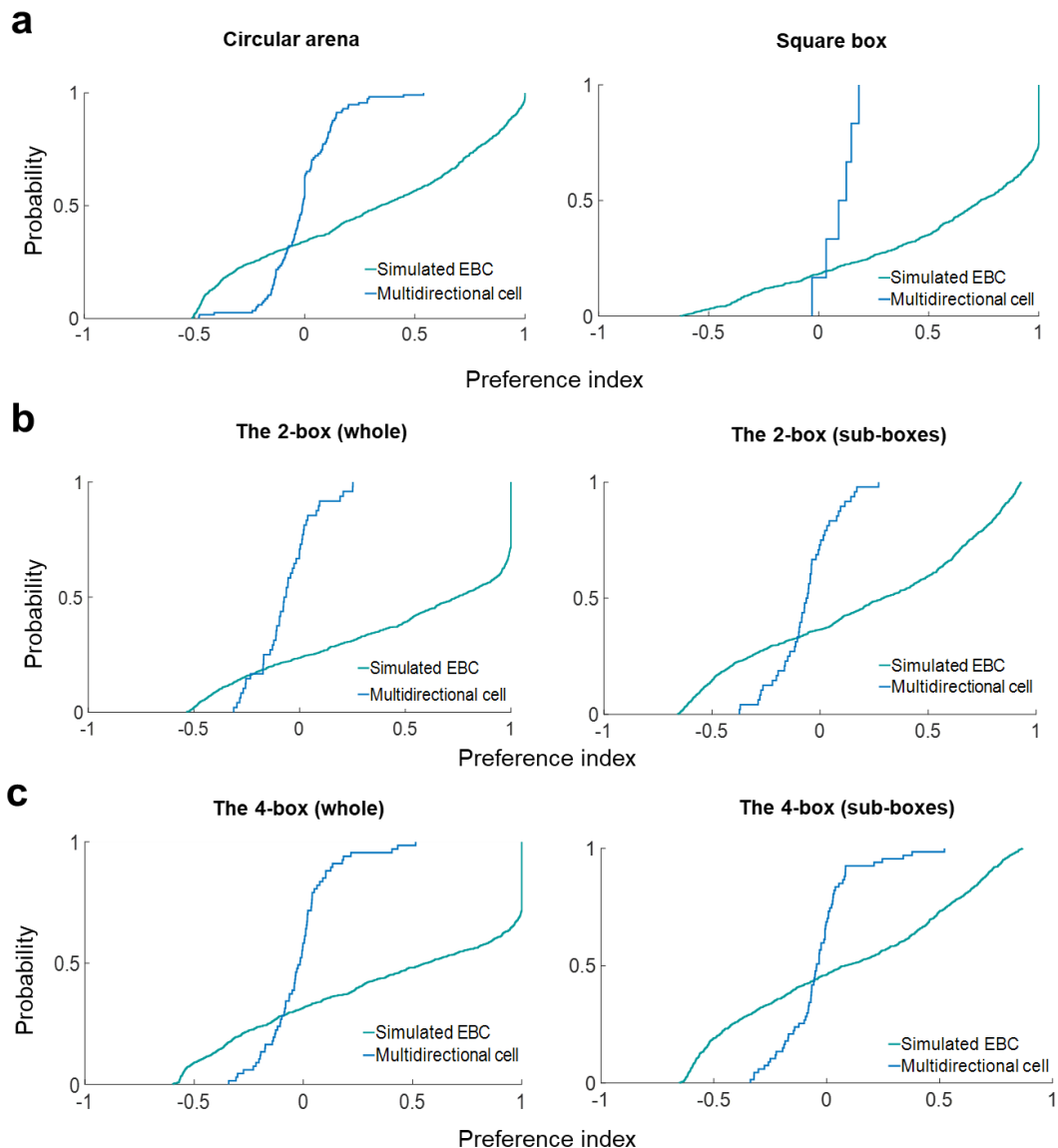


Figure 5-12. Distinct spiking preferences of multidirectional cell and simulated EBCs. Cumulative probability of the spiking preference index of the multidirectional cells (blue) and the simulated EBCs (cyan) in different environments: 1-boxes shown in (a), the 2-box and its sub-boxes (mean of two single sub-compartments) in (b), the 4-box and its sub-boxes (mean of four single sub-compartments) shown in (c). Note small sample size of multidirectional cells in the square box. The higher the index (> 0), spiking activity is closer to the boundaries; the lower the index (< 0), spiking activity is centred in the middle of an arena. Index value towards one indicates preferred firing around boundaries, seen in the simulated EBCs in the square box, 2-box and 4-box.

In contrast, the simulated EBCs showed significantly higher spiking preference index values than the multidirectional cells in all four environments (circular arena: median = 0.34, KStest with the multidirectional cells, $D = 0.51, p < .001$; square box: median = 0.74, $D = 0.76, p < .001$; the whole 2-box: median = 0.75, $D = 0.69, p < .001$; sub-boxes of the 2-box: median = 0.29, $D = 0.53, p < .001$; the whole 4-box: median = 0.56, $D = 0.58, p < .001$; sub-boxes of the 4-box: median = 0.08, $D = 0.42, p < .001$).

Taken together, the result suggests that unlike the EBCs or egocentric boundary cells, the multidirectional cells did not selectively fire along the walls or in the centre of the arena, but their spikes were homogenously distributed in both simple and complex environments.

5.4 Discussion

5.4.1 Summary

The overall results supported the first hypothesis in this chapter: EBCs yield a multidirectional pattern, reflecting geometric features of the environment; and disproved the second hypothesis that the multidirectional cells are EBCs. The supportive evidence is reviewed below.

First, the EBCs in the current dataset, as simulated from the model, shared highly comparable EB tuning characteristics with the real RSC EBCs (Alexander et al., 2020). This confirmed the performance of the EBC selection criteria in all environment types used in the current experiments. This validation is important because it would eliminate false negatives in real data due to potentially fragile analysis methods.

The results of EBC HD tuning largely supported the predictions made by Alexander et al. (2020). Specifically, the simulated EBCs yielded a four-way allocentric directional

tuning in the square box, but the symmetric pattern was absent in the circular arena. The simulated EBCs also yielded a four-way directional pattern in the 4-box that consists of four square boxes (fourfold inner and outer boundaries) and a two-way directional pattern in the 2-box that consists of two rectangular boxes (twofold inner boundaries). The results supported the first hypothesis of the chapter (Hypothesis 3 of the thesis) that the allocentric directional pattern of EBCs is an artefact of boundary representations, reflecting geometry-related features of both simple and complex environments.

Accordingly, it was not unreasonable for the authors in the RSC EBC experiment (Alexander et al., 2020) to speculate that restrained egocentric firing along the two opposite walls in the 2-box can result in a BD-pattern. However, further analyses demonstrated that the artefact was not the case for multidirectional cells. This was evident in the results supporting the second hypothesis: the recorded multidirectional cells did not show significant EB tuning and were different from the EBC characteristics in many aspects: a lack of significant or stable EB firing field, presence of between-compartment cells, a uniform distribution of preferred directions and spikes in an environment. The possibility that multidirectional cells encode borders as suggested by Alexander et al. (2020) was refuted, because egocentric boundary related property was unlikely to be acquired by RSC multidirectional cells. Detailed discussions on these two hypotheses are provided below.

5.4.2 HD tuning of EBCs as a by-product of egocentric boundary encoding

Although HD tuning of EBCs showed prominent symmetries, looking like the multidirectional cells, the resemblance in pattern does not mean that they should be considered as the same neural code. Here I first discuss the HD tuning formation of EBCs, and extra reasons in support of the argument are listed in the next section.

First, it should be reiterated that HD tuning curves in the simulated EBCs do not reflect any direction ‘encoding’ of the cells, because there were no pre-defined parameters for head direction encoding in the simulation. Thus the cell’s firing probability was determined only by the built-in egocentric parameters: the preferred distance and egocentric bearing (see section 5.2.3). Thus, HD tuning of the simulated EBCs should be treated as a by-product of pure EB tuning relationships, an artefact due to environmental boundary constraints, instead of intrinsic functional properties of the cells.

One crucial difference between the recorded multidirectional cells and EBCs was a general absence of unidirectional HD tuning that rotates accordingly with the sub-box rotations (and landmark rotations in real experiments; see **Chapter 4**). In EBCs, the cross-correlations of the sub-box tuning curves showed that the peaks were largely found at $\pm 90^\circ$, in contrast to the multidirectional cells that their preferred directions follow the rotations of visual landmarks and peaked at 90° . Thus, the multidirectional cells primarily encode allocentric directions as defined by external landmarks, while EBCs are primarily sensitive to geometric features such as the conjunctions of walls forming 90° -corners in the square box (Alexander et al., 2020). For instance, an EBC with a preferred EB field close to boundaries would continue firing when an animal travels clockwise or counterclockwise along the walls of the square box.

Although corners are important in deciding EBC HD tuning, more factors such as the lengths of boundaries and how inner walls are orientated along two allocentric axes largely influence the egocentric boundary representations, and thus EBC HD tuning. For example, the current results showed that EBC HD tuning in the 2-box and its rectangular sub-boxes showed a bimodal pattern instead of four peaks. This was due to inhomogeneous egocentric firing probability distributed in the 2-box (see below). More intuitively, although in the

previous chapter (and in Jacob et al., 2017), the 2-box was conceptualised as a multicompartiment environment with a twofold visual symmetry, a slightly different perspective might be taken here to think the 2-box as a square box with two inner walls inserted in the middle. Accordingly, egocentric sampling in this case might not be as homogenous as in the square box.

Specifically, as illustrated in **Figure 5-13**, because the lengths of the walls are equal in the square box, for an EBC in favour of firing along the walls lateral to the animal, the chance for it to spike is in theory equally distributed along the four walls in a square box (**Figure 5-13a**; analogously in the 4-box). The egocentric firing probability should be generally homogenously distributed in four directions of a fourfold symmetric environment. Thus, the four-way HD tuning pattern was normally observed in the two environments.

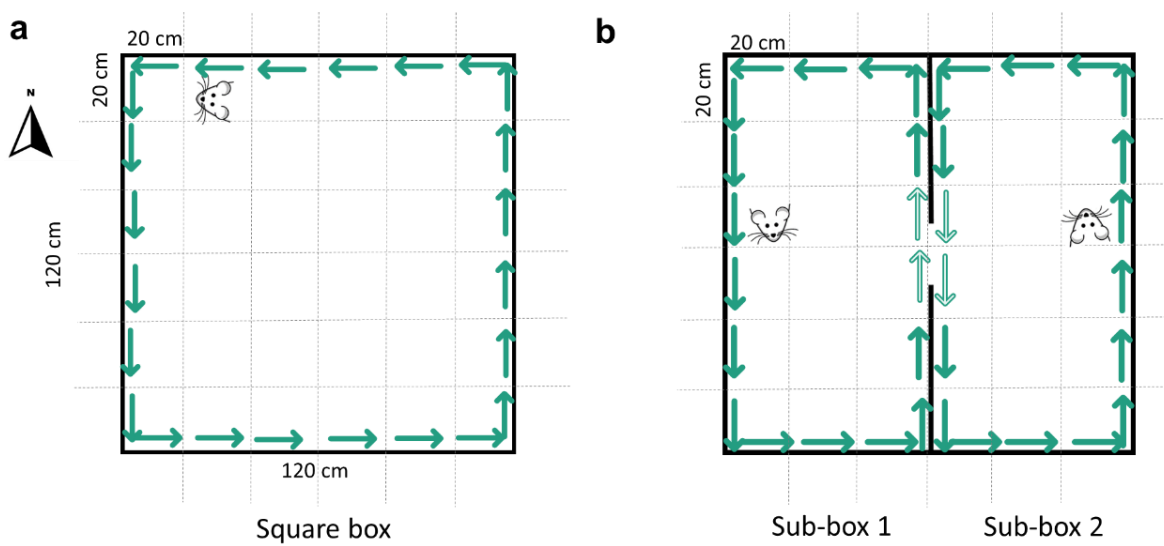


Figure 5-13. Schematics for EBC bimodal pattern in the square box and the 2-box.
The schematic describes a typical scenario where an EBC shows close boundary representations in the square box (a) and the 2-box (b). For simplicity, the cell fires as the animal (the cartoon rat head) moves in counterclockwise direction whenever there is a wall within 5 cm to its right in the environment. Dotted lines separate the environment into 36 grids (20 cm x 20 cm), and the solid arrows denote intensity of firing in corresponding head directions. The egocentric sampling is homogenously distributed in all directions in the square box but not the 2-box: the cell fires more in ‘North’ and ‘South’ directions due to the additional walls in the middle, albeit that it may fire slightly less around the central doorway (denoted by more transparent arrows). The number of vertical arrows is as doubled as the horizontal arrows in the 2-box, thus different sizes of HD tuning peaks.

However, egocentric sampling is different and biased in the 2-box due to the two opposite inner walls. For the same EBC which has close a representation to walls on the right, the likelihood for it to spike along the long-wall axis (120 cm) is doubled over the short one (60 cm; **Figure 5-13b**) in the rectangular sub-box. Accordingly, this would result in unequal sizes of HD tuning peaks, and any imprecision in tuning would produce wide, non-separable peaks (in 90°). Due to biases in egocentric sampling of the EBCs, a bimodal HD tuning is normally formed in the rectangular sub-box and the whole 2-box (see **Figure 5-7**). Interestingly, this account is consistent with some empirical S1 egocentric border cells recently reported by Long, Deng et al. (2021, see example cells in their Figure 2C).

Furthermore, the HD tuning of EBCs, as an artefact, also shows large variabilities. For example, in empirical EBCs reported by others, the cells also show a wide, onefold tuning pattern in the square box (Alexander et al., 2020; their Figure 5A), although this was left unquantified. Due to variations in their data, the authors only considered the HD pattern from the population mean. In the current simulation dataset, allocentric directional patterns of EBCs also showed some variabilities within an environment, and not all EBCs showed a fourfold pattern in the square box or 4-box, or a twofold pattern in the 2-box (see **Figure 5-7**; **Figure 5-8**). In the simulation, the allocentric behavioural sampling in each environment was controlled and remained the same for all cells. Therefore, different EB encoding characteristics of the cells and the egocentric sampling bias should primarily account for individual differences in EBC HD tuning.

5.4.3 Distinctions between the multidirectional cells and EBCs

Next, let us consider the second hypothesis: should the recorded multidirectional cells be considered as an independent population from the EBCs? The answer is yes, based on several

observations in this chapter. The distinctions between the multidirectional cells and simulated EBCs are summarised as follows:

1. In HD tuning results (section 5.3.2), the preferred firing directions of the multidirectional cells were distributed homogenously, representing all 360° in the 2-box and 4-box. It suggests that the multidirectional cells, like HD cells, encode allocentric direction orientations. In contrast, the distribution of EBC HD tuning was biased in all environments, especially in parallel with the walls in the onefold square box, suggesting strong influences by boundary constraints and egocentric boundary representations.
2. In section 5.3.3, most of the multidirectional cells showed low selectivity in EB tuning and failed the EB detection criteria. Their EB tuning characteristics were in contrast with the significant EBCs that show focal, selective firing fields to either the animal's left, right (sometimes slightly off to the left-back or right-back).
3. Even if a small number of multidirectional cells occasionally passed the EB criteria in one of the trials, they did not show any stable or reproducible EB tuning in second baseline trials. Similarly, cells that passed the criteria in the multi-boundary environments did not show persistent EB firing in the circular arena. In contrast, the EBCs show consistent EB tuning relationships in all environments with physical boundaries (Alexander et al., 2020; and the current simulation). As mentioned earlier, this suggests that a few cells that passed the criteria only in the 2-box and 4-box were likely to be false positives.
4. As illustrated in section 5.3.4, the spiking preference with respect to environmental boundaries of the multidirectional cells was centred on zero in all environments, indicating a uniform distribution of spikes of the cells. However,

the distribution of EBCs were skewed towards representations near the boundaries, suggesting that the firing probability of EBCs is dominated by environment geometric features.

5. As discussed earlier, although HD tuning of the EBCs also showed a high level of symmetries in the square box, the 2-box and the 4-box, the patterns differed from real multidirectional cells in many ways, such as the angular position of correlation peak, Rayleigh vector lengths and so on. In particular, a lack of between-compartment HD tuning in EBCs strongly distinguished them from the multidirectional cells. The directional pattern seen in the simulated EBCs do not essentially represent the direction orientations, but an artefact from the EB relationships.

In sum, dissimilar properties of multidirectional cells from the simulated EBCs support the second hypothesis that the multidirectional cells are not EBCs, and they encode head direction orientation in allocentric reference frames. Accordingly, the observed multidirectional firing pattern (see **Chapter 4**) should not be regarded as a direct consequence of the cell's egocentric sampling or tuning in the 2-box and 4-box.

5.4.4 Limitations and implications

Of note, so far in literature, it was not clear whether using head direction or movement direction would yield more accurate detection of EBCs. In the study by Hinman et al. (2019), the authors stated that using the rat's movement direction rather than the head direction in constructing the EBC rate maps has detected a higher amount of EBCs in the striatum. Although both head direction and movement direction were used in the RSC study by Alexander et al. (2020), the authors found a higher number of EBCs (21.4%) when using the movement direction than using head direction (16.4%). Moreover, the authors reported no

statistical difference in stability of receptive fields of a subset of detected EBCs referenced to head direction versus movement direction (Alexander et al., 2020), and EB tunings are comparable for robust EBCs regardless of analysed using movement or head direction (see examples in their Supplementary Figure 3).

Given the main purpose of the current analyses was potential EBC detection, the movement direction was used as the angular reference. Based on the previous results, using head direction should not produce significantly different findings. However, it would be useful to compare the current results with referencing to head direction in future analyses. This would foster a clearer definition of egocentric reference frames.

Moreover, regarding an absence of EBCs in the recorded dataset, it is hypothesised that it might be due to potential differences in their distribution along the retrosplenial rostral-caudal axis, and the current recordings did not sample along this axis. In the original report of biological EBCs in RSC (Alexander et al., 2020), the majority of EBCs (~80%) were recorded from AP -3 and -4 relative to the Bregma, and only a few EBCs (~10%) were recorded around AP -5, where the multidirectional cells were concentrated (see **Chapter 6** for detailed histological analyses). However, the full set of EBC analyses has only been applied to the direction-selective neurons. In future work, it would be interesting to apply the analysis to the non-directional cells, in addition to the spiking preference analysis to detect potential EBCs.

The extended analyses in the current chapter have several important implications: first, a high performance of the simulation model confirmed its robustness in generating a dataset comparable to the real EBCs that others reported (Hinman et al., 2019; Alexander et al., 2020). The simulation model and the simulation results could be considered an instantiation of hypothesis regarding the relationship between EBC firing property and

environment symmetry. The results provided clear insights for future experimental work into how biological EBCs would behave in complex environments that comprise multiple inner walls.

Second, the analyses on HD tuning of EBCs confirmed previous predictions and some observations by Alexander et al. (2020). So far in the literature, there was a lack of detailed HD tuning characterisation of EBCs even in simple environments. Although sometimes HD polar plots were presented together with the EBC rate maps (Alexander et al., 2020; Long, Deng et al., 2021), a systematic description of the HD tuning pattern was missing. The current symmetry analysis methods not only quantified the HD tuning of EBCs but also made comparisons with the real multidirectional cells in multiple environment types.

It should be noted that some asymmetries of EBC HD tuning correlations seen in the present study were likely due to biased egocentric sampling of the cells: most of the EBCs only fire when boundaries are lateral to the agent. In addition, as the whole population of cells shared the same behavioural sampling (i.e., the same trajectory in one environment), it is difficult to rule out any possible effect due to systematic bias (e.g., head directional sampling), which could be amplified in a much larger population ($n = 940$) and reflected in the HD tuning curves. This again would support that the EBC HD tuning is prone to any minor inhomogeneity during sampling. One possible way to optimise the simulation model is to feed real experimental trajectories to the random walk process, so that to produce behavioural sampling comparable to the real data. This is an important direction for future work.

Moreover, a comparison between the EBCs and the recorded multidirectional cells critically disentangled the possibility that they are the same type of neurons in RSC. Their distinctions in many aspects allow us to refute the hypothesis that EB tuning contributes to

multiple peaks observed in real multidirectional cells. Several spatial tuning features such as the distribution of directional peaks and spike preference index could be used as additional characteristics to describe EBCs.

Nevertheless, one should note that it remains unclear if and how biological EBCs may interact with the directional codes in RSC. A more thorough exploration of this question is beyond the scope of the current thesis, but an important future direction. For example, future work may consider co-record EBCs, multidirectional cells, and HD cells together, then analyse the temporal relationship between spike trains (whether one fires before or after another) to characterise potential information flow between egocentric and allocentric systems. This point is revisited in **Chapter 7**, in which some possibilities are suggested to dissociate the two cell populations experimentally.

To conclude, the results in this chapter illustrated how HD tuning of EBC arises an artefact of egocentric boundary representations, which are not the feature of multidirectional cells as described in Chapter 4. The results together suggest that egocentric spatial encoding was not ubiquitous in the recorded RSC cells, and the multidirectional cell activity in the current experiments and the previous study (Jacob et al., 2017) was not due to encoding of egocentric boundary relationships.

CHAPTER 6

CHAPTER 6 MULTIDIRECTIONAL CELLS ARE A SEPARABLE SUBCLASS FROM HEAD DIRECTION CELLS

6.1 Introduction

Results from the previous chapters demonstrated that the unusual fourfold (TD-pattern) and twofold (BD-pattern) firing symmetries of retrosplenial neurons were not intrinsic, or egocentric, but driven by environment symmetry in an allocentric space. Those cells clearly showed directional tuning patterns distinct from the canonical HD cells in RSC and other brain regions of the HD circuits (e.g., PoS and ADN; Jacob et al., 2017). Moreover, Jacob et al. (2017) reported that the BD-pattern cells were found exclusively in the dysgranular RSC sub-region. The TD-pattern cells are believed to be the same category with BD-pattern cells and referred to as multidirectional cells together. Thus, the possibility of multidirectional cells being confined to dysgranular RSC was examined in this chapter.

Brennan et al. (2020) recently performed whole-cell recordings on brain slices in mice and reported two distinct subtypes of excitatory neurons in superficial granular RSC. Their biophysical modelling results suggest that the two excitatory cell types (namely, low rheobase and regular spiking) encode PoS HD inputs differently. This finding interestingly suggests a potential link between neuronal intrinsic properties and head direction encoding within the RSC. Thus, it is important to consider how neural properties of the cells might relate to directional tuning types. Therefore, this short chapter performed extended analyses on histology and neural properties in RSC, to examine the last hypothesis of the thesis: are multidirectional cells a different subclass from HD cells? Specifically, the analyses focused on: do TD-pattern and BD-pattern cells share comparable electrophysiological characteristics that are different from HD cells?

6.2 Methods

6.2.1 Data analyses

All analyses were performed on data from the 1st baseline trial of the multicompartment boxes for TD-pattern cells, BD-pattern cells, and HD cells. The electrophysiological properties were examined as described below.

- *Waveform:* The waveform width (peak-to-trough latency) and the amplitude were extracted for each cell. I collated the waveform features for all directional cells and applied a K-means clustering method (MATLAB functions *kmeans*) to decide cluster centroid locations.
- *Burst index:* The burstiness of neurons was measured by the spike-burst index, which was defined as the proportion of spiking activities (of all spikes) occurred within 6 ms of the peak of the inter-spike interval histogram.
- *Inter-spike interval:* For each cell, the inter spike interval of a spike train was analysed within a time window of 50 ms. An Epanechnikov kernel (bandwidth = 6) was fitted to the time interval distribution to get a smoothed density estimate. I calculated the latency between the points where the spiking probability first and last dropped below half of the maximum, and then compared the population data between cell groups.
- *LFP phase and spiking activity:* The LFP analysis methods were established and described in a previous study (Grieves et al., 2020). To obtain a theta phase angle for each spike, the saved LFP signals were first bandpass filtered in the 6-12 Hz range (fourth-order Butterworth, MATLAB functions *butter* and *filtfilt*) before a Hilbert transform was applied to obtain the instantaneous phase angle (MATLAB function

hilbert). For each cell, the instantaneous theta phase of every spike was calculated by linear interpolation of the instantaneous theta phase signal (MATLAB function *Phase*). The cell's phase angles were binned between $-\pi$ and π in 0.1 radian bins. The cell's preferred theta phase was defined as the circular mean of these angles, and the strength of the modulation (phase-locking) was defined as the mean resultant vector length of these angles (MATLAB functions *circ_mean* and *circ_r* respectively). For each cell, the number of spikes was normalised to its maximum in the baseline trial. At the population level, the average number of spikes per angular bin was calculated, and all cell preferred phases were collated.

6.2.2 Histological analysis

At the end of experiments, as described in **Chapter 3** (section 3.5), animals were anaesthetised with isoflurane and injected with an overdose of sodium pentobarbital for euthanasia. Half of the 18 animals underwent an electrolytic lesion: passing a small 15-20 μA current through two electrical channels (on different tetrodes) for 6-12 seconds prior to a perfusion. After a trans-cardiac perfusion (see **Chapter 3** for details), the brain was extracted from the skull, fixed, and stored in cold paraformaldehyde (4%) for at least two weeks, then transferred to sucrose solution (30%) for cryoprotection. The brains were sliced using a freezing cryostat (Leica Biosystems, UK) under -21°C, and 35-40 μm coronal sections through the caudal extent of the RSC were taken, stored in wells containing phosphate buffered saline (PBS), and wet-mounted on the slides.

After at least two weeks from the time of mounting, the sections were stained with a 0.1% cresyl violet solution and imaged by Olympus microscope (Olympus Keymed, UK). While imaging, the deepest point of the electrode track was found by referencing to an online version of Paxinos and Watson rat brain atlas

(<https://github.com/mattgaidica/RatBrainAtlasAPI>). The history of tetrode movements was used together with these points to estimate the recording depth of each experimental session.

6.3 Results

6.3.1 Multidirectional cells were generally confined to dysgranular RSC

First, example histological sections of implanted animals are shown in **Figure 6-1a**. In most animals, the tetrodes went through both dysgranular and granular sub-regions (**Figure 6-1b**, **Table 6-1**). As reported in previous chapters, a total number of 115 multidirectional cells (10.1%; n = 1138) and 102 unidirectional HD cells (9%) were identified from two experiments (see **Table 6-1** for contributions by individual animals).

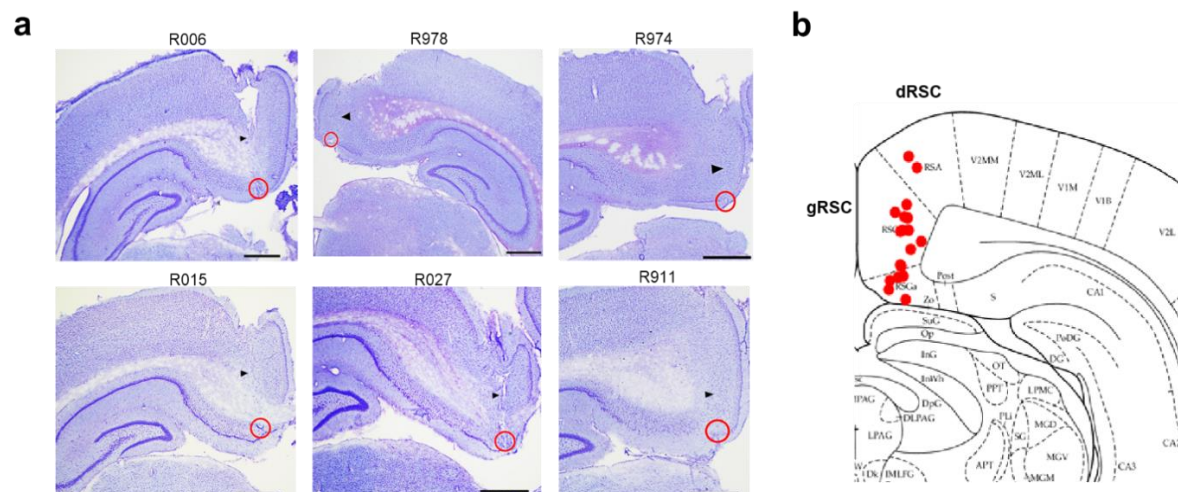


Figure 6-1. Histology and locations of tetrode tracks. **a.** Example histological slices of six animals implanted with 8-tetrode (R006, R978, R015, and R027) or 4-tetrode bundles (R974, R911). Animals of these representative sections received a small electrolytic lesion under anaesthesia prior to perfusion, showing visible brain tissue damage at the tip of electrodes, indicated by red circles. Black arrow points to the trajectory of the electrode bundle. Scale bar denotes 1mm. **b.** Superimposed histological diagram corresponding to the population median recording coordinates (AP: -5.5, ML: ± 0.83) of all animals (n=18), filled red dots mark the estimated sites at the end of recordings for each animal. In all eighteen animals, the electrode tracks went descended into the RSC (dRSC and gRSC were referred to as RSA, RSGb/a in the Atlas diagram).

One prominent difference between the multidirectional and HD cells is their anatomical distributions in RSC subregions (**Figure 6-2**). Of the whole population, 49.5%

(n=564/1138) of recordings were sampled from dysgranular RSC, 27.3% (311/1138) from granular and 23.1% (263/1138) from the intersection of the two sub-regions. Specifically, most multidirectional cells were localised in dysgranular RSC, a few in the conjunction between dysgranular and granular RSC, and the least from granular RSC. In contrast, the majority of HD cells were recorded from granular RSC and the border, but a small proportion was from dysgranular RSC (Chi-Square test showed significant differences between the multidirectional and HD cell groups (group: $\chi^2(2, N=217) = 101.89, p <.001$; TD vs. HD: $\chi^2(2, N = 169) = 79.85, p <.001$; BD vs HD: $\chi^2(2, N = 150) = 72.19, p <.001$), but non-significant difference within multidirectional cell groups (TD vs BD: $\chi^2(2, N = 115) = 5.23, p = 0.073$). The results showed that the distribution of directional cells was related to anatomical segregation of RSC sub-regions.

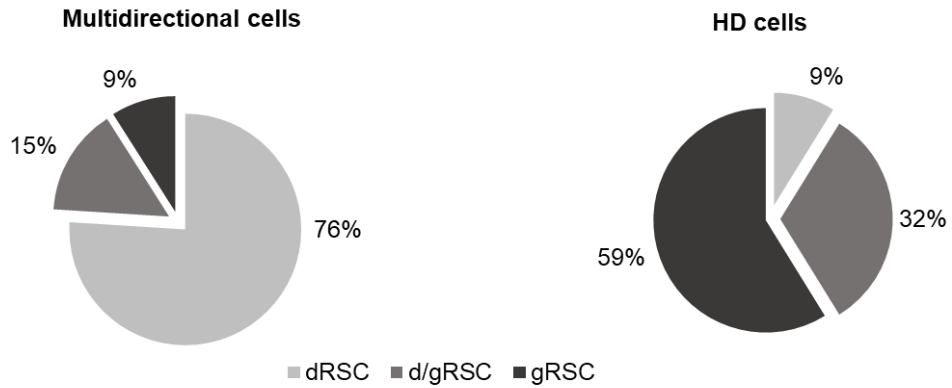


Figure 6-2. Different distributions of multidirectional and HD cells in RSC sub-regions. Proportion of the directional cells shown in pie charts, upper: Multidirectional, n = 115; lower: HD, n = 102) recorded in each RSC sub-region (light grey: dysgranular RSC; dark grey: intersection between dysgranular and granular RSC; space grey: granular RSC).

Table 6-1. Summary of cells recorded per animal in the 2-box and the 4-box experiments.

Note that the multidirectional cell refers to BD-pattern cells and TD-pattern cells recorded from the two experiments. The recording sites were checked from the histological slides of each animal at the end of the recording. Four animals (R973, R974, R975, R976) participated in both experiments, and recordings in the 2-box were made only from their dRSC while the 4-box experiments sampled both sub-regions.

Experiment	Rat	Single units		HD cell		Multidirectional cell		Recording site
				% of n	% of total	n	% of total	
			n	total	n	total	n	% of total
The 2-box	863	15	3.1	0	0.0	1	2.1	dRSC (l)
	872	7	1.5	4	14.8	1	2.1	gRSC (r)
	887	24	5.0	2	7.4	4	8.3	d&gRSC (l)
	889	33	6.9	6	22.2	3	6.3	d&gRSC (r)
	890	33	6.9	4	14.8	6	12.5	d&gRSC (l)
	891	37	7.7	0	0.0	4	8.3	dRSC (r)
	892	116	24.3	5	18.5	6	12.5	d&gRSC (l)
	910	52	10.9	6	22.2	3	6.3	d&gRSC (r)
	911	88	18.4	0	0.0	4	8.3	d&gRSC (r)
	912	13	2.7	0	0.0	7	14.6	dRSC (l)
	973	9	1.9	0	0.0	1	2.1	dRSC (r)
	974	10	2.1	0	0.0	4	8.3	dRSC (l)
The 4-box	975	22	4.6	0	0.0	3	6.3	dRSC (r)
	976	19	4.0	0	0.0	1	2.1	dRSC (l)
	Total n	14	478	27		48		
	973	9	1.4	1	1.3	0	0.0	gRSC (r)
	974	74	11.2	12	16.0	6	9.0	d&gRSC (l)
	975	45	6.8	2	2.7	1	1.5	d&gRSC (r)
	976	163	24.7	24	32.0	8	11.9	d&gRSC (l)
	978	27	4.1	3	4.0	2	3.0	d&gRSC (r)
	006	178	27.0	19	25.3	39	58.2	d&gRSC (l)
	015	93	14.1	10	13.3	1	1.5	d&gRSC (l)
	027	71	10.8	4	5.3	10	14.9	d&gRSC (l)
	Total n	8	660	75		67		

dRSC: dysgranular sub-region; gRSC: granular sub-region; (r): right hemisphere; (l): left hemisphere.

6.3.2 Is RSC functional dissociation related to the electrophysiological properties?

Next, across cells with different firing patterns (i.e., TD, BD and HD), I compared the following electrophysiological characteristics of the cells: waveform features, burstiness, inter-spike intervals and local field potential (LFP) modulation (see statistical summary in **Table 6-2**). As shown in **Figure 6-3**, compared to most HD cells that exhibited narrow-width waveforms, TD-pattern and BD-pattern cells generally had wider waveforms. This possibly suggest that the multidirectional group primarily were composed of more putative principal neurons. However, it was unclear if the HD group consisted of more inhibitory neurons.

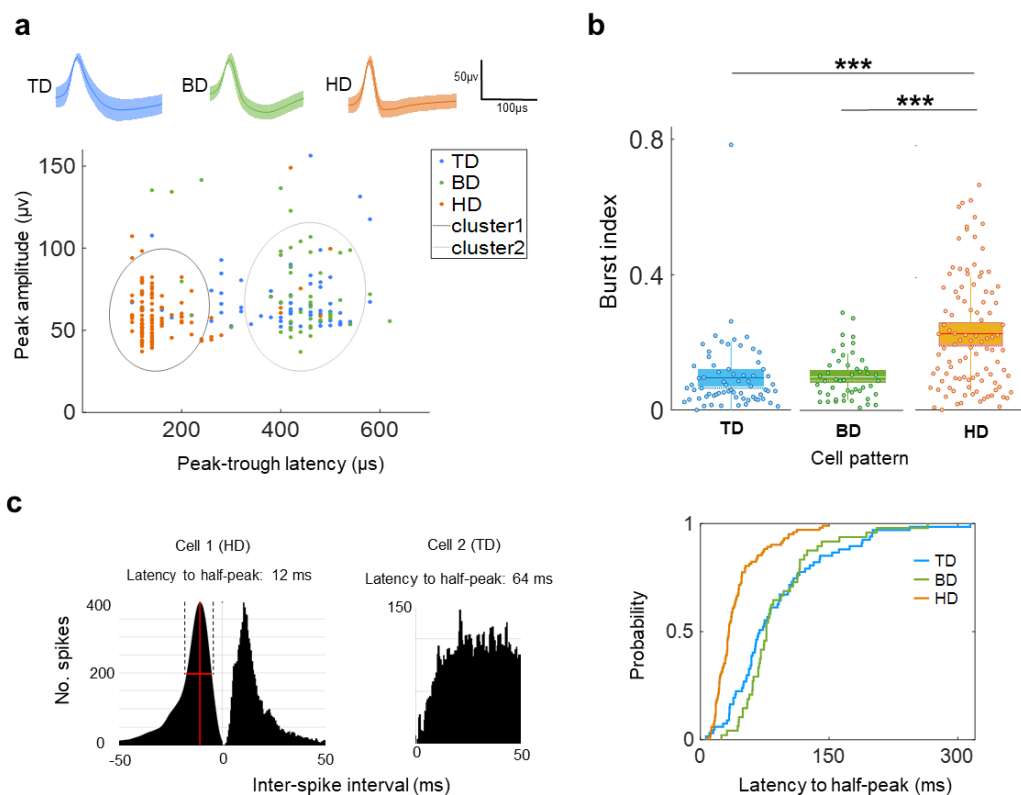


Figure 6-3. Distinguishable electrophysiological properties of multidirectional cell from HD cell. **a.** Top: Example waveforms of a TD-pattern (blue), BD-pattern (green) and HD cell (orange) of the channel with the highest amplitude (Mean±SEM), numbers denote of waveform peak amplitude and peak-trough latency. Bottom: scatter plots shown multidirectional cell cluster (cluster 1, dark circle) distinct from HD cells (cluster 2, pale circle), K-Means clustering, best total sum of distance between two clusters = 11946.3. The distributions were plotted as ellipses specified by population mean and covariance. **b.** Box plots of burst index show significantly different distributions between TD and HD, BD and HD cells, but not between TD and BD (solid line: mean, dotted line: median). **c.** Left: Example of an HD cell (top) and TD-pattern cell (bottom), showing distinct spiking distribution in inter-spike intervals analysis. Right: cumulative probability distributions of latency to half-peak (FWHM) for TD and BD patterns were similar, while different from HD cells.

Moreover, HD cells were significantly burstier than multidirectional cells and had shorter decay latency (i.e., full width of half maximum) to half-peak in the inter-spike interval histogram than that of multidirectional cells (**Figure 6-3**). The latter finding is consistent with the previous comparison of HD cells and BD-pattern cells solely (Jacob et al., 2017).

Furthermore, the relationship of cell firing to LFP was investigated. It was found that the BD-pattern cells, TD-pattern cells, especially HD cells, did not exhibit prominent theta rhythmic spiking, as evident in their low Rayleigh vector lengths at the population level (see **Table 6-2; Figure 6-4**). However, the relationship between theta LFP and directional cell spiking did differ slightly between HD and BD cells: HD cells showed the lowest level of phase-locking, marginally significantly lower than BD-pattern cells.

Some additional differences between multidirectional cells and HD cells should be noted: a few more multidirectional cells did show higher phase-locking strength. As Alexander et al. (2020) quantified theta-modulated cells in RSC using a similar method (see their Fig 6), their population median of modulation strength ($r = 0.13$, for non-EBC cells) was thus used here as a reference. It was found that significantly more BD-pattern cells ($n = 8$, 16.7%) had their theta-modulation strength higher than 0.13 (as shown in **Figure 6-4a**), compared with the HD group (HD, $n = 5$, 4.9%; Chi-Squared test showed significant differences between them: $\chi^2(2, N = 169) = 5.71, p = 0.017$). The difference was not significant between the BD-pattern and TD-pattern groups (TD, $n = 5$, 7.5%; $\chi^2(2, N = 115) = 2.36, p = 0.124$) or between the TD-pattern and the HD groups ($\chi^2(2, N = 169) = 0.48, p = 0.490$). Overall, the number of cells that exhibited stronger theta-modulation was not significantly different between multidirectional and HD cell groups ($\chi^2(2, N=217) = 2.91, p = 0.088$). The results were consistent with the comparisons of their

modulation strengths as listed in **Table 6-2**. The LFP results suggest that although multidirectional cells in general were not coupled to theta LFP, some subsets seemed more likely to show theta phase-locking spiking activity than the RSC HD cells.

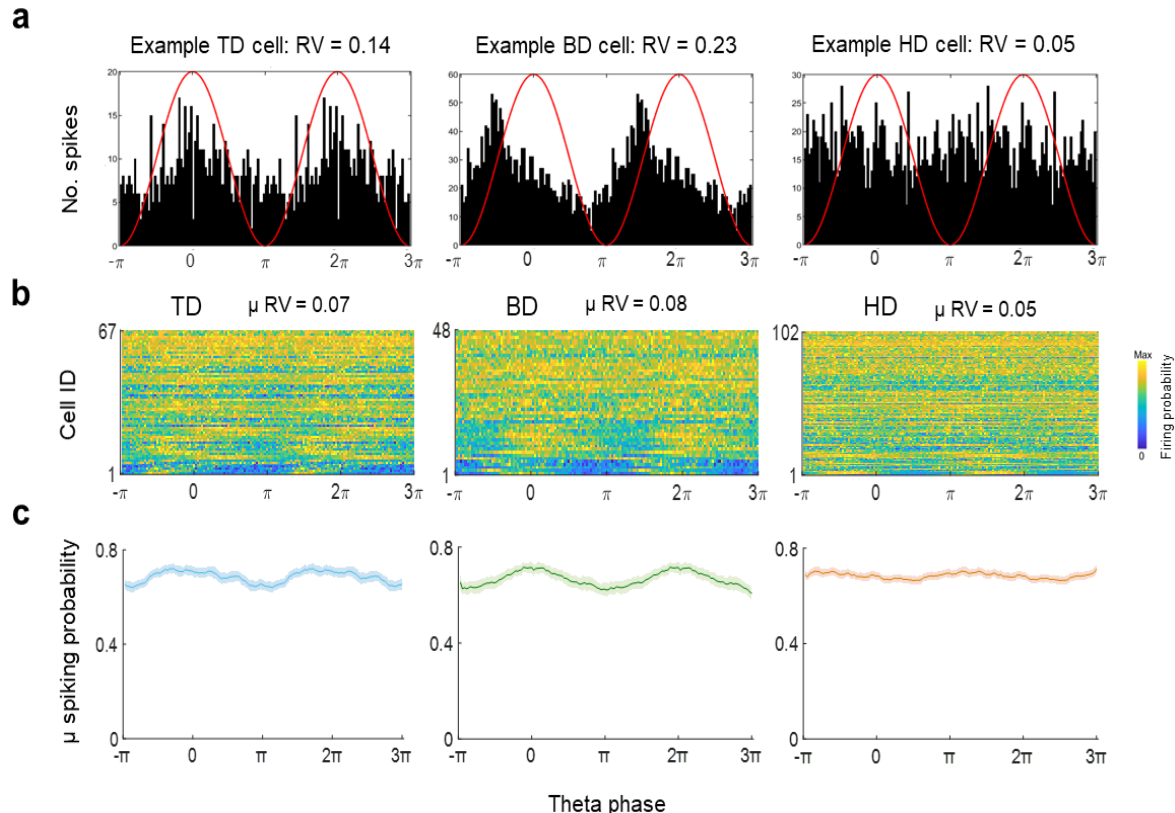


Figure 6-4. Multidirectional cells and HD cells are generally not theta-modulated.

- a.** Histograms show the spiking activity of three example cells relative to theta phase. The red lines trace the amplitude of a theta wave at every phase. Note that these cells vary in their theta modulation strengths, as denoted by the RV values (Rayleigh vector length). The multidirectional cell examples (as in bottom rows in b) do not represent the population level, but the HD example is typical.
- b.** Heatmaps show spiking activity as a function of theta phase for three patterns. Cell ID was sorted by their Rayleigh vector lengths (maximum at the bottom), representing the strength of phase-locking. The number denotes the population mean strength of phase-locking. **c.** Normalised spiking activity (mean \pm SEM) over two theta phases. The relationship between theta and cell spiking was not significantly different between the BD vs. TD groups or TD vs. HD groups, but it was slightly different between BD vs. HD groups; see text for a detailed description.

Table 6-2. Summary of cell electrophysiological properties and statistics.

The electrophysiological firing properties of directional cells (Mean \pm SEM) showed that multidirectional cells were different from HD cells in many aspects.

Neural properties	TD pattern	BD pattern	HD cells	Welch's ANOVA*	Post-hoc comparisons
Peak amplitude (μ V)	68.51 \pm 2.35	74.69 \pm 3.94	60.40 \pm 1.64	$F(2, 101.87) = 7.84,$ $p = 0.001$	TD vs BD: $p = 0.374;$ TD vs HD: $p = 0.015;$ BD vs HD: $p = 0.004.$
Peak-trough latency (μ s)	402.39 \pm 13.72	405.83 \pm 17.51	162.75 \pm 7.99	$F(2, 100.98) = 159.73,$ $p < .001$	TD vs BD: $p = 0.987;$ TD vs HD: $p < .001;$ BD vs HD: $p < .001.$
Burst index	0.10 \pm 0.01	0.10 \pm 0.01	0.23 \pm 0.02	$F(2, 140.61) = 24.81,$ $p < .001$	TD vs BD: $p = 0.926;$ TD vs HD: $p < .001;$ BD vs HD: $p < .001.$
Latency to ISI half-peak (ms)	88.17 \pm 7.28	89.67 \pm 6.62	42.12 \pm 2.91	$F(2, 94.87) = 33.64, p < .001$	TD vs BD: $p = 0.987;$ TD vs HD: $p < .001;$ BD vs HD: $p < .001$
Theta modulation strength	0.07 \pm 0.01	0.08 \pm 0.01	0.05 \pm 0.005	$F(2, 108.37) = 2.98,$ $p = 0.055$	TD vs BD: $p = 0.523;$ TD vs HD: $p = 0.252;$ BD vs HD: $p = 0.07.$

* The assumption of homogeneity of variances was violated, and so Welch's ANOVA was used as an alternative to the classic One-way ANOVA. Games-Howell test was used to compare all possible combinations to detect group differences.

6.4 Discussion

In this chapter, the results revealed that the multidirectional cells as a whole population were anatomically distributed differently from HD cells, and their electrophysiological properties were different. They together supported Hypothesis 5 of the thesis: multidirectional cells are a distinct subclass of neurons from the canonical HD cells.

Specifically, directional neurons in RSC showed clear anatomical segregations: multidirectional cells were localised primarily in the dysgranular RSC, whereas more HD cells were found in the granular sub-region. The results were consistent with the earlier finding that BD-pattern cells were recorded almost exclusively in the dysgranular RSC (Jacob et al., 2017; RSC HD cell distribution was not specified in particular). They suggest that the multidirectional and HD cells are distributed disparately in different RSC sub-regions. However, it should be noted that the current recordings only sampled around AP -5~5.5, and there might be variations along the rostral-caudal axis of RSC, because the anterior part is closely in contact with motor cortices (Yamawaki et al., 2016) while the posterior part is connected with visual areas (Van Groen and Wyss, 1992). Future work should sample along different caudal-rostral parts of RSC.

The results also reflect a gradual dorsal-to-ventral difference in directional encoding in RSC. The current finding interestingly echoes with previous results in MEC. Giocomo et al. (2014) reported that dorsal HD cells in layer III of MEC showed sharper tuning than ventral MEC HD cells. However, the MEC cell population displayed unimodal distribution in their directional phase, indicating that those HD cells are just different variants relating to anatomical segregation, rather than different subclasses of neurons as shown in the current results. Nevertheless, given reciprocal connections between the MEC and RSC (Czajkowski et al., 2013; van Wijngaarden et al., 2020; see **Chapter 2**), one might expect to see similar

multidirectional cells in MEC. However, specific projections from RSC sub-regions to the dorsal-ventral MEC layers were not clear. Also, it remains unknown whether the widely tuned cells observed in ventral MEC (Giocomo et al., 2014) can ever ‘become’ multidirectional (also see Kornienko et al., 2018), like the RSC neurons, if systematically tested in symmetric environments. The current study therefore has provided reliable experimental set-ups (1-boxes, 2-box and 4-box) for future studies to explore the issue.

Second, the analyses revealed the novel finding that several electrophysiological characteristics of multidirectional cells are distinct from HD cells. Spike waveform analysis allowed us to classify recorded units roughly as fast-spiking neurons or putative excitatory interneurons, although they had significantly shorter peak-trough latency in their waveforms than multidirectional cells, suggesting that at least RSC multidirectional cells are likely to be regular-spiking, putative pyramidal neurons. Interestingly, Keshavarzi et al. (2021) reported that approximately 20% of the recorded RSC HD cells were putative inhibitory cells. Long et al. (2020) found that 10% of somatosensory HD cells show fast-spiking characteristics. suggesting that cortical HD neurons may have some similar characteristics.

A more in-depth categorisation of cell types requires high resolution-investigations through juxtacellular recordings or recordings *in vitro*. Brennan et al. (2020) dissected intrinsic properties of RSC neuronal subtypes more precisely. They reported small, excitable pyramidal neurons (low-rheobase) that receive local feedforward inhibition from layer II/III fast-spiking neurons, which possibly convey PoS HD signals to RSC. How might the intrinsic physiological properties of RSC neurons determine the cell’s capacity for direction encoding? Currently it remains unknown whether multidirectional cells and HD cells receive excitatory

or inhibitory inputs differently, and whether there is any crosstalk between the two types (although see theoretical considerations in **Chapter 7**).

One possible way to explore interactions between the HD cells and multidirectional cells experimentally is to cross-correlate the spike trains of units simultaneously recorded from the same trial. For example, strongly correlated firing at brief time scale might suggest monosynaptic connection between the cells (Csicsvari et al., 1998). This type of analysis might provide some hints as to whether HD inputs arrive at the synapses of multidirectional cells within a short period of time (see section 7.3.1 for discussion on the Hebbian model). However, due to the limited number of simultaneously recorded HD and multidirectional cells in the current study, such analysis was not possible. To characterise information transmission within the retrosplenial circuit, future research should adopt large-scale recording techniques to co-record a larger population of HD cells and multidirectional cells to examine the temporal relationship between their spiking activity.

Furthermore, it was found that HD cells are burstier than multidirectional cells. Again, there was not enough resolution for us to characterise how burst firing is functionally relevant to RSC directional cells. Nevertheless, previous findings in the hippocampal place cells supply some hints. It has been shown that bursts sharpen spatial tuning in the CA1 place cells (Harris et al., 2001), and this may be the case for RSC HD cells that have tighter HD tuning width (see Chapter 4). Besides, sparsely-bursting cells may carry more spatial information than dominantly bursting cells in the subiculum (Simonnet and Brecht, 2019). Likewise, in the RSC, one may infer that multidirectional cells that encode multiple head direction orientations carry more direction information, and their firing is more sparse than unidirectional HD cells.

Finally, the current findings have several implications. Future research may explore the following directions: first, can we use electrophysiological characteristics as ‘markers’ to classify RSC directional cells while screening in a simple environment? It is a challenge for the experimenter to identify the multidirectional cells until recordings are performed in the multicompartment boxes. Therefore, identifying unique electrophysiological features will provide hints as to how to classify the cells. Second, future analyses may also look at whether the electrophysiological features relate to the cells’ cytoarchitectonic (i.e., cellular composition) features in granular, dysgranular, and the intermediate area within the RSC. The analysis could also be extended to the whole cell population recorded in RSC, including those non-directional cells.

Third, how do spiking properties of RSC neurons such as the burstiness of discharges and their temporal correlations relate to directional encoding? As mentioned earlier, simultaneous recordings of a large number of multidirectional and HD cells can help answer this question; and fourth, what specific cell types might multidirectional and HD cells be, and do they receive excitatory versus inhibitory synaptic inputs differently? Are those synaptic inputs homogeneous? These questions are beyond the resolution of extracellular single-unit recordings. The data generated from the current study provided useful directions for future research to characterise how information transmission happens at microcircuit level between different neuronal subclasses in RSC.

Together, the data showed that TD-pattern and BD-pattern cells share comparable neural properties but are distinct from HD cells, indicating that multidirectional and HD cells are two separable subclasses of neurons. The results supported the last hypothesis of the thesis, reflecting functional dissociation in relation to anatomical segregation in RSC.

CHAPTER 7

CHAPTER 7 GENERAL DISCUSSION

7.1 An overview of results

The principal aim of the current thesis was to uncover the neural basis of spatial orientation in rat retrosplenial cortex (RSC), so as to explore a potential capacity of RSC in resolving directional ambiguity while rats navigate in multi-fold symmetric environments. To achieve this, I used extracellular single-unit recordings to record direction-selective neurons in RSC while rats freely and randomly foraged in multiple environments that varied in symmetry order (e.g., onefold, twofold and fourfold). The level of visual and directional ambiguity changed accordingly. The recordings were conducted in two separate sets of experiments. The cell activity was analysed extensively throughout three results chapters: in relation to allocentric head direction orientations, egocentric boundary vectors and electrophysiological properties, respectively.

The first experiment, the ‘2-box’ experiment, was not only to replicate the intriguing finding of a retrosplenial bi-directional (BD) tuning pattern reported by Jacob et al. (2017), but also to test these two hypotheses (Hypothesis 1 & 2): first, whether the atypical BD pattern was intrinsic to RSC neurons or arose from an environment; and second, if the twofold pattern was driven by a twofold environment symmetry, did the pattern follow the environment symmetry order, as suggested by previous theoretical work (Page and Jeffery, 2018). Thus, the second set of experiments, termed the ‘4-box’ experiment, specifically investigated the two hypotheses further: especially whether the noncanonical directional pattern would show a fourfold symmetry in a fourfold symmetric environment. Both experiments also looked at whether the cells would show onefold symmetry in 1-boxes.

At the time the two experiments were completed, interestingly, others reported egocentric boundary vector cells (EBC) in rat RSC (Alexander et al., 2020; see section 1.4.4.2). The authors proposed that the bidirectional pattern reported by Jacob et al. (2017) might be produced by unnoticed egocentric tuning, raising the possibility that whether the cells recorded from the current experiments encode egocentric boundaries, thus accounting for their HD tuning. Accordingly, two additional hypotheses (Hypothesis 3 & 4) were examined: whether EBCs produce multidirectional tuning in multicompartiment environments and whether the multidirectional cells are EBCs. I did extended analyses on a simulated egocentric cell dataset and the recorded data.

Furthermore, the final hypothesis (Hypothesis 5) was tested: whether the noncanonical directional cells was a distinct subclass from HD cells. Their anatomical distributions in RSC and several electrophysiological characteristics were examined. Next, I summarise the results and review the five hypotheses respectively.

7.2 Review of hypotheses

The original five hypotheses examined in the current thesis were listed in section 2.4 of Chapter 2, and some of them were supported and others were refuted. In this section, for clarity, based on the current findings, they are rephrased as conclusions in subheadings and reviewed systematically.

7.2.1 Hypothesis 1: the bidirectional pattern is not an intrinsic property of the cells

As shown in **Chapter 4**, in the 2-box experiment, the BD pattern did not persist when the environment changed from twofold to onefold symmetry (i.e., 1-box, an open circular arena). Instead, a subset of BD-pattern cells showed a onefold firing pattern (single-peaked) in the 1-boxes as well as in single sub-compartments of the 2-box. When the environment

symmetry order was increased to fourfold in the 4-box experiment, rather than keeping the BD pattern, the RSC cells showed a prominent tetra-directional (TD) pattern, and the four tuning peaks were separated by 90°. Similarly, the TD pattern again was demolished if the environment symmetry was reduced to onefold in 1-boxes (i.e., the single-cued circular arena and square box). The results clearly rejected the hypothesis that the multidirectional pattern is an intrinsic tendency of these neurons.

More importantly, the hypothesis was also refuted by an absence of multi-directionality in the 1-boxes when the animal was naïve to the multicompartment environments. Due to technical difficulties in obtaining a large sample of data from naïve animals (as discussed in **Chapter 4**), it remains unknown whether the onefold firing pattern is a built-in feature of some cells. The data obtained in the cylinder provided some hints that some cells showed single peaks and could follow visual landmark rotations, even if when the animal is naïve to multicompartment environments (albeit preliminary).

For future work, using large-scale recording techniques (e.g., high-density silicon probes) in freely moving animals would foster simultaneously sampling of a large population of neurons from naïve rats, before an exposure to the multicompartment environments. It might help answer the question of to what extent these RSC neurons might be intrinsically unidirectional in onefold symmetric environments. The current results of onefold firing in 1-boxes suggest that the single landmark (in the cylinder) and multiple distal landmarks in the room (around the arena) may drive the single peaks of the cells (see section 7.3 below for discussion). This is consistent with the view that RSC processes allocentric, landmark-based directional information (Jacob et al., 2017; Page and Jeffery, 2018).

7.2.2 Hypothesis 2: the multidirectional pattern of the cells is driven by environment symmetry

The main findings of the two experiments showed that a population of RSC neurons displayed a fourfold, twofold, or onefold firing patterns in the 4-box, 2-box, and 1-boxes respectively, following the order of environment symmetry. Together, these noncanonical directional cells were referred to as multidirectional cells. In contrast, the canonical HD cells in RSC maintained a unidirectional firing pattern in all environments and their subspaces.

Interestingly, based on the firing symmetry within single sub-compartments in the multicompartment environments, the multidirectional cells were divided into two subsets: the within-compartment (WC) and between-compartment (BC) cells. The BC cells showed single peaks within single sub-boxes, displaying an overall multidirectional pattern in the whole environment. In contrast, analogously to the current finding of a twofold pattern in a single sub-compartment (i.e., the WC-BD cells; also in Jacob et al., 2017), some WC multidirectional cells expressed a fourfold pattern even in a single sub-compartment, indicating new learning of multiple directions from experience in the 4-box. This result clearly ruled out the possibility that the multidirectional pattern could have been intrinsic and instead supports the environment-dependent account.

The observation of a fourfold pattern within a sub-compartment was particularly interesting, as it did not break down when the symmetry order was as high as fourfold, in contrast to the theoretical prediction by Page and Jeffery (2018). That model and formation of the multidirectional pattern are discussed in detail later. Together, the findings not only confirm the earlier report in Jacob et al. (2017) but also provide new support and detailed characterisation of the multidirectional pattern, which is unlikely to be an intrinsic property of retrosplenial cells but driven by environment symmetries. Critically, the results of

within-compartment pattern support that the multidirectional pattern was learned from the environment.

7.2.3 Hypothesis 3: egocentric boundary vector cells yield a multidirectional pattern as an artefact

The rationale of the third hypothesis was mentioned earlier. It was examined by analysing the HD tuning of the simulated EBCs in four experiments: simple circular arena and square box that comprise the peripheral boundaries only; and the 2-box and 4-box that comprise multiple inner and outer walls. The simulated EBCs generated from our model (see methods in **Chapter 5**) do not ‘encode’ allocentric head directions but only egocentric parameters, and they share similar features with the empirical RSC EBCs (Alexander et al., 2020).

The simulated EBCs generally showed a four-way symmetry in HD tuning in the square box and the 4-box, due to restrained spiking activity of EBCs along the neighbouring walls with a 90° conjunction offset between two allocentric axes. However, the four-way pattern was slightly deformed in some of the sub-boxes, possibly because of the discontinuity at the doorway. The EBCs showed a two-way pattern in the 2-box and its rectangular sub-boxes, possibly due to marked inhomogeneous distribution of spikes along the long-wall versus the short-wall axes (see discussion in **Chapter 5**). The symmetry pattern was lost in the circular arena. The data showed that the HD tuning pattern of EBCs arises as the cells exhibit substantial spiking biases in heading associated with boundary directions (or angular offsets between walls) in an environment. Moreover, a lack of single-peaked sharp tuning in the HD pattern of EBCs supported that they do not encode true head directions. The findings from the simulation supported the view that HD tuning of EBCs reflects environmental geometric features (Alexander et al., 2020), but, critically, they should be considered as an artefact of representations of egocentric boundary relationships. It should also be emphasised

that the phenomena of HD tuning of EBCs should be considered mechanistically different from the multidirectional cells. The mechanism for the former has been discussed earlier (section 5.4.2), and the latter is discussed in section 7.3.1 below.

The simulation work and testing of this hypothesis had two important implications: first, they confirmed the speculations made by Alexander et al. (2020); and second, they confirmed the EBC detection methods and allowed comparisons with the HD tuning of the recorded data. This leads to the next question: whether the multidirectional cells truly encode allocentric head direction orientations in symmetric environments or any egocentric boundary related features?

7.2.4 Hypothesis 4: the multidirectional cells are not egocentric boundary vector cells

As shown in **Chapter 5**, the directional data collected in the two experiments were analysed in egocentric reference frame using established methods as validated here. In general, the multidirectional cells did not show significant egocentric coding characteristics in any environment. Although a few multidirectional cells seemed to pass the EBC detection threshold, they were likely to be false positives because they were not stable or reproducible in second trials or between different environments.

More importantly, the recorded multidirectional cells were distinct from the EBCs in various aspects, as summarised in **Chapter 5**. If the egocentric position of boundaries drives HD tuning of the cells, the boundary directions would have been associated with the cells' preferred directions, as reported in simulation data and previous observations (Alexander et al., 2020; also see S1 egocentric cell examples in Long, Deng et al., 2021). However, this was not the case in the recorded directional cells. Homogenous distribution of multidirectional preferred tuning peaks in the 2-box and 4-box supports that multidirectional cells, like HD cells, encodes the animal's head orientations uniformly in allocentric space.

Moreover, homogenous distributions of spiking activity of multidirectional cells suggest that the cells fire neither along the walls nor in the centres of the arena, whereas the EBCs showed conspicuous spiking preference along the boundaries. These results revealed that the RSC multidirectional cells robustly encode head directions in a world-centred reference frame and clearly ruled out the possibility that the multidirectional cells could have been egocentric. The reasons for the fact that EBCs were not present in the current dataset were discussed in **Chapter 5**. In short, this was probably because of differences in cell distributions along the rostral-caudal RSC, and the current recordings were only sampled from the caudal part of RSC.

7.2.5 Hypothesis 5: the multidirectional and HD cells are different subclasses

In **Chapter 6**, histological analyses of recording sites showed that most multidirectional cells were found in the dysgranular RSC, whereas majority of HD cells were in the granular RSC. The current results largely agree with previous findings in Jacob et al. (2017). In addition, a more careful characterisation showed that TD-pattern and BD-pattern cells displayed a prominent level of homogeneity in characteristics of the waveforms, inter-spike interval and burst index, making them distinguishable from HD cells.

Although cell-type-specific information was not available using the current recording methods, the waveform information could supply some hints about cell types (Peyrache et al., 2012). More multidirectional cells are likely to be regular-spiking pyramidal neurons, whereas unidirectional HD cells in RSC are fast-spiking, bursty neurons, although it is unknown if the HD cells are inhibitory interneurons. The results suggested that the multidirectional neurons may be a distinct cell type from the canonical HD cells in RSC, and their functional segregation is associated with anatomical segregation.

Interestingly, the fact that retrosplenial HD cells tend to be fast-spiking, less theta-modulated and show burstier firing mode corroborate the features of some HD cells in S1 (Long et al., 2020). Long et al. (2020) found that 10% of S1 HD cells show fast-spiking characteristics and are more sharply tuned than the regular-spiking HD cells in S1. In short, the present findings of multidirectional cells and HD cells in RSC suggest that co-existence of fast-spiking and regular-spiking direction-selective cells may be a general phenomenon of direction encoding in the cortex.

7.3 The underlying mechanisms of multidirectional encoding

This section is dedicated to discussing how multidirectional cells encode multiple head direction orientations in multi-fold symmetric environments.

7.3.1 What generates the pattern of multidirectional cells?

To account for the first RSC BD pattern reported by Jacob et al. (2017), Page and Jeffery (2018) devised a computational model that simulated the BD pattern in the 2-box and a tri-modal pattern in a trifold symmetric environment, delineating a dynamic interaction between landmark and HD processing in RSC. Specifically, according to that model (Page and Jeffery, 2018; as reconceptualised in **Figure 7-1**), RSC HD cells inherit the canonical HD signal from thalamic nuclei such as the ADN and ATN as part of the HD circuit. For example, an HD cell only becomes active if the animal faces ‘North’ and receives a presynaptic signal from a global ‘North’ HD signal through pre-wired connectivity with thalamic nuclei, regardless of environment symmetry or type (**Figure 7-1a**).

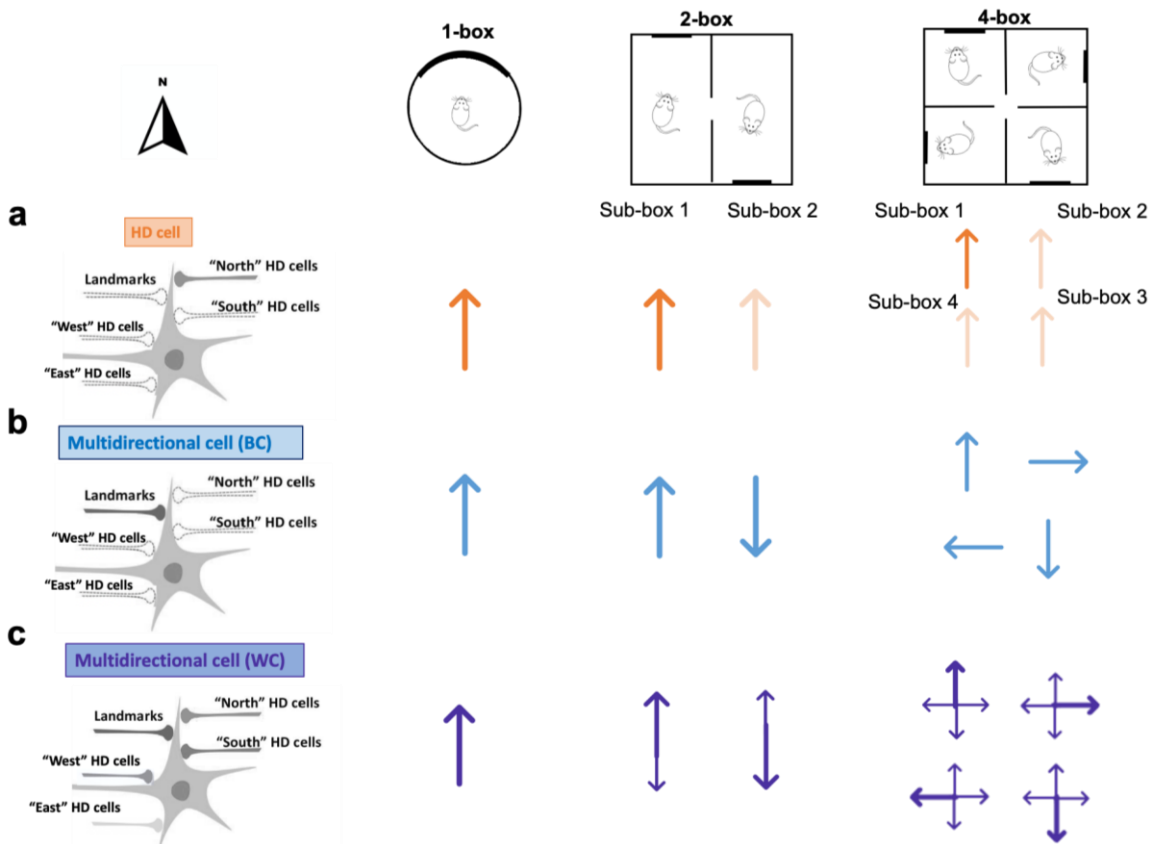


Figure 7-1. Multidirectional encoding appears from landmark learning and Hebbian plasticity. Page and Jeffery (2018) proposed the original model (see their Fig. 2), here this has been modified to capture the fourfold symmetry. **a.** A canonical HD cell receives a global HD signal (left: 'North' signal, via pre-wired synaptic inputs in dark grey) from the HD attractor system. It becomes active when the rat faces North (denoted by an orange solid upward arrow) in different environments and their sub-boxes; it does not fire (faded arrow) when the animal faces other directions, but other HD cells would become active. **b.** A between-compartment (BC) multidirectional cell (blue) becomes active when it receives a presynaptic signal (grey) from local environmental landmarks. When the animal faces the cue card, the landmark direction is coincident with 'North' direction in one sub-compartment and 'South' in the other in the 2-box, as denoted by the arrows. The arrows follow landmark rotation in sub-boxes in the 4-box. In 1-box, the cell shows a one-way peak driven by the landmark. **c.** It is more complicated for the within-compartment (WC) multidirectional cells. The WC cell becomes active by receiving not only landmark inputs but also co-activated HD cell signals. As an example, activity in the sub-box 3 of the 4-box is denoted in the neuron illustration on the left: the connectivity is strengthened if the 'South' HD signal aligns with the 'South' cue card direction (denoted as dark-grey synapses), as the animal faces away from the cue card, it receives inputs from other co-active HD cells, so weaker connectivity and firing (denoted as light-grey synapses). The weaker inputs lead to a second peak in the single compartments of 2-box, as well as the third and fourth peaks in the 4-box. In the 1-box, the cell shows one-way peak driven by the landmark and/or the HD signal.

The between-compartment (BC) cells mainly receive active inputs from salient visual landmarks and show a local, unidirectional pattern in the current local environments (**Figure 7-1b**). When the environmental landmark is present in the local view of the animal (e.g., the

field of view width was set to 90° for simulations by Page and Jeffery, 2018), some landmark-detectors, possibly located in the visual area, encode landmark bearings similarly to HD attractor dynamics (e.g., forming a Gaussian peak) and send landmark bearing information to the BC multidirectional cell, yielding its maximal firing. As the animal faces a different landmark in another sub-box, the cell's PFD follows directional rotations subsequently.

The within-compartment (WC) cells are driven by inputs from HD cells and environmental landmarks (**Figure 7-1c**). Critically, once encoding of the landmark bearing in each sub-compartment is coincident with the current HD signal, their synaptic connectivity gets strengthened due to Hebbian plasticity: prolonging changes in the synapse conductance as the result of association between pre- and postsynaptic activity. For instance, when the animal faces ‘North’ and a north landmark in sub-box 1, the WC cell fires with its largest peak pointing to ‘North’. As the animal moves into a different sub-box facing ‘East’, the cell’s largest peak rotates accordingly due to Hebbian co-activation - the local East landmark aligns with the now-online ‘East’ HD signal. Other peak(s), although smaller, are present as the animal heads other directions in local subspaces, because previously activated synapses of HD cells (those were in 180° apart in the 2-box; in 90° apart in the 4-box) also provide slightly weaker inputs via Hebbian plasticity. Accordingly, the WC cells showed asymmetric two peaks in sub-boxes of the 2-box and asymmetric four peaks in sub-boxes of the 4-box.

This Hebbian learning account also reflects mnemonic processing in RSC because landmark learning happens rapidly, as evident in the current finding that the firing symmetry can be established from Day 1 exposure. The Hebbian learning aspect also suggests that new association of landmark inputs and HD inputs is established and cached in the system at the time of learning, supporting cognitive mapping in RSC (see section 2.1.2.3).

In sum, the current experimental observations of WC and BC cell firing activity could largely be explained by the Hebbian learning of environmental landmarks, as delineated by the model (referred to as the landmark model hereafter; Page and Jeffery, 2018). However, some important aspects of the data not entirely consistent with the theoretical account are worth highlighting below.

7.3.2 Is there a theoretical limit on symmetry order?

First, the landmark model illustrated that as the number of peaks in HD tuning increases, the multidirectional cell's responses become less precise to a given direction: thus, there would be a limit to the number of multiple sub-boxes in a symmetric environment to drive the multidirectional pattern. Their simulation results, as shown in **Figure 7-2**, demonstrated how theoretical limits on environment symmetry order and HD tuning peaks arise: as the agent learned a relationship between HD inputs and landmark inputs that rotate by different angular amounts in symmetric environments (e.g., 120° in a 3-box, 90° in a 4-box, 60° in a 6-box), the standard deviation of the Gaussian profile was set to different values, describing changes in the connectivity from landmark detectors to multidirectional cells. The number and widths of HD tuning peaks of the cell increased accordingly with the number of sub-compartments within an environment. According to the model, the HD tuning curves eventually lost their precision as the number of sub-compartments reached as high as four and above. For example, when $\sigma = 30$, although the four peaks seem to be preserved in the fourfold, the directional precision would be low and fail the threshold; this was prominent when $\sigma = 40$.

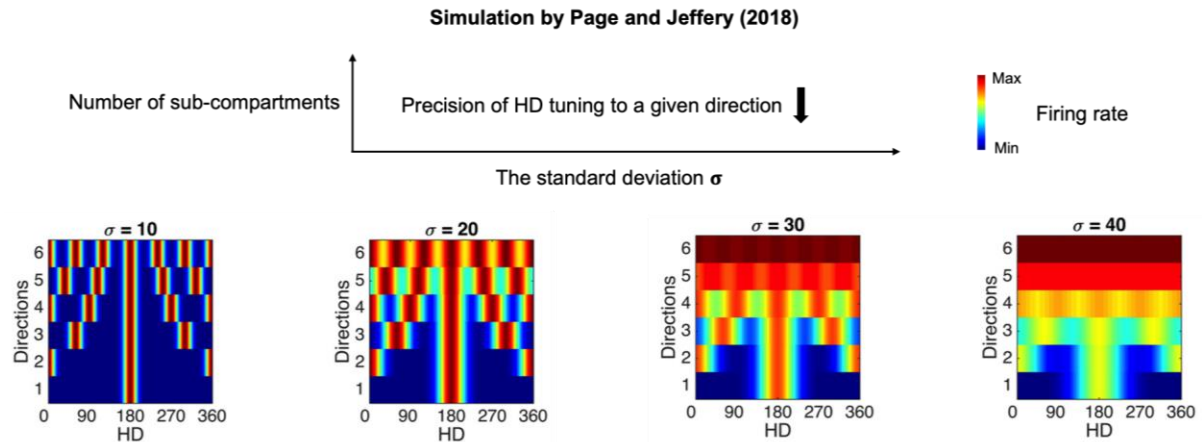


Figure 7-2. Simulated effects of sub-compartment numbers on HD tuning specificity.

First row: the main message conveyed by the simulation results (subplots below) reported by Page and Jeffery (2018). The colour bar denotes HD cell firing intensity in the subplots. Second row: as the number of sub-compartments and multiple directions increases (y-axis), a multidirectional cell adds tuning peaks separated evenly in a range from 0° to 360° (x-axis); as the sigma value increases, accordingly, the cell's tuning becomes broader and lose the resolution in differentiating multiple directions of the sub-compartments. Adapted from Page and Jeffery (2018; their Fig 10).

On the contrary, the experimental observation of the WC-TD pattern in the 4-box broke the theoretical limit suggested by the landmark model. Instead, the RSC HD network clearly acquired the ability to differentiate multiple directions in a four-way symmetric environment. Therefore, the parameters (e.g., the sigma value) used in that model describing the Hebbian weights of landmark inputs onto the cells need some modification for simulation in multi-fold symmetric environments. Simulation work in more than trifold symmetric environments is currently lacking, and it would be an important future direction. It would also be interesting for future experimental work to test if the cells form fivefold pattern in a pentagonal environment and sixfold pattern in a hexagonal environment with multiple directions and subspaces.

Nevertheless, although the WC-TD pattern was not captured by the landmark model, the current preliminary data that TD-pattern cells lost their TD pattern in the square box (see section 4.3.3 of Chapter 4) was consistent with their simulated results in an open field (Page and Jeffery, 2018; their Figure 11). The simulated uniform pattern was also consistent with

the current 1-box data in which many cells lost their directional specificity in the circular arenas, albeit some showed a onefold tuning peak. Thus, this raised an interesting question: whether the synaptic weights from landmarks and/or HD inputs to multidirectional cells differ in a onefold, independent square box (and 1-box in general, including the circular arenas) from a quadrant of the 4-box. If so, what may cause the difference? Two possible accounts are proposed below.

7.3.3 Learning multimodal environmental cues

First, it is possible that the miscellaneous cell activity in the 1-box was due to contextual changes. The 1-box trials were all performed in experiment rooms different from the multicompartiment one with an aim of achieving the best chance of cue control for the latter. Moreover, the multicompartiment boxes, but not the 1-boxes, were scented with odour cues to help spatial disambiguation. It is possible that some neurons were probably sensitive to contextual changes (i.e., room, odour) between the 1-boxes and multi-fold boxes and lost the directional specificity due to contextual modulation, analogously to a mixed of global and partial remapping of hippocampal place cells modulated by contextual inputs such as wall colours and odours (Anderson and Jeffery, 2003; section 1.4.1.2). It should be noted that the odour is not necessary for the multidirectional pattern to appear (as shown in Chapter 4).

This account is consistent with the view that RSC is involved in contextual learning (Todd et al., 2019), suggesting that the environment inputs learned by the RSC HD network are multimodal. This was also mentioned by the model in which the landmark detector layers are not purely ‘visual’ (Page and Jeffery, 2018), corroborating the current finding of a sustained TD pattern (and persistent BD pattern in Jacob et al., 2017) in the dark. However, since the landmark detector layer stays theoretical, to what extent their pre-synaptic weights

to the multidirectional cells are influenced by contexts is an open question for future research (see section 7.4.3 below).

Second, it is possible that the landmark detectors did not detect their ‘favourite’ landmarks (those present in the multicompartment box) in the 1-boxes. A lack of co-activated HD signal with the ‘favoured’ landmark bearing may account for an absence of directional specificity in the 1-boxes. One prominent difference between the 1-box and the multi-box is the central doorway. For example, it is possible not only that the landmark detectors process the visual cue card bearings in the multicompartment environments, but that the doorway also acts as a salient landmark in maintaining environment symmetry. In addition, knowing the angular offsets between sets of cue cards or doorway-to-cue-card may be sufficient to establish the wiring. This account corroborates the view that RSC neurons are particularly involved in processing landmarks (see section 2.1.2.1).

7.3.4 Reference frame transformation

The reference frames possessed by onefold and multi-fold environments are different due to their structures: multiple sub-boxes are connected via the central doorway in the latter, whereas physical transition between local and global space is not applicable in simple 1-boxes. This leads to an interesting but unexplored question considering the relationship between environmental connectivity and the multi-fold firing symmetry. To be more precise, would transitioning from one sub-box to another enable the BC cells to be driven (more) by landmark detectors, and would it particularly engage both landmark and HD inputs to the WC cell?

Transitions between sub-boxes in multi-fold symmetric environments involve reference frame transformation in two aspects that are not mutually exclusive to each other: first, transformation from local (as defined by directions in subspaces inside a whole space)

to a global direction network as described earlier (section 1.5.1.2); as well as transformation from egocentric to allocentric spatial representations. The RSC multidirectional cell activity clearly reveals these processes: reflecting that spatial mapping relies on a combination of idiothetic and allothetic information sources and spatial orientation involves converting directions of egocentric ‘snapshots’ (e.g., the animal’s current visual scenes) into an allocentric relationship of landmark arrays (section 1.3.1).

The reference frame transformation account of RSC multidirectional cells is in line with evidence that visual scene processing and imagery are the key functions of RSC (Byrne et al., 2007; Epstein and Higgins, 2007). They are especially useful for spatial orientation (Shine et al., 2016; section 2.1.2.2). This account also corroborates the RSC function in encoding subspace information such as route segments and converting egocentric information into an allocentric framework to produce repetitive firing activity (Alexander and Nitz, 2017). Therefore, spatial connectivity of subspaces to a global space might contribute to RSC firing symmetry.

As mentioned in **Chapter 2**, connectivity encoding was recently examined in the hippocampal place cells by Duvelle, Grieves et al. (2021) in four-connected-rooms with identical geometric features with distal room cues. The place cells encode locations in a global reference frame rather than changes in local spatial connectivity. It would be interesting for future experimental work to explore how RSC directional encoding may be influenced by changes in environmental connectivity using similar, but cue-controlled set-ups.

In summary, the multidirectional cells encode multiple head direction orientations from the animal’s experience in the multi-boxes. The firing symmetry arises as a result of Hebbian learning of multimodal environmental landmarks. This is different from the HD

tuning of egocentric boundary vector cells as discussed earlier. The next question is, what are the multidirectional cells for?

7.4 Functional significance of two directional systems

This section is dedicated to discussing potential advantages of having multidirectional cells as well as HD cells in RSC and implications extended from the current work.

7.4.1 Assessment of landmark stability

First, let us briefly review how the canonical HD cells maintain a global signal (**Chapter 2**).

Path integration is useful in supporting the global direction signal (Taube and Burton, 1995). In the present experiments, the animal walked freely between sub-compartments in the door-open trials in the 4-box and 2-box. Through experience that the sub-compartments were connected, the animal acquired the knowledge of a global environment structure, and the HD cells form a homogeneous onefold firing peak across subspaces (Dudchenko and Zinyuk, 2005; Smith et al., 2021).

However, as reviewed previously, the HD system (also the hippocampal position system; section 1.5.1.2) is prone to landmark instability and experience (section 2.3.2), and HD cells fail to follow landmark rotations if they are perceived unstable (Knierim et al., 1995). How do the HD cells ‘know’ about landmark instability?

The answer seems to be via the multidirectional cells. According to the landmark model (Page and Jeffery, 2018), RSC HD cells receive competing inputs from the BC and WC cells, depending on which is coincident with the animal’s current heading signal. The BC cells keep track of the changing-by-moving local views, while the WC cells also integrate the expected heading from HD inputs. When there is a match or congruence between the ‘sense of direction’ and the perceived orientation indicated by the current visual panorama,

the multidirectional cells teach the HD system to stay stable, as signified by the largest peak of WC cells, suggesting that the landmark in view is stable.

This Hebbian congruence detection mechanism may help the RSC HD system to resolve the directional ambiguity arising from identical subspaces. For instance, a proper Hebbian learning process in the HD network could have saved Jim Marshall from his disorientated wrong-way-run (section 1.1). His system clearly did not dissociate the HD activity from the multidirectional cells by weakening their connectivity to avoid directional ambiguity. This was probably because an incongruence signal between his estimated HD signal and the current scene of ‘rival’s goal post’, for some reason, was either not generated or was delayed in reaching the system. Therefore, the multidirectional cells may serve as a mechanistic link for teaching the HD system to assess the stability of landmarks during spatial orientation. It corroborates previous evidence on engagement of RSC in processing landmark permanence, which could be generalised to a non-spatial domain (Auger et al., 2018).

7.4.2 A working model for the network to resolve spatial ambiguity

It is hypothesised that the noncanonical directional cells can ‘report’ whether the perceived sensory information matches with the upcoming HD inputs via their interconnections. In this way, the system decides which part of the environment is trustworthy for orientation. This decision process involves procedures such as environment cue weighting, direction signal computation, and reference frame translations in line with the functional characteristics of RSC in spatial cognition (section 2.1.2). The next question is, how may a broader spatial map system benefit from this decision process? To be more precise, how may the two direction codes interact with other circuitries at network level?

As reviewed in **Chapter 2**, RSC has abundant anatomical and functional connectivity with cortical and subcortical regions. A working model for the spatial network is summarised in **Figure 7-3**, centred on the Hebbian landmark weighting mechanism (section 7.3.1) of the current multidirectional cells found in RSC, with a majority from the dysgranular RSC but not exclusively (see **Chapter 6**). More importantly, this working model reconciles the evidence reviewed previously (section 2.1.1) and summarises several candidate brain regions as potential sensory origin and/or the output sites of RSC.

First, the landmark detectors remain hypothetical in the brain, but they may locate in the visual association areas such as V2M, especially given that V2M contains HD cells (Chen et al., 1994). V2M has dense connections with the dysgranular RSC (Van Groen and Wyss, 1992) and para-hippocampal regions such as MEC and POR (Olsen et al., 2017). Accordingly, the BC cells in the dysgranular RSC are hypothesised to receive visuo-spatial sensory information from V2M and send (may receive as well) local landmark-based directional signal to the MEC and POR due to their reciprocal connectivity (Sugar and Witter, 2016). This proposition, although awaits investigation, is in agreement with the fact that some MEC directional cells are considered to be driven by salient visual cues and flip their PFDs accordingly (Kornienko et al., 2018). Similarly, some cells in POR showed a bidirectional tuning in a cylinder adorned with two opposite visual landmarks, and the mechanism is still under investigation (LaChance et al., 2020, *iNAV*). This finding also corroborates the observation that cortical afferent projections into POR heavily originate from dysgranular RSC (as well as visual association areas; Burwell and Amaral, 1998), suggesting functional crosstalk between the two regions. It would also be interesting to investigate whether MEC and POR send landmark inputs into the RSC.

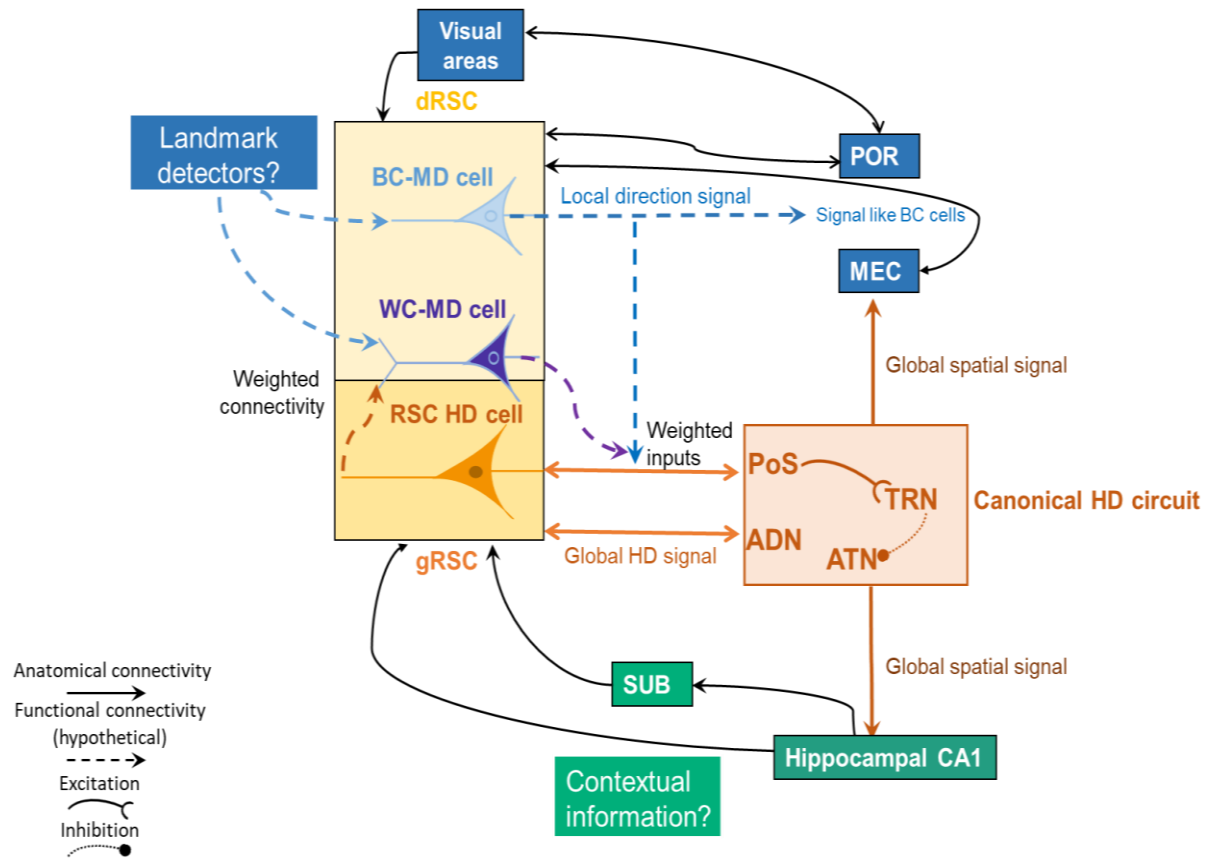


Figure 7-3. Model schematics for the network to resolve spatial ambiguity.

The dysgranular RSC (dRSC, light yellow panel) contains mostly the noncanonical multidirectional cells (blues and purple) while granular RSC (gRSC, yellow) contains the canonical HD cells (orange). As described in the landmark model, hypothetical landmark detectors (navy panel) send landmark inputs (dotted arrow) to both BC (blue) and WC cells (purple); the latter also receive inputs from unidirectional HD cells (orange), and their connection is modulated by Hebbian plasticity. HD cells receive the weighted inputs from the BC/WC cells (where the dotted purple and blue arrows converge) and update the HD circuit and its structures (light orange panel). The hypothetical point where the weighted inputs converge remains unknown. The two RSC subregions receive segregated projections (solid arrow) from different regions: dRSC receives inputs from the visual areas, (and to) the postrhinal cortex and medial entorhinal cortex. Note that V2M is also interconnected with the parahippocampal regions, the postrhinal cortex has dense connectivity with the dRSC and visual association areas. Therefore, visual areas (possibly PoR and MEC as well) are considered as potential landmark sources (coloured in navy). PoR and MEC largely contain global spatial signals, for simplicity, this is not denoted in their panels. The gRSC has more cross-talks between the canonical HD circuit anatomically and functionally: within the HD circuit, RSC and PoS send excitatory inputs to the thalamic reticular nucleus, which functionally inhibits the anterior thalamic nuclei that projects directly back to gRSC. The green panel denotes the hippocampal-subiculum circuit which may send contextual signals to gRSC, which receives direct projection from the subiculum and CA1.

Furthermore, the lateral part of the entorhinal cortex (LEC) may also serve as tentative candidate for landmark processing, because its central role is to process landmarks egocentrically (Wang et al., 2018) and allocentrically (Deshmukh and Knierim, 2011),

although its projection to RSC seems sparse (Haugland et al., 2019). Neunuebel et al. (2013) reported that LEC cell activity was controlled by local cue rotations while the rat ran in one-way direction on a circular track, instead of being controlled by the surrounding distal cues. The results suggest that LEC may prioritise local, multimodal cue processing. It would be interesting for future work to consider how this ‘what’ (i.e., object or item processing) pathway may contribute to landmark-based direction encoding in the network.

Second, RSC is directly connected with the canonical HD circuit, especially the PoS and ADN (Van Groen and Wyss, 1990b; Clark et al., 2010; see section 2.1.1.4) and sends inputs to the anterodorsal thalamic reticular nucleus (TRN) as well (Vantomme et al., 2020). The study by Vantomme et al. (2020) suggests TRN as an entry point to gate information flow to the ATN by receiving excitatory synaptic input from the PoS and RSC. The TRN-dependent inhibition is then fed forward to the ATN (comprises ADN) to sharpen HD tuning. It is possible that when landmark conflicts are resolved within the RSC, the landmark stability signal is then processed from RSC/PoS through TRN to help update the HD tuning in the canonical circuit to maintain a global, coherent directional signal. The global HD signal is sent back to HD cells in RSC and the hippocampal-entorhinal circuitry. This account supports that the HD signal in the ADN and PoS remain unidirectional in the 2-box (Jacob et al., 2017). This account also agrees with abundant evidence that the positional map system encodes space in a global reference frames if the HD system functions properly (Harland et al., 2017; see section 1.5.3). Therefore, the retrosplenial multidirectional cells feed reliability information of environmental cues into the map and direction system in service of resolving spatial ambiguity.

At the same time, the map system might feed multimodal information through long-range projections from the CA1 and dorsal subiculum (SUB) to granular RSC

(Yamawaki et al., 2019; see 2.1.1.3). Interestingly, a recent study showed that subicular neurons send a linear running speed signal directly to RSC (Kitanishi et al., 2021), corroborating the function of RSC in path integrating visual-motor signals (Mao et al., 2020). Moreover, it is also possible that via this subicular-hippocampal circuit, allocentric spatial information such as place and context information could be transported to RSC, and the retrosplenial spatial code gets sharpened by inhibitory CA1 inputs (Ranganath and Ritchey, 2012; Opalka et al., 2020). This hypothesis is in line with the finding that place-like code in RSC depends on an intact hippocampus (Mao et al., 2018). However, it remains unknown to what extent the multidirectional code may interact directly with hippocampal-subicular neurons.

In summary, this working model has delineated a rich (although not complete yet) picture of the thalamic-hippocampal-retrosplenial network (also see Chapter 2 for references). It reveals multiple pathways for future work to manipulate with such as to alter synaptic plasticity between neurons in RSC and these regions. For example, future research could co-record multidirectional cells in the RSC and HD cells while optogenetically or chemogetically cutting off (e.g., via administration of NMDA receptor antagonist) the inputs from 1) visual and landmark-related areas; 2) the canonical HD inputs from thalamic regions and 3) the hippocampal-subicular complex. A series of systematic manipulations would help decipher direction and spatial information flow through RSC to the broader spatial map system.

7.4.3 Future directions

The limitations of the current study were discussed in individual chapters earlier. A couple of routes for future work have been suggested in earlier sections. In addition, this final section highlights how recent technical advances provide an exciting new opportunity for future

investigation into two lines of research: first, how could the proposed landmark-based Hebbian learning model (**Figure 7-1**) be tested experimentally? Second, although the multidirectional cells have been dissociated from the EBCs by simulation, is it possible to dissociate the two codes experimentally?

Recent technical advances have been made in two-photon imaging with a rotating headplate system that allows a large degree of freedom in head movements in an open arena (Voigts and Harnett, 2019). For example, Voigts and Harnett demonstrated differential HD signalling in apical dendrites from somatic activities while imaging layer 5 pyramidal neurons in RSC. This nonlinearity in RSC dendritic computation provides a practical window to examine Hebbian landmark weighting and an integration of multimodal contextual information of the multidirectional cells. Future research could study dendritic processing of RSC multidirectional cells and HD cells by simultaneously imaging many neurons while the animal actively walks and rotates in symmetric environments. Then to examine the calcium transients between somatic and dendritic signals, as well as their temporal relationship, so that to illustrate any spike timing dependent plasticity (i.e., how the precise timing of spikes affects the changes in synaptic strength; Bi and Poo, 1998).

Moreover, the two-photon imaging technique would be ideally combined with a 2D VR system (Chen et al., 2018; Chen, Lu et al., 2019), which allows rapid experimental manipulations in refreshing environmental landmarks and changing orders of symmetry and contexts. It would also resolve the technical difficulties met in the current study in obtaining limited data from naive animals. These cutting-edge set-ups provide promising opportunities to characterise direction computation in RSC in a high resolution. These experiment proposals would help uncover how environment landmarks are learned and how they interact with head direction inputs at a synaptic level.

Furthermore, a combination of a rotating headpost plus a VR system may be particularly useful to design experiments to dissociate egocentric boundary vector coding from multidirectional encoding. The stability of EBCs requires the presence of physical boundaries (Alexander et al., 2020), and their activity and HD tuning should in theory deform in a boundary-less environment as well as in VR. It would be very interesting to test whether multidirectional cells maintain their symmetry firing in visually identical, symmetric environments in VR. If the cells encode true allocentric head directions, like the HD cells, which preserve the unidirectional firing pattern even if the animal's head was restrained to some extent (Chen et al., 2018), their firing pattern should be comparable to the current results.

A final note is that whether (and how) the directional system and the egocentric coding system in RSC might interact remains an unknown question. It is even unclear what exactly the egocentric cells are encoding - boundaries, doorway (centre), corners, or landmarks? It has been suggested that the egocentric sensory information should be temporally coupled with self-motion (Alexander et al., 2020), and the egocentric signal may arrive slightly before it gets transformed into allocentric representations (Bicanski and Burgess, 2020). As discussed in **Chapter 5**, EBCs may potentially be concentrated in more anterior part of RSC while the multidirectional cells are localised more in the posterior part (this needs testing). Future experiments should try to sample along the rostral-caudal axis of RSC to simultaneously record EBCs and HD cells, probably on simple, linear environments as a start and examine temporal relationship between their spikes.

Moreover, although HD tuning of the EBCs reflects geometrical features of the environment, they are not sufficient in resolving disorientation problem, as evident in animal's rotational errors made in the Ken Cheng task (Cheng, 1986; see section 1.3.1).

Therefore, referencing to landmarks or allocentric environmental cues by the multidirectional cells might be more efficient in resolving directional ambiguity.

7.5 Concluding remarks

The current thesis has demonstrated a multidirectional code that is not intrinsic, not purely sensory, and not egocentric, but is determined by environment symmetry. The work included in the current thesis has advanced from the previous work by Jacob et al. (2017) to show that environment symmetry is the key to producing multidirectional tuning of RSC cells. Clearly, the cells encode multiple directions in allocentric space, rather than egocentric boundary relationships. HD inputs and multimodal information are fed into the RSC; thus, the firing symmetry is hypothesised to arise from Hebbian learning and weighting of environmental landmarks. It is summarised that the network would benefit from having a second directional system signalling local directional information, because it can assess landmark stability, recalibrate the system rapidly by converting current egocentric panoramic views into allocentric representations.

Importantly, through an interaction between internal and external information exchange, RSC facilitates cognitive mapping of space. The cognitive mapping account is in line with the classic theory of learning formation by Harlow (1949): past experience drives the acquisition of abstract structure. The animal only acquires the knowledge of the whole environment structure as being fourfold through traversing across four sub-compartments, and this piece of knowledge may be memorised somehow, as it is informative about spatial orientation. That is to say, by representing direction information that reflects a global structure in a local space such as one quarter (or half) of an environment, the animal would be able to know its current heading as well as the global direction and the map in general,

reflecting structural abstraction. By this view, whether the regular, structural code in RSC can be generalised beyond a spatial domain is an important question of future research interests.

To conclude, the finding of a multidirectional code in the current study has not only clarified important attributes of direction encoding in RSC, but also delineated clearly how it is driven by a global environment symmetry and how it incorporates local multisensory signals. These processes involve landmark processing, local-global/egocentric-allocentric transformation and possibly mnemonic processing. The important observation of a multidirectional pattern within subspaces illustrates a map-like, allocentric spatial encoding beyond merely the perceptual, egocentric domain, reflecting cognitive mapping. Interaction of the two direction systems consequently confers more flexibility and higher efficacy for signal computation. They make RSC a credible candidate to flexibly guide spatial orientation and resolve direction ambiguity in complex, multi-fold-symmetrical environments. It is hoped that, by the help of a properly functioning RSC and interaction between the multidirectional cells and canonical HD cells, we would avoid similar incidence of Jim Marshall's wrong-way-run when navigating in symmetric environments.

APPENDIX

The appendices consist of four parts: first, the cluster quality analyses of all single units included in the current thesis; second, more representative RSC neurons showing multi-fold symmetric pattern in the two experiments; third, the characteristics of locomotion behaviours in the multi-fold symmetric environments and analyses of the relationship between self-motion and the cell activity; and finally, an analysis of dwelling time of the animal spent in different sub-compartments insides the multi-fold symmetric environments.

APPENDIX I: Cluster quality

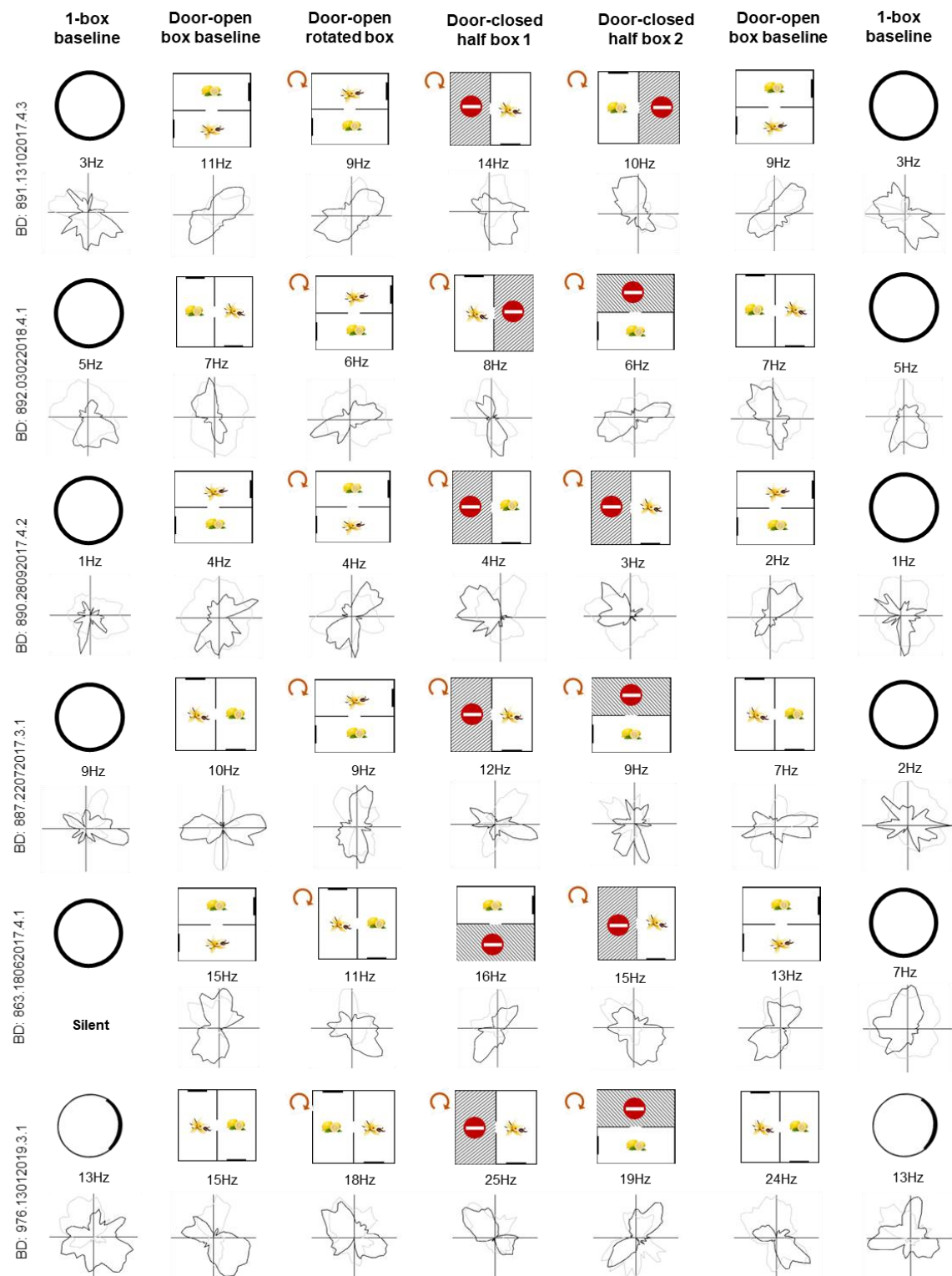
The table below (**Appendix Table 1**) summarised the cluster quality metrics, including the isolation distance, the L-ratio and refractory period contamination rates (see description in **Chapter 3**). They were computed for all single units, and comparisons were conducted between groups with different firing patterns (TD, BD, and HD). As reported in the t-tests, the sample sizes for isolation distance and L-ratio were individual sessions. The cluster-cutting was performed on a session-by-session basis to ensure cluster stability across multiple trials. The sample sizes for refractory period analysis were individual trials.

In general, there was no significant group difference in cluster quality for directional cells with different firing patterns, nor between different patterns of the cells. This suggests homogeneity in the cluster quality of all clusters. Therefore, functional characteristics of the cells described in the results chapters were not due to any confounding factors during cluster cutting. Although, compared to all population clusters, TD and HD cells had significantly lower refractory period violation rates, indicating that the clusters of HD cells and TD cells may have contained fewer noise spikes. Nevertheless, there was no such difference across three groups (TD, BD, HD), supporting that the directional cells had homogenous cluster quality, regardless of their firing pattern.

Appendix Table 1. Summary of cluster quality metrics

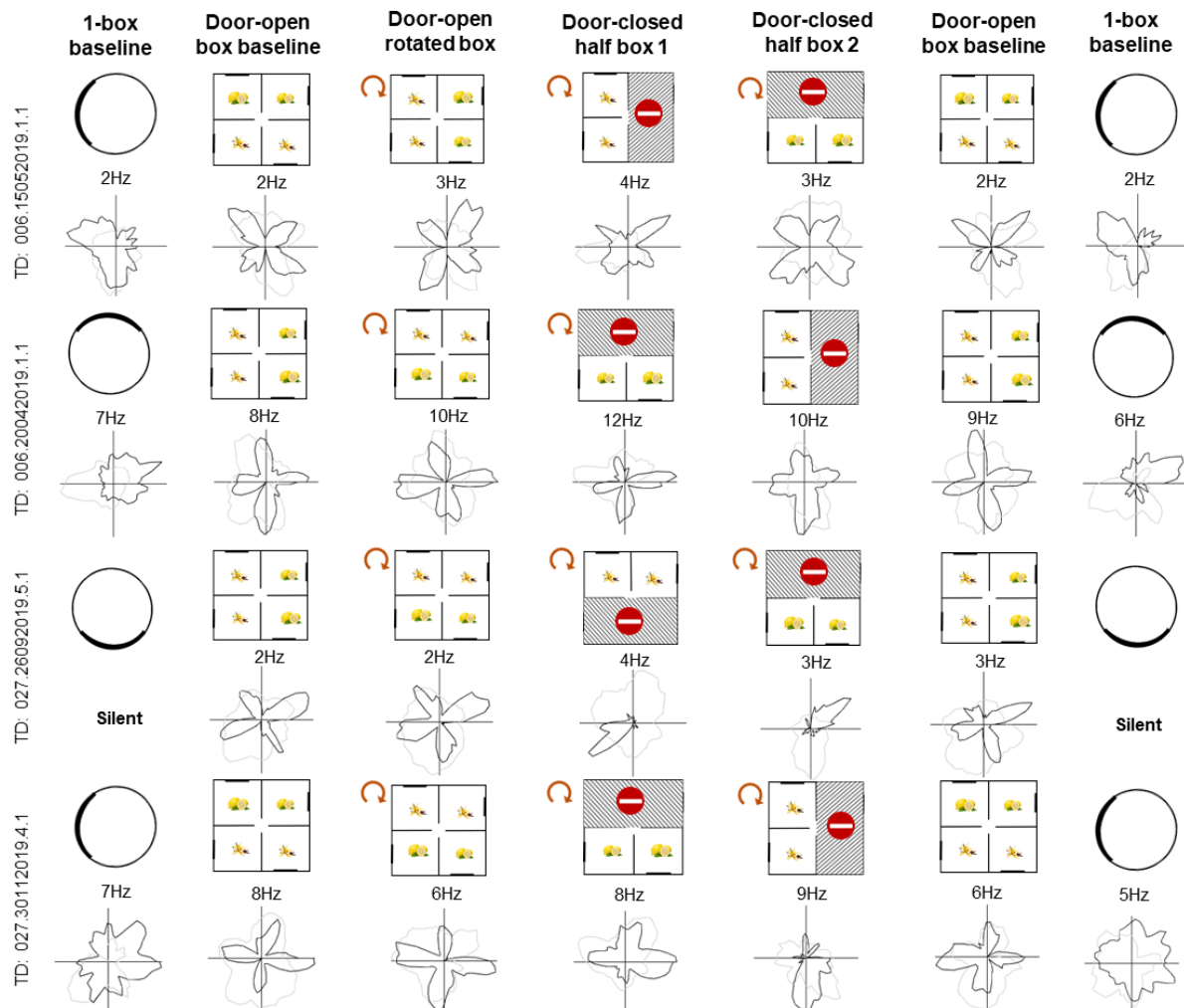
		Mean			Statistical comparisons
Cluster quality metrics	All single-units	HD cells	BD-pattern cells	TD-pattern cells	t-tests (cell type vs. unit population mean & between cell types)
Isolation distance	43.295	48.378	48.371	40.402	HD: $t(90) = 1.13, p = 0.262$; BD: $t(47) = 0.40, p = 0.694$; TD: $t(57) = -0.47, p = 0.639$
L-ratio	0.008	-0.003	0.009	-0.011	HD vs. BD: $t(137) = 0.001, p = 0.999$; HD vs. TD: $t(147) = 1.07, p = 0.287$; TD vs. BD: $t(104) = -0.59, p = 0.555$
Refractory period violation rate	0.003	0.002	0.002	0.002	HD: $t(90) = -0.93, p = 0.357$; BD: $t(47) = 0.38, p = 0.759$; TD: $t(57) = -1.07, p = 0.291$
					HD vs. BD: $t(137) = -0.70, p = 0.483$; HD vs. TD: $t(147) = 0.40, p = 0.69$; TD vs. BD: $t(104) = 0.99, p = 0.323$
					HD: $t(766) = -2.82, p = 0.005$; BD: $t(360) = -1.16, p = 0.248$; TD: $t(654) = -4.56, p < .001$
					HD vs. BD: $t(1126) = -0.40, p = 0.688$; HD vs. TD: $t(1420) = 1.39, p = 0.165$; TD vs. BD: $t(1126) = -1.44, p = 0.151$

APPENDIX II: Multidirectional cells in the multi-fold symmetric environments

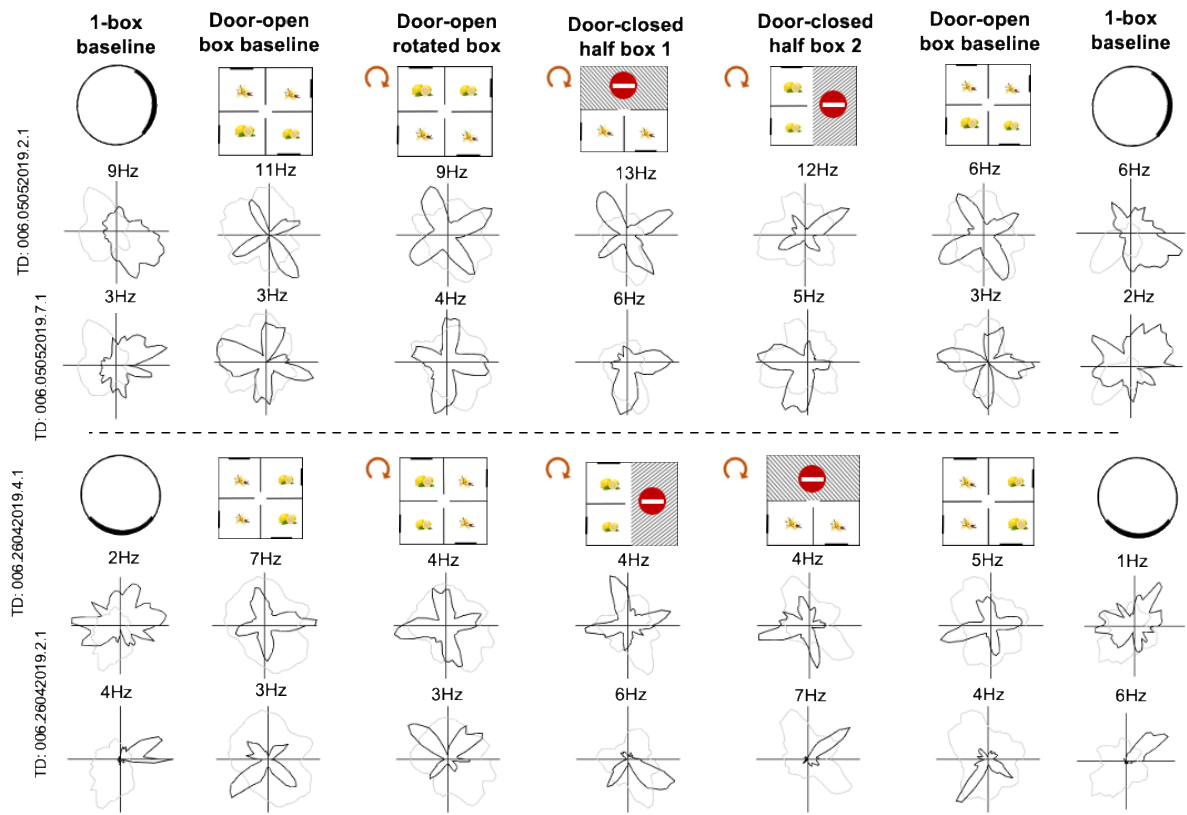


Appendix Figure 1. BD-pattern in the 2-box experiment. Six example BD-pattern cells recorded from different animals in the 2-box experiment. Polar plots show the standard seven-trial recording sessions, the rotation mark denotes the box orientation being different from that in the baseline. The last row shows a session recorded in the single-cued cylinder. Note that the BD-pattern cell firing patterns were miscellaneous in the 1-box.

The figures below showed more example TD-pattern cells recorded from the 4-box experiment. Note that the four peaks of the fourfold tuning curves were uniformly distributed in the 4-box, and usually did not align with the 4-box boundaries or the inner walls.



Appendix Figure 2. TD-pattern in the 4-box experiment. Four example TD-pattern cells recorded from different animals in the 4-box experiment. Polar plots show the standard seven-trial recording sessions, the rotation mark denotes the box orientation being different from that in the baseline. Note that TD-pattern firing patterns are miscellaneous in the 1-box baseline trials: some cells are onefold and some are zerofold.



Appendix Figure 3. Co-recorded TD-pattern cells in the 4-box experiment. Four example TD-pattern cells: two cells were simultaneously recorded from different tetrodes in one session (upper) and another two were recorded from another session (below the dotted line). Plots show the standard seven-trial recording sessions. Note that co-recorded cells have different PFDs within the same session. The decoupled HD tuning of co-recorded cells strongly supports that the firing symmetry is unlikely due to merely movement-related factors of the animal during recordings.

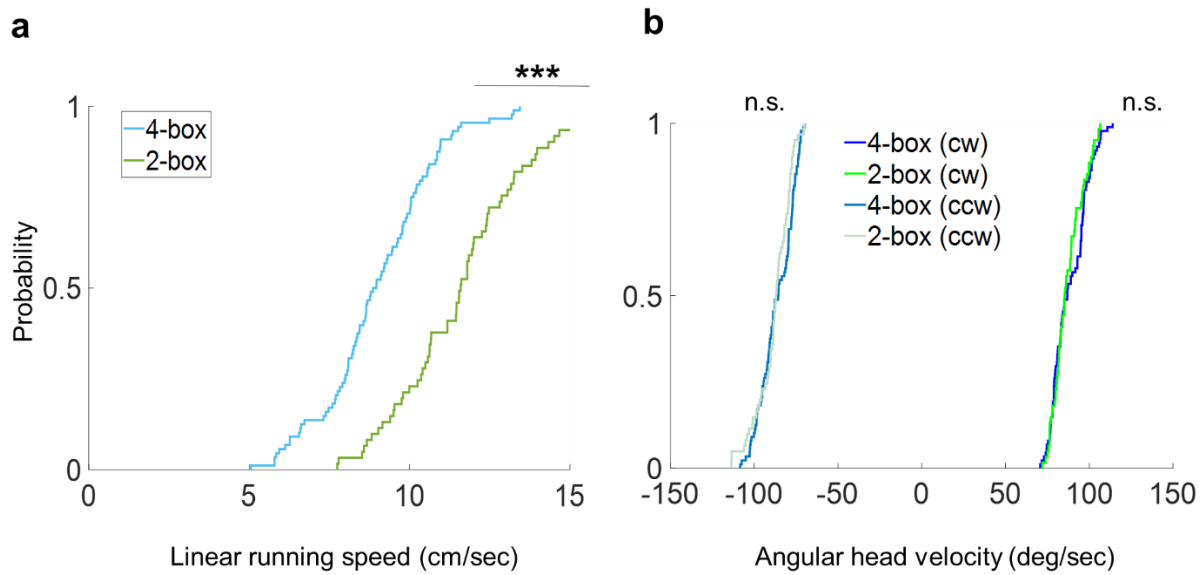
APPENDIX III: Locomotion and neural encoding in multi-fold symmetric environments

1. Foraging behaviours

To characterise the animal's locomotion during pellet-chasing behaviours in the multicompartment environments, animal's linear running speed and angular head velocity (AHV; clockwise and counterclockwise) in the 2-box and 4-box and their sub-compartments and were calculated.

The animal's linear running speed and AHV were calculated in individual recording sessions in which directional cells (including multidirectional cells and HD cells) were recorded (the 4-box experiment: $n = 88$; 2-box experiment: $n = 61$). When extracting linear running speed and AHV profiles for each trial, the instantaneous speed estimate derived from two successive positions in a window of 40 ms. The values of both variables were smoothed using 5-point Gaussian (100 ms window) to minimise tracking artefacts, and the medians were computed.

As shown in **Appendix Figure 4**, the results showed that animals ran slightly faster in the 2-box than in the 4-box (Mean \pm SEM in the 4-box: 9.0 ± 0.19 cm/sec; 2-box: 11.67 ± 0.27 cm/sec; 4-box vs. 2-box, independent-sample t-test: $t(147) = -8.40, p < .001$). It was probably because the 2-box contains fewer number of walls (i.e., obstacles), thus was more 'obstacle-free' for animals to run between different sub-compartments. Whereas in the 4-box that contain more sub-compartments as choices, the animal sometimes pauses briefly at the central doorway, then went into one of the four sub-compartments.



Appendix Figure 4. Locomotion features in multi-fold symmetric boxes. **a.** Cumulative probability of linear running speed in the 4-box and 2-box door-open baseline trials (blue: 4-box; green: 2-box). **b.** Cumulative probability of angular head velocity in the 4-box and 2-box door-open baseline trials (cw: clockwise; ccw: counter-clockwise).

The speeds of head turning were similar in the two environments: the AHVs were not significantly different (Clockwise AHV, 4-box: 88.48 ± 1.11 deg/sec; 2-box: 87.28 ± 1.15 deg/sec; $t(147) = 0.73$, $p = 0.467$; Counter-clockwise AHV, 4-box: -86.25 ± 1.07 deg/sec; 2-box: 88.07 ± 1.31 deg/sec; $t(147) = 1.08$, $p = 0.282$). These results together suggest that the animal's locomotion behaviours were comparable while the animal navigates in the 2-box and the 4-box. This supports that locomotion is unlikely contributing to different multidirectional patterns observed in the two environments.

2. In relationship to neural activity

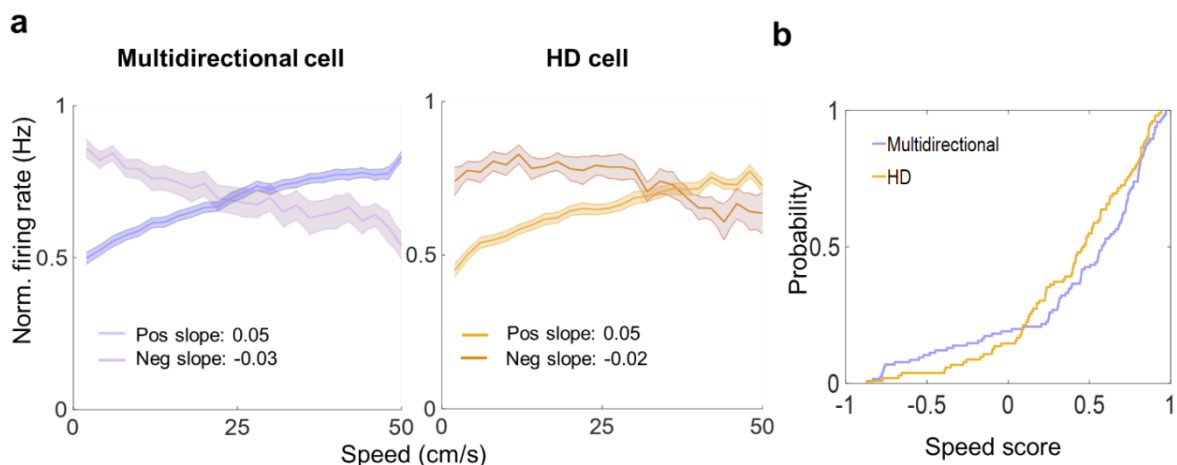
Next, I examined if there was any unnoticed encoding of self-motion variables in the directional cell activity. The cell activity in relation to movement correlates including linear running speed and angular head velocity was analysed, as described below.

- *Linear running speed:* to quantify the relationship between the animal's linear running speed and the cell's firing rate, the instantaneous firing rate (the total distance

travelled in every 40ms window) was estimated as the smoothed spike histogram (in 260 ms Gaussian smoothing window using MATLAB function *fspecial*). The running speeds were binned in 2cm/sec increments, and the mean firing rate for each running speed bin and the total time spent moving at that speed were calculated. The speed score was used to show modulation strength, defined as the Pearson correlation coefficient (Kropff et al., 2015). A linear regression model was fitted to the average firing rate/speed data using a least-squares approach (MATLAB function *polyfit*, 1 degree, and curve fitting toolbox), where the SEM, slope and intercept were extracted and compared between groups.

- *Angular head velocity*: to quantify the relationship between the animal's AHV and the cell's firing rate, spikes emitted during active clockwise (CW) and counterclockwise (CCW) head turns were analysed separately. The CW condition was defined as samples for which the angular velocity of the head $> 30^\circ/\text{sec}$, the CCW condition was defined as samples for which the AHV $<-30^\circ/\text{sec}$. If the AHV fell within -30° to $30^\circ/\text{sec}$, then the sample was not included in the analysis. A cell's instantaneous firing rate (angles sampled in 40ms window) was estimated as the smoothed spike histogram (in 100 ms Gaussian smoothing window using MATLAB function *fspecial*). The animal's AHV was binned in $6^\circ/\text{sec}$ increments, and the mean firing rate for angular bin and the total time spent moving at that speed were calculated. Similar to the speed score, an AHV score was used to indicate modulation strength. For each cell, it was defined as the Pearson product-moment correlation between the cell's instantaneous firing rate and the rat's instantaneous angular speed and calculated for CW and CCW tuning curves respectively.

The results showed that 81% ($n=93/115$) of the multidirectional cells' firing rate was positively correlated with the linear running speed (**Appendix Figure 5a**). However, the relationship between directionality and linear running speed was not significantly different between the multidirectional cells and HD cells (speed intercept: *Wilcoxon rank-sum Z* = 0.37, $p = 0.710$; slope: $Z = 0.43, p = 0.667$). Speed tuning (**Appendix Figure 5b**), as measured by the speed score of HD cells (median = 0.46, $t(101) = 9.59, p <.001$) and multidirectional cells (median = 0.58, $t(114) = 8.65, p <.001$) was significantly higher than zero for both groups. However, they were not significantly different between the two groups (KStest, $D = 0.15, p = 0.14$).



Appendix Figure 5. Speed correlates of multidirectional and HD cells. **a.** The mean and SEM firing rate at various running speeds averaged across multidirectional cells (TD and BD combined, left) and HD cells (right), plotted separately for positive and negative slopes (Mean \pm SEM). **b.** Cumulative probabilities of speed scores for multidirectional cells (violet) and HD cells (orange).

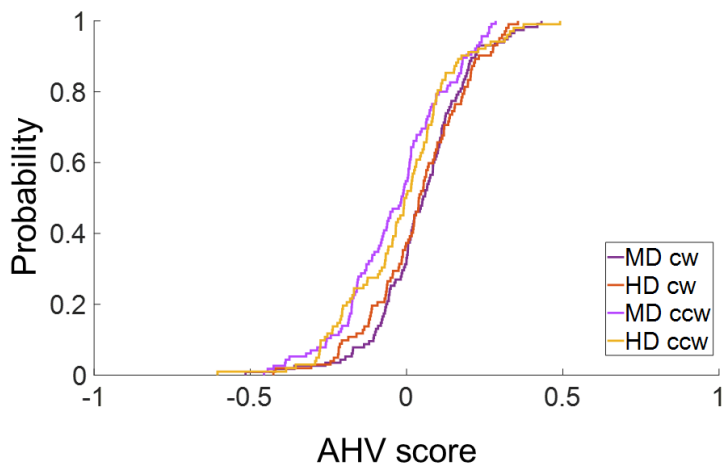
Regarding AHV encoding (**Appendix Figure 6**), the multidirectional cells and HD cells showed a slight encoding of angular head motion signal to some extent while the animal was making clockwise head turns, as evident in low, but-non-zero AHV scores (median, multidirectional, $AHV_{cw} = 0.05, t(101) = 3.41, p <.001$; $AHV_{ccw} = -0.02, t(101) = -2.12$,

$p = 0.036$; HD, AHVcw = 0.04, $t(101) = 2.44$, $p = 0.016$; AHVccw = 0.00, $t(101) = -0.9$,

$p = 0.368$). In contrast, HD cells did not show encoding of AHV for CCW head turns.

Nevertheless, the multidirectional and HD cells did not show significant differences in AHV

tuning (KStest, AHVcw, D = 0.10, $p = 0.62$; AHVccw, D = 0.11, $p = 0.46$).



Appendix Figure 6. Head-motion correlates of multidirectional and HD cells.

The figure shows the cumulative probability of angular head velocity scores for multidirectional (MD) cells (violet; clockwise: dark; counterclockwise: light) and HD cells (orange; clockwise: dark; counterclockwise: light).

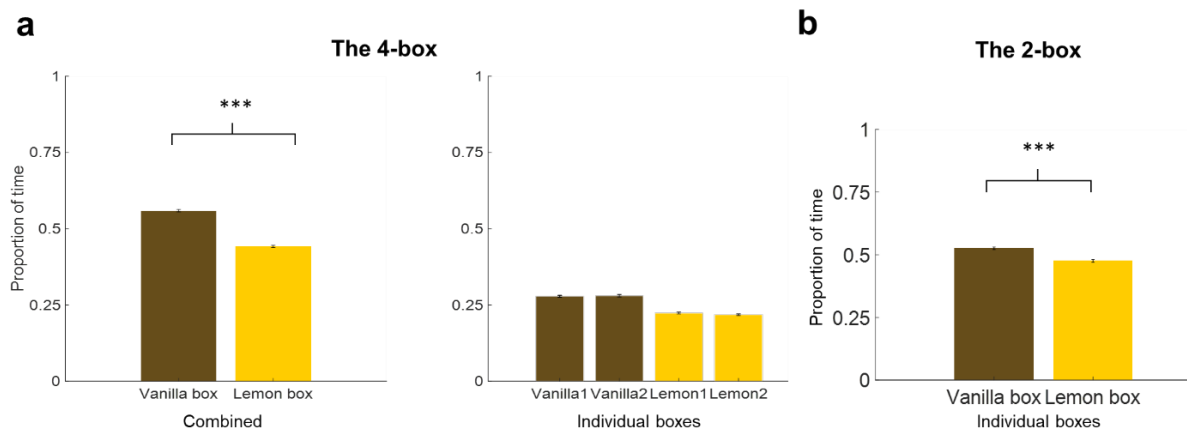
Overall, the relationship between symmetry firings and linear running speed or angular head velocity was not significantly different between the multidirectional cells and HD cells. Although some cells showed a slight speed tuning, which may indicate a potential role by optic flow to facilitate information processing in RSC, consistent with previous findings (Fischer et al., 2020; Powell et al., 2020; Mao et al., 2020). The results indicated that animal's movement correlates with cell tuning were not variant for HD cells and multidirectional cells. This leads to the conclusion that differences observed in RSC directional encoding were not simply due to locomotion related factors – which is also evident in simultaneously recorded directional cells (multidirectional cells with HD cells), as shown in **Chapter 4** (also see **Appendix Figure 3**).

APPENDIX IV: Dwelling time in the multi-fold symmetric environments

Finally, the multi-fold symmetric environments comprise complex cues, it would be interesting to consider if rats have any preference of single sub-compartments scented with different contextual cues. Thus, I compared the dwelling time of rats spent in vanilla- scented versus lemon-scented sub-compartments. The analysis was done with recording sessions where multidirectional cells were recorded. In both environments, it was found that animals generally preferred the vanilla box than the lemon box (**Appendix Figure 7**).

In the 4-box, the animal spent significantly longer time exploring the vanilla sub-compartments than lemon ones. The sum of two single sub-compartments of vanilla (mean = 55.9%) was significantly higher than combined time in the lemon ones (mean = 44.2%; *Wilcoxon signed-ranks test Z* = 11.11, $p < .001$). Individual vanilla 1 (mean 27.85%, $Z = 8.09, p < .001$) and vanilla 2 (mean 28.03%, $Z = 6.45, p < .001$) showed significantly higher than chance level (25%), whereas single box lemon1 (mean 22.35%, $Z = -7.71, p < .001$) and lemon 2 (mean 21.82%, $Z = -10.40, p < .001$) were significantly lower than 25%.

Likewise, in the 2-box, the animal tended to spend more time in the vanilla sub-compartments (mean = 52.6%) than in the lemon ones (mean = 47.5%; *Wilcoxon signed-ranks test Z* = 4.75, $p < .001$).



Appendix Figure 7. Dwelling time in sub-compartment of the multi-fold symmetric boxes. Bar charts show the dwelling time (population mean in proportion) in the 4-box (a) and the 2-box (b). For each recording session, data from three door-open box trials was pooled and averaged. In the 4-box, the sampling time in each individual sub-compartment as well as the sum of same-scented ones was shown. Colours denote different scents (brown: vanilla; yellow: lemon).

The fact that the animal showed a slight behavioural bias in visiting the vanilla sub-compartments suggests that it makes use of contextual cues to disambiguate different sub-compartments in ambiguous environments (Anderson and Jeffery, 2003). Moreover, the bias suggests that lemon odour might be a bit aversive for rats. Nevertheless, it should be noted that the odour-related differences observed in the dwelling time does not affect the interpretation RSC directional encoding, because the dwelling time in sub-compartment was normalised in constructing HD tuning curves in individual sub-compartments. However, to avoid potential behavioural bias in sampling, future study might use other non-citric based odour (e.g., apple or apricot) as contextual odour cues.

REFERENCES

REFERENCES

- Aggleton JP. 2014. Looking beyond the hippocampus: Old and new neurological targets for understanding memory disorders. *Proc R Soc B Biol Sci* **281**: 20140565. doi:10.1098/rspb.2014.0565
- Aggleton JP. 2010. Understanding retrosplenial amnesia: Insights from animal studies. *Neuropsychologia* **48**:2328–2338. doi:10.1016/j.neuropsychologia.2009.09.030
- Alexander AS, Carstensen LC, Hinman JR, Raudies F, Chapman GW, Hasselmo ME. 2020. Egocentric boundary vector tuning of the retrosplenial cortex. *Sci Adv* **6**: eaaz2322. doi:10.1101/CBO9781107415324.004.
- Alexander AS, Nitz DA. 2017. Spatially periodic activation patterns of retrosplenial cortex encode route sub-spaces and distance traveled. *Curr Biol* **27**:1551-1560.e4. doi:10.1016/j.cub.2017.04.036
- Alexander AS, Nitz DA. 2015a. Retrosplenial cortex maps the conjunction of internal and external spaces. *Nat Neurosci* **18**:1143–1151. doi:10.1038/nn.4058
- Alexander AS, Robinson JC, Dannenberg H, Kinsky NR, Levy SJ, Mau W, Chapman GW, Sullivan DW, Hasselmo ME. 2020. Neurophysiological coding of space and time in the hippocampus, entorhinal cortex, and retrosplenial cortex. *Brain Neurosci Adv* **4**:239821282097287. doi:10.1177/2398212820972871
- Alyan S, Jander R. 1994. Short-range homing in the house mouse, *mus musculus*: stages in the learning of directions. *Anim Behav* **48**: 285–298. doi:10.1006/anbe.1994.1242
- Alyan S, McNaughton BL. 1999. Hippocampectomized rats are capable of homing by path integration. *Behav Neurosci* **113**:19–31. doi:10.1037/0735-7044.113.1.19
- Anderson MI, Jeffery KJ. 2003. Heterogeneous modulation of place cell firing by changes in

context. *J Neurosci* **23**:8827–8835. doi: 10.1523/JNEUROSCI.23-26-08827.2003

Aronov D, Nevers R, Tank DW. 2017. Mapping of a non-spatial dimension by the hippocampal-entorhinal circuit. *Nature* **543**:719–722. doi:10.1038/nature21692

Auger SD, Maguire EA. 2013. Assessing the mechanism of response in the retrosplenial cortex of good and poor navigators. *Cortex* **49**:2904–2913.
doi:10.1016/j.cortex.2013.08.002

Auger SD, Mullally SL, Maguire EA. 2012. Retrosplenial cortex codes for permanent landmarks. *PLoS One* **7**. doi:10.1371/journal.pone.0043620

Auger SD, Zeidman P, Maguire EA. 2015. A central role for the retrosplenial cortex in de novo environmental learning. *eLife* **4**:1–26. doi:10.7554/eLife.09031

Baleydier C, Mauguiere F. 1985. Anatomical evidence for medial pulvinar connections with the posterior cingulate cortex, the retrosplenial area, and the posterior parahippocampal gyrus in monkeys. *J Comp Neurol* **232**:219–228. doi:10.1002/cne.902320207

Barlow JS. 1964. Inertial navigation as a basis for animal navigation. *J Theor Biol* **6**:76–117.
doi:10.1016/0022-5193(64)90067-0

Barry C, Ginzberg LL, O’Keefe J, Burgess N. 2012. Grid cell firing patterns signal environmental novelty by expansion. *Proc Natl Acad Sci U S A* **109**:17687–17692.
doi:10.1073/pnas.1209918109

Barry C, Hayman R, Burgess N, Jeffery KJ. 2007. Experience-dependent rescaling of entorhinal grids. *Nat Neurosci* **10**:682–684. doi:10.1038/nn1905

Barry C, Lever C, Hayman R, Hartley T, Burton S, O’Keefe J, Jeffery KJ, Burgess N. 2006. The boundary vector cell model of place cell firing and spatial memory. *Rev Neurosci* **17**:71–97. doi:10.1515/REVNEURO.2006.17.1-2.71

Bassett JP, Wills TJ, Cacucci, F. 2018. Self-organized attractor dynamics in the developing head direction circuit. *Curr Biol* **48**: 609-615. doi:10.1016/j.cub.2018.01.010.

Bassett JP, Taube JS. 2001. Neural correlates for angular head velocity in the rat dorsal tegmental nucleus. *J Neurosci* **21**:5740–5751. doi:10.1523/JNEUROSCI.21-15-05740.2001

Bassett JP, Tullman ML, Taube JS. 2007. Lesions of the tegmentomammillary circuit in the head direction system disrupt the head direction signal in the anterior thalamus. *J Neurosci* **27**:7564–7577. doi:10.1523/JNEUROSCI.0268-07.2007

Bassett JP, Zugaro MB, Muir GM, Golob EJ, Muller RU, Taube JS. 2005. Passive movements of the head do not abolish anticipatory firing properties of head direction cells. *J Neurophysiol* **93**:1304–1316. doi:10.1152/jn.00490.2004

Baumann O, Mattingley JB. 2010. Medial parietal cortex encodes perceived heading direction in humans. *J Neurosci* **30**:12897–12901. doi:10.1523/JNEUROSCI.3077-10.2010

Behrens TEJ, Muller TH, Whittington JCR, Mark S, Baram AB, Stachenfeld KL, Kurth-Nelson Z. 2018. What is a cognitive map? organizing knowledge for flexible behavior. *Neuron* **100**:490–509. doi:10.1016/j.neuron.2018.10.002

Bellmund JLS, Deuker L, Schröder TN, Doeller CF. 2016. Grid-cell representations in mental simulation. *eLife* **5**:1–21. doi:10.7554/eLife.17089

Ben-Yishay E, Krivoruchko K, Ron S, Ulanovsky N, Derdikman D, Gutfreund Y. 2020. Head-direction coding in the hippocampal formation of birds. *bioRxiv* 2020.08.31.274928. doi:10.1101/2020.08.31.274928

Benhamou S, Poucet B. 1998. Landmark use by navigating rats (*rattus norvegicus*):

- contrasting geometric and featural information. *J Comp Psychol* **112**:317–322.
doi:10.1037/0735-7036.112.3.317
- Berens P. 2009. Circstat: a matlab toolbox for circular statistics. *J Stat Softw* **31**:1–21.
doi:10.18637/jss.v031.i10
- Best PJ, Thompson LT. 1989. Persistence, reticence, and opportunism of place-field activity in hippocampal neurons. *Psychobiology* **17**:236–246. doi:10.1007/BF03337775
- Bi GQ, Poo MM. 1998. Synaptic modifications in cultured hippocampal neurons: Dependence on spike timing, synaptic strength, and postsynaptic cell type. *J Neurosci* **18**:10464–10472. doi:10.1523/jneurosci.18-24-10464.1998
- Bicanski A, Burgess N. 2020. Neuronal vector coding in spatial cognition. *Nat Rev Neurosci* **21**:453–470. doi:10.1038/s41583-020-0336-9
- Bicanski A, Burgess N. 2018. A neural-level model of spatial memory and imagery. *eLife* **7**:1–45. doi:10.7554/eLife.33752
- Bjerknes TL, Moser EI, Moser MB. 2014. Representation of geometric borders in the developing rat. *Neuron* **82**:71–78. doi:10.1016/j.neuron.2014.02.014
- Blair HT, Cho J, Sharp PE. 1999. The anterior thalamic head-direction signal is abolished by bilateral but not unilateral lesions of the lateral mammillary nucleus. *J Neurosci* **19**:6673–6683. doi:10.1523/jneurosci.19-15-06673.1999
- Blair HT, Cho J, Sharp PE. 1998. Role of the lateral mammillary nucleus in the rat head direction circuit: A combined single unit recording and lesion study. *Neuron* **21**:1387–1397. doi:10.1016/S0896-6273(00)80657-1
- Boccara CN, Sargolini F, Thoresen VH, Solstad T, Witter MP, Moser EI, Moser MB. 2010. Grid cells in pre-and parasubiculum. *Nat Neurosci* **13**:987–994. doi:10.1038/nn.2602

Brennan EKW, Sudhakar SK, Jedrasiak-Cape I, John TT, Ahmed OJ. 2020. Hyperexcitable neurons enable precise and persistent information encoding in the superficial retrosplenial cortex. *Cell Rep* **30**:1598–1612.e8. doi:10.1016/j.celrep.2019.12.093

Buckley MJ, Mitchell AS. 2016. Retrosplenial cortical contributions to anterograde and retrograde memory in the monkey. *Cereb Cortex* **26**:2905–2918. doi:10.1093/cercor/bhw054

Burgess N, Becker S, King JA, O’Keefe J. 2001. Memory for events and their spatial context: models and experiments. *Philos Trans R Soc Lond B Biol Sci* **356**:1493–503. doi:10.1098/rstb.2001.0948

Burwell RD, Amaral DG. 1998. Cortical efferents of the perirhinal, postrhinal, and entorhinal cortices of the rat. *J Comp Neurol* **398**:179–205. doi:10.1002/hipo.20578

Bush D, Barry C, Burgess N. 2014. What do grid cells contribute to place cell firing? *Trends Neurosci* **37**:136–145. doi:10.1016/j.tins.2013.12.003

Bush D, Barry C, Manson D, Burgess N. 2015. Using grid cells for navigation. *Neuron* **87**:507–520. doi:10.1016/j.neuron.2015.07.006

Butler WN, Smith KS, van der Meer MAA, Taube JS. 2017. The head-direction signal plays a functional role as a neural compass during navigation. *Curr Biol* **27**:1259–1267. doi:10.1016/j.cub.2017.03.033

Byrne M, Dacke M, Nordström P, Scholtz C, Warrant E. 2003. Visual cues used by ball-rolling dung beetles for orientation. *J Comp Physiol A Neuroethol Sensory, Neural, Behav Physiol* **189**:411–418. doi:10.1007/s00359-003-0415-1

Byrne P, Becker S, Burgess N. 2007. Remembering the past and imagining the future: A neural model of spatial memory and imagery. *Psychol Rev* **114**:340–375.

doi:10.1037/0033-295X.114.2.340

Cacucci F, Level C, Wills TJ, Burgess N, O'Keefe J. 2004. Theta-modulated place-by-direction cells in the hippocampal formation in the rat. *J Neurosci* **24**:8265–8277.
doi:10.1523/JNEUROSCI.2635-04.2004

Calton JL, Stackman RW, Goodridge JP, Archey WB, Dudchenko PA, Taube JS. 2003. Hippocampal place cell instability after lesions of the head direction cell network. *J Neurosci* **23**:9719–9731. doi:10.1523/jneurosci.23-30-09719.2003

Campbell MG, Ocko SA, Mallory CS, Low IIC, Ganguli S, Giocomo LM. 2018. Principles governing the integration of landmark and self-motion cues in entorhinal cortical codes for navigation. *Nat Neurosci* **21**:1096–1106. doi:10.1038/s41593-018-0189-y

Cartwright BA, Collett TS. 1983. Landmark learning in bees - experiments and models. *J Comp Physiol* **151**:521–543. doi:10.1007/BF00605469

Cenquizca LA, Swanson LW. 2007. Spatial organization of direct hippocampal field CA1 axonal projections to the rest of the cerebral cortex. *Brain Res Rev* **56**:1–26.
doi:10.1016/j.brainresrev.2007.05.002

Chaudhuri R, Gerçek B, Pandey B, Peyrache A, Fiete I. 2019. The intrinsic attractor manifold and population dynamics of a canonical cognitive circuit across waking and sleep. *Nat Neurosci* **22**:1512–1520. doi:10.1038/s41593-019-0460-x

Chen G, King JA, Lu Y, Cacucci F, Burgess N. 2018. Spatial cell firing during virtual navigation of open arenas by head-restrained mice. *Elife* **7**:1–20. doi:10.1101/246744

Chen G, Lu Y, King JA, Cacucci F, Burgess N. 2019. Differential influences of environment and self-motion on place and grid cell firing. *Nat Commun* **10**:1–11.
doi:10.1038/s41467-019-08550-1

- Chen LL, Lin LH, Barnes CA, McNaughton BL. 1994. Head-direction cells in the rat posterior cortex - II. Contributions of visual and ideothetic information to the directional firing. *Exp Brain Res* **101**:24–34. doi:10.1007/BF00243213
- Cheng K. 1986. A purely geometric module in the rat's spatial representation. *Cognition* **23**:149–178. doi:10.1016/0010-0277(86)90041-7
- Cho J, Sharp PE. 2001. Head direction, place, and movement correlates for cells in the rat retrosplenial cortex. *Behav Neurosci* 3–25. doi:10.1037/0735-7044.115.1.3
- Clancy KB, Orsolic I, Mrsic-Flogel TD. 2019. Locomotion-dependent remapping of distributed cortical networks. *Nat Neurosci* **22**:778–786. doi:10.1038/s41593-019-0357-8
- Clark BJ, Bassett JP, Wang SS, Taube JS. 2010. Impaired head direction cell representation in the anterodorsal thalamus after lesions of the retrosplenial cortex. *J Neurosci* **30**:5289–302. doi:10.1523/JNEUROSCI.3380-09.2010
- Clark BJ, Taube JS. 2012. Vestibular and attractor network basis of the head direction cell signal in subcortical circuits. *Front Neural Circuits* **6**:1–12. doi:10.3389/fncir.2012.00007
- Collett TS, Cartwright BA, Smith BA. 1986. Landmark learning and visuo-spatial memories in gerbils. *J Comp Physiol A Sensory, Neural, Behav Physiol* **158**:835–851. doi:10.1007/BF01324825
- Collett TS, De Ibarra NH, Riabinina O, Philippides A. 2013. Coordinating compass-based and nest-based flight directions during bumblebee learning and return flights. *J Exp Biol* **216**:1105–1113. doi:10.1242/jeb.081463
- Constantinescu AO, O'Reilly JX, Behrens TE. Organizing conceptual knowledge in humans

with a gridlike code. *Science*. **352**:1464-8. doi: 10.1126/science.aaf0941

Cooper BG, Mizumori SJ. 2001. Temporary inactivation of the retrosplenial cortex causes a transient reorganization of spatial coding in the hippocampus. *J Neurosci* **21**:3986–4001. doi: 10.1523/JNEUROSCI.21-11-03986.2001

Cressant A, Muller RU, Poucet B. 1997. Failure of centrally placed objects to control the firing fields of hippocampal place cells. *J Neurosci* **17**:2531–2542. doi:10.1523/jneurosci.17-07-02531.1997

Cullen KE, Taube JS. 2017. Our sense of direction: Progress, controversies and challenges. *Nat Neurosci* **20**:1465–1473. doi:10.1038/nn.4658

Czajkowski R, Sugar J, Zhang S-J, Couey JJ, Ye J, Witter MP. 2013. Superficially projecting principal neurons in layer v of medial entorhinal cortex in the rat receive excitatory retrosplenial input. *J Neurosci* **33**:15779–15792. doi:10.1523/JNEUROSCI.2646-13.2013

Darwin C. 1873. Perception in the lower animals. *Nature* **7**: 360. doi:10.1038/007360c0

Dashiell, JF. 1930. An experimental analysis of some group effects. *J Abnorm Soc Psych* **25**: 190–199. doi:10.1037/h0075144

DeCamp JE. 1921. Relative distance as a factor in the white. *Psychobiology* **II**:245–253. doi:10.1037/h0075411

Derdikman D. 2009. Are the boundary-related cells in the subiculum boundary-vector cells? *J Neurosci* **29**:13429–13431. doi:10.1523/JNEUROSCI.4176-09.2009

Dudchenko PA, Zinyuk LE. 2005. The formation of cognitive maps of adjacent environments: Evidence from the head direction cell system. *Behav Neurosci* **119**:1511–1523. doi:10.1037/0735-7044.119.6.1511

Dunn AR, Neuner SM, Ding S, Hope KA, O'Connell KMS, Kaczorowski CC. 2018. Cell-type-specific changes in intrinsic excitability in the subiculum following learning and exposure to novel environmental contexts. *eNeuro* **5**. doi:10.1523/ENEURO.0484-18.2018

Duvelle É, Grieves RM, Liu A, Jedidi-Ayoub S, Holeniewska J, Harris A, Nyberg N, Donnarumma F, Lefort JM, Jeffery KJ, Summerfield C, Pezzulo G, Spiers HJ. 2021. Hippocampal place cells encode global location but not connectivity in a complex space. *Curr Biol* **31**:1221-1233.e9. doi:10.1016/j.cub.2021.01.005

Ekstrom AD, Kahana MJ, Caplan JB, Fields TA, Isham EA, Newman EL, Fried I. 2003. Cellular networks underlying human spatial navigation. *Nature* **425**:184–187. doi:10.1038/nature01964

el Jundi B, Pfeiffer K, Heinze S, Homberg U. 2014. Integration of polarization and chromatic cues in the insect sky compass. *J Comp Physiol A Neuroethol Sensory, Neural, Behav Physiol* **200**:575–589. doi:10.1007/s00359-014-0890-6

Elduayen, C, Save E. 2014. The retrosplenial cortex is necessary for path integration in the dark. *Behav Brain Res* **272**:303-307. doi: 10.1016/j.bbr.2014.07.009

Epstein RA. 2008. Parahippocampal and retrosplenial contributions to human spatial navigation. *Trends Cogn Sci* **12**:388–396. doi:10.1016/j.tics.2008.07.004

Epstein RA, Higgins JS. 2007. Differential parahippocampal and retrosplenial involvement in three types of visual scene recognition. *Cereb Cortex* **17**:1680–1693. doi:10.1093/cercor/bhl079

Epstein RA, Patai EZ, Julian JB, Spiers HJ. 2017. The cognitive map in humans: Spatial navigation and beyond. *Nat Neurosci* **20**:1504–1513. doi:10.1038/nn.4656

Epstein RA, Vass LK. 2014. Neural systems for landmark-based wayfinding in humans.

Philos Trans R Soc London **369**:20120533. doi:10.1098/rstb.2012.0533

Etienne AS, Jeffery KJ. 2004. Path integration in mammals. *Hippocampus* **14**:180–192.

doi:10.1002/hipo.10173

Etienne AS, Maurer R, Saucy F. 1988. Limitations in the assessment of path dependent

information. *Behaviour* **106**:81–111. doi:10.1163/156853988X00106

Etienne AS, Maurer R, Saucy F, Teroni E. 1986. Short-distance homing in the golden

hamster after a passive outward journey. *Anim Behav* **34**:696–715. doi:10.1016/S0003-3472(86)80054-9

Etienne AS, Maurer R, Séguinot V. 1996. Path integration in mammals and its interaction

with visual landmarks. *J Exp Biol* **199**:201–209. doi:10.1242/jeb.199.1.201

Etienne AS, Teroni E, Hurni C, Portenier V. 1990. The effect of a single light cue on homing

behaviour of the golden hamster. *Anim Behav* **39**:17–41. doi:10.1016/S0003-

3472(05)80723-7

Fee MS, Mitra PP, Kleinfeld D. 1996. Automatic sorting of multiple unit neuronal signals in

the presence of anisotropic and non-Gaussian variability.[Erratum appears in J Neurosci

Methods 1997 Feb;71(2):233]. *J Neurosci Methods* **69**:175–188.doi:10.1016/S0165-

0270(96)00050-7

Fenton AA, Csizmadia G, Muller RU. 2000. Conjoint control of hippocampal place cell

firing by two visual stimuli. *J Gen Physiol* **116**:211–222. doi:10.1085/jgp.116.2.211

Fiete IR, Burak Y, Brookings T. 2008. What grid cells convey about rat location. *J Neurosci*

28:6858–6871. doi:10.1523/JNEUROSCI.5684-07.2008

Finkelstein A, Derdikman D, Rubin A, Foerster JN, Las L, Ulanovsky N. 2014. Three-

dimensional head-direction coding in the bat brain. *Nature* **517**.

doi:10.1038/nature14031

Fischer LF, Soto-Albors RM, Buck F, Harnett MT. 2020. Representation of visual landmarks in retrosplenial cortex. *eLife* **9**:1–25. doi:10.7554/eLife.51458

Fisher YE, Lu J, D'Alessandro I, Wilson RI. 2019. Sensorimotor experience remaps visual input to a heading-direction network. *Nature* **576**:121–125. doi:10.1038/s41586-019-1772-4

Fox GE, Li M, Zhao F, Tsien JZ. 2017. Distinct retrosplenial cortex cell populations and their spike dynamics during ketamine-induced unconscious state. *PLoS One* **12**:1–23. doi:10.1371/journal.pone.0187198

Frank LM, Brown EN, Wilson MA. 2001. A comparison of the firing properties of putative excitatory and inhibitory neurons from CA1 and the entorhinal cortex. *J Neurophysiol* **86**:2029–2040. doi:10.1152/jn.2001.86.4.2029

Fuhs MC, VanRhoads SR, Casale AE, McNaughton B, Touretzky DS. 2005. Influence of path integration versus environmental orientation on place cell remapping between visually identical environments. *J Neurophysiol* **94**:2603–2616. doi:10.1152/jn.00132.2005

Fyhn M, Hafting T, Treves A, Moser MB, Moser EI. 2007. Hippocampal remapping and grid realignment in entorhinal cortex. *Nature* **446**:190–194. doi:10.1038/nature05601

Fyhn M, Molden S, Witter MP, Moser EI, Moser MB. 2004. Spatial representation in the entorhinal cortex. *Science* **305**:1258–1264. doi:10.1126/science.1099901

Gallistel CR. 1990. *The organization of learning*. The MIT Press.

Garcia D. 2011. A fast all-in-one method for automated post-processing of PIV data. *Exp*

Fluids **50**:1247–1259. doi:10.1007/s00348-010-0985-y

Garvert MM, Dolan RJ, Behrens TEJ. 2017. A map of abstract relational knowledge in the human hippocampal–entorhinal cortex. *eLife* **6**:1–20. doi:10.7554/eLife.17086

Gener T, Perez-Mendez L, Sanchez-Vives M V. 2013. Tactile modulation of hippocampal place fields. *Hippocampus* **23**:1453–1462. doi:10.1002/hipo.22198

Gentry G, Brown VVL, Lee HUN. 1948. Spatial location in the learning of a multiple-T maze. *J Comp Physiol* **41**:312–318. doi: 10.1037/h0056159

Gentry G, Brown WL, Kaplan SJ. 1947. An experimental analysis of the spatial location hypothesis in learning. *J Comp Physiol Psychol* **40**:309–322. doi:10.1037/h0061537

Giocomo LM, Stensola T, Bonnevie T, Cauter T Van, Moser M, Moser EI. 2014. Topography of head direction cells in medial entorhinal cortex. *Curr Biol* **24**:252–262. doi:10.1016/j.cub.2013.12.002

Goodridge JP, Dudchenko PA, Worboys KA, Golob EJ, Taube JS. 1998. Cue control and head direction cells. *Behav Neurosci* **112**:749–761. doi:10.1037/0735-7044.112.4.749

Goodridge JP, Taube JS. 1997. Interaction between the postsubiculum and anterior thalamus in the generation of head direction cell activity. *J Neurosci* **17**:9315–9330. doi:10.1523/jneurosci.17-23-09315.1997

Goodridge JP, Taube JS. 1995. Preferential use of the landmark navigational system by head direction cells in rats. *Behav Neurosci* **109**:49–61. doi:10.1037/0735-7044.109.1.49

Gouteux S, Thinus-Blanc C, Vauclair J. 2001. Rhesus monkeys use geometric and nongeometric information during a reorientation task. *J Exp Psychol Gen* **130**:505–519. doi:10.1037/0096-3445.130.3.505

Graf W, Gerrits N, Yatim-Dhiba N, Ugolini G. 2002. Mapping the oculomotor system: The power of transneuronal labelling with rabies virus. *Eur J Neurosci* **15**:1557–1562.
doi:10.1046/j.1460-9568.2002.01994.x

Greene CM, Cook RG. 1997. Landmark geometry and identity controls spatial navigation in rats. *Anim Learn Behav* **25**:312–323. doi:10.3758/BF03199089

Grieves RM, Duvelle É, Dudchenko PA. 2018. A boundary vector cell model of place field repetition. *Spat Cogn Comput* **18**:217–256. doi:10.1080/13875868.2018.1437621

Grieves RM, Duvelle É, Wood ER, Dudchenko PA. 2017. Field repetition and local mapping in the hippocampus and the medial entorhinal cortex. *J Neurophysiol* **118**:2378–2388.
doi:10.1152/jn.00933.2016

Grieves RM, Jedidi-Ayoub S, Mishchanchuk K, Liu A, Renaudineau S, Jeffery KJ. 2020. The place-cell representation of volumetric space in rats. *Nat Commun* **11**:789.
doi:10.1101/698175

Grieves RM, Jeffery KJ. 2017. The representation of space in the brain. *Behav Processes* **135**:113–131. doi:10.1016/j.beproc.2016.12.012

Grieves RM, Jenkins BW, Harland BC, Wood ER, Dudchenko PA. 2016. Place field repetition and spatial learning in a multicompartment environment. *Hippocampus* **26**:118–134. doi:10.1002/hipo.22496

Hafting T, Fyhn M, Molden S, Moser MB, Moser EI. 2005. Microstructure of a spatial map in the entorhinal cortex. *Nature* **436**:801–806. doi:10.1038/nature03721

Harker KT, Whishaw IQ. 2002. Impaired spatial performance in rats with retrosplenial lesions: importance of the spatial problem and the rat strain in identifying lesion effects in a swimming pool. *J Neurosci* **22**:1155–1164. doi:22/3/1155 [pii]

Harland B, Grieves RM, Bett D, Stentiford R, Wood ER, Dudchenko PA. 2017. Lesions of the head direction cell system increase hippocampal place field repetition. *Curr Biol* **27**:2706-2712.e2. doi:10.1016/j.cub.2017.07.071

Harlow HF. 1949. The formation of learning sets. *Psychol Rev* **56**:51–65.
doi:10.1037/h0062474

Harris KD, Henze DA, Csicsvari J, Hirase H, Buzsáki G. 2000. Accuracy of tetrode spike separation as determined by simultaneous intracellular and extracellular measurements. *J Neurophysiol* **84**:401–414. doi:10.1152/jn.2000.84.1.401

Harris KD, Hirase H, Leinekugel X, Henze DA, Buzsáki G. 2001. Temporal interaction between single spikes and complex spike bursts in hippocampal pyramidal cells. *Neuron* **32**:141–149. doi:10.1016/S0896-6273(01)00447-0

Hartley T, Burgess N, Lever C, Cacucci F, O’Keefe J. 2000. Modeling place fields in terms of the cortical inputs to the hippocampus. *Hippocampus* **10**:369–379. doi:10.1002/1098-1063(2000)10:4<369::AID-HIPO3>3.0.CO;2-0

Hartley T, Lever C, Burgess N, O’Keefe J. 2014. Space in the brain: How the hippocampal formation supports spatial cognition. *Philos Trans R Soc B Biol Sci* **369**.
doi:10.1098/rstb.2012.0510

Haugland KG, Sugar J, Witter MP. 2019. Development and topographical organization of projections from the hippocampus and parahippocampus to the retrosplenial cortex. *Eur J Neurosci* **50**:1799–1819. doi:10.1111/ejn.14395

Hayman RM, Jeffery KJ. 2008. How heterogeneous place cell responding arises from homogeneous grids - A contextual gating hypothesis. *Hippocampus* **18**:1301–1313.
doi:10.1002/hipo.20513

Hermer L, Spelke ES. 1994. A geometric process for spatial reorientation in young children. *Nature* **370**:57–59. doi:10.1038/370057a0

Herzog LE, Pascual LM, Scott SJ, Mathieson ER, Katz DB, Jadhav SP. 2019. Interaction of taste and place coding in the hippocampus. *J Neurosci* **39**:3057–3069. doi:10.1523/JNEUROSCI.2478-18.2019

Hindley EL, Nelson AJD, Aggleton JP, Vann SD. 2014. Dysgranular retrosplenial cortex lesions in rats disrupt cross-modal object recognition. *Learn Mem* **21**:171–9. doi:10.1101/lm.032516.113

Hinman JR, Brandon MP, Climer JR, Chapman GW, Hasselmo ME. 2016. Multiple running speed signals in medial entorhinal cortex. *Neuron* **91**:666–679. doi:10.1016/j.neuron.2016.06.027

Hinman JR, Chapman GW, Hasselmo ME. 2019. Neuronal representation of environmental boundaries in egocentric coordinates. *Nat Commun* **10**:1–8. doi:10.1038/s41467-019-10722-y

Honda Y, Ishizuka N. 2015. Topographic distribution of cortical projection cells in the rat subiculum. *Neurosci Res* **92**:1–20. doi:10.1016/j.neures.2014.11.011

Honzik CH. 1936. The sensory basis of maze learning in rats. *Comp Psych Mono* **13**: 113.

Hopkins, DA. 2005. Neuroanatomy of head direction cell circuits. *Head direction cells and the neural mechanisms of spatial orientation*. MIT Press, Cambridge, MA, 17-44.

Hulse BK, Jayaraman V. 2020. Mechanisms underlying the neural computation of head direction. *Annu Rev Neurosci* **43**:31–54. doi:10.1146/annurev-neuro-072116-031516

Ichinohe N. 2012. Small-scale module of the rat granular retrosplenial cortex: An example of the minicolumn-like structure of the cerebral cortex. *Front Neuroanat*.

doi:10.3389/fnana.2011.00069

Ismakov R, Barak O, Jeffery K, Derdikman D. 2017. Grid cells encode local positional information. *Curr Biol* **27**:2337–2343.e3. doi:10.1016/j.cub.2017.06.034

Jacob P-Y, Casali G, Spieler L, Page H, Overington D, Jeffery K. 2017. An independent, landmark-dominated head-direction signal in dysgranular retrosplenial cortex. *Nat Neurosci* **20**:173–175. doi:10.1038/nn.4465

Jacob P-Y, Capitano F, Poucet B, Save E, Sargolini F. 2019. Path integration maintains spatial periodicity of grid cell firing in a 1D circular track. *Nat Commun* **10**:1–13. doi:10.1038/s41467-019-108795-w

Jankowski MM, Islam MN, Wright NF, Vann SD, Erichsen JT, Aggleton JP, O’Mara SM. 2014. Nucleus reuniens of the thalamus contains head direction cells. *eLife* **3**:1–10. doi:10.7554/eLife.03075

Jankowski MM, Paszecker J, Islam N, Vann S, Erichsen JT, Aggleton JP, O’Mara SM. 2015. Evidence for spatially-responsive neurons in the rostral thalamus. *Front Behav Neurosci* **9**:1–18. doi:10.3389/fnbeh.2015.00256

Jayakumar RP, Madhav MS, Savelli F, Blair HT, Cowan NJ, Knierim JJ. 2019. Recalibration of path integration in hippocampal place cells. *Nature* **566**:533–537. doi:10.1038/s41586-019-0939-3

Jeffery KJ. 1998. Learning of landmark stability and instability by hippocampal place cells. *Neuropharmacology* **37**:677–687. doi:10.1016/S0028-3908(98)00053-7

Jeffery KJ. 1997. LTP and spatial learning - Where to next? *Hippocampus* **7**:95–110. doi:10.1002/(SICI)1098-1063(1997)7:1<95::AID-HIPO10>3.0.CO;2-D

Jeffery KJ, Anderson MI, Hayman R, Chakraborty S. 2004. Studies of the hippocampal

cognitive map in rats and humans. Online at: www. ucl. ac. uk/jefferylab/publications

Jeffery KJ, Donnett JG, Burgess N, O'Keefe J. 1997. Directional control of hippocampal place fields. *Exp Brain Res* **117**:131–142. doi:10.1007/s002210050206

Jeffery KJ, Grieves R, Donnett J. 2018. Recording the spatial mapping cells: place, head direction, and grid cells. *Handb Behav Neurosci* **28**:95–121. doi:10.1016/B978-0-12-812028-6.00005-7

Jeffery KJ, O'Keefe JM. 1999. Learned interaction of visual and idiothetic cues in the control of place field orientation. *Exp Brain Res* **127**:151–161. doi:10.1007/s002210050785

Jeffery KJ, Page HJI, Stringer SM. 2016. Optimal cue combination and landmark-stability learning in the head direction system. *J Physiol* **594**:6527–6534. doi:10.1113/JP272945

Jones BF, Witter MP. 2007. Cingulate cortex projections to the parahippocampal region and hippocampal formation in the rat. *Hippocampus* **17**:957–976. doi:10.1002/hipo

Kelly DM, Spetch ML, Heth CD. 1998. Pigeons' (*columba livia*) encoding of geometric and featural properties of a spatial environment. *J Comp Psychol* **112**:259–269. doi:10.1037/0735-7036.112.3.259

Keshavarzi S, Bracey EF, Faville RA, Campagner D, Tyson AL, Lenzi SC, Branco T, Margrie TW. 2021. The retrosplenial cortex combines internal and external cues to encode head velocity during navigation. *bioRxiv*. 2021.01.22.427789. doi: 10.1101/2021.01.22.427789

Kim SS, Hermundstad AM, Romani S, Abbott LF, Jayaraman V. 2019. Generation of stable heading representations in diverse visual scenes. *Nature* **576**:126–131. doi:10.1038/s41586-019-1767-1

Kitanishi T, Umaba R, Mizuseki K. 2021. Robust information routing by dorsal subiculum

- neurons. *Sci Adv* **7**. doi:10.2139/ssrn.3641932
- Knierim JJ. 2006. Neural representations of location outside the hippocampus. *Learn Mem* **13**:405–415. doi:10.1101/lm.224606
- Knierim JJ. 2002. Dynamic interactions between local surface cues, distal landmarks, and intrinsic circuitry in hippocampal place cells. *J Neurosci* **22**:6254–6264. doi:10.1523/jneurosci.22-14-06254.2002
- Knierim JJ. 1996. Vestibular and visual cues in navigation: a tale of two cities. *Ann N Y Acad Sci* **8**:399–406. doi:10.1111/j.1749-6632.1996.tb15715.x
- Knierim JJ, Kudrimoti HS, McNaughton BL. 1998. Interactions between idiothetic cues and external landmarks in the control of place cells and head direction cells. *J Neurophysiol* **80**:425–446. doi:10.1152/jn.1998.80.1.425
- Knierim JJ, Kudrimoti HS, McNaughton BL. 1995. Place cells, head direction cells, and the learning of landmark stability. *J Neurosci* **15**:1648–1659.
- Knierim JJ, Zhang K. 2012. Attractor dynamics of spatially correlated neural activity in the limbic system. *Annu Rev Neurosci* **35**:267–285. doi:10.1146/annurev-neuro-062111-150351
- Knight R, Piette CE, Page H, Walters D, Marozzi E, Nardini M, Stringer S, Jeffery KJ. 2014. Weighted cue integration in the rodent head direction system. *Philos Trans R Soc Lond B Biol Sci* **369**:20120512. doi:10.1098/rstb.2012.0512
- Koay SA, Thibierge SY, Brody CD, Tank DW. 2019. Neural correlates of cognition in primary visual versus neighboring posterior cortices during visual evidence-accumulation-based navigation. *bioRxiv* 1–84. doi:10.1101/568766
- Koganezawa N, Gisetstad R, Husby E, Doan TP, Witter MP. 2015. Excitatory postrhinal

- projections to principal cells in the medial entorhinal cortex. *J Neurosci* **35**:15860–15874. doi:10.1523/JNEUROSCI.0653-15.2015
- Kononenko NL, Witter MP. 2012. Presubiculum layer III conveys retrosplenial input to the medial entorhinal cortex. *Hippocampus* **22**:881–895. doi:10.1002/hipo.20949
- Kornblith S, Cheng X, Ohayon S, Tsao DY. 2013. A network for scene processing in the macaque temporal lobe. *Neuron* **79**:766–781. doi:10.1016/j.neuron.2013.06.015
- Kornienko O, Latuske P, Bassler M, Kohler L, Allen K. 2018. Non-rhythmic head-direction cells in the parahippocampal region are not constrained by attractor network dynamics. *eLife* **7**:1–25. doi:10.7554/eLife.35949
- Kropff E, Carmichael JE, Moser MB, Moser EI. 2015. Speed cells in the medial entorhinal cortex. *Nature* **523**:419–424. doi:10.1038/nature14622
- Krupic J, Bauza M, Burton S, Barry C, O’Keefe J. 2015. Grid cell symmetry is shaped by environmental geometry. *Nature* **518**:232–235. doi:10.1038/nature14153
- LaChance PA, Todd TP, Taube JS. 2019. A sense of space in postrhinal cortex. *Science* **365**. doi:10.1126/science.aax4192
- LaChance PA, Graham J, Shapiro BL, Taube JS. 2020. Landmark-based representations of spatial context in postrhinal cortex. *iNAV* **2020**. doi: inavsymposium.com/wp-content/uploads/2020/10/Data_Blitz_Booklet_2020.pdf
- Landler L, Ruxton GD, Malkemper EP. 2018. Circular data in biology: advice for effectively implementing statistical procedures. *Behav Ecol Sociobiol* **72**. doi:10.1007/s00265-018-2538-y
- Langston RF, Ainge JA, Couey JJ, Canto CB, Bjerknes TL, Witter MP, Moser EI, Moser MB. 2010. Development of the spatial representation system in the rat. *Science* (80-)

328:1576–1580. doi:10.1126/science.1188210

Le Tarnec L, Garcia D. 2012. Erratum: Robust smoothing of gridded data in one and higher dimensions with missing values (Computational Statistics and Data Analysis (2010) 54 1167-1178). *Comput Stat Data Anal* **56**:2182. doi:10.1016/j.csda.2011.12.001

Leutgeb S, Ragazzino KE, Mizumori SJY. 2000. Convergence of head direction and place information in the CA1 region of hippocampus. *Neuroscience* **100**:11–19. doi:10.1016/S0306-4522(00)00258-X

Lever C, Burton S, Jeewajee A, O’Keefe J, Burgess N. 2009. Boundary vector cells in the subiculum of the hippocampal formation. *J Neurosci* **29**:9771–9777. doi:10.1523/JNEUROSCI.1319-09.2009

Lomi E, Mathiasen ML, Cheng HY, Zhang N, Aggleton JP, Mitchell AS, Jeffery KJ. 2021. Evidence for two distinct thalamocortical circuits in retrosplenial cortex. *bioRxiv*. doi: 10.1101/2021.06.11.448056

Long X, Deng B, Cai J, Chen ZS, Zhang S, Hospital X. 2021. Egocentric asymmetric coding in sensory cortical border cells. *bioRxiv*. doi:10.1101/2021.03.11.434952

Long X, Young CK, Zhang SJ. 2020. Sharp tuning of head direction by somatosensory fast-spiking interneurons. *bioRxiv*. doi:10.1101/2020.02.03.933143

Long X, Zhang SJ. 2021. A novel somatosensory spatial navigation system outside the hippocampal formation. *Cell Res* 1–15. doi:10.1038/s41422-020-00448-8

Lozano YR, Page H, Jacob P-Y, Lomi E, Street J, Jeffery K. 2017. Retrosplenial and postsubicular head direction cells compared during visual landmark discrimination. *Brain Neurosci Adv* **1**:239821281772185. doi:10.1177/2398212817721859

Ludvig N, Tang HM, Gohil BC, Botero JM. 2004. Detecting location-specific neuronal firing

rate increases in the hippocampus of freely-moving monkeys. *Brain Res* **1014**. 97-109.

doi: 10.1016/j.brainres.2004.03.071

Maguire E. 2001. The retrosplenial contribution to human navigation: A review of lesion and neuroimaging findings. *Scand J Psychol* **42**:225–238.

Makino H, Komiyama T. 2015. Learning enhances the relative impact of top-down processing in the visual cortex. *Nat Neurosci* **18**:1116–1122. doi:10.1038/nn.4061

Mankin EA, Thurley K, Chenani A, Haas O V., Debs L, Henke J, Galinato M, Leutgeb JK,

Leutgeb S, Leibold C. 2019. The hippocampal code for space in Mongolian gerbils.

Hippocampus **29**:787–801. doi:10.1002/hipo.23075

Mao D, Avila E, Caziot B, Laurens J, Dickman JD, Angelaki DE. 2020a. Spatial

representations in macaque hippocampal formation. *bioRxiv*.

doi:10.1101/2020.10.03.324848

Mao D, Kandler S, McNaughton BL, Bonin V. 2017. Sparse orthogonal population

representation of Spatial Context in the Retrosplenial Cortex. *Nat Commun* 1–9.

doi:10.1038/s41467-017-00180-9

Mao D, Molina LA, Bonin V, McNaughton BL. 2020b. Vision and Locomotion Combine to

Drive Path Integration Sequences in Mouse Retrosplenial Cortex. *Curr Biol* **30**:1680-

1688.e4. doi:10.1016/j.cub.2020.02.070

Mao D, Neumann AR, Sun J, Bonin V, Mohajerani MH, McNaughton BL. 2018.

Hippocampus-dependent emergence of spatial sequence coding in retrosplenial cortex.

Proc Natl Acad Sci U S A **115**:8015–8018. doi:10.1073/pnas.1803224115

Marchette SA, Vass LK, Ryan J, Epstein RA. 2014. Anchoring the neural compass: coding of

local spatial reference frames in human medial parietal lobe. *Nat Neurosci* **17**:1598–

1606. doi:10.1038/nn.3834

Markus EJ, Qin YL, Leonard B, Skaggs WE, McNaughton BL, Barnes CA. 1995.

Interactions between location and task affect the spatial and directional firing of hippocampal neurons. *J Neurosci* **15**:7079–7094. doi:10.1523/jneurosci.15-11-07079.1995

Marozzi E, Ginzberg LL, Alenda A, Jeffery KJ. 2015. Purely translational realignment in grid cell firing patterns following nonmetric context change. *Cereb Cortex* **25**:4619–4627. doi:10.1093/cercor/bhv120

Marozzi E, Jeffery KJ. 2012. Place, space and memory cells. *Curr Biol* **22**:R939–R942. doi:10.1016/j.cub.2012.10.022

Mackintosh NJ. 1975. A theory of attention: Variations in the associability of stimuli with reinforcement. *Psycho Rev* **82**: 276–298. doi:10.1037/h0076778

Mallory CS, Hardcastle K, Campbell MG, Attinger A, Low II, Raymond JL, Giocomo LM. 2021. Mouse entorhinal cortex encodes a diverse repertoire of self-motion signals. *Nat Commun* **12**:1-20. doi: 10.1038/s41467-021-20936-8

Mathiasen ML, Dillingham CM, Kinnavane L, Powell AL, Aggleton JP. 2017. Asymmetric cross-hemispheric connections link the rat anterior thalamic nuclei with the cortex and hippocampal formation. *Neuroscience* **349**:128–143. doi:10.1016/j.neuroscience.2017.02.026

Matthews DB, Best PJ. 1997. Evidence for the flexible use of spatial knowledge in the rat. *Psychobiology* **25**:294–302. doi:10.3758/BF03331940

Mcnaughton BL, Barnes CA, Gerrard JL, Gothard K, Jung MW, Knierim JJ, Kudrimoti H, Qin Y, Skaggs WE, Suster M, Weaver KL. 1996. Deciphering the hippocampal

polyglot: The hippocampus as a path integration system. *J Exp Biol* **199**:173–185.

McNaughton BL, Barnes CA, O’Keefe J. 1983. The contributions of position, direction, and velocity to single unit activity in the hippocampus of freely-moving rats. *Exp Brain Res* **52**:41–49. doi:10.1007/BF00237147

McNaughton BL, Battaglia FP, Jensen O, Moser EI, Moser MB. 2006. Path integration and the neural basis of the “cognitive map.” *Nat Rev Neurosci* **7**:663–678. doi:10.1038/nrn1932

McNaughton BL, Chen LL, Markus EJ. 1991. “Dead reckoning,” landmark learning, and the sense of direction: A neurophysiological and computational hypothesis. *J Cogn Neurosci* **3**:190–202. doi:10.1162/jocn.1991.3.2.190

Mehlman ML, Winter SS, Taube JS. 2019. Functional and anatomical relationships between the medial precentral cortex, dorsal striatum, and head direction cell circuitry. II. Neuroanatomical studies. *J Neurophysiol* **121**:371–395. doi:10.1152/jn.00144.2018

Milczarek MM, Vann SD, Sengpiel F. 2018. Spatial memory engram in the mouse retrosplenial cortex. *Curr Biol* **28**:1975-1980.e6. doi:10.1016/j.cub.2018.05.002

Minderer M, Brown KD, Harvey CD. 2019. The spatial structure of neural encoding in mouse posterior cortex during navigation. *Neuron* **102**:232-248.e11. doi:10.1016/j.neuron.2019.01.029

Mitchell AS, Czajkowski R, Zhang N, Jeffery K, Nelson AJD. 2018. Retrosplenial cortex and its role in spatial cognition. *Brain Neurosci Adv* **2**:239821281875709. doi:10.1177/2398212818757098

Mittelstaedt ML, Mittelstaedt H. 1980. Homing by path integration in a mammal. *Naturwissenschaften* **67**:566–567. doi:10.1007/BF00450672

Mittelstaedt H, Mittelstaedt ML. 1982. Homing by path integration. In: Papi F, Wallraff HG, editors. *Avian navigation*. New York: Springer. p 290–297

Miyashita T, Rockland KS. 2007. GABAergic projections from the hippocampus to the retrosplenial cortex in the rat. *Eur J Neurosci* **26**:1193–1204. doi:10.1111/j.1460-9568.2007.05745.x

Mizumori SJY, Ragazzo KE, Cooper BG. 2000. Location and head direction representation in the dorsal striatum of rats. *Psychobiology* **28**:441–462. doi:10.3758/BF03332003

Mizumori SJY, Williams JD. 1993. Directionally selective mnemonic properties of neurons in the lateral dorsal nucleus of the thalamus of rats. *J Neurosci* **13**:4015–4028. doi:10.1523/jneurosci.13-09-04015.1993

Morris RGM. 1981. Spatial localization does not require the presence of local cues. *Learn Motiv* **12**:239–260. doi:10.1016/0023-9690(81)90020-5

Muir GM, Brown JE, Carey JP, Hirvonen TP, Della Santina CC, Minor LB, Taube JS. 2009. Disruption of the head direction cell signal after occlusion of the semicircular canals in the freely moving chinchilla. *J Neurosci* **29**:14521–14533. doi:10.1523/JNEUROSCI.3450-09.2009

Muller RU, Bostock E, Taube JS, Kubie JL. 1994. On the directional firing properties of hippocampal place cells. *J Neurosci* **14**:7235–7251. doi:10.1523/jneurosci.14-12-07235.1994

Muller RU, Kubie JL. 1987. The effects of changes in the environment on the spatial firing of hippocampal complex-spike cells. *J Neurosci* **7**:1951–1968. doi:10.1523/jneurosci.07-07-01951.1987

Muller RU, Kubie JL, Ranck JB. 1987. Spatial firing patterns of hippocampal complex-spike

cells in a fixed environment. *J Neurosci* **7**:1935–1950. doi:10.1523/jneurosci.07-07-01935.1987

Nelson AJD, Hindley EL, Haddon JE, Vann SD, Aggleton JP. 2014. A novel role for the rat retrosplenial cortex in cognitive control. *Learn Mem* **21**:90–7.
doi:10.1101/lm.032136.113

Neunuebel JP, Yoganarasimha D, Rao G, Knierim, JJ. 2013. Conflicts between local and global spatial frameworks dissociate neural representations of the lateral and medial entorhinal cortex. *J Neurosci* **33**: 9246-9258. doi: 10.1523/JNEUROSCI.0946-13.2013

O’Keefe J. 1979. A review of hippocampal place cell. *Prog Neurobiol* **13**:419–439. doi: 10.1016/0301-0082(79)90005-4

O’Keefe J, Burgess N. 1996. Geometric determinants of the neurons. *Nature* **381**:425–428.
doi: 10.1038/381425a0

O’Keefe J, Dostrovsky J, J. O’Keefe JD. 1971. The hippocampus as a spatial map. Preliminary evidence from unit activity in the freely-moving rat. *Brain Res* **34**:171–175.
doi: 10.1016/0006-8993(71)90358-1

O’Keefe J, Nadel L. 1978. *The hippocampus as a cognitive map*. Philosophical Studies.
doi:10.5840/philstudies19802725

O’Keefe J, Speakman A. 1987. Single unit activity in the rat hippocampus during a spatial memory task. *Exp Brain Res* **68**:1–27. doi:10.1007/BF00255230

Oh SW, Harris JA, Ng L, Winslow B, Cain N, Mihalas S, Wang Q, Lau C, Kuan L, Henry AM, Mortrud MT, Ouellette B, Nguyen TN, Sorensen SA, Slaughterbeck CR, Wakeman W, Li Y, Feng D, Ho A, Nicholas E, Hirokawa KE, Bohn P, Joines KM, Peng H, Hawrylycz MJ, Phillips JW, Hohmann JG, Wohnoutka P, Gerfen CR, Koch C, Bernard

- A, Dang C, Jones AR, Zeng H. 2014. A mesoscale connectome of the mouse brain. *Nature* **508**:207–214. doi:10.1038/nature13186
- Olsen GM, Ohara S, Iijima T, Witter MP. 2017. Parahippocampal and retrosplenial connections of rat posterior parietal cortex. *Hippocampus* **27**:335–358. doi:10.1002/hipo.22701
- Olson JM, Tongprasearth K, Nitz DA. 2017. Subiculum neurons map the current axis of travel. *Nat Neurosci* **20**:170–172. doi:10.1038/nn.4464
- Olton DS, Walker JA, Gage FH. 1978. Hippocampal connections and spatial discrimination. *Brain Res* **139**:295–308. doi:10.1016/0006-8993(78)90930-7
- Opalka AN, Huang W qiang, Liu J, Liang H, Wang D V. 2020. Hippocampal Ripple Coordinates Retrosplenial Inhibitory Neurons during Slow-Wave Sleep. *Cell Rep* **30**:432-441.e3. doi:10.1016/j.celrep.2019.12.038
- Opalka AN, Wang D V. 2020. Hippocampal efferents to retrosplenial cortex and lateral septum are required for memory acquisition. *Learn Mem* **27**:310–318. doi:10.1101/2020.03.23.003996
- Packard MG, McGaugh JL. 1996. Inactivation of hippocampus or caudate nucleus with lidocaine differentially affects expression of place and response learning. *Neurobiol Learn Mem* **65**:65–72. doi:10.1006/nlme.1996.0007
- Page HJI, Jeffery KJ. 2018. Landmark-based updating of the head direction system by retrosplenial cortex: a computational model. *Front Cell Neurosci* **12**:1–17. doi:10.3389/fncel.2018.00191
- Papez, JW. 1937. A proposed mechanism of emotion. *Arch Neuro Psychi*, **38**: 725-743. doi: 10.1001/archneurpsyc.1937.02260220069003

Park S, Chun MM. 2009. Different roles of the parahippocampal place area (PPA) and retrosplenial cortex (RSC) in panoramic scene perception. *Neuroimage* **47**:1747–1756. doi:10.1016/j.neuroimage.2009.04.058

Patai EZ, Javadi AH, Ozubko JD, O'Callaghan A, Ji S, Robin J, Grady C, Winocur G, Rosenbaum RS, Moscovitch M, Spiers HJ. 2019. Hippocampal and retrosplenial goal distance coding after long-term consolidation of a real-world environment. *Cereb Cortex* **29**:2748–2758. doi:10.1093/cercor/bhz044

Pavlov IP. 1927. *Conditioned reflexes: an investigation of the physiological activity of the cerebral cortex*. Oxford Univ. Press.

Payne HL, Lynch GF, Aronov D. 2020. Precise spatial representations in the hippocampus of a food-caching bird. *bioRxiv*. doi:10.1101/2020.11.27.399444

Paxinos G, Watson C. 2006. *The rat brain in stereotaxic coordinates: hard cover edition*. Elsevier.

Pérez-Escobar JA, Kornienko O, Latuske P, Kohler L, Allen K. 2016. Visual landmarks sharpen grid cell metric and confer context specificity to neurons of the medial entorhinal cortex. *eLife* **5**:1–21. doi:10.7554/eLife.16937

Peyrache A, Lacroix MM, Petersen PC, Buzsáki G. 2015. Internally organized mechanisms of the head direction sense. *Nat Neurosci* **18**:569–575. doi:10.1038/nn.3968

Peyrache A, Schieferstein N, Buzsáki G. 2017. Transformation of the head-direction signal into a spatial code. *Nat Commun* **8**. doi:10.1038/s41467-017-01908-3

Pothuizen HHJ, Aggleton JP, Vann SD. 2008. Do rats with retrosplenial cortex lesions lack direction? *Eur J Neurosci* **28**:2486–2498. doi:10.1111/j.1460-9568.2008.06550.x

Pothuizen HHJ, Davies M, Albasser MM, Aggleton JP, Vann SD. 2009. Granular and

- dysgranular retrosplenial cortices provide qualitatively different contributions to spatial working memory: Evidence from immediate-early gene imaging in rats. *Eur J Neurosci* **30**:877–888. doi:10.1111/j.1460-9568.2009.06881.x
- Pouget A, Sejnowski TJ. 1997. Spatial Transformations in the Parietal Cortex Using Basis Function. *J Cogn Neurosci* **9**:222–237. doi:10.1215/9780822383680-004
- Powell A, Connelly WM, Vasalauskaite A, Nelson AJD, Vann SD, Aggleton JP, Sengpiel F, Ranson A. 2020. Stable encoding of visual cues in the mouse retrosplenial cortex. *Cereb Cortex* **30**:4424–4437. doi:10.1093/cercor/bhaa030
- Preston-Ferrer P, Coletta S, Frey M, Burgalossi A. 2016. Anatomical organization of presubiculum head-direction circuits. *eLife* **5**:1–20. doi:10.7554/eLife.14592
- Morris RMG. 1981. Spatial localization does not require the presence of local cue. *Learn Motiv* **12**:239-260. doi: 10.1016/0023-9690(81)90020-5
- Morris RMG, Garrud P, Rawlins JNP, O’Keefe J. 1982. Place navigation impaired in rats with hippocampal lesions. *Nature* **297**:681–683. doi:10.1038/297681a0
- Ranck JB Jr. 1984. Head-direction cells in the deep cell layers of dorsal presubiculum in freely moving rats. *Soc Neurosci Abstr.* **10**: 599.
- Ranganath C, Ritchey M. 2012. Two cortical systems for memory-guided behaviour. *Nat Rev Neurosci* **13**:713–726. doi:10.1038/nrn3338
- Redish A, Elga A, Touretzky D. 1996. A coupled attractor model of the rodent head direction system. *Netw Comput Neural Syst* **7**:671–685. doi:10.1088/0954-898X/7/4/004
- Renaudineau S, Poucet B, Save E. 2007. Flexible use of proximal objects and distal cues by hippocampal place cells. *Hippocampus* **17**:381–395. doi:10.1002/hipo

- Robertson RG, Rolls ET, Georges-François P, Panzeri S. 1999. Head direction cells in the primate pre-subiculum. *Hippocampus* **9**:206–219. doi:10.1002/(SICI)1098-1063(1999)9:3<206::AID-HIPO2>3.0.CO;2-H
- Rolls ET, Treves A, Robertson RG, Georges-François P, Panzeri S. 1998. Information about spatial view in an ensemble of primate hippocampal cells. *J Neurophysiol* **79**:1797–1813. doi:10.1152/jn.1998.79.4.1797
- Rotenberg A, Mayford M, Hawkins RD, Kandel ER, Muller RU. 1996. Mice expressing activated CaMKII lack low frequency LTP and do not form stable place cells in the CA1 region of the hippocampus. *Cell* **87**:1351–1361. doi:10.1016/S0092-8674(00)81829-2
- Saleem AB, Ayaz AI, Jeffery KJ, Harris KD, Carandini M. 2013. Integration of visual motion and locomotion in mouse visual cortex. *Nat Neurosci* **16**:1864–1869. doi:10.1038/nn.3567
- Saleem AB, Diamanti EM, Fournier J, Harris KD, Carandini M. 2018. Coherent encoding of subjective spatial position in visual cortex and hippocampus. *Nature* **562**:124–127. doi:10.1038/s41586-018-0516-1
- Sams CF, Tolman EC. 1925. Time discrimination in white rats. *J Comp Psychol* **5**:255–263. doi:10.1037/h0074866
- Samsonovich A, McNaughton BL. 1997. Path integration and cognitive mapping in a continuous attractor neural network model. *J Neurosci* **17**:5900–5920. doi:10.1523/jneurosci.17-15-05900.1997
- Sargolini F, Fyhn M, Hafting T, McNaughton BL, Witter MP, Moser MB, Moser EI. 2006. Conjunctive representation of position, direction, and velocity in entorhinal cortex. *Science* **312**:758–762. doi:10.1126/science.1125572

Save E, Nerad L, Poucet B. 2000. Contribution of multiple sensory information to place field stability in hippocampal place cells. *Hippocampus* **10**:64–76. doi:10.1002/(SICI)1098-1063(2000)10:1<64::AID-HIPO7>3.0.CO;2-Y

Savelli F, Yoganarasimha D, Knierim JJ. 2008. Influence of boundary removal on the spatial representations of the medial entorhinal cortex. *Hippocampus* **18**:1270–1282. doi:10.1002/hipo.20511

Schmitzer-Torbert N, Jackson J, Henze D, Harris K, Redish AD. 2005. Quantitative measures of cluster quality for use in extracellular recordings. *Neuroscience* **131**:1–11. doi:10.1016/j.neuroscience.2004.09.066

Seelig JD, Jayaraman V. 2015. Neural dynamics for landmark orientation and angular path integration. *Nature* **521**:186–191. doi:10.1038/nature14446

Shapiro ML, Tanila H, Eichenbaum H. 1997. Cues that hippocampal place cells encode: Dynamic and hierarchical representation of local and distal stimuli. *Hippocampus* **7**:624–642. doi:10.1002/(SICI)1098-1063(1997)7:6<624::AID-HIPO5>3.0.CO;2-E

Sharp PE. 1999. Subicular place cells expand or contract their spatial firing pattern to fit the size of the environment in an open field but not in the presence of barriers: Comparison with hippocampal place cells. *Behav Neurosci* **113**:643–662. doi:10.1037//0735-7044.113.4.643

Sharp PE, Blair HT, Cho J. 2001. The anatomical and computational basis of the rat head-direction cell signal. *Trends Neurosci* **24**:289–294. doi:10.1016/S0166-2236(00)01797-5

Sharp PE, Green C. 1994. Spatial correlates of firing patterns of single cells in the subiculum of the freely moving rat. *J Neurosci* **14**:2339–2356. doi:10.1523/jneurosci.14-04-02339.1994

Shibata H. 1993. Direct projections from the anterior thalamic nuclei to the retrohippocampal region in the rat. *J Comp Neurol* **337**:431–445. doi:10.1002/cne.903370307

Shibata H, Kondo S, Naito J. 2004. Organization of retrosplenial cortical projections to the anterior cingulate, motor, and prefrontal cortices in the rat. *Neurosci Res* **49**:1–11. doi:10.1016/j.neures.2004.01.005

Shine JP, Valdes-Herrera JP, Hegarty M, Wolbers T. 2016. The human retrosplenial cortex and thalamus code head direction in a global reference frame. *J Neurosci* **36**:6371–6381. doi:10.1523/JNEUROSCI.1268-15.2016

Simonnet J, Brecht M. 2019. Burst firing and spatial coding in subiculum principal cells. *J Neurosci* **39**:3651–3662. doi:10.1101/303354

Skaggs WE, Knierim JJ, Kudrimoti HS, McNaughton BL. 1995. A model of the neural basis of the rat's sense of direction. *Adv Neural Inf Process Syst* **7**:173–180.

Skaggs WE, McNaughton BL. 1998. Spatial firing properties of hippocampal CA1 populations in an environment containing two visually identical regions. *J Neurosci* **18**:8455–8466. doi:10.1523/jneurosci.18-20-08455.1998

Smith AE, Wood ER, Dudchenko PA. 2021. The stimulus control of local enclosures and barriers over head direction and place cell spatial firing. *Brain Behav* e02070. doi:10.1002/brb3.2070

Smith DM, Barredo J, Mizumori SJY. 2012. Complementary roles of the hippocampus and retrosplenial cortex in behavioral context discrimination. *Hippocampus* **22**:1121–1133. doi:10.1002/hipo.20958

Solstad T, Boccara CN, Kropff E, Moser M-B, Moser EI. 2008. Representation of geometric borders. *Science* **322**:1865–1868. doi: 10.1126/science.1166466

Spalla D, Treves A, Boccaro CN. 2021. Angular and linear speed cells in the parahippocampal circuits. *bioRxiv*. doi: 2021.01.28.428631

Spiers HJ, Hayman RMA, Jovalekic A, Marozzi E, Jeffery KJ. 2015. Place field repetition and purely local remapping in a multicompartment environment. *Cereb Cortex* **25**:10–25. doi:10.1093/cercor/bht198

Sreenivasan S, Fiete I. 2011. Grid cells generate an analog error-correcting code for singularly precise neural computation. *Nat Neurosci* **14**:1330–1337. doi:10.1038/nn.2901

Stachenfeld KL, Botvinick MM, Gershman SJ. 2017. The hippocampus as a predictive map. *Nat Neurosci* **20**:1643–1653. doi:10.1038/nn.4650

Stackman RW, Clark AS, Taube JS. 2002. Hippocampal spatial representations require vestibular input. *Hippocampus* **12**:291–303. doi:10.1002/hipo.1112

Stackman RW, Golob EJ, Bassett JP, Taube JS. 2003. Passive transport disrupts directional path integration by rat head direction cells. *J Neurophysiol* **90**:2862–2874. doi:10.1152/jn.00346.2003

Stackman RW, Taube JS. 1998. Firing properties of rat lateral mammillary single units: Head direction, head pitch, and angular head velocity. *J Neurosci* **18**:9020–9037. doi:10.1523/jneurosci.18-21-09020.1998

Stackman RW, Taube JS. 1997. Firing properties of head direction cells in the rat anterior thalamic nucleus: Dependence on vestibular input. *J Neurosci* **17**:4349–4358. doi:10.1523/jneurosci.17-11-04349.1997

Sugar J, Witter MP. 2016. Postnatal development of retrosplenial projections to the parahippocampal region of the rat. *Elife* **5**:1–29. doi:10.7554/eLife.13925

- Sugar J, Witter MP, van Strien NM, Cappaert NLM. 2011. The retrosplenial cortex: intrinsic connectivity and connections with the (para)hippocampal region in the rat. An interactive connectome. *Front Neuroinform* **5**:7. doi:10.3389/fninf.2011.00007
- Sutherland RJ, Whishaw IQ, Kolb B. 1988. Contributions of cingulate cortex to two forms of spatial learning and memory. *J Neurosci* **8**:1863–872. doi: 10.1523/JNEUROSCI.08-06-01863.1988
- Suzuki K, Yamadori A, Hayakawa Y, Fujii T. 1998. Pure topographical disorientation related to dysfunction of the viewpoint dependent visual system. *Cortex* **34**:589–599. doi:10.1016/S0010-9452(08)70516-1
- Suzuki S, Augerinos G, Black AH. 1980. Stimulus control of spatial behavior on the eight-arm maze in rats. *Learn Motiv* **11**:1–18. doi:10.1016/0023-9690(80)90018-1
- Takahashi N, Kawamura M, Shiota J, Kasahata N, Hirayama K. 1997. Pure topographic disorientation due to right retrosplenial lesion. *Neurology* **49**:464–469. doi:10.1212/WNL.49.2.464
- Tan HM, Wills TJ, Cacucci F. 2017. The development of spatial and memory circuits in the rat. *Wiley Interdiscip Rev Cogn Sci* **8**:1–16. doi:10.1002/wcs.1424
- Tanila H. 1999. Hippocampal place cells can develop distinct representations of two visually identical environments. *Hippocampus* **9**:235–246. doi:10.1002/(SICI)1098-1063(1999)9:3<235::AID-HIPO4>3.0.CO;2-3
- Tanila H, Shapiro ML, Eichenbaum H. 1997. Discordance of spatial representation in ensembles of hippocampal place cells. *Hippocampus* **7**:613–623. doi:10.1002/(SICI)1098-1063(1997)7:6<613::AID-HIPO4>3.0.CO;2-F
- Taube JS. 2007. The head direction signal: Origins and sensory-motor integration. *Annu Rev*

Neurosci **30**:181–207. doi:10.1146/annurev.neuro.29.051605.112854

Taube JS. 1995. Head direction cells recorded in the anterior thalamic nuclei of freely moving rats. *J Neurosci* **15**:70–86. doi:10.1523/jneurosci.15-01-00070.1995

Taube JS, Burton HL. 1995. Head direction cell activity monitored in a novel environment and during a cue conflict situation. *J Neurophysiol* **74**:1953–1971. doi:10.1152/JN.1995.74.5.1953

Taube JS, Goodridge JP, Golob EJ, Dudchenko PA, Stackman RW. 1996. Processing the head direction cell signal: A review and commentary. *Brain Res Bull* **40**:477–484. doi:10.1016/0361-9230(96)00145-1

Taube JS, Muller RU. 1998. Comparisons of head direction cell activity in the postsubiculum and anterior thalamus of freely moving rats. *Hippocampus* **8**:87–108. doi:10.1002/(SICI)1098-1063(1998)8:2<87::AID-HIPO1>3.0.CO;2-4

Taube JS, Muller RU, Ranck JB. 1990. Head-direction cells recorded from the postsubiculum in freely moving rats. I. Description and quantitative analysis. *J Neurosci* **10**:420–35. doi:10.1212/01.wnl.0000299117.48935.2e

Taube JS, Muller RU, Ranck JB. 1990. Head-direction cells recorded from the postsubiculum in freely moving rats. II. Effects of environmental manipulations. *J Neurosci* **10**:436–447. doi:10.1212/01.wnl.0000299117.48935.2e

Thorndike, EL. 1898. Animal intelligence. *Nature* **58**: 390. doi:10.1038/058390b0

Todd TP, Fournier DI, Bucci DJ. 2019. Retrosplenial cortex and its role in cue-specific learning and memory. *Neurosci Biobehav Rev* **107**:713–728. doi:10.1016/j.neubiorev.2019.04.016

Todd TP, Mehlman ML, Keene CS, DeAngeli NE, Bucci DJ. 2016. Retrosplenial cortex is

- required for the retrieval of remote memory for auditory cues. *Learn Mem* **23**:278–88.
doi:10.1101/lm.041822.116
- Tolman EC, Ritchie BF, Kalish D. 1946. Studies in spatial learning. I. Orientation and the short-cut. *J Exp Psychol* **36**: 13–24. doi:10.1037/h0053944
- Tolman EC. 1948. Cognitive maps in rats and men. *Image Environ Cogn Mapp Spat Behav* 27–50. doi:10.4324/9780203789155-11
- Tsanov M, Chah E, Vann SD, Reilly RB, Erichsen JT, Aggleton JP, O’Mara SM. 2011. Theta-modulated head direction cells in the rat anterior thalamus. *J Neurosci* **31**:9489–9502. doi:10.1523/JNEUROSCI.0353-11.2011
- Ulanovsky N, Moss CF. 2007. Hippocampal cellular and network activity in freely moving echolocating bats. *Nat Neurosci* **10**:224–233. doi:10.1038/nn1829
- Valerio S, Taube JS. 2016. Head direction cell activity is absent in mice without the horizontal semicircular canals. *J Neurosci* **36**:741–754. doi:10.1523/JNEUROSCI.3790-14.2016
- Vale R, Campagner D, Iordanidou P, Arocás OP, Tan YL, Stempel AV, Keshavarzi S, Petersen R, Margrie T, Branco T. 2020. A cortico-collicular circuit for accurate orientation to shelter during escape. *bioRxiv*. doi:10.1101/2020.05.26.117598
- van der Meer M a a, Knierim JJ, Yoganarasimha D, Wood ER, van Rossum MCW. 2007. Anticipation in the rodent head direction system can be explained by an interaction of head movements and vestibular firing properties. *J Neurophysiol* **98**:1883–97.
doi:10.1152/jn.00233.2007
- Van Groen T, Wyss JM. 1990. The connections of presubiculum and parasubiculum in the rat. *Brain Res* **518**:227–243. doi:10.1016/0006-8993(90)90976-I

Van Groen T, Wyss JM. 2003. Connections of the retrosplenial granular b cortex in the rat. *J Comp Neurol* **463**:249–263. doi:10.1002/cne.10757

Van Groen T, Wyss JM. 1992. Connections of the retrosplenial dysgranular cortex in the rat. *J Comp Neurol* **315**:200–216. doi:10.1002/cne.903150207

Van Groen T, Wyss JM. 1990. Connections of the retrosplenial granular a cortex in the rat. *J Comp Neurol* **300**:593–606. doi:10.1002/cne.10757

van Wijngaarden JBG, Babl SS, Ito HT. 2020. Entorhinal-retrosplenial circuits for allocentric-egocentric transformation of boundary coding. *eLife* **9**:1–25. doi:10.7554/eLife.59816

Vann SD, Aggleton JP. 2005. Selective dysgranular retrosplenial cortex lesions in rats disrupt allocentric performance of the radial-arm maze task. *Behav Neurosci* **119**:1682–1686. doi:10.1037/0735-7044.119.6.1682

Vann SD, Aggleton JP. 2004. Testing the importance of the retrosplenial guidance system: Effects of different sized retrosplenial cortex lesions on heading direction and spatial working memory. *Behav Brain Res* **155**:97–108. doi:10.1016/j.bbr.2004.04.005

Vann SD, Aggleton JP, Maguire EA. 2009. What does the retrosplenial cortex do? *Nat Rev Neurosci* **10**:792–802. doi:10.1038/nrn2733

Vantomme G, Rovó Z, Cardis R, Béard E, Katsioudi G, Guadagno A, Perrenoud V, Fernandez LMJ, Lüthi A. 2020. A thalamic reticular circuit for head direction cell tuning and spatial navigation. *Cell Rep* **31**. doi:10.1016/j.celrep.2020.107747

Vedder LC, Miller AMP, Harrison MB, Smith DM. 2017. Retrosplenial cortical neurons encode navigational cues, trajectories and reward locations during goal directed navigation. *Cereb Cortex* **27**:3713–3723. doi:10.1093/cercor/bhw192

- Vélez-Fort M, Bracey EF, Keshavarzi S, Rousseau CV, Cossell L, Lenzi SC, Strom M, Margrie TW. 2018. A circuit for integration of head-and visual-motion signals in layer 6 of mouse primary visual cortex. *Neuron* **98**: 179–91. doi: 10.1016/j.neuron.2018.02.023
- Vesuna S, Kauvar I V., Richman E, Gore F, Oskotsky T, Sava-Segal C, Luo L, Malenka RC, Henderson JM, Nuyujukian P, Parvizi J, Deisseroth K. 2020. Deep posteromedial cortical rhythm in dissociation. *Nature* **586**:87–94. doi:10.1038/s41586-020-2731-9
- Vogt BA, Miller MW. 1983. Cortical connections between rat cingulate cortex and visual, motor, and postsubiculum cortices. *J Comp Neurol* **216**:192–210.
doi:10.1002/cne.902160207
- Vogt BA, Peters A. 1981. Form and distribution of neurons in rat cingulate cortex: Areas 32, 24, and 29. *J Comp Neurol* **195**:603–625. doi:10.1002/cne.901950406
- Voigts J, Harnett MT. 2019. Somatic and dendritic encoding of spatial variables in retrosplenial cortex differs during 2d navigation. *Neuron* **105**: 1–9.
doi:10.1016/J.NEURON.2019.10.016
- Von Helmholtz H. 1925. *Helmholtz's treatise on physiological optics (Vol. 3)*. Optical Society of America.
- Wagner AD, Shannon BJ, Kahn I, Buckner RL. 2005. Parietal lobe contributions to episodic memory retrieval. *Trends Cogn Sci* **9**. doi:10.1016/j.tics.2005.07.001
- Wang C, Chen X, Knierim JJ. 2020. Egocentric and allocentric representations of space in the rodent brain. *Curr Opin Neurobiol* **60**:12–20. doi:10.1016/j.conb.2019.11.005
- Wang C, Chen X, Lee H, Deshmukh SS, Yoganarasimha D, Savelli F, Knierim JJ. 2018. Egocentric coding of external items in the lateral entorhinal cortex. *Science* **362**:945–949. doi:10.1126/science.aau4940

- Whitlock JR, Derdikman D. 2012. Head direction maps remain stable despite grid map fragmentation. *Front Neural Circuits* **6**:1–10. doi:10.3389/fncir.2012.00009
- Wiener SI. 1993. Spatial and behavioral correlates of striatal neurons in rats performing a self-initiated navigation task. *J Neurosci* **13**:3802–3817. doi:10.1523/jneurosci.13-09-03802.1993
- Wilber AA, Clark BJ, Forster TC, Tatsuno M, McNaughton BL. 2014. Interaction of egocentric and world-centered reference frames in the rat posterior parietal cortex. *J Neurosci* **34**:5431–5446. doi:10.1523/JNEUROSCI.0511-14.2014
- Wills TJ, Cacucci F, Burgess N, O’Keefe J. 2010. Development of the hippocampal cognitive map in preweanling rats. *Science (80-)* **328**:1573–1576. doi:10.1126/science.1188224
- Winter SS, Taube JS. 2014. Head Direction Cells: From Generation to Integration. In: Derdikman D., Knierim J. (eds) *Space, Time and Memory in the Hippocampal Formation*. Springer, Vienna. doi:10.1007/978-3-7091-1292-2_4
- Winter SS, Clark BJ, Taube JS. 2015. Disruption of the head direction cell network impairs the parahippocampal grid cell signal. *Science* **347**:1–6. doi: 10.1126/science.1259591
- Wood ER, Dudchenko PA, Eichenbaum H. 1999. The global record of memory in hippocampal neuronal activity. *Nature* **397**:613–616. doi:10.1038/17605
- Wyss JM, Sripanidkulchai K. 1984. The topography of the mesencephalic and pontine projections from the cingulate cortex of the rat. *Brain Res* **293**:1–15. doi:10.1016/0006-8993(84)91448-3
- Wyss JM, Van Groen T, Sripanidkulchai K. 1990. Dendritic bundling in layer I of granular retrosplenial cortex: Intracellular labeling and selectivity of innervation. *J Comp Neurol* **295**:33–42. doi:10.1002/cne.902950104

Yamawaki N, Li X, Lambot L, Ren LY, Radulovic J, Shepherd GMG. 2019. Long-range inhibitory intersection of a retrosplenial thalamocortical circuit by apical tuft-targeting CA1 neurons. *Nat Neurosci* **22**:618–626. doi:10.1038/s41593-019-0355-x

Yamawaki N, Radulovic J, Shepherd G. 2016. A corticocortical circuit directly links retrosplenial cortex to M2 in the mouse. *J Neurosci* **36**:9365–9374. doi:10.1523/JNEUROSCI.1099-16.2016

Yoder RM, Clark BJ, Taube JS. 2011. Origins of landmark encoding in the brain. *Trends Neurosci* **34**:561–571. doi:10.1016/j.tins.2011.08.004

Yoder RM, Peck JR, Taube JS. 2015. Visual landmark information gains control of the head direction signal at the lateral mammillary nuclei. *J Neurosci* **35**:1354–1367. doi:10.1523/JNEUROSCI.1418-14.2015

Yoganarasimha D, Knierim JJ. 2005. Coupling between place cells and head direction cells during relative translations and rotations of distal landmarks. *Exp Brain Res* **160**:344–359. doi:10.1007/s00221-004-2016-9

Yoganarasimha D, Yu X, Knierim JJ. 2006. Head Direction Cell Representations Maintain Internal Coherence during Conflicting Proximal and Distal Cue Rotations: Comparison with Hippocampal Place Cells. *J Neurosci* **26**:622–631. doi:10.1523/JNEUROSCI.3885-05.2006

Yoon K, Buice MA, Barry C, Hayman R, Burgess N, Fiete IR. 2013. Specific evidence of low-dimensional continuous attractor dynamics in grid cells. *Nat Neurosci* **16**:1077–1084. doi:10.1038/nn.3450

Zanforlin M., Poli G. 1970. The burrowing rat: a new technique to study place learning and orientation. *Attice Memorie dell'Accademia patavia di Scienze, Lettere e Arti* **82**: 653-70.

Zhang K. 1996. Representation of spatial orientation by the intrinsic dynamics of the head-direction cell ensemble: a theory. *J Neurosci* **16**:2112–2126.
doi:10.1523/JNEUROSCI.5154-08.2009

Zhang N, Jeffery KJ. 2019. Retrosplenial ‘bi-directional’ cells become tetra-directional in a fourfold-symmetric environment. *Soc Neurosci Abstr* **45**: 694.26.

Zugaro MB, Berthoz A, Wiener SI. 2001. Background, but not foreground, spatial cues are taken as references for head direction responses by rat anterodorsal thalamus neurons. *J Neurosci* **21**:1–5. doi:10.1523/jneurosci.21-14-j0001.2001

Zugaro MB, Tabuchi E, Wiener SI. 2000. Influence of conflicting visual, inertial and substratal cues on head direction cell activity. *Exp Brain Res* **133**:198–208.
doi:10.1007/s002210000365